UNIVERSITY OF NAPLES FEDERICO II

Polytechnic and Basic Sciences School

DOCTORATE SCHOOL IN BIOLOGY

Cycle XXXVI

Toxicity of Rare Earth Elements on human and environmental health

Coordinator

Prof. Sergio Esposito

Supervisors

Prof. Marco Trifuoggi

Prof. Marco Guida

Prof. Giovanni Libralato

Candidate

Antonios Apostolos Brouziotis

ACADEMIC YEAR 2022 – 2023

There is nothing impossible to him who will try

Alexander the Great

Funding

This research has received funding from European Union's Horizon 2020 research and innovation program under the Marie Sklodowska-Curie Grant Agreement N°857989.

Antonios Apostolos Brouziotis

Toxicity of Rare Earth Elements on human and environmental health

Antonios Apostolos Brouziotis, 2023: Toxicity of Rare Earth Elements on human and environmental health

Total number of pages of the thesis: 238

Number of Figures: 63

Number of Tables: 73

Number of graphs: 3

Number of bibliographic references: 557

Published papers

1. Siciliano, A., Guida, M., Pagano, G., Trifuoggi, M., Tommasi, F., Lofrano, G., Suarez, E.G.P., Gjata, I., **Brouziotis, A.A.,** Liguori, R., Libralato, G., 2021. Cerium, gadolinium, lanthanum, and neodymium effects in simplified acid mine discharges to *Raphidocelis subcapitata*, *Lepidium sativum*, and *Vicia faba*. Science of the Total Environment 787, 147527. https://doi.org/10.1016/j.scitotenv.2021.147527. I.F.: 9.8. Citations: 6
2. Siciliano, A., Guida, M., Serafini, S., Micillo, M., Galdiero, E., Carfagna, S., Salbitani, G., Tommasi, F., Lofrano, G., Suarez, E.G.P., Gjata, I., **Brouziotis, A.A.,** Trifuoggi, M., Liguori, R., Race, M., Fabbricino, M., Libralato, G., 2021. Long-term multi-endpoint exposure of the microalga *Raphidocelis subcapitata* to lanthanum and cerium. Science of the Total Environment 790, 148229. https://doi.org/10.1016/j.scitotenv.2021.148229. I.F.: 9.8. Citations: 12
3. **Brouziotis, A.A.,** Giarra, A., Marano, A., Di Nunzio, A., Lombardo, F., Guida, M, Libralato, G., Trifuoggi, M., 2022. Comparative study of two methods for rare earth elements analysis in human urine samples using inductively coupled plasma-mass spectrometry. Frontiers in Environmental Science 10, 942441. https://doi.org/10.3389/fenvs.2022.942441. I.F.: 4.6. Citations: 0
4. Siciliano, A., Sabatino, M., Paone, A., Padilla, E.G., Toscanesi, M., **Brouziotis, A.A.,** Gambino, E., Saviano, L., Trifuoggi, M., Guida, M., Libralato, G., 2022. A first attempt to evaluate the toxicity to *Phaeodactylum tricornutum Bohlin* exposed to rare earth elements. Frontiers in Environmental Science 10, 957943. https://doi.org/10.3389/fenvs.2022.957943. I.F.: 4.6. Citations: 1
5. **Brouziotis, A.A.,** Giarra, A., Libralato, G., Pagano, G., Guida, M., Trifuoggi, M., 2022. Toxicity of rare earth elements: An overview on human health impact. Frontiers in Environmental Science 10, 948041. https://doi.org/10.3389/fenvs.2022.948041. I.F.: 4.6. Citations: 16
6. Pagano, G., **Brouziotis, A.A.,** Lyons, D., Čarapar, I., Oral, R., Tez, S., Thomas, P.J., Tommasi, F., Libralato, G., Guida, M., Trifuoggi, M., 2023. Hormetic effects of cerium, lanthanum and their combination at sub‐micromolar concentrations in sea urchin sperm. Bulletin of Environmental Contamination and Toxicology 110, 65. https://doi.org/10.1007/s00128-023-03701-z. I.F.: 2.7. Citations: 0
7. Saviano, L., **Brouziotis, A.A.,** Suarez, E.G.P., Siciliano, A., Spampinato, M., Guida, M., Trifuoggi, M., Del Bianco, D., Carotenuto, M., Spica, V.R., Lofrano, G., Libralato, G., 2023.

Catalytic activity of rare earth elements (REEs) in advanced oxidation processes of wastewater pollutants: A review. Molecules 28(17), 6185. https://doi.org/10.3390/molecules28176185. I.F.: 4.6. Citations: 1

Submitted or under preparation papers

1. **Brouziotis, A.A.,** Heise, S., Saviano, L., Zhang, K., Tommasi, F., Guida, M., Libralato, G., Trifuoggi, M., 2024. Levels of rare earth elements on three abandoned mining sites in Southern Italy: A comparison between TXRF and ICP-MS. Submitted
2. **Brouziotis, A.A.,** Aiani, M.R., Pagano, G., Mascagni, P., Borea, L., Teze, S., Orale, R., Guida, M., Libralato, G., Giarra, A., Toscanesi, M., Ranieri, P., Marano, A., Giampaolo, F., Galbiati, E., Mariani, S., Cucco, M.G., Thomas, P.J., Trifuoggi, M., 2024. Occupational exposure to rare earth elements in mechanic workshops. Submitted
3. Albarano, L., Guida, M., Tommasi, F., Lofrano, G., Suarez, E.G.P., Gjata, I., **Brouziotis, A.A.,** Trifuoggi, M., Giarra, A., Libralato, G., 2024. Species sensitivity distribution of rare earth elements: a full overview. Submitted

Scientific conferences participation

1. **Brouziotis, A.A.,** Pagano, G., Giarra, A., Toscanesi, M., Di Nunzio, A., Lombardo, F., Libralato, G., Guida, M., Trifuoggi, M., 2021. REEs exposure and related toxicity to car repair workers. SCI 2021. 14-23/09/2021. Poster presentation
2. Suarez, E.G.P., Siciliano, A., Guida, M., Pagano, G., Trifuoggi, M., Serafini, S., Galdiero, E., Tommasi, F., Lofrano, G., Gjata, I., **Brouziotis, A.A.,** Liguori, R., Libralato, G., 2021. Toxicological efects of rare earth elements to photosynthetic organisms. GeoKarlsruhe 2021. 19-24/09/2021. Co-author on oral presentation
3. Suarez, E.G.P., Siciliano, A., **Brouziotis, A.A.,** Guida, M., Trifuoggi, M., Libralato, G., 2022. Influence of pH in the toxicology of rare earth elements Lu, Sm, Y and Yb to model organisms. SETAC 2022 15-19/05/2022. Co-author on poster presentation
4. **Brouziotis, A.A.,** Guida, M., Libralato, Trifuoggi, M., 2022. REE-related toxicity on human and environment. 2nd PANORAMA summer school. 31/10/2022 – 04/11/2022. Oral presentation
5. **Brouziotis, A.A.,** Pagano, G., Giarra, A., Marano, A., Libralato, G., Guida, M., Trifuoggi, M., 2023. Toxicity of rare earth elements on human health. SETAC 2023. 30/04/2023 – 04/05/2023. Poster presentation
6. **Brouziotis, A.A.,** Heise, S., Saviano, L., Giarra, A., Tommasi, F., Guida, M., Trifuoggi, M., 2023. REE levels in abandoned mining sites in Southern Italy. GoldSchmidT 2023. 09-14/07/2023. Poster presentation
7. **Brouziotis, A.A.,** Heise, S., Giarra, A., Guida, M., Libralato, G., Lombardo, F., Manfredi, C., Marano, A., Saviano, L., Tommasi, F., Toscanesi, M., Trifuoggi, 2023. Rare earth elements (REEs) on three abandoned mining sites in the region of Puglia. Congress ABC 2023. 28/09/2023 – 01/10/2023. Oral presentation

Secondments out of UNINA

1. University of bari Aldo Moro, Bari, Italy. 26/09/2022 – 27/10/2022 & 01/05/2023 – 30/06/2023. During the secondment at this university, environmental samples from three abandoned mining sites were collected. The final data were analyzed, a statistical analysis was elaborated and a scientific paper was concluded concerning REEs on these areas.
2. Hamburg University of Applied Sciences, Hamburg, Germany. 1/11/2022 – 1/02/2023. During the secondment at this university, the environmental samples collected in the region of Puglia were digested and analyzed by TXRF. The data received from these analyses have been included in the paper mentioned before, which has been submitted for publication.

Acknowledgments

Contents

General comment on graphical abstracts

The following section provides in an illustrative way the main findings of the current PhD thesis. Graphical abstracts, providing the main points of the three basic chapters of the thesis (Chapter 2: Human Toxicology of REEs; Chapter 3: Environmental Toxicology of REEs; Chapter 4: Environmental Chemistry of REEs) can be found.

Overall graphical abstract

REE-related toxicity on human and environmental health

Chapter 1: Introduction

The extensive use of rare earth elements (REEs) in a number of technologies is expected to impact both human and environmental health. This project seeks to investigate the toxicity of REEs on 3 different levels: human toxicology of REEs, environmental toxicology of REEs and environmental chemistry of REEs.

Chapter 2: Human toxicology

Bibliographic review of REE toxicity on human health. Determining REE-levels in urine and scalp hair samples of car mechanics. Validating methods before analysis by ICP-MS.

Chapter 3: Environmental Toxicology

Investigating the hazardness of REEs on several living organisms (e.g., *R. subcapitata*, *L. sativum*, *Vicia faba*, *P. tricornutum*, *S. granularis*)

Chapter 4: Environmental Chemistry

Examining the REE levels on abandoned mining sites of Southern Italy (Gargano, Otranto, Spinazzola) and their potential as catalysts for removing pollutants from aquatic solutions

Chapter 5: Overall Conclusions

REEs have been proved to be potentially hazardous for both human and environmental health. Human exposure to REEs could occur via several ways. REEs have been associated with a number of diseases. Two methods for preparing urines before analysis by ICP-MS were validated. REEs could potentially be accumulated in human urines and hair due to occupational exposure. REEs have been tested against living organisms and have proven to possess a risk for environmental health. REEs could be used as catalysts for removing toxic substances in aqueous solutions. Last, but not least, their levels in abandoned mining sites of southern Italy, are ideal for a potential future extraction.

Graphical abstract of Chapter 2: Human Toxicology of REEs

Introduction

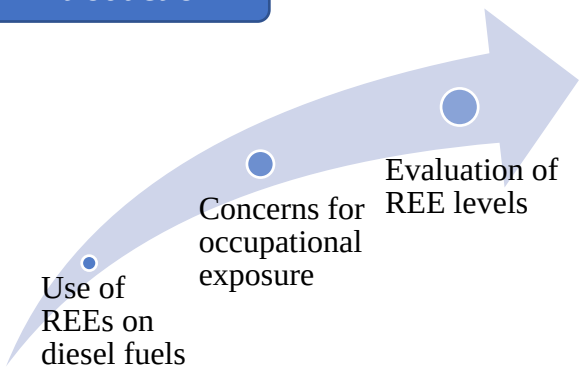

i) Literature review about human toxicity of REEs
ii) Analysis of REE levels on urine and scalp hair of car mechanics
iii) Validation of urine methods

Methods

3 methods

- Dilution 1:5 with HNO_3 2% (DIL)
- Digestion overnight with HNO_3 69% (v/v) (DIG)
- Microwave digestion with HNO_3 69% (v/v) (MIN)

1 method

- Digestion on 80ºC with HNO_3 69% (v/v)

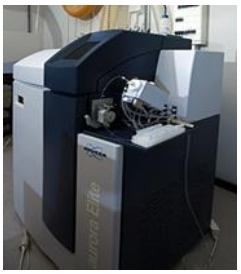

Results

DIL & MIN methods are validated for preparing human urine samples before analysis with ICP-MS. Levels of REEs, 1-OHP and creatinine were significantly higher in urines of Avellino workers. REEs in scalp hair were not significantly different between the two groups. According to our review, Ce is the most studied REE and hair the most studied biological matrix. There are several ways of exposure to REEs, and they are associated with several diseases.

Conclusions

There is a potential occupational exposure to REEs during work-time and a direct excretion. The elevated levels of 1-hydroxypyrene and creatinine in the urines of Avellino workers indicate a higher exposure to combustion products and a higher probability of problems with health issues, respectively.

Graphical abstract of Chapter 3: Environmental Toxicology of REEs

Introduction

The release of REEs into the environment due to the anthropogenic activity (mining, use for production of devices, etc.) has increased concerns for environmental health. Several models have been used to evaluate the ecotoxicity of REEs. The real concentration by ICP-MS was determined before the elaboration of the trials.

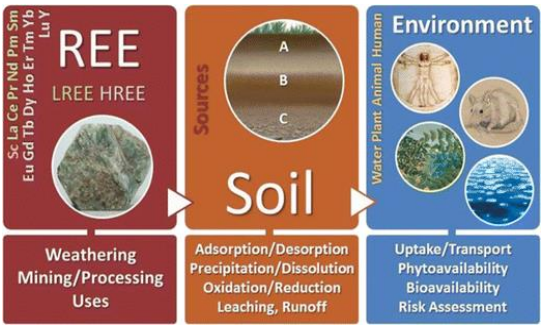

Methods

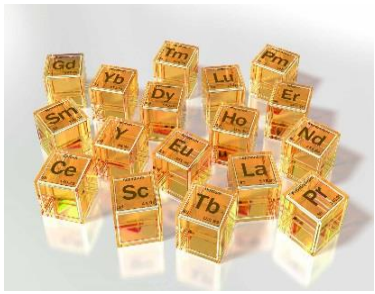

ICP-MS

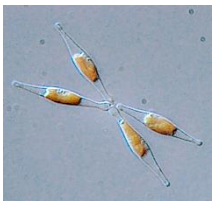

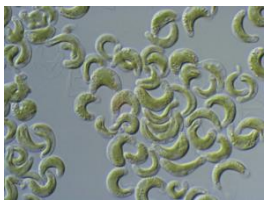

Results

Gd was the most toxic element against *R. subcapitata*, *L. sativum*, and *V. faba* at pH 4, followed by La, Nd, and Ce. On pH 6 the toxicity of REEs was reduced. La and Ce were also toxic against *R. subcapitata* on short-and long-term. La, Ce, Nd, Sm, Eu, Gd, Dy and Er were found toxic against *P. tricornutum Bohlin*. La and Ce increased the fertilization of *S. granularis* in small concentrations, and decreased it in higher.

Conclusions

The increase of the pH seems to mitigate the toxic effects of REEs. Even low concentrations can be toxic to living organisms with the potential to be bioaccumulated and transferred along the food web. Actions are suggested for the managements of the REE impact in seawater environments. REEs could demonstrate a hormetic effect on various organisms.

Graphical abstract of Chapter 4: Environmental Chemistry of REEs

Introduction

The mining of REEs has increased cocerns about their safety for environmental health. In addition, there is a continuous interest on finding new areas for a potential REE-extraction. Environmental samples were collected from three abandoned mining sites in the region of Puglia, Southern Italy.

Methods

Soil Sediments Rocks	•US EPA 3051a
Biota	•Donohue & Friedricks, 1984
Water	•US EPA 3015a

TXRF

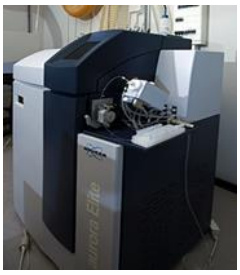

ICP-MS

Results

The LOD valus of ICP-MS were 1000 times lower than the LOD values of TXRF. Only 6 REEs were detected by TXRF; the spectra of some REEs is covered by the spectra of other elements. Generally, there are no significant differences between the two techniques for the analysis of Y, La and Ce. There is a correlation of REE-levels between soil and biota, but they are not bioaccumulative.

Conclusions

There are two main disadvantages when determining REE-levels in environmental samples by TXRF compared to ICP-MS. The very higher LOD values, and the overlap of the spectra of some REEs by the spectra of other elements. Instead, in ICP-MS there are no interferences for the analysis of REEs. Cerium is the most abundant REE in all three regions. Spinazzola is the site containing the highest amount of these elements making it the most interesting among all for a possible REE extraction.

Abstract

The Rare Earth Elements (REEs) are a group of metals consisting of the 15 lanthanides (La, Ce, Pr, Nd, Pm, Sm, Eu, Gd, Tb, Dy, Ho, Er, Tm, Yb, Lu) generally along with Sc and Y. These metals have similar ionic radii and physicochemical properties. Their continuous application in sectors like agriculture and medicine, as well as their necessary utilization for the production of electronic devices, have increased concerns over the last years for both human and environmental health. Previous studies on animal models showed that REEs could cause several types of toxicity.

Therefore, this PhD project investigated the potential hazardness of REEs on three different levels: i) on human toxicity, through the biomonitoring of the REE levels on human matrices; ii) on environmental toxicity, through elaborating ecotoxicity trials with several organisms; and on environmental chemistry, through determing the REE levels on abandoned mining sites.

A literature review concerning the toxicity of REEs exclusively on human health was elaborated. Ce is the most studied REE, cytotoxicity the most studied field, while hair, blood and blood serum are the most studied human matrices. Human exposure to REEs can happen via many ways, such as environmental exposure, exposure through the food web or due to the lifestyle. REEs have been associated with several dieases, like neural tube defects, anemia and endomyordical fibrosis. GBCAs could be accumulated in kidney or muscles causing renal failure and fibromyalgia. The mining of REEs does not affect only the mining workers, but also residents near the mining areas. REEs have been shown to affect a number of metabolic pathways. They could activate metabolic pathways resulting to ROS production, DNA damage and apoptosis. However, they could be potential anticancer agents, since they are more cytotoxic on cancer compared to normal cells.

Due to the implementation of REEs in diesel fuels as additives, concerns have increased about the potential human exposure to them through the car exhausts. For that reason, urine and scalp hair samples of car mechanics were collected from two different types of workshops. The car mechanics in the workshops of Avellino are lacking the use of means of protection, while those of Como are using them properly.

Before the analysis of REEs on the human matries, it was essential to determine the LOD and LOQ values of REEs on ICP-MS, as well as validating the methods of preparation before analysis by ICP-MS. For determining the LOD and LOQ values, the REE content in 10 blank samples containing only HNO_3 2% (v/v) was determined. LOD values ranged from 0.001 to 0.004 μg/L, while LOQ values ranged from 0.005 to 0.013 μg/L. Due to the lack of certified reference materials for REEs on human urine and hair, only the two methods for preparing human urines were validated following a method of spiking. Both methods showed adequate precision of repeatability and intra-laboratory reproducibility. The CVr% values of repeatability ranged from 1.5 to 12% for the DIL and from 8.4 to 16% for the MIN method. The CVr% values of reproducibility ranged from 6.2–23% for the DIL and from 8.6 to 24% for the MIN method. REE recoveries for both methods were very close to 100%. Therefore, both methods proved to be effective for the determination of REE levels in human urine matrices.

Proceeding with the human matrices, the levels of REEs were determined in urines and hair. In addition, the levels of creatinine and 1-OHP were determined in urines. Our results showed significantly elevated levels of La, Ce, Gd, Tb and Total REEs in the urines of the exposed group, as well as levels of creatinine and 1-OHP. No REE or Total REEs were significantly different in the scalp hair between the two groups. Statistical analysis revealed that levels of La and Ce were

significantly higher in the scalp hair of smokers when the use of hair dye does not affect the levels of any REE. These results indicate a highly possible occupational exposure of car mechanics to REEs due to car exhausts and a direct excretion through urines. There are also indications that smoking affects the levels and bioaccumulation of La and Ce.

Several models were used in the lab for investigating the environmental toxicity of REEs. The real concentration of REEs in the samples prepared for elaborating the ecotoxicity trials was determined by ICP-MS with respect to the nominal concentration.

The effect of Ce, Gd, La, and Nd was investigated in a simulated AMD at pH 4 and 6 considering a number of photosynthetic organisms (*R. subcapitata, L. sativum,* and *V. faba*) according to a multipleendpoint approach (growth inhibition, germination index, and mutagenicity). Gd was the most toxic element at pH 4, followed by La, Nd, and Ce. At pH 6, their effects significantly decreased, and Nd evidenced the highest toxicity. Gd, La and Nd evidenced at pH 4 their potential mutagenicity, that was not present at pH 6. These results indicate that the toxicity of REEs is increased in acidic environments, while the increase of the pH could mitigate their toxic effects.

The microalagae *R. subcapitata* was exposed to La and Ce for 3 days (short-term exposure) to derive the EC_{10} values that were consequently used for the long-term exposure (21 days) to observe growth inhibition, biomarkers of stress, and bioconcentration. La and Ce increased the growth inhibition and were bioconcentrated. La increased also the ROS production. These results indicate that even low concentrations of La and Ce could be toxic to R. subcapitata with the potential to be bioaccumulated and transferred through the food web.

The toxicity of eight REEs (La, Ce Nd, Sm, Eu, Gd, Dy, and Er) to the microalga *Phaeodactylum tricornutum Bohlin* was investigated. The EC_{50} values ranged from 0.98 mg/L to 13.21 mg/L and the elements were ranked according to their toxicity as follows: Gd > Ce > Er > La > Eu > Nd > Dy > Sm. Based these results, the presence of REEs in the marine environment does not seem to represent a widespread environmental risk except at some hotspots which may become more severe with the increase of REE application.

Ce, La and their combination were tested across a concentration range for their effects on the sperm of *S. granularis*. A significantly decreased fertilization rate and increased developmental defects were noticed in higher concentrations, while an increased fertilization rate and decreased developmental defects were observed in lower concentrations. These results indicate that REEs could have a hormetic effect on several models.

REEs can be used as catalysts on Advanced Oxidation Processes for the enhancement of the degradation of organic pollutants from aqueous solutions, including pharmaceuticals, dyes, and other molecules such as alkaloids, herbicides, and phenols. Ce and La are the most studied REEs on this field, and their mechanism of action is based on the oxygen vacancies and REE ion concentration in the catalysts. Metal oxide surfaces improve the decomposition of hydrogen peroxide to form hydroxide species, which degrade the organics.

The REE content was analyzed in environmental samples collected from three abandoned mining sites in the region of Puglia (Gargano, Otranto and Spinazzola). After the digestion, the REE content was determined by TXRF and ICP-MS. TXRF performed much higher LOD levels than ICP-MS. Only by ICP-MS, could all REEs be traced in the samples. Ce seems to be the most abundant REE in all sites, while Spinazzola seems to be the site containing the highest amount of these elements,

making it the most interesting among all for a possible REE extraction. According to the calculation of BCF, REEs are not bioaccumulative.

All in all, this project has shown that REEs are potentially hazardous for both human and environmental health. They have been associated with several diseases, they could be bioaccumulated in human matrices and they are toxic for a number of living organisms. In the future, other research projects should consider of investigating the safety of these elements as well, since their human utilization and environmental concentration is increasing overtime.

Table of abbreviations

Abbreviation	Full name
1-OHP	1-hydroxypyrene
AOPs	Advanced Oxidation Processes
GBCAs	Gadolinium-based contrast agents
HCl	Hydrochloric acid
HNO_3	Nitric acid
ICP-MS	Inductively Coupled Plasma Mass Spectrometry
LOD	Limit of Detection
LOQ	Limit of Quantification
REEs	Rare Earth Elements
RF	Radiofrequency
TXRF	Total X-Ray Fluorescence

Chapter 1: Introduction

Rare Earth Elements (REEs)

The metals known as rare earth elements (REEs), include the 15 lanthanide elements [Lanthanum (La), Cerium (Ce), Praseodymium (Pr), Neodymium (Nd), Promethium (Pm), Samarium (Sm), Europium (Eu), Gadolinium (Gd), Terbium (Tb), Dysprosium (Dy), Holmium (Ho), Erbium (Er), Thulium (Tm), Ytterbium (Yb), and Lutetium (Lu)], and also Scandium (Sc) and Yttrium (Y). They have been dubbed as a treasure of novel materials due to their significant contributions to both the advancement of traditional industries and technology (Du and Graedel, 2011; Wang et al., 2009). These metals are grouped into three groups based on their atomic number and masses and share comparable ionic radii and physicochemical characteristics (Brown et al., 1990): Light rare earth elements (LREEs) are La, Ce, Pr, Nd, and Pm; medium rare earth elements (MREEs) are Sm, Eu, Gd, Tb, Dy, and Ho; and heavy rare earth elements (HREEs) are Er, Tm, Yb, and Lu. An illustration of the position of REEs on the periodic table is shown in Figure 1.

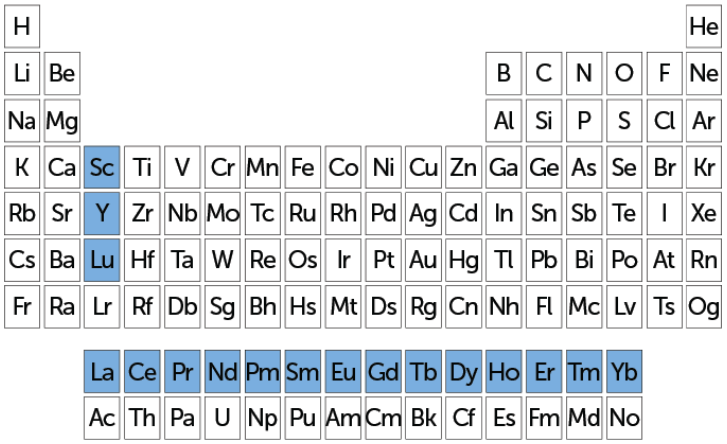

Figure 1. A simple illustration of the periodic table, highlighting the metals belonging to the group of the rare earth elements (REEs), including scandium and yttrium.

The chemistry of REEs differs from main group elements and transition metals because of the nature of the 4f orbitals, which are shielded from the atom's environment by the 4d and 5p electrons (Table 1) (Vogler and Kunkely, 2006). These orbitals give to REEs unique catalytic, magnetic, and electronic properties, which can be exploited to accomplish new types of applications that are not possible with transition and main group metals (Celardo et al., 2011b; Kuchma et al., 2010; Pagano et al., 2015a).

All REEs exhibit the +3 oxidation state, whether they are in solid compounds or solutions in water or other solvents. A few solid compounds that represent the +4 state have been created, but only Ce^{4+} has a long enough half-life to be significant in aqueous solutions. Even though all REEs were trapped in solid alkaline earth halide matrices and obtained in the +2 state, dissolution in aqueous environments causes all species with the exception of Eu^{2+} to rapidly oxidize to the +3 state. Even in aqueous solution, the half-life of oxidation for Eu^{2+} is only fairly brief.

In the case of cerium, which has two partially filled sub-shells of electrons, 4f and 5d, with several excited sub-states predicted, the +4 state with the stable electronic configuration of xenon is preferentially formed. When cerium oxide crystallizes in the fluorite structure, every cerium atom is surrounded by eight oxygen anions and every oxygen atom occupies a tetrahedral position. Nonetheless, a significant concentration of intrinsic defects is usually present, with a portion of cerium present in the Ce^{3+} valence state having the deficiency of positive charge compensated by oxygen vacancies (Conesa, 1995; Sverjensky, 1984). The ratio of Ce^{3+} to Ce^{4+} ions depends on the size of the particles. In general, when particle size decreases, the fraction of Ce^{3+} ions in the particles rises (Zhao et al., 2011).

Table 1. Electronic properties of REEs.

Element	Symbol	Oxidation State	Z	A	Electronic Configuration
Scandium	Sc	+3	21	45	$(3d4s)^3$
Yttrium	Y	+3	39	89	$(4d5s)^3$
Lanthanum	La	+3	57	139	$4f^0(5d6s)^3$
Cerium	Ce	+3, +4	58	140	$4f^1(5d6s)^3$
Praseodymium	Pr	+3	59	141	$4f^2(5d6s)^3$
Neodymium	Nd	+3	60	144	$4f^3(5d6s)^3$
Promethium	Pm	+3	61	145	$4f^4(5d6s)^3$
Samarium	Sm	+3	62	150	$4f^5(5d6s)^3$
Europium	Eu	+2, +3	63	152	$4f^7(5d6s)^2$
Gadolinium	Gd	+3	64	157	$4f^7(5d6s)^3$
Terbium	Tb	+3	65	159	$4f^8(5d6s)^3$
Dysprosium	Dy	+3	66	163	$4f^9(5d6s)^3$
Holmium	Ho	+3	67	165	$4f^{10}(5d6s)^3$
Erbium	Er	+3	68	167	$4f^{11}(5d6s)^3$
Thulium	Tm	+3	69	169	$4f^{12}(5d6s)^3$
Ytterbium	Yb	+3	70	173	$4f^{14}(5d6s)^2$
Lutetium	Lu	+3	71	175	$4f^{14}(5d6s)^3$

Although the production of catalysts for the cracking of crude oil is one of the primary industrial uses of REEs, involving millions of tons of raw materials annually, their use in the production of strong permanent magnets for electro-mechanical devices, of displays, glass, and lenses, for laser technology, and for their use in solid state microwave devices (for radar and communications systems) illustrates the relatively widespread involvement of REEs in industry (Bellin and Van Der Molen, 2008; Corma et al., 2004; Khan et al., 2011).

Low quantities of rare earth elements, such as lanthanides, Y, and Sc, exist naturally in the soil, water, and atmosphere. These elements can build up as a result of anthropogenic inputs from farming, animal husbandry, and industrial waste applications. These substances were not regarded as pollutants for a very long time due to their poor mobility. However, in recent years, REEs have generated a great deal of worry due to their toxicity to living things as well as their persistence in the environment and bioaccumulation in the biota. In fact, recent data from many world locations, including China, Canada, the Netherlands, and Australia, show an increase in the concentration of REE in soil and

water (Ding et al., 2006; Li et al., 2010, 2013; Liang et al., 2014; Turra et al., 2011; Wyttenbach et al., 1998; Diatloff et al., 1996; Volokh et al., 1990).

Despite the increasing interest in REEs, the early and sparse database referring to the last two decades has led to the contentious current knowledge on the healthy versus toxic effects of these materials. The attention seems to be focused only on a restricted number of REEs, namely Ce, La, Gd, Nd, and Y. The manufacturing, processing, and use of REEs raise numerous environmental concerns. According to a growing body of data, the chemicals employed in the refining process have contributed to sickness, occupational poisoning of locals, water contamination, and the degradation of farmland. At several stages, including mining and refining, transportation, processing, waste disposal, and decommissioning, occupational and public safety and health issues associated with REEs may be taken into consideration (Marubashi et al., 1998; Rim et al., 2013; Wu et al., 2013; US EPA, 2012).

Inductively Coupled Plasma – Mass Spectrometry (ICP-MS)

1 General Discussion

Using the inductively coupled plasma-mass spectrometry (ICP-MS) method, metals and metalloids can be discovered in surface, ground, and drinking waters. Although it works best for ambient or pristine freshwater matrices, this method can be used to analyze wastewater, soils, sediments, sludge, and biological samples after proper digestion, followed by dilution and/or cleanup to limit matrix effects to a manageable level (Montaser and Golightly, 1992; Date and Gray, 1989). Many elements may not require mathematical interference correction thanks to the use of collision cell technology (CCT) (Nelms, 2005; Becker, 2008). The strategy is intended to be performance-based, allowing for the adoption of new cleaning and preparation techniques as well as other necessary adjustments as technology develops, such as the expansion of the elemental analyte list. Any underlying technique modifications must be confirmed using the necessary quality control standards (US EPA, 1994; Longbottom et al., 1994; US EPA, 1995). The ICP-MS procedure, interpreting spectrum and matrix interferences, and applying correction techniques should all be familiar to the analysts who use this approach. Before producing data, analysts should accurately evaluate a performance evaluation sample for each type of matrix to demonstrate their proficiency with this approach. Figure 1 shows an Aurora M90 ICP-MS instrument, which was also used in this project for all the REE analyses.

Figure 1. An Aurora M90 ICP-MS instrument.

1.1 Principle

In this procedure, nebulization is used to introduce the sample material to an argon-based, high-temperature radio-frequency plasma. The energy from the plasma is transferred to the sample stream, dissolving, atomizing, and ionizing the target element. Through a differential vacuum interface, the resultant ions are removed from the plasma and then separated by a mass spectrometer according to their mass-to-charge (m/z) ratio. The two most common mass spectrometers are quadrupole and magnetic sector (high-resolution). The separated ions are counted using an electron multiplier detector, and the information obtained is processed by a computer-based data-management system.

The employment of a high-temperature plasma discharge to produce positively charged ions is the core idea of ICP-MS. The sample introduction system, which consists of a spray chamber and a

nebulizer, is pumped with the sample, which is in liquid form. It appears as an aerosol and finally makes its way into the plasma's base via a sample injector. It is dried, evaporated, atomized, and ionized as it passes through the various heating zones of the plasma torch. The sample undergoes a series of changes throughout this period, going from a liquid aerosol to solid particles to a gas. When it eventually reaches the analytical zone of the plasma, at around 6000–7000 K, it exists as excited atoms and ions, which indicates the sample's elemental composition.

Atomic emission's fundamental mechanism is the excitation of an atom's outer electron, which results in photons of light with a certain wavelength. The plasma does, however, also contain sufficient energy to liberate one electron from its orbital and produce an ion. The hallmark ultratrace detection capabilities of ICP-MS are due to the creation, transportation, and detection of large numbers of these positively charged ions. It is also crucial to note that although ICP-MS is primarily used to detect positive ions, the plasma can also produce negative ions such halogens. However, the majority of commercial equipment are not made to monitor negative ions because their extraction and transportation differ from those of positive ions.

1.2 Applicable elements and analytical limits

As long as the established acceptance limits are followed and the quality assurance procedures are used, this approach has been shown to be suitable for a number of metals. The instrument detection limit (IDL) and method detection limit (MDL) for each analyte should be established prior to method implementation. When complicated matrices, such as seawater, brines, and industrial effluents, are studied, figuring out the MDL for each constituent is crucial. Due to background analyte levels introduced during sample preparation, laboratory-derived contamination, and matrix-based interferences, the MDL in these situations will often be higher than the IDL. When first applying this procedure, both IDL and MDL should be determined. They should then be redone annually or anytime the instrument configuration changes or significant maintenance takes place, whichever comes first. In order to take into consideration potential inter-element effects, the linear dynamic range (LDR) for all method analytes, including multi-element combinations, should also be computed. LDR is the greatest concentration of an analyte above the highest calibration point at which the analyte response is within 10% of its theoretical response. Unnecessarily high analyte concentrations should be avoided while determining LDRs since they could harm the detector. LDR should be established when adopting this method for the first time, and then done annually (US EPA, 1994).

1.3 Interferences

There are various forms of interferences that can affect ICP-MS, including the following:

1. Isobars. A quadrupole or a high-resolution mass spectrometer cannot distinguish between isotopes of different elements that produce ions with the same nominal atomic mass units/charge number (m/z) ratio. These ions are known as isobars. Normally, all known isobaric interferences are included in ICP-MS operating software, and the relevant calculations are done automatically. For instance, ^{82}Kr on ^{82}Se, ^{98}Ru on ^{98}Mo, ^{114}Sn on ^{114}Cd, ^{115}Sn on ^{115}In, and ^{123}Te on ^{123}Sb can all result in isobaric interference. The accuracy and suitability of all elemental and molecular correction equations for the sample matrix and the mass spectrometer utilized in this procedure should be confirmed. There are no isobaric interferences for REEs.

2. Abundance sensitivity. The likelihood that the low and high "wings" of any abundant mass peak may contribute to or hide nearby masses is known as abundance sensitivity. To reduce these interferences, the quadrupole pole bias and mass spectrometer resolution should be modified.

3. Polyatomics. A polyatomic is an ion with more than one atom that has the same nominal m/z ratio as the isotope of interest. Polyatomics are molecular ion interferences, the majority of which have been found. Hydrochloric acid is not advised for use in ICP-MS sample preparation due to the severe chloride ion interference on critical analytes. Analysts must employ chloride-correction equations for affected masses since the majority of environmental samples contain some chloride ions. In quadrupole-based ICP-MS systems, CCT efficiently decrease the majority of polyatomic species to analytically inconsequential levels, sometimes negating the need for complicated correction equations. Many, but not all, interferences brought on by polyatomic ions are eliminated using a high-resolution ICP-MS. Polyatomic interferences can occasionally be decreased by carefully modifying nebulizer gas flow and other instrument operating parameters. Polyatomic interferences are greatly impacted by instrument design and plasma operating conditions.

4. Double-charged. Under typical plasma conditions, several elements, like barium and strontium, form considerable amounts of M^{2+} ions. In the case of Ba and Sr, the M^{2+} ions will interfere with some isotopes of zinc and calcium, respectively, because they are present in the mass spectrum at M/2. There are no elements that make up amounts of M^{2+} in the case of REEs.

5. Physical interferences. These include variations between samples and calibration standards in viscosity, surface tension, and dissolved solids. Analytical samples shouldn't include more than 0.5% of dissolved solids in order to reduce these effects. Prior to analysis, samples of water and wastewater with higher dissolved solids levels should be diluted. To adjust for physical interferences, it is advised to employ internal standards, provided that their analytical behavior is comparable to the elements being determined. For all analytes, a quadrupole ICP mass spectrometer with CCT is advised because it does away with a lot of the equations that are generally required in the standard operating mode.

6. Memory interferences. When analytes from a previous sample or standard are analyzed in the present sample, such interferences could happen. To reduce these interferences, it is advised to give the samples enough time to rinse between them. Consistent memory hiccups could be a sign of issues with the sample-introduction system. Analysts may need to disassemble and clean the entire sample-introduction system, including the plasma torch and the sampler and skimmer cones, in the case of severe memory interferences.

7. Interferences due to ionization. These happen when little amounts of a matrix ion - between 0.1% and 1% - change the analyte signal. By applying internal standardization techniques, this effect, also known as suppression, which typically decreases the analyte signal, can be rectified (Baird et al., 2017).

2 The sample-introduction system

The process of adding a liquid to an ICP-MS can be done in a variety of ways, but they all essentially provide the same result in the end: they make the sample into a thin aerosol that can be effectively ionized in the plasma discharge. Because it is thought to be the instrument's weakest part, with about 1% to 2% of the sample making it into the plasma, the sample-introduction system has been the Achilles heel of the ICP-MS. Although there has been significant advancement in this field recently,

since the technique's inception in 1983, the fundamental design of an ICP-MS sample introduction system has not significantly changed.

The two events that make up the mechanism for introducing a liquid sample into analytical plasma are the droplet selection through a spray chamber and the aerosol production using a nebulizer. Both procedures were thoroughly examined by (Sharp, 1980).

Figure 2 demonstrates the typical positions of the spray chamber and nebulizer in an ICP-MS system.

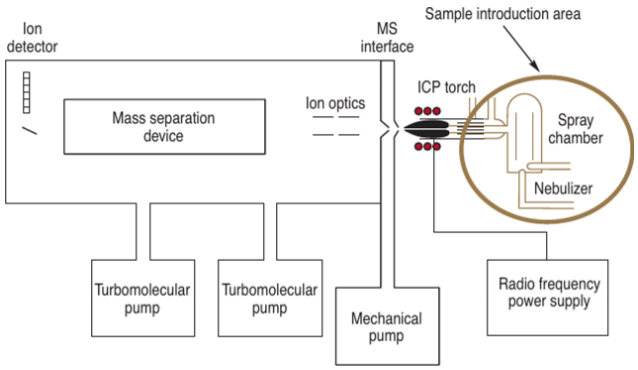

Figure 2. Positions of the spray chamber and nebulizer in an ICP-MS.

2.1 Aerosol generation

The sample introduction system's primary purpose is to produce a fine aerosol of the sample. It uses a nebulizer and a spray chamber to do this. A peristaltic pump generally pumps the sample into the nebulizer at a rate of around 1 mL/min. A peristaltic pump is a tiny pump with numerous little rollers that spin continuously. The sample is fed to the nebulizer by the continual rotation and pressure of the rollers on the pump tube. Peristaltic pumps have the advantage of maintaining a steady flow of liquid despite variations in viscosity between samples, standards, and blanks.

The liquid is broken up into a fine aerosol after the sample enters the nebulizer by the pneumatic action of gas flow (1 L/min), which is quite similar to the spray mechanism of a can of deodorant. However, some pneumatic nebulizers, like the concentric design, do not require a pump since they rely on the natural venturi effect of the positive pressure of the nebulizer gas to suck the sample through the tubing. Pumping the sample is still the most popular method of introducing it.

2.2 Droplet selection

The spray chamber's main purpose is to only permit small droplets into the plasma because the plasma discharge is ineffective at separating large droplets. Its secondary function is to reduce pulses that happen during nebulization, primarily because of the peristaltic pump. The most popular method of ensuring that only tiny droplets pass through is to employ a double-pass spray chamber, in which the aerosol exits the nebulizer and is directed into a central tube that extends the whole length of the chamber.

The huge droplets (more than 10 mm in diameter) fall out by gravity and leave through the drain tube at the end of the spray chamber after traveling the length of this tube. The tiny droplets (5–10 m in diameter) eventually exit the spray chamber and are carried into the sample injector of the plasma

torch by passing between the outer wall and the central tube. The spray chamber's primary purpose is to only permit the tiniest droplets into the plasma in order to dissociate, atomize, and ultimately ionize the sample's elemental constituents (Bates and Olesik, 1990).

2.3 Nebulizers

The pneumatic nebulizer, which creates the sample aerosol mechanically using a gas flow (most often argon at a pressure of 20–30 psi), is by far the most popular design used for ICP–MS. Pneumatic nebulizers come in a variety of configurations, but concentric, microconcentric, microflow, and crossflow are the most widely used. Although they are typically composed of glass, other nebulizer materials, such as different kinds of polymers, are gaining popularity, especially for specific applications and highly corrosive samples. The concentration of matrix components must typically be kept below 0.2% since the sampler and skimmer cones used in ICP-MS have such narrow orifice diameters (0.6-1.2 mm). Therefore, high-solids nebulizers like the Babbington, V-groove, or cone-spray nebulizers, which are designed to handle as much as 20% dissolved solids, are not the best choices for usage with ICP-MS. The concentric and crossflow designs of pneumatic nebulizers are the most often utilized ones in industrial ICP mass spectrometers. While the crossflow is typically more tolerant to samples having higher amounts of particles or particulate matter, the concentric design is better suited for clean samples (Houk, 1986).

2.4 Spray chambers

Commercial ICP-MS apparatus mostly uses double pass and cyclonic spray chamber designs. The cyclonic kind is becoming more and more widespread, although the double pass is by far the most prevalent. The early ICP-MS systems explored a different kind of spray chamber based on the impact bead design, but it is not typically used nowadays. As was already established, the spray chamber's job is to both reject larger aerosol particles and smooth out peristaltic pump pulses. Additionally, some ICP-MS spray chambers have external cooling (usually to 2–5 °C) to maintain the sample's thermal stability and reduce the amount of solvent entering the plasma. Depending on the application, this may have a variety of advantageous effects, but the main advantages are the reduction of oxide species and the capacity to aspirate volatile organic solvents (Beres et al., 1994).

3 The plasma source

3.1 The plasma torch

A plasma torch, a Radiofrequency (RF) coil, and an RF power supply are the three fundamental parts that make up the plasma source. Figure 3 demonstrates a view of the plasma torch and RF coil, while Figure 4 shows the typical position of a plasma source in an ICP-MS system. Three concentric tubes, typically formed of quartz, make up the plasma torch. The torch may be constructed in two ways: either as a single unit with the three tubes attached, or as a demountable unit with the tubes and sample injector separated. Approximately 12–17 L/min of gas, most often argon, is transferred between the outer and central tube to create the plasma. The auxiliary gas, a second gas flow between the central tube and the sample injector, moves the position of the sample injector in relation to the plasma at a rate of around 1 L/min. The sample is physically punched through the center of the plasma by a third gas flow, the nebulizer gas, which is also flowing at a rate of less than 1 L/min and brings the sample from the sample introduction system, in the form of a fine-droplet aerosol, into the plasma. If highly corrosive materials need to be examined, the sample injector is frequently made of substances other

than quartz, such as alumina, platinum, and sapphire. Although argon is the best gas to utilize for all three flows, employing different gas mixes, particularly in the nebulizer flow, has analytical advantages. The plasma torch is horizontally installed and placed in the center of the RF coil, around 10–20 mm away from the interface. The coil used in ICP-MS plasma differs slightly from the one used in ICP Optical Emission Spectroscopy (ICP-OES). Due to capacitive coupling between the RF coil and the plasma, there is a potential difference of a few hundred volts in every plasma. This would cause a secondary discharge between the interface cone and the plasma in an ICP mass spectrometer, which would impair the device's functionality. The coil needs to be grounded in order to make up for this and maintain the interface region's potential as near to zero as possible (Lam and McLaren, 1990).

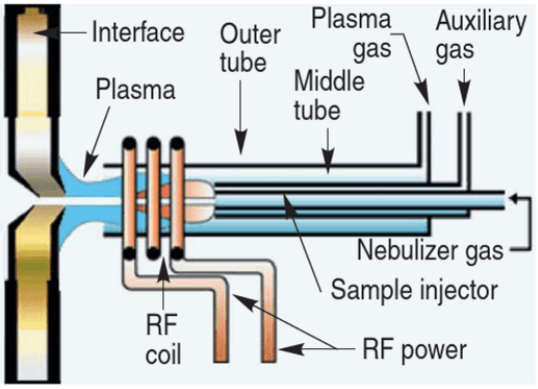

Figure 3. Detailed view of a plasma torch and RF coil relative to the interface region.

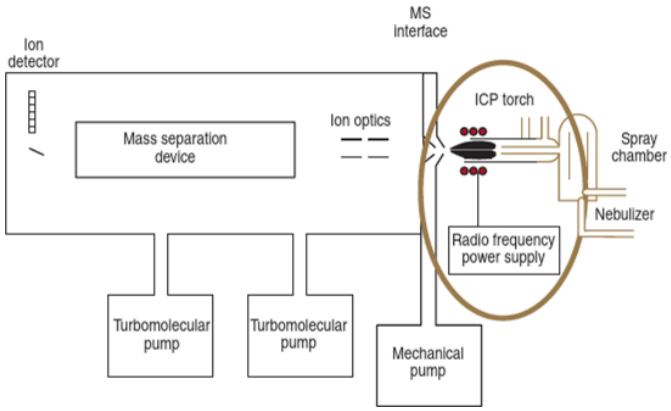

Figure 4. Positions of the plasma torch and radio frequency (RF) power supply in an ICP-MS system.

3.2 Formation of an ICP discharge

The first step is to direct a spiral flow of argon gas between a quartz torch's central and outer tubes. Around the torch's upper end there is a load coil made of typically copper that is coupled to a radio frequency generator. An alternating current oscillates within the load coil at a rate corresponding to the generator's frequency when RF power—typically 750–1500 W, depending on the sample—is delivered. This frequency is often either 27 or 40 MHz in ICP generators. A powerful electromagnetic field is generated in the region at the torch's top due to the RF oscillation of the coil's current. A high-voltage spark is used to ignite the argon gas as it passes past the torch, which results in some electrons

being taken away from their argon atoms. These in the magnetic field trapped and accelerated electrons then crash with other argon atoms, removing even more electrons. An inductively coupled plasma discharge is created when the argon is broken down into argon atoms, argon ions, and electrons as a result of collision-induced ionization. Then, when RF energy is continuously supplied to it via the inductive coupling process, the ICP discharge is maintained within the torch and load coil. The sample injector, a third tube, is used to introduce the sample aerosol into the plasma. Figure 3 conceptually depicts this entire procedure.

3.3 The function of the RF generator

Some of the earliest nitrogen or air-based generators needed 5–10 kW of electricity to maintain the plasma discharge and practically filled up the entire room. Since the majority of generators today employ solid-state electronics, vacuum power amplifier tubes are no longer necessary. Because vacuum tubes were infamously unreliable and unstable, this results in substantially smaller and more suitable for routine operation current devices.

ICP RF generators are typically operated at 27 and 40 MHz. These frequencies are dedicated to RF applications of this kind and wil not conflict with those used for other forms of communication. The most modern designs prefer 40 MHz while the older RF generators used 27 MHz. It seems that neither form has a clear analytical advantage over the other. It is important to note that the 40-MHz design often operates at lower power levels, which results in a weaker signal and less background noise. This might be useful for long-term use of the generator because it consumes a little less electricity.

The RF generator's coupling efficiency to the coil is the most crucial factor to take into account. Most current solid-state RF generators are between 70 and 75 percent efficient, which means that between 70 and 75 percent of the given power actually enters the plasma. It wasn't always like this, and some of the earlier vacuum tube-designed generators were infamously inefficient, losing as much as 50% of their output in some cases. The way the matching network adjusts for variations in solvent volatility or changes in impedance, which are caused by the matrix components of the sample, is another crucial factor to take into account.

This was often accomplished using servo-driven capacitors in earlier crystal-controlled generators. They performed admirably with the majority of sample types, but because they were mechanical devices, they had trouble adjusting for some samples' incredibly quick impedance changes. As a result, the plasma burned out quickly, especially when volatile organic solvents were aspirated.

The use of free-running RF generators, whose matching networks were based on electronic tuning of minute changes in frequency caused by the sample solvent or matrix components, helped to partially alleviate these issues. The main advantage of this method was that there were no moving elements, and so correction for impedance changes was practically immediate. As a result, several sample types that would have likely extinguished the plasma of a crystal-controlled generator may now be successfully analyzed.

3.4 Ionization of the sample

The sample aerosol enters the sample injector through the spray chamber, as was already explained. It leaves the sample injector traveling so quickly that it actually rips a hole through the plasma discharge's core. Then, after undergoing a series of physical transformations in the preheating zone, radiation zone, and analytical zone, it finally becomes a positively charged ion. Let's assume that the

element exists as a trace metal salt in solution in order to very simply explain this. Desolvation of the droplet is the initial process. It then turns into a very small solid particle after the water molecules have been removed. The solid particle transforms into a gaseous form at first when the sample advances further into the plasma, and subsequently into a ground-state atom. The intense argon electrons (and to a lesser extent, argon ions) collide with the groundstate atom to produce the final process that transforms an atom into an ion. The ion subsequently leaves the plasma and is directed toward the mass spectrometer's interface (Hasegawa and Haraguchi, 1992).

4 The interface region

4.1 Sampling the ions

The proximity of the interface region to the remainder of the instrument is depicted in Figure 5. The function of the interface is to move the ions from the plasma, which is at atmospheric pressure (760 Torr), to the mass spectrometer analyzer zone, which is at a pressure of about 10^{-6} Torr, efficiently, consistently, and with electrical integrity. By first directing the ions toward the interface region, one can accomplish this. Two metallic cones with extremely small orifices make up the interface, which is kept at a vacuum of 2 Torr by a mechanical roughing pump. The sampler cone is the first cone the ions pass through once they are created in the plasma, and has an opening diameter of 0.8-1.2 mm. Then, they go a short distance to the skimmer cone, which has an aperture that is significantly smaller (0.4–0.8 mm) and typically sharper than the sampler cone. Although both cones are often constructed of nickel, they can also be manufactured from materials that are much more resistant to corrosive liquids, such as platinum. The interface housing is built of a heat-dissipating material, such as copper or aluminum, and is water-cooled to lessen the impact of the high-temperature plasma on the cones. The ions then exit the skimmer cone, travel via the ion lenses, and are eventually led into the mass separation apparatus.

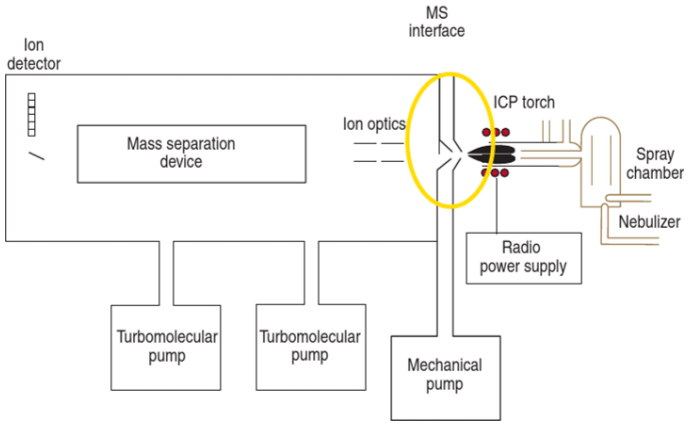

Figure 5. Position of the interface region in an ICP-MS system.

4.2 Capacitive coupling

It may seem simple enough, but during the early stages of ICP-MS development, an undesirable capacitive coupling between the load coil and the plasma discharge—which results in a potential difference of 100–200 V—made this process very difficult. The fact that the sampler cone and plasma are electrically discharged by the capacitive coupling in an ICP mass spectrometer makes this potential, which is a physical trait of all ICP discharges, more dangerous in this situation. The pinch

effect or secondary discharge, as it is often known, manifests as arcing in the area where the plasma is in contact with the sampler cone (Gray and Date, 1983).

This arcing can lead to a variety of issues if it isn't addressed, such as an increase in doubly charged interfering species, a large kinetic energy spread of the sampled ions, the generation of ions generated from the sampler cone, and a shorter orifice lifetime. Numerous early practitioners of the approach acknowledged these issues (Houk et al., 1981; Date and Gray, 1981). In reality, the source of the secondary discharge was initially believed to be an electro-gasdynamic process that led to an increase in electron density at the orifice because the arcing increased with sampler cone orifice size. After conducting numerous experiments, it was eventually determined that the secondary discharge was caused by the load coil's electrostatic coupling to the plasma. The radio frequency (RF) potential was first reduced to a few volts by grounding the induction coil at the center, which solved the issue (Gray and Date, 1981).

Initially, the grounding was accomplished by physically fastening a grounding strap from the coil's center turn to the interface housing. Depending on how the interface is designed, there are several approaches to ground today's instruments. The oscillator inside the RF generator's circuitry is balanced (Tanner, 1995), a grounded shield or plate is placed between the coil and the plasma torch, or two interlaced coils with opposing RF fields are some of the most widely used designs. All of them operate differently but ultimately reduce or do away with secondary discharge (Sakata and Kawabata, 1994).

4.3 Ion kinetic energy

Regarding its impact on the kinetic energy of the ions being tested, the impact of a secondary discharge cannot be overstated. It is widely known that to enable efficient and complete electrical focus by the ion optics and the mass separation device, the energy distribution of the ions entering the mass spectrometer must be as low as feasible. Depending on their mass-to-charge ratios, the ions' kinetic energy will vary when they leave the argon plasma. Since they are all governed by the bulk plasma's rapid expansion, which will remain neutral as long as its potential is kept at zero, their velocities ought to be comparable. The ion beam will expand as it travels from the sampler cone to the skimmer cone, but if the plasma is neutral, its composition and integrity will be preserved.

As the ions enter the sampler or skimmer cone, electrodynamic forces are not a factor because the Debye length, or the distance over which the ions impact one another, is short (usually 10^{-3}-10^{-4} mm) in comparison to the orifice diameter (0.5-1.0 mm) (Douglas and French, 1986).

Therefore, it is obvious that maintaining a neutral plasma is crucial to ensuring the ion beam's electrical integrity as it travels over the interface area. If a secondary discharge occurs, it modifies the plasma's electrical properties, which will have a variable impact on the ions' kinetic energy depending on their mass. Ion energy spread is in the range of 5–10 eV if the plasma is at zero potential. However, the presence of a secondary discharge makes ion focusing considerably more difficult since it causes a significantly larger dispersion of ion energies to enter the mass spectrometer (usually 20–40 eV) (Douglas and French, 1986).

5 The ion focusing system

Despite being universally acknowledged as being better to all other atomic spectroscopy techniques, ICP-MS is most likely to be affected by the components of the sample's matrix. One ion out of every

million that are created in the plasma actually makes it to the detector, which is the fundamental issue on ICP-MS. The larger concentration of the matrix components than the analyte, which has the impact of defocusing the ions and changing the transmission properties of the ion beam, is one of the main causes of the low efficiency. When the matrix ions are heavier in mass than the analyte ions, a phenomenon known as the "space charge effect" may be more pronounced. The purpose of the ion focusing system is to reject as many matrix elements and species that are not analyte-based and to transfer as many analyte ions as feasible from the interface region to the mass separation device (Olivares and Houk, 1986).

5.1 Role of the ion optics

The position of the ion optics relative to the interface region is shown in Figure 6. The mass separation device and the skimmer cone are separated by the ion optics, which are made up of one or more electrostatically controlled lens components. They are made up of a number of metallic plates, barrels, or cylinders that have a voltage applied to them rather than the conventional optics that identified on ICP emission or atomic absorption. The ion optic system's purpose is to direct ions into the mass analyzer, which is operating in high vacuum, from the hostile environment of the plasma at atmospheric pressure using interface cones. The plasma discharge, interface region, and ion optics must all be constructed in collaboration with one another. It is crucial that the ion beam's composition and electrical integrity are preserved as it enters the ion optics. To ensure that the magnitude and spread of ion energies are as small as possible, it is crucial that the plasma be at zero potential (Douglas and French, 1986).

The ion optic system's secondary but equally crucial function is to block particles, neutral species, and photons from reaching the mass analyzer and the detector. These species contribute to background levels and signal instability, both of which have an impact on the system's performance. For instance, if photons or neutral species enter the detector, the background noise will increase, lowering the detector's capacity for detection. Additionally, if matrix particles enter the mass spectrometer zone further, they could deposit on lens components or, in rare circumstances, enter the mass analyzer. This will cause in short-term a signal instability and in long-term an increase in cleaning and periodic maintenance frequency.

There are essentially two methods that can be used to lessen the likelihood that these unwanted species enter the mass spectrometer. Putting a grounded metal disk behind the skimmer cone is the first technique. The particles, photons, and neutral species are physically prevented from moving downstream by this disk, which permits the ion beam to pass through it. The other strategy is to position the mass analyzer or ion lens just off axis. The photons, neutral, and nonionic species are expelled out of the ion beam, and the positively charged ions are subsequently guided by the lens system into the mass analyzer.

In order to electrostatically remove the ions from the interface region, certain lens systems contain an extraction lens following the skimmer cone. This benefits a more uniform response across the entire mass range of 0-300 amu by increasing the transmission and detection limits of the low-mass elements (which frequently get pushed out of the ion beam by the heavier elements). Some previous systems used lens components to speed the ions downstream in an effort to lessen the effects of space charge. Because of the substantially higher kinetic energy of the accelerated ions when they enter the mass analyzer, this can unfortunately have the effect of decreasing the instrument's resolving power and abundance sensitivity (Denoyer et al., 1995).

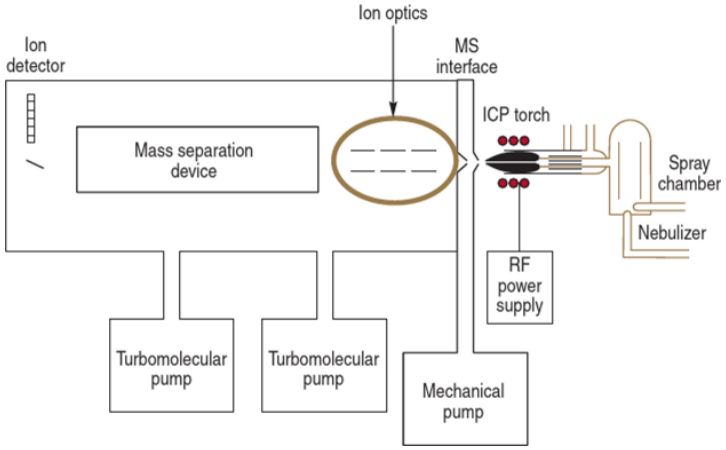

Figure 6. Position of the ion optics in an ICP-MS system.

5.2 Dynamics of ion flow

Understanding the kinetics of ion flow from the plasma via the interface region into the mass spectrometer is crucial to comprehending the function of the ion optics in ICP-MS. With a turbomolecular pump, the pressure in the lens chamber is decreased from 760 Torr (atmospheric pressure) to roughly 10^{-3} to 10^{-4} Torr when the ions produced in the plasma exit from the skimmer cone. This causes a rapid expansion of the ion beam. Because the expansion at this stage is governed by regular gas dynamics rather than electrodynamics, the composition of the ion beam immediately behind the cone is the same as the composition in front of the cone. The Debye length, or the distance over which ions exert effect on one another, is modest in the ion sampling process compared to the orifice diameter of the sampler or skimmer cone, which is one of the primary causes of this. As a result, there is not much electrical interaction between the individual ions in the beam or between the ion beam and the cone. This keeps the ion beam's compositional integrity intact across the interaction area. Electrons diffuse out of the ion beam as a result of this abrupt pressure reduction in the lens chamber. The electrons diffuse farther from the beam than the positively charged ions due to their smaller size in comparison to them, giving rise to an ion beam with a net positive charge (Tanner and Douglas, 1984).

The initial step in the charge separation process is the creation of a positively charged ion beam. Unfortunately, the ion beam's net positive charge has resulted in a natural inclination for the ions to reject one another. If nothing is done to make up for this, the center of the ion beam will be dominated by ions with a greater mass-to-charge ratio, pushing the lighter ions to the periphery. Ions with high kinetic energy (high mass elements) will be transported preferentially compared to those with medium (mid-mass elements) or low kinetic energy (low-mass elements), which will determine the extent of loss. By applying voltage to one or more ion lens components, the ions of interest are then electrostatically guided back into the center of the ion beam for the second stage of charge separation. But keep in mind that this is only possible if the interface is maintained at zero potential, which guarantees a neutral gas-dynamic flow over the interface and preserves the ion beam's compositional integrity. Additionally, it ensures that each ion entering the lens systems has an average and energy distribution that are optimal for mass separation. It will be highly challenging to optimize the ion lens system if the interface region is improperly grounded because stray capacitance would cause a

discharge between the plasma and sampler cone and raise the kinetic energy of the ion beam (Thomas, 2001).

5.3 Commercial ion optic designs

Ion optic designs have changed considerably over time. They all have unique traits, but they all serve the same basic purpose: separating out unwanted matrix- or solvent-based ions so that only the analyte ions are sent to the mass spectrometer. The most typical ion optics configuration in use today consists of a number of lens elements, each of which plays a particular part in the transmission of the analyte ions. To achieve the necessary ion specificity, the voltage can be tuned on each lens of the ion optics using these multicomponent lens systems. This particular lens arrangement has demonstrated to provide very low background levels and has a very long lifespan, especially when used in conjunction with an off-axis mass analyzer. However, the more complicated the lens system, the more variables need to be optimized, especially if many distinct sample types are being examined because of the interaction nature of parameters that affect the signal response. Since the lens voltages are completely computer-controlled and procedures may be recorded for each new sample setting, this is not a huge issue (Kishi, 1997).

With this arrangement, the analyzer's (usually a quadrupole) mass scan works in tandem with dynamically ramping voltage on-the-fly. The advantage of this method is that the optimal lens voltage is applied to each mass in a multielement run to let the most analyte ions through while minimizing the matrix ions. Each component has a unique optimal value that is used to calibrate the system and enable ramp scanning of the lens over the whole mass range. The mass analyzer and detector are often protected from particles, neutral species, and photons by using this kind of strategy in conjunction with a grounded stop. This design delivers great long-term stability despite producing slightly higher background levels. It works well for a variety of sample types, but it performs best when determining low mass elements while high mass matrix elements are present.

A few of ICP-MS systems include what is known as a high-sensitivity interface, which provides up to ten times the sensitivity of a conventional interface by combining a slightly altered cone geometry, a greater vacuum at the interface, one or more extraction lenses, and a slightly altered ion optic design (Brenner et al., 1998). However, especially for samples with a heavy matrix, this improved sensitivity is frequently accompanied by decreased stability and an increase in background levels. The systems' applicability for real-world samples is constrained by the necessity of diluting the samples prior to analysis to avoid this performance decrease. They have, however, been put to use in non-liquid-based applications where great sensitivity is essential, such as the examination of minute patches on the surface of a geological specimen using laser ablation ICP-MS. A single laser pulse is employed in this application to ablate the sample and sweep a minute quantity of the dry sample aerosol into the ICP-MS, hence the instrument needs to have high sensitivity (Howe et al., 2001).

6 The mass-analyzer

The ions of interest were predominantly separated using conventional quadrupole mass filter technology for the first ten years of inductively coupled plasma-mass spectroscopy's development (ICP-MS) before it was marketed in 1983. These performed remarkably well in the majority of applications, but they had drawbacks when trying to identify challenging elements or handle more complicated sample matrices. Because of this, alternative mass separation tools were created, pushing capabilities of ICP-MS and enabling it to be employed for more difficult applications.

A second turbomolecular pump is used to keep the mass analyzer, which is situated between the ion optics and the ion detector, as shown in Figure 7, at a vacuum of around 10^{-6} Torr. Assuming the ions are leaving the ion optics at the ideal kinetic energy, they are prepared to be separated by the mass analyzer based on their mass-to-charge ratio. In general, there are four different types of mass analyzers that are commercially available: quadrupole mass filters, double focusing magnetic sectors, time-of-flight, and collision-reaction cell technology. Each of them has particular advantages and disadvantages (Thomas, 2001).

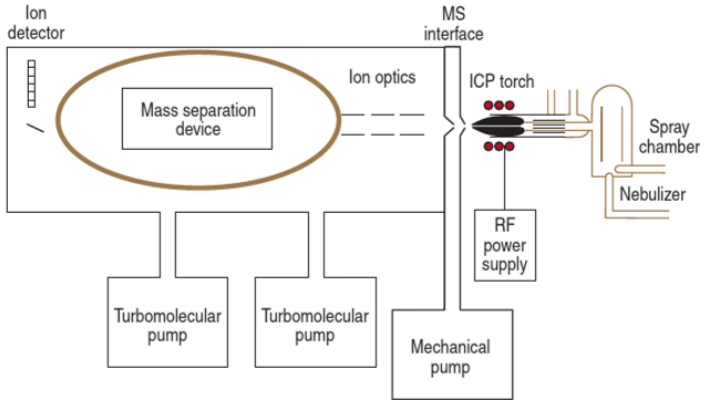

Figure 7. Position of the mass analyzer in an ICP-MS system.

6.1 Quadrupole mass filter technology

Quadrupole-based systems, which were created in the early 1980s, make up around 90% of all ICP mass spectrometers in use today. Due to the fact that this design was the first to be marketed, quadrupole ICP-MS technology is now regarded as a highly developed, common, high-throughput, trace-element technique. Four identically sized and shaped metallic cylindrical or hyperbolic rods make comprise a quadrupole. They are frequently made of molybdenum or stainless steel, and they may have a ceramic coating for corrosion resistance. ICP-MS quadrupoles typically have dimensions of 15-20 cm in length, 1 cm in diameter, and a frequency range of 2-3 MHz.

6.2 Basic principles of operation

Ions with a particular mass are permitted to pass through the rods and into the detector by applying a direct current (dc) field to one pair and a RF field to the other pair, while the others are ejected from the quadrupole.

In this streamlined illustration, the analyte ion and four additional ions have arrived at the entrance to the quadrupole's four rods. The positive or negative bias on the rods will electrostatically direct the target analyte ion along the middle of the four rods to the end, where it will emerge and be transformed into an electrical pulse by the detector when a specific RF-dc voltage is supplied to the rods. Other ions with various mass-to-charge ratios will go through the gaps between the rods and emerge out the quadrupole. After measuring all of the analytes in a multielement analysis, this scanning procedure is repeated for a different analyte with a completely different mass-to-charge ratio.

6.3 Quadrupole performance criteria

The ability of a mass analyzer to distinguish between an analyte peak and a spectral interference is controlled by two crucial performance requirements. The first is resolving power (R), which is represented by the following equation in conventional mass spectrometry: R is defined as R = m/Dm, where Dm is the mass difference between two resolved peaks and m is the nominal mass at which the peak appears (Adams et al., 1988). However, the term resolution is more frequently used in relation to quadrupole technology and is typically defined as the breadth of a peak at 10% of its height. The second specification is abundance sensitivity, which is the signal contribution from the tail of a peak that is next to the analyte peak but has a mass that is one mass lower and one mass higher than it (Montaser, 1998). While they both define a quadrupole's quality and are slightly connected, the abundance sensitivity is probably the most important. It is frequently impossible to measure an ultratrace analyte peak next to a significant interfering mass if a quadrupole has strong resolution but poor abundance sensitivity.

6.4 Resolution

The shape, diameter, and length of the rods, the frequency of the quadrupole power supply, the operating vacuum, the applied RF-dc voltages, and the motion and kinetic energy of the ions entering and exiting the quadrupole are some of the factors that affect a quadrupole's capacity to separate different masses. All of these elements will directly affect how stable the ions are as they move through the middle of the rods, which will affect the quadrupole's capacity to distinguish between ions with various mass-to-charge ratios. A quadrupole mass filter has a theoretical resolution range of 0.3 to 3.0 amu. However, increased resolution is invariably accompanied by a loss in sensitivity. (Dawson, 1995).

6.5 Abundance sensitivity

The quadrupole's abundance sensitivity, which is influenced by a number of variables including the rods' design, the power supply's frequency, and the operating vacuum, determines the overall peak form, especially its low mass and high mass tail. Even though they are all significant, the mobility and kinetic energy of the ions as they enter and exit the quadrupole are likely to have the greatest effects on abundance sensitivity. The stability boundaries of each mass are less clearly defined (not as sharp) on the low mass side as they are on the high mass side. Since the low mass boundary's ion motion characteristics differ from those at the high mass boundary, the low mass side's abundance sensitivity is lower than it is on the high mass side. Additionally, the ion motion will be influenced by the velocity (and consequently the kinetic energy) of the ions entering the quadrupole, which will directly affect the abundance sensitivity. Because of this, the instrument's sensitivity to abundance will be reduced by elements that influence the kinetic energy of the ions, such as high plasma potential and the employment of lens components to accelerate the ion beam (Denoyer et al., 1995).

6.6 Different quadrupole designs

ICP-MS employs a wide variety of quadrupole designs, all of which are constructed from distinct materials and have varying sizes, shapes, and physical properties. They all also run at various frequencies and are maintained at slightly variable vacuum chamber pressures. According to theory, hyperbolic rods should produce an elliptical hyperbolic field that is superior to cylindrical rods, resulting in stronger ion transmission at higher resolution. It also reveals that when the ions go down

the quadrupole, a higher operating frequency corresponds to a higher rate of oscillation and, consequently, separation. The fact that a higher vacuum results in fewer collisions between gas molecules and ions, a narrower spread in the kinetic energy of the ions, and consequently less of a tail at the low mass side of a peak, is also well acknowledged. Despite all these variances in specifications, the majority of contemporary quadrupole ICP-MS apparatus performs relatively similarly in practice.

7 Collision/Reaction cell technology

ICP-MS has identified a small subset of elements as having low detection limits. The majority of these elements are those that are severely affected by spectrum interferences brought on by ions from the plasma gas, matrix components, or the solvent-acid used to dissolve the sample. Some of such interferences are:

- $^{40}Ar^{16}O$ on the determination of ^{56}Fe
- ^{38}ArH on the determination of ^{39}K
- ^{40}Ar on the determination of ^{40}Ca
- $^{40}Ar^{40}Ar$ on the determination of ^{80}Se
- $^{40}Ar^{35}Cl$ on the determination of ^{75}As
- $^{40}Ar^{12}C$ on the determination of ^{52}Cr
- $^{35}Cl^{16}O$ on the determination of ^{51}V.

The cold/cool plasma approach, which uses a lower temperature to reduce the formation of the argon-based interferences, is a very effective way to get around some of these issues (Sakata and Kawabata, 1984); however, it can be time-consuming to switch between normal- and cool-plasma conditions, it is only suitable for a few interferences, and it is sometimes difficult to optimize. In the late 1990s, collision/reaction cells were developed in response to these performance constraints and a drive to enhance efficiency. They were employed in ICP-MS to prevent the emergence of numerous argon-based spectrum interferences. Originally developed for organic MS to generate daughter species to confirm identification of the parent molecule's structure (Thomson et al., 1995). A layout of a typical collision/reaction cell instrument is shown in Figure 8.

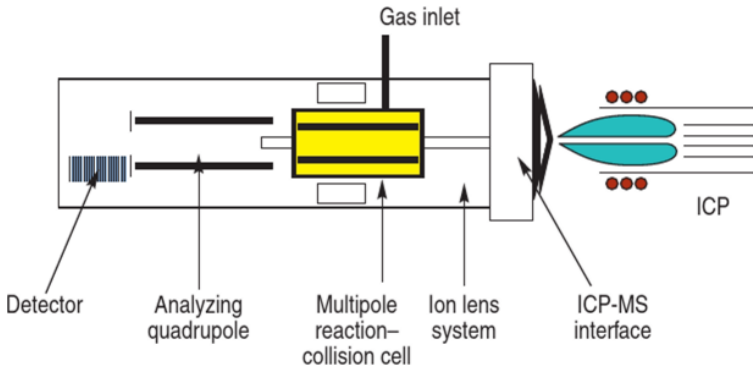

Figure 8. A layout of a typical collision/reaction cell instrument.

7.1 Basic principles of collision/reaction cells

With this method, ions entering the interface as usual, are extracted into a collision/reaction cell that is placed in front of the analyzer quadrupole while under vacuum. The cell, which comprises of a multipole (a quadrupole, hexapole, or octapole), is then bled with a collision/reaction gas like hydrogen or helium and is typically operated in the RF-only mode. The RF-only field instead has the effect of focusing the ions, which then collide and react with molecules of the collision/reaction gas, as opposed to separating the masses as a regular quadrupole would. Polyatomic interfering ions like ^{40}Ar, $^{40}Ar^{16}O$, and ^{38}ArH will either be transformed to harmless non-interfering species or the analyte will be converted to another ion which is not interfered with by a variety of different ion-molecule collision and reaction mechanisms. The reaction [1], which demonstrates the use of hydrogen gas to lessen the 38ArH polyatomic interference in the determination of ^{39}K, serves as an illustration of this. Although hydrogen gas does not react with potassium, it transforms ^{38}ArH into the innocuous H_3^+ ion and atomic argon. The ^{39}K analyte ions then leave the collision/reaction cell, interference-free, and are sent in the direction of the quadrupole analyzer for standard mass separation.

$^{38}ArH^+ + H_2 = H_3^+ + Ar$

$^{39}K^+ + H_2 = {}_{39}K^+ + H_2$ (no reaction) [1]

7.2 Different collision/reaction approaches

An extremely simplified illustration of a collision/reaction cell's operation is provided by the prior example. In reality, complicated secondary reactions and collisions occur, producing a large number of unwanted interfering species. These species might cause additional spectrum interferences if they are not eradicated or rejected. Discrimination by kinetic energy or discrimination by mass are essentially the two methods utilized to reject the byproducts of these undesirable interactions. The sorts of multipoles used and their fundamental interference rejection mechanisms are where the two approaches diverge most (Thomson et al., 1995).

8 Detectors

The position of an ion detector in an ICP-MS system is demonstrated in Figure 9. The most widely utilized ion detection systems since the invention of inductively coupled plasma-mass spectrometry (ICP-MS) in the early 1980s include electron multipliers for low ion-count rates and Faraday collectors for high ion-count rates. Modern ICP-MS systems for ultratrace analysis commonly employ detectors based on active film or discrete dynode electron multipliers. Compared to prior designs, these are extremely sophisticated pieces of machinery that transform ion currents into electrical impulses very well.

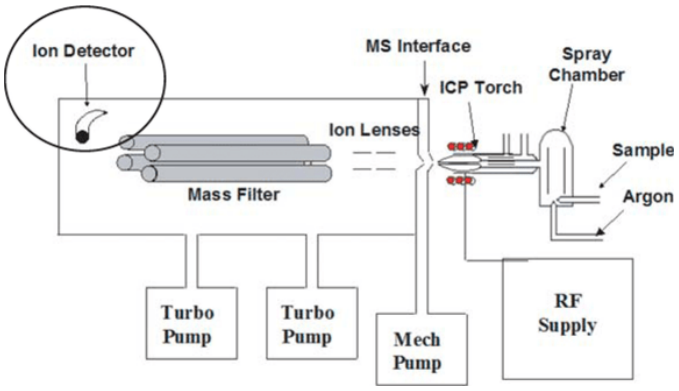

Figure 9. Position of the ion detector in an ICP-MS system.

Discrete dynodes are used in discrete dynode electron multipliers to multiply electrons (Hunter, 1994). In order to reduce the background radiation and neutral species coming from the ion source, the detector is typically positioned off-axis. An ion travels along a curved path after leaving the quadrupole before making contact with the first dynode. The first dynode is struck, releasing secondary electrons. These secondary electrons are accelerated to the following dynode, where they produce more electrons, thanks to the dynode's electron-optic architecture. At every dynode, this procedure is repeated, producing an electron pulse that is eventually collected by the multiplier collector or anode. The discrete dynode detector is often more sensitive than channeltron technology due to the materials used in it and the different ways that electrons are produced.

Even though the majority of discrete dynode detectors operate relatively similarly, there are slight variations in how the measuring circuitry manages low and high ion-count rates. When ICP-MS was first marketed, it had a maximum dynamic range of five orders. However, when attempts were made to increase the dynamic range, issues arose.

ICP-MS typically has a linear dynamic range of roughly five orders when employing the pulse counting technique. This indicates that, generally speaking, ICP-MS calibration curves are linear from ng/L levels to as high as a few hundred parts-per-billion. To work from sub-part-per-trillion levels to as much as 100 mg/L, there are a number of techniques to add another three to four orders of magnitude to the dynamic range of the ICP-MS.

Filtering the ion beam by applying a non-optimal voltage to one of the ion lens components or the quadrupole itself to reduce the amount of ions that reach the detector was one of the first methods used to increase the dynamic range in ICP-MS. The individual mass-based voltage offset served as an energy filter to electronically screen the ion beam and lower the succeeding ion signal to a level that could be detected by pulse-counting ion detection. The key drawback of this strategy was that the operator needed to be familiar with the sample beforehand in order to know what voltage to apply to the high concentration masses.

Another method was to utilize two separate detectors, such as a channel electron multiplier to monitor low current signals and a Faraday cup to measure high ion currents, in some of the early quadrupole ICP-MS instruments. Due to the quick switching between the two detectors, this method suffered with some applications but generally functioned okay. The issue was that choosing the best detector required physically deflecting the ion stream. In addition to lowering the measuring duty cycle, this resulted in detector switching and stabilization durations of several seconds, which made it unable to detect transient signals quickly.

The most contemporary method is to increase the dynamic range by using only one detector. High and low concentrations can be found in the same sample by employing the detector in the pulse-counting and analog modes. This type of detection method is used in three different approaches, two of which require two scans of the sample and the third only one.

The first method employs an electron multiplier that can function in digital and analog modes. The highest sensitivity is attained with digital counting, while analog operation (achieved by lowering the high voltage provided to the detector) reduces the detector's sensitivity and increases the concentration range over which ion signals can be measured. The system is put into practice by running each sample through the spectrometer twice. The detector's analog mode is used for the initial scan, which produces signals for elements with high concentrations. For elements present at low levels, a second scan with the detector voltage changed to digital-pulse counting mode offers high sensitivity detection. Because the system automatically scans all items in both modes, one important benefit of this technology is that users do not need to know in advance whether to employ analog or digital detection. Its drawback is that two separate mass scans must be performed in order to collect data over a wide signal range. Because mode switching is typically too sluggish, the system cannot be used for fast transient signal analysis of unknown samples in addition to resulting in decreased measurement efficiency and slower analyses (Montaser, 1998).

The first scan is used as an investigative tool to look at the sample spectrum before analysis. The second method of increasing the dynamic range is identical to the first method. The mass points at which the analog and pulse modes will be applied in order to later gather the spectral signal are established by this initial prescan. The technology shifts the detector rapidly between pulse and analog mode depending on the concentration of each analytical mass during the second analytical scan, which is subsequently employed for data collecting.

The fundamental drawback of these two methods is that measuring high and low levels necessitates two independent scans. This is not a huge issue with conventional nebulization, but it can slow down sample throughput. However, it does become an issue when dealing with transient peaks produced by flow injection, electrothermal vaporization, or laser sampling in ICP-MS. For the best detection limits, all the time that is available must be spent measuring the masses of interest because these transitory peaks frequently only last a few seconds. Two scans are required, which consume significant time and degrade the analytical signal quality (Hutton et al., 1990).

Due to the drawbacks of using two scans, a third strategy using a dual-stage discrete dynode detector was created. With the use of measurement circuitry, this technology can determine both high and low concentrations in a single scan. The ion signal is measured as an analog signal at the midpoint dynode to achieve this. The signal is processed through the analog circuitry when more ions are found than a threshold amount. Less than the required number of ions must be found for the signal to cascade down the remaining dynodes and be monitored as a pulse signal as is customary. This procedure is fully automatic and results in the simultaneous collection of both the analog and pulse signals in a single scan (Denoyer et al., 1997).

While analog circuitry is acceptable from 10^4 to 10^9 counts/s, the pulse-counting mode is typically linear from zero to roughly 10^6 counts/s. A cross calibration is done to cover concentration levels that could produce a pulse and an analog signal in order to normalize both ranges. This is achievable because, based on knowledge of the voltage at the first analog stage, the output current, and a conversion factor determined by the detecting circuitry electronics, the analog and pulse outputs may be specified in identical terms of incoming pulse counts per second. A dual-mode detector of this

kind may achieve about eight to nine orders of dynamic range in one simultaneous scan by carrying out a cross calibration throughout the mass range.

This kind of detection system comes in subtle variations, but its main advantage is that it only needs one scan to identify both high and low concentrations. This means that the most data may be gathered on a transitory signal that only lasts a few seconds, in addition to the possibility of improving sample throughput.

The PANORAMA programme and the ESR 13 project

1 An introduction to the PANORAMA programme

The goal of PANORAMA's research is to clarify how man-made environmental dispersion of rare earth elements (REEs) affects environmental health. To address the above-mentioned European and global challenges, the inter(multi)disciplinary training of a new generation of young researchers is essential, as the understanding of REE environmental behavior is becoming a hot topic regarding the opening of new mines, recycling plants, or medical and industrial use. In addition to supporting the strategy for achieving a competitive low-carbon economy by 2050, REEs offer access to cutting-edge low-carbon technology. With relation to China's mining practices, the European REE sector seeks to reduce the creation of REE footprints (e.g. The Norra Kärr REE Project). Beyond ensuring that supply chains adhere to ethical and environmental standards, however, there are still many unanswered questions regarding how REEs are dispersed in the environment.

In order to support Europe's efforts to develop an environmentally clean REE circular economy, PANORAMA aims to play this role by integrating 15 early stage researchers (ESRs) into an ambitious research and training program. This will enable them to contribute to the achievement of all scientific (and technical) objectives and to disseminate the results to the scientific community and relevant stakeholders.

2 The PANORAMA Work Packages

PANORAMA is organized into four scientifically based work packages (WP) that will be useful in providing ESRs with an integrated way of thinking in this new major scientific, environmental, and societal topic. These WPs include (geo)chemistry, hydrogeology, (eco)toxicology, and support with environmental decision-making and new original analytical devices (Figure 1).

To encourage cross-talk, the four research WPs will be operated simultaneously. Crucial data for speculating on bioavailability, bioaccumulation, transfer, etc., and for establishing experimental settings that may be evaluated and utilized in WP2 and WP3 will be provided by WP1, which is devoted to the speciation of REEs. The WP4 will employ all generated datasets and developed procedures to create models that forecast the environmental behavior of REE. Most ESRs will have connections to two or more scientific WPs. Along with the scientific WPs, WP5 and WP6 will ensure effective project management, open communication amongst the scientific WPs, ongoing progress monitoring, and adherence to the excellent planned training program. The requirements related to ethics will be covered in a WP7.

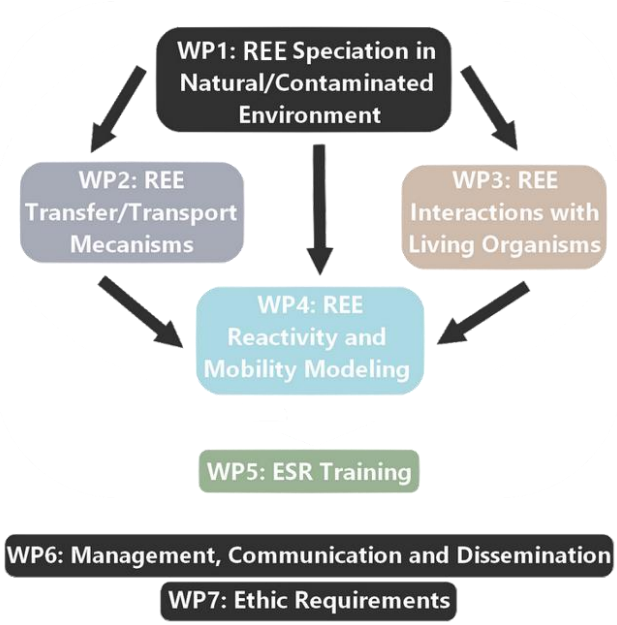

Figure 1. Inter-relationships of the work package of PANORAMA programme.

3 The ESR 13 project

The project of the Early Stage Researcher 13 (ESR 13) aims to investigate the REE content and related toxicity on both human and environmental health. For this reason, this project was constructed in three parts of investigation.

The first part concerns the REE related toxicity of REEs on human health. ESR 13 elaborated a litarture review concerning the toxicity of REEs on human health, validated two methods for preparing human urine samples before analysis by ICP-MS and determined the REE content in urine and scalp hair samples of car mechanics (see Chapter 2).

The second part concerns the ecotoxicity of REEs. Ecotoxicity trials were elaborated by preparing solutions that included specific nominal concentrations of REEs and were tested against several living organisms. The main work of ESR 13 on this part was to determine the real concentration, with respect to the nominal concentration, in such solutions that were collected either before the beginning of the trials or at specific times during the trials.

The third part concerns the environmental chemistry of REEs. ESR 13 elaborated a litarture review about the catalytic activity of REE in Advanced Oxidation Processes for the removal of pollutants from aquatic solutions. In addition, he collected environmental samples from three abandoned mining sites in the region of Puglia and determined the REE content in them.

Chapter 2: Human Toxicology of REEs

In this chapter, the contributions of the PhD project concerning the human toxicity of REEs are presented. Two of the three following subchapters are already published in *Frontiers in Environmental Science* (Brouziotis et al., 2022a, 2022b), while the third has been submitted for publication.

General introduction about chapter 2

It is anticipated that the widespread usage of REEs in numerous technologies, including occupational and environmental REE exposures, will have an effect on human health (Pagano et al., 2019; Rim, 2016). Since they are required in many industries, including agriculture and medical, as well as for the manufacturing of electrical gadgets, such as TVs, smartphones, electric cars, and wind turbines, REEs have become an essential component of our daily lives during the past few years (Pagano et al., 2015a; Pagano et al., 2019). The effects of REE exposures on human health have received considerably less research than experimental trials. A new line of research is necessary to address the potential environmental risks brought on by REE exposures (Pagano et al., 2015a).

Investigations on occupational exposures to noxious agents have been conducted in auto repair and maintenance facilities. Beyond those well-known by-products of hydrocarbon combustion, REEs may be also linked to engine exhaust and harmful health impacts. Cerium and lanthanum are two of these elements that are used in the production of diesel fuel as catalytic additives as well as oil refining processes (Cassee et al., 2011; Rim et al., 2013; Sajeevan et al., 2013; Pagano et al., 2019). Because there are numerous ways to be exposed to these elements, concern over whether they are safe for human health has grown (Brouziotis et al., 2022a).

The bioaccumulation of REEs in human urine matrices was the subject of several research. For the detection of REEs in urine matrices, a few novel techniques based on Inductively Coupled Plasma Mass Spectrometry (ICP-MS) have been developed. Even though numerous studies have looked at the amounts of REE in human matrices, there is still no defined standard method for testing these elements in human matrices. To guarantee the accuracy of the process and the traceability of the analytical data, the sample analysis should be of the highest caliber, and the methodologies should be thoroughly validated. Therefore, developing techniques for accurately detecting REEs in human matrices, such as urine, is crucial.

For all the above reasons, the first goal of the PhD project was to investigate the toxicity of REEs on human health, and determine their levels on human matrices. A literature review concerning the toxicity of REEs on human health was elaborated at first place, investigating the research gaps on this field and the exposome of REEs to human health. Subsequently, urine and scalp hair samples were collected from car repair workers with the aim to investigate the potentially augmented levels of REEs on the matrices of this type of workers due to the occupational exposure to the car exhausts. In addition, two methods for preparing human urine samples before analysis by ICP-MS were validated in the laboratory following a method validation protocol.

Toxicity of rare earth elements: An overview on human health impact

1 Introduction

The term rare earth elements (REEs) refers to a group of metals that consists of the 15 lanthanides [Lanthanum (La), Cerium (Ce), Praseodymium (Pr), Neodymium (Nd), Promethium (Pm), Samarium (Sm), Europium (Eu), Gadolinium (Gd), Terbium (Tb), Dysprosium (Dy), Holmium (Ho), Erbium (Er), Thulium (Tm), Ytterbium (Yb), and Lutetium (Lu)] generally along with Scandium (Sc) and Yttrium (Y)] (Wall, 2013). These metals have similar ionic radii and physicochemical properties and are sub-divided into three groups according to their atomic number and masses (Brown et al., 1990): La, Ce, Pr, Nd, and Pm are called light rare earth elements (LREEs); Sm, Eu, Gd, Tb, Dy, and Ho are called middle rare earth elements (MREEs); Er, Tm, Yb, and Lu are called heavy rare earth elements (HREEs).

China is the leader country in the production of REEs, having provided since recently more than approximately 90% of the global REE supply (Long, 2011). However, China's development in REE production has been decreased during the last years, resulting in production of only 60% of the global REE supply in 2021 (USGS, 2022). REEs are used in several technological applications since the manufacturing of many devices relies on their utilization (Du and Graedel, 2011, 2013; Pagano et al., 2019; US EPA, 2012), with the glass industry being the number one consumer of REE raw materials (Van Gosen et al., 2017).

Human exposures to REEs occur due to anthropogenic activity in many ways. Atmospheric particulates undergo an REE-enrichment by anthropogenic sources and are influenced by strong winds (Wang and Liang, 2014). Workers in recycling facilities are exposed to significant amounts of REEs through inhalation, ingestion, and skin contact (Shin et al., 2019). REEs can be transferred to the human body also through the food chain since they are used as feed additives to improve animal health and production without affecting their safety (Abdelnour et al., 2019; He et al., 2010, 2001), and in pesticides, herbicides, and fertilizers to improve crop yield and quality (Pang and Peng, 2002). However, unlike animals, an REE accumulation occurs not only in soil (Naccarato et al., 2020) but also in the roots and tops of plants (Xu et al., 2002). As a result, many concerns about human health due to REE exposure have been raised.

Some review papers have investigated the hazards of REEs to human health based on research of REE toxicity both to humans and generally to several biota (Cassee et al., 2011; Gwenzi et al., 2018; Hirano and Suzuki, 1996; Pagano et al., 2015b, 2015a; Rim, 2016). In a recent review paper, we investigated the environmental species sensitivity distribution of REEs and calculated the environmental hazard concentration of each REE for the 5% (HC5) and the 50% (HC50) of the species, including only research concerning acute toxicity and bioaccumulation of REEs to animals, plants and microorganisms (Albarano et al., 2022).

In the present review, we attempt to investigate the impacts of REEs on human health and find out the main knowledge gaps. Through this literature review, we wish to accomplish three critical issues: i) to gather all the studies that investigated REE toxicity to the human body; ii) to find out the gaps concerning the information about the exposure and toxicity of REEs directly to human health, and iii) to investigate the exposome of REEs directly to human health, i.e. to understand by which routes REEs can enter the human body, its tropism, and the level of toxicity they can exert.

2 Data collection and comparison

We used the following main keywords for searching activities: rare earth elements, human, toxicity, accumulation. The literature search was made up to 28th July 2022 using SCOPUS, PubMed and Google Scholar as the main search engines. We found 135 articles mainly about accumulation due to REE mining, risk assessment to human health, cytotoxicity to human cell lines. They were categorized into seven sections: environmental exposure, association of REEs with health problems, exposure to REEs due to daily habits, REE exposure through the food chain, Gd contrast agents causing health problems, occupational exposure to REEs, cytotoxicity studies of REEs. Table 1 is demonstrating a schematic summary of this review paper. The relative abundance (%) of papers for each section studied in response to REEs are shown in Figure 1.

Comparing the sections studied about REE toxicity, 37.8% of papers included cytotoxicity studies, followed by a 11.9% for environmental exposure, association of REEs with health problems and Gd-based contrast agents. The comparison among the analyzed biological matrices is shown in Figure 2. Hair was the most analyzed matrix (19%), followed by blood serum (16%) and blood (13%). Comparing the percentage of the articles considering the investigated REEs, Ce was present in 65.9% of the papers, La in 48.9%, Gd in 42.2%, while Nd in 37%. The complete data is shown in Figure 3. Comparing the different types of Ce for which we found information, more than half of them (52%) were reports in which Ce levels were traced in biological matrices, and studies about the cytotoxicity of CeO_2 nanoparticles (NPs) were 24%. Comparison of the relative abundance (%) of each type of Ce studied is shown in Figure 4.

Table 1. Schematic summary table demonstrating the different sections that each REE has been studied about at least once, and the relative abundance (%) of papers including information for the toxicity of each REE to human health.

Element	Sections studied	Articles percentage (%)
Sc	Environmental exposure, Food chain	2.2
Y	Environmental exposure, Health disorders, Lifestyle, Food chain, Occupational exposure, Cytotoxicity studies	24.4
La	Environmental exposure, Health disorders, Lifestyle, Food chain, Occupational exposure, Cytotoxicity studies	48.9
Ce	Environmental exposure, Health disorders, Lifestyle, Food chain, Occupational exposure, Cytotoxicity studies	65.9
Pr	Environmental exposure, Health disorders, Lifestyle, Food chain, Occupational exposure, Cytotoxicity studies	29.6
Nd	Environmental exposure, Health disorders, Lifestyle, Food chain, Occupational exposure, Cytotoxicity studies	37.0
Sm	Environmental exposure, Health disorders, Lifestyle, Food chain, Occupational exposure, Cytotoxicity studies	28.1
Eu	Environmental exposure, Health disorders, Lifestyle, Food chain, Occupational exposure, Cytotoxicity studies	31.1
Gd	Environmental exposure, Health disorders, Lifestyle, Food chain, Gd contrast agents, Occupational exposure, Cytotoxicity studies	42.2
Tb	Environmental exposure, Health disorders, Lifestyle, Food chain, Occupational exposure, Cytotoxicity studies	25.9
Dy	Environmental exposure, Health disorders, Lifestyle, Food chain, Occupational exposure, Cytotoxicity studies	25.2
Ho	Environmental exposure, Health disorders, Lifestyle, Food chain, Occupational exposure, Cytotoxicity studies	23.0
Er	Environmental exposure, Health disorders, Lifestyle, Food chain, Occupational exposure, Cytotoxicity studies	24.4
Tm	Environmental exposure, Health disorders, Lifestyle, Food chain, Occupational exposure, Cytotoxicity studies	23.0
Yb	Environmental exposure, Health disorders, Lifestyle, Food chain, Occupational exposure, Cytotoxicity studies	27.4
Lu	Environmental exposure, Health disorders, Lifestyle, Food chain, Occupational exposure, Cytotoxicity studies	26.7

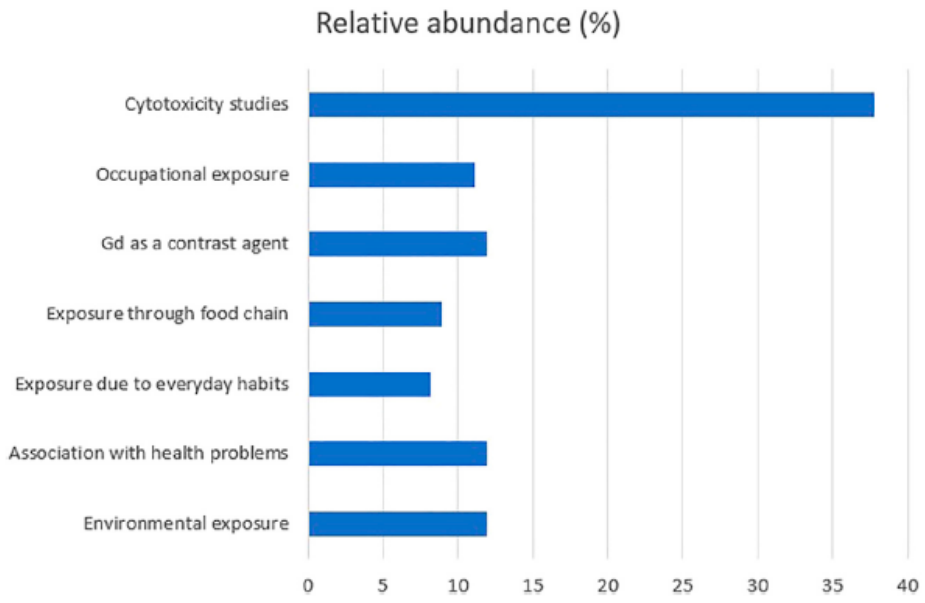

Figure 1. Comparison of the relative abundance (%) of papers for each section studied in response to REEs.

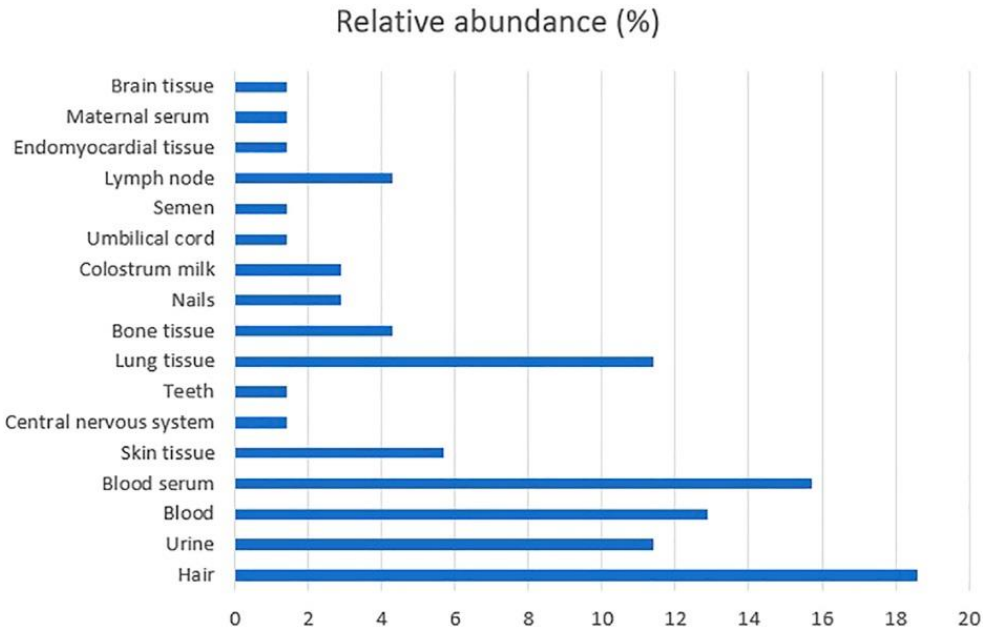

Figure 2. Comparison of number of available articles in which each biological matrices was analyzed for the toxicity of REEs.

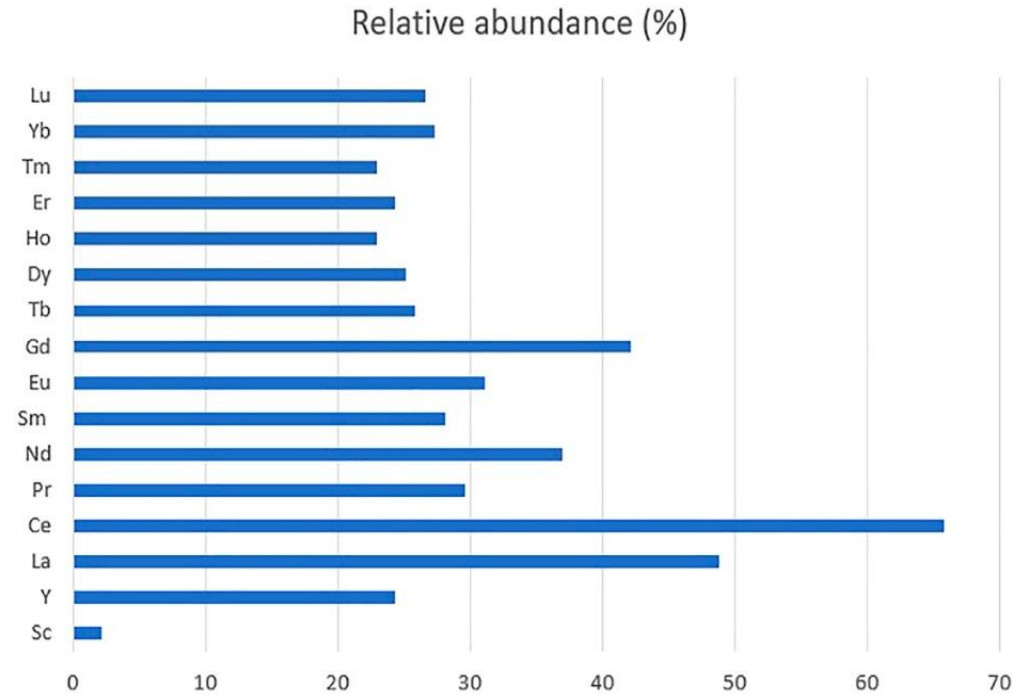

Figure 3. Comparison of the relative abundance (%) of papers including information for the toxicity of each REE to human health.

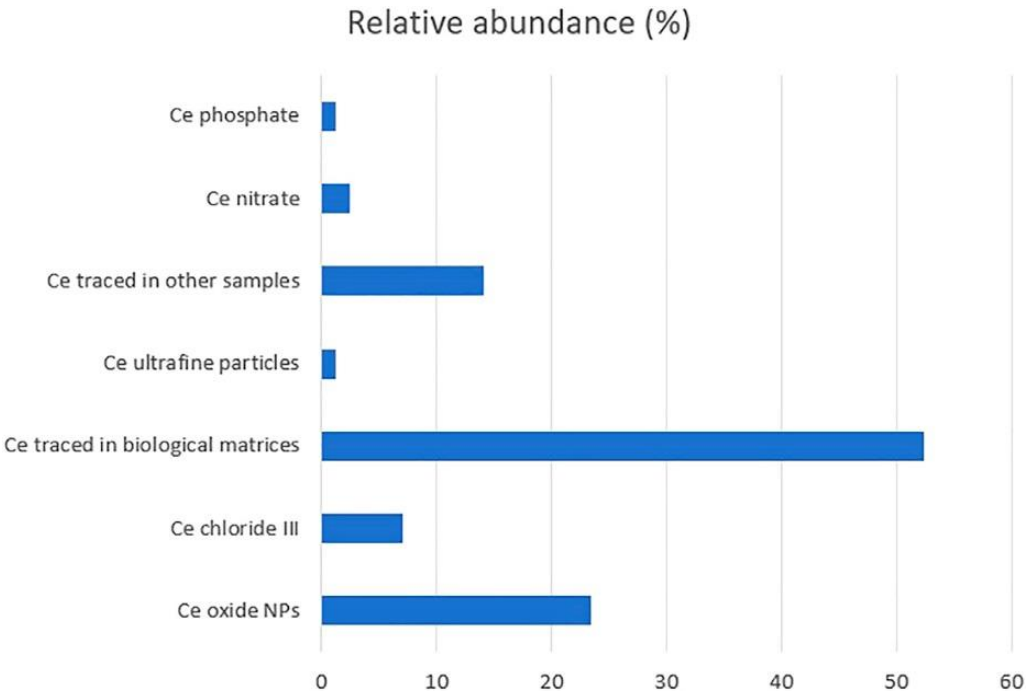

Figure 4. Comparison of the relative abundance (%) of each type of Ce studied about its toxicity to human health.

3 Environmental exposure

Some studies showed that REE mining affected the residents in the areas near the mining sites by analyzing the REE levels in human samples. Urine REE concentrations of people living near Baiyun Obo mining area were significantly higher than in residents outside the mining area (Hao et al., 2015; Liang et al., 2018). Other studies have investigated the REEpollution through analyses of hair

samples. In the study of Wei et al. (2013), scalp hair of people living near a mining site in Inner Mongolia contained significantly higher REE levels compared to people from the control area. In a similar study, the hair of children living in Shang and Liao villages, near a mining site, contained higher REE levels versus children from reference areas (Tong et al., 2004). As reported by Yu et al. (2007), REE blood levels were higher in people living near the mining site of Xunwu. They had some effects on the peripheral blood mononuclear cells, such as increasing telomerase activity, promoting the diploid DNA replication, and increasing the percentage of cells in the S-phase and the G_2/M phase. The blood and hair of people living near a large-scale mining site in southwest Fujian Province, China, were found enriched with REEs but much more with LREEs (Li et al., 2014). A correlation between the concentration of REEs in soil and human samples was found in Hezhang County, China, where REEs levels (mostly La, Ce, and Nd) in the soil near a smelting area were higher than those in the soil near a mining area, and the same applied for urine and hair of residents near these two areas (Meryem et al., 2016). Tian et al. (2019) found an enrichment of Ce in dust from mining areas and the potential of causing health problems through inhalation. According to the Life Cycle Assessment of Wang C. et al. (2020), the most significant impact of Sc_2O_3 production from Bayan Obo mine is the non-cancerous human toxicity. All these studies indicated that the REE mining process influenced the environment in mining areas and the people living nearby.

However, REEs environmental exposure can occur, not only due to REE mining but also to other factors. Ugandan children presented significantly higher REE concentrations in their primary teeth than the children from the United Kingdom (Brown et al., 2004) due to an environmental exposure. The levels of REEs were significantly higher in the blood of Moroccans than in Canarians, possibly related to the improper management of e-waste (Henríquez-Hernández et al., 2018). Lanthanum and Ce levels were higher in resident serum from an e-waste area and were associated with higher thyroid-stimulating hormone (TSH) (Guo et al., 2020). Hollriegl et al. (2010) associated the increased Ce levels in the serum of women in Madrid with the high traffic volume in this town. The accumulated concentration of REEs in the rib bone tissue was found to be age dependent by Zaichick et al. (2011). Street dust in industrial cities is enriched with REEs mainly due to heavy local soil and less due to anthropogenic pollution, however, the existing REE levels were not found as a threat to cancer occurrence (Sun et al., 2017). Analysis of soil samples from a tropical area and a subsequent health risk assessment from Ferreira et al. (2022) showed that REEs represent less than 20% of the metal content and the risk for cancer due to these metals is very low.

4 Rare earth elements-associated health disorders

Some studies have investigated the association between REEs and specific diseases, with different results. Brown et al. (2004) concluded that the higher Ce concentration in primary teeth of Ugandan children, compared to children from the United Kingdom, failed to be associated with endomyocardial fibrosis. Huo et al. (2017) suggested that although LREEs are higher in the hair of women with neural tube defects (NTDs) affected pregnancies, they are not associated with the risk of NTDs, even if Wei et al. (2020) found that the REEs levels were higher in the maternal serum of pregnant women affected by NTDs and that the risk for NTDs increases with REE concentrations, especially La. Henríquez-Hernández et al. (2017) have pointed out the possibility of REEs playing a role in the development of anemia since they were found to be higher in the blood of sub-Saharan immigrants with anemia and independent of Fe levels. De Vathaire et al. (1998) identified an excess of mortality due to lung and bladder cancer in a French population living near a site where Ce was extracted. Similarly, Kutty et al. (1996) found that deposits of monazite elements, like Ce, increase

the rate of occurrence of endomyocardial fibrosis (EMF). In utero exposure to REEs, mainly La and Nd, increase the risk of orofacial clefts to infants (L. Liu et al., 2021). Exposure of pregnant women to Ce and Yb has decreased TSH levels in infants (Y. Liu et al., 2019). REEs may accumulate in the cerebral cortex by long-term environmental intake of a small amount and cause subclinical damage (Zhu et al., 1997). REEs, especially La, Ce, and Gd, are significantly higher in brain-tumor tissues of patients with astrocytoma compared to normal brain tissues (Zhuang et al., 1996). People living near high-REE background areas have illnesses like indigestion, diarrhea, abdominal distension, anorexia, weakness, and fatigue. They have been shown to have lower levels of total protein, globulin, albumin, and serum-glutamic pyruvic transaminase (SGPT) and higher levels of IgM in their blood serum (Zhu et al., 2005). A high amount of REEs in hair has been associated with low levels of Ca in hair and a high risk of hypertension among housewives (B. Wang et al., 2017). Lanthanum levels in the serum of women undergoing in vitro fertilization-embryo transfer have been associated with a 30% increase in clinical pregnancy failure, a 230% increase in preclinical spontaneous abortion, and a negative correlation with the number of good-quality oocytes (Li et al., 2021). Cerium levels in toenails have been associated with an increased risk of acute myocardial infarction (Gómez-Aracena et al., 2006). In the study of Medina-Estévez et al. (2020), Ce levels were higher in control people group than in the subjects, and so, inversely associated with the risk of stroke. Increased REEs in the hair of housewives have been correlated with indoor air pollution and the risk of hypertension by Wang et al. (2018).

5 Rare earth elements exposure as related to lifestyle

Everyday habits can also affect the concentration of metals, including REEs, in the human body. Marzec-Wroblewska et al. (2015) found that the concentrations of La, Ce, Eu, and Gd were significantly lower in the non-drinkers' and short-term smokers' semen than in the semen from drinkers and long-term smokers. Moreover, Zhang et al. (2020) evidenced that smoking was positively associated with Dy, Er, and Yb levels, whereas drinking habits showed no significant effect on REE levels, while La, Ce, Pr, and Nd were higher in hair and nails of smokers (Rodushkin and Axelsson, 2000). Poniedziałek et al. (2017) found that Nd concentration was significantly higher in the colostrum milk of smoking women compared to those who had never smoked. Zhang et al. (2020) confirmed also that REE levels are higher in biological matrices of smokers, but not in drinkers. Housewives exposed to REEs due to passive smoking presented elevated levels of REEs in their hair according to Na et al. (2022).

The rolling paper, especially a flavored paper, is the part of the cigarette that contains the highest amount of hazardous metals, including REEs, while black tobacco contains more REEs compared to the other tobacco types, and so, smokers are exposed to REEs mainly due to the rolling paper, as well as to the tobacco (Zumbado et al., 2019). LREEs are contained in the flint of lighters, and even short-term contact with the flint during the light-up could result in exposure to LREEs (Kastury et al., 2020; Rodushkin and Axelsson, 2000).

Tobacco smoking has been rated as one of the most significant sources of REEs in indoor inhalable particles. Cerium and La levels significantly increased in the households of smokers and hospitality pubs like restaurants, pubs, dance clubs, offices, and cafeterias due to tobacco smoke, and imply a threat to the human respiratory system (Böhlandt et al., 2012; Slezakova et al., 2009). Increased indoor Ce and La have also been associated with indoor smoking and respiratory symptoms in children (Drago et al., 2018). Although REEs in PM10 are higher in smokers' households, their

dissolution in PM10 and inhalation bioaccessibility are higher in non-smokers' households (Kastury et al., 2020).

E-cigarettes can be considered also as a source of an increased REE intake. Badea et al. (2018) found that REE levels are higher in serum of e-cigarette users than cigarette users, and the longer someone uses e-cigarettes, the higher the levels of Ce and Er in their blood serum. Ytterbium levels were found higher in teeth of people wearing porcelain bridges, and so the latter can be considered as well as another potential source of REEs intake (Rodushkin and Axelsson, 2000).

6 Rare earth elements exposure through the food chain

REEs can be transferred in the human body also via the food chain. In the study by Zhang et al. (2020), centenarians who consumed smoked and pickled food, egg, milk, and high amounts of salt had higher REE levels in their hair. REE oxides (LREOs) in Oolong tea consider a negligible threat for human health as its consumption does not exceed the accepted daily intake (ADI) of REE levels (Guo et al., 2015). Cereals, especially wheat, and vegetables, especially leaf vegetables, bioaccumulate significantly high amounts of LREEs when growing near mining areas; however, these concentrations are much lower than the ADI (Zhuang et al., 2017b, 2017a). Jiang et al. (2012) investigated the REE levels in the most consumed foods in China and concluded that REEs are at a shallow concentration and do not exert a hazard for human health. Freshwater and marine fish in Shandong Province, the largest center for fishery production and processing in China, contain a much higher amount of LREEs versus HREEs; however, the estimated daily intake (EDI) of REEs through fish food were significantly lower than the ADI; therefore, its consumption presented little risk to human health (Yang et al., 2016). The health risk assessment of Li et al. (2013) concluded that vegetable consumption would not exceed the EDI values for REEs. The same applies for the health risk assessment of Shi et al. (2022) concerning fruit and vegetable consumption. REE levels are higher in the aquatic than the terrestrial food, get lower at higher trophic levels in the environment and their human intake at present is acceptable (Dai et al., 2022). To the best of our knowledge, the studies, up to now, about the REEs level in food showed that they are present in low concentrations and can hardly exert problems in human health. Squadrone et al. (2019) analyzed REEs level in several terrestrial and marine matrices and organisms. Although the highest REE levels were found at low trophic levels in both environments, they suggested a biomonitoring of these elements for possible cumulative effects to human health, since they can be transferred to human body through the trophic chain.

Zhang et al. (2000) indicated that exposure to REEs through the food chain could result in low total serum protein (TSP), albumin, β-globulin, glutamic pyruvic transaminase, serum triglycerides, and immunoglobulin, but high cholesterol. Cerium concentration was found higher in endomyocardial samples of people dying from endomyocardial fibrosis and has been associated with the Ce levels in leafy vegetables and root tubers like tapioca and yam (Valiathan et al., 1986).

7 Gd contrast agents are causing health problems

Gadolinium-based contrast agents (GBCAs) have been used for years in magnetic resonance imaging (MRI) and magnetic resonance angiography (MRA). In the first research about the safety of these agents to human health, no side effects were caused to patients. Carr et al. (1984) found that a small intravenous administration of Gd-diethylenetriamine pentaacetic acid (Gd-DTPA) could enhance the contrast of tumors during an MRI operation, causing no side effects to patients. However, subsequent

studies reported that these agents are not completely safe for human health. GBCAs can cause acute renal failure in patients with underlying chronic renal insufficiency (Sam et al., 2003). Chien et al. (2011) found out that potential acute kidney injury is after administration of a GBCA, under sepsis condition, at the dose given for MRI and MRA examinations in patients with renal impairment. Ergun et al. (2006) reported that an acute renal failure (ARF) can occur after a GBCA administration in patients with moderate to severe chronic renal failure. Risk factors for ARF after Gd toxicity include diabetic nephropathy and low glomerular filtration rate (GFR). Similarly, Thomsen (2004) reported that GBCAs can induce nephropathy even at doses below 0.2 mmol/kg body weight (a usual dose of GBCA for MRI) in patients with multiple risk factors. Gd-DTPA could play a role in developing nephrogenic fibrosing dermopathy (NFD) in renal disease patients undergoing MRA (Grobner, 2006). There is a high risk of nephrogenic systemic fibrosis in patients with chronic kidney disease at stage 5 due to exposure to gadodiamide during MRI (Rydahl et al., 2008). Gadolinium remained in human bone tissue after administration of a standard clinical dose (0.1 mmol/kg) of Omniscan or Prohance a few days before surgery to patients undergoing hip replacement (Gibby et al., 2004; White et al., 2006). GBCAs can induce central torso and peripheral arm and leg distribution pain in patients (Semelka et al., 2016). Gadovist, a GBCA was reported to cause fibromyalgia in one patient following repeated administrations (Lattanzio and Imbesi, 2020).

A few studies have investigated the potential toxicity of GBCAs to human health by a number of cytotoxicological experiments. Four GBCAs, Gadovist, Magnevist, Multihance, and Omniscan, were not toxic to the embryonic fetal lung fibroblast cell line Hel-299, which rapidly recovered after the initial antiproliferative effects of the agents (Wiesinger et al., 2010). Omniscan increased the proliferation and the levels of the matrix metalloproteinase-1 (MMP-1) and the inhibitor of metalloproteinases-1 (TIMP-1) to monolayer culture of human dermal fibroblasts and to organ culture of human dermal skin, but they did not stimulate the proliferation of epidermal keratinocytes (Bhagavathula et al., 2009; Varani et al., 2009). Magnevist, Multihance, and Prohance (i.e., another GBCAs) increased the proliferation and levels of MMP-1 and TIMP-1 in human dermal fibroblasts like Omniscan did (Varani et al., 2009). Edward et al. (2010) examined the effect of several GBCAs on human skin fibroblasts. Some of them stimulated cell proliferation and hyaluronan production, while no GBCA could affect collagen synthesis. Omniscan increased MMP-1 and TIMP-1 in a human skin organ culture, but reduced the collagenolytic activity (Perone et al., 2010). Gadolinium chloride had similar effects with the GBCAs, having no effect on epidermal keratinocytes, enhancing the proliferation and the levels of MMP-1 and TIMP-1, and having no effect on type I procollagen in fibroblasts via activation of the PDGF receptor signaling pathway (Bhagavathula et al., 2010).

8 Occupational exposure to rare earth elements

The content of REEs in the hair of miners, particularly light REEs (La, Ce, Pr, and Nd), was much higher than the values in the hair of non-miners from both mining area and control area (Wei et al., 2013). Liu et al. (2015) found higher REE hair levels in miners working at the Baiyun Obo mining area (China), affecting the levels of proteins in serum that participate in various biological processes. Increased La levels were also found in the lung tissue of deceased smelter workers (Gerhardsson and Nordberg, 1993). Elevated REE levels were found in the hair of miners, which were associated with Fe and Ca in hair and a lower bone mineral density at lumbar vertebrae, femoral neck, greater trochanter, and intertrochanter (H. Liu et al., 2021). These studies suggested that the miners can be exposed to increased REE levels in their occupational environment.

Rare earth pneumoconiosis is an uncommon occupational disease caused by the inhalation of REE-containing dust and has been associated with dendriform pulmonary ossification (Yoon, 2005). Some early studies showed that workers active in movie projection were exposed to REEs, produced in the fumes and dust of arc carbon lamps that contained a significant REEs amount. A movie projectionist who had approximately 25 years of occupational exposure to carbon arc lamp fumes was found to be exposed to La, Ce, and Nd, with evidence of their redistribution throughout the reticuloendothelial system. However, the exposed did not suffer from pneumoconiosis, as there were no respiratory symptoms or radiographic or histological pulmonary changes attributable to a progressive REEs accumulation (Waring and Watling, 1990). Porru et al. (2001) investigated another movie projectionist exposed for 12 years to REE-containing dust from cored arc light carbon electrodes. The exposed presented interstitial lung disease, emphysema, and a severe obstructive impairment with a marked decrease of carbon monoxide diffusion capacity. The biopsy confirmed the diffuse interstitial lung fibrosis and significantly higher concentrations of Ce, La, Nd, Sm, Tb, and Yb compared to the unexposed control subjects. Three other cases of photoengravers, exposed for many years to the fumes and dust from carbon arc lamps, suffered from pneumoconiosis and the clinical analyses showed evident high REEs concentration in the pulmonary and lymph node biopsies, suggesting a relationship between the pneumoconiosis and the occupational exposure to REE dusts, and the need to define air exposure threshold limit values of REEs to prevent workers' occupational exposure (Sabbioni et al., 1982; Vocaturo et al., 1983).

Rare earth elements are biopersistent and can remain in the human body many years after occupational exposure (Pairon et al., 1995, 1994). High Ce, La, and Nd levels were found in the lung tissue of a subject having worked in printing shops and exposed to carbon-arc lamp emissions (Dufresne et al., 1994). REE dust exposure in a lens grinder was reported by Yoon et al. (2005), who found pneumoconiosis associated with dendriform pulmonary ossification. The urines of workers producing ultrafine and nano-sized particles containing Ce and La oxide; especially those at separation and packaging locations presented greater levels of La and Ce (Y. Li et al., 2017). In the study by Li et al. (2016), the REE levels in the urine of workers that manufacture cerium and lanthanum oxide ultrafine and nano-sized particles were more than five times higher versus controls. Their results, however, suggested that only the urinary levels of La, Ce, Nd, and Gd among the exposed workers were significantly higher than the levels measured in the control subjects. High REE levels in the blood have been associated with significant DNA oxidative damage and high blood concentration of Cr in chromate exposed workers (Bai et al., 2019). The urines and blood of e-waste recyclers contain more Eu, but for La, this applies only for urines (Takyi et al., 2021). An uptake of REEs has been found in triple negative breast cancer cells of a woman having worked in the ceramic industry (Roncati et al., 2018).

9 Cytotoxicity of rare earth elements

Nanoparticles (NPs) of Ce can significantly mitigate reactive oxygen species (ROS) production and DNA oxidative damage in the BEAS-2B cell line (Rubio et al., 2016). The co-exposure of CeO_2 NPs and diesel exhaust on a sophisticated in vitro 3D co-culture model of the human epithelial airway barrier indicates that a short-term co-exposure filed to result in adverse effects, long-term co-exposure caused undesired effects to human respiratory health (Steiner et al., 2012). CeO_2 NPs induced mitochondrial damage and overexpression of apoptosis to human peripheral blood monocytes ($CD14^+$) (Hussain et al., 2012) and human lung adenocarcinoma (A549) (Mittal and Pandey, 2014). CeO_2 NPs protected human colon cells (CRL 1541) from radiation by reducing ROS production and

increasing the expression of superoxide dismutase 2 (SOD2) (Colon et al., 2010). CeO_2 NPs enhanced the antitumor effect of anthracycline doxorubicin, one of the most effective anti-cancer drugs, in human melanoma cells (A375), and even protected human dermal fibroblasts from doxorubicin-induced cytotoxicity (Sack et al., 2014). Nanoparticles of CeO_2 did not cause any cytotoxicity to human hepatic carcinoma cell line (HepG2) and human lung carcinoma cell line (A549) during a short-term exposure (24 h) but only during a long-term period (10 days); moreover, they did not cause any cytotoxicity to cells from human colon carcinoma (CaCo2) at any of the investigated times (De Marzi et al., 2013).

Diesel particulate matter containing CeO_2 and $Fe(C_5H_5)_2$ NPs decrease the viability of human-type II cell alveolar epithelial cells (A549) (Zhang and Balasubramanian, 2017). Nanoparticles of CeO_2 enhanced the proliferation of human keratinocytes and human microvascular endothelial cells (Chigurupati et al., 2013). Nanoparticles of CeO_2 were not found to be genotoxic to eye lens epithelial cells (ATCC-LGC CRL-11421), suggesting a potential safe use in drug delivery for treating cataract (Pierscionek et al., 2010). They were not toxic to the cell lines T98G (from a human glioblastoma multiform tumor) but caused cell death to BEAS-2B cell line (Park et al., 2008) and human bronchoalveolar carcinoma derived cell line (A549) (Lin et al., 2006) by an apoptotic process, mainly by increasing the levels of ROS and decreasing the levels of GSH and α-tocopherol. In the study of Alpaslan et al. (2015), the dextran-coated nanoceria killed much more effectively the osteosarcoma cell line MG-63 (ATCC CRL-1427) than the osteoblast noncancerous cell line (PromoCell, C-12720), suggesting that nanoceria can promisingly be used for treating bone cancer without the appearance of adverse effects to healthy bone cells. CeO_2 NPs showed a rapid uptake from human keratinocyte cells (HaCaT) and co-localized with mitochondria, lysosomes, endoplasmic reticulum, cytoplasm, and nucleus, suggesting that they act as cellular antioxidants in multiple compartments (Singh et al., 2010). CeO_2 NPs are taken up into caveolin-1 endosomal compartments by BEAS-2B cells without causing inflammation or cytotoxicity (Xia et al., 2008). Tarnuzzer et al. (2005) showed that CeO_2 NPs could protect almost 100% of the normal breast epithelial cell line CRL8798 and simultaneously did not protect the breast carcinoma cell line MCF-7. According to the study by Celardo et al. (2011), in two tumor cell lines, the human tumor monocytes U937 and the human tumor T lymphocytes Jurkat, the intracellular antioxidant effect of CeO_2 NPs is due to their anti-apoptotic and prosurvival activity. They also found that doping of CeO_2 NPs with increasing concentrations of Sm^{3+} blunted these effects by decreasing Ce^{3+} and not affecting oxygen vacancies, demonstrating that Ce^{3+}/Ce^{4+} redox reactions might be responsible for the biological properties of nanoceria.

In Yongxing et al. (2000), La and Gd were indicated as possible mutagenic factors for human primary peripheral lymphocytes. The compounds $LaCl_3$ and $CeCl_3$ inhibited the growth of the leukemic cell lines HL-60 and NB4, respectively, and simultaneously $LaCl_3$ had no inhibitory effect on normal bone marrow hematopoietic progenitor cells (Dai et al., 2002). Lanthanum and Ce nitrates decrease the proliferation of the human osteoblast MG63 cell line when combined with radiation but not alone (Da F. Iwahara et al., 2019). Lanthanum oxyiodide nanosheets with low dose of doxorubicin, an anticancer drug, can kill more effectively the A375 cells compared to the doxorubicin alone (Xu et al., 2020). Nd_2O_3 and La_2O_3 NPs are cytotoxic, while Gd_2O_3 and CeO_2-Gd NPs enhance ROS production to the U-87 MG tumor cell line (Lu et al., 2019). Lanthanum is cytotoxic through the necrosis pathway and genotoxic by increasing ROS production in Jurkat cells and human peripheral lymphocytes (Paiva et al., 2009). The ionic forms La^{3+} and Tb^{3+} caused disruptions on potassium channels on the plasma membrane of HEK293 cells (L. Wang et al., 2017). Lanthanides can decrease the ATP production and the cell viability of the HepG2 cells, and also can decrease the mitochondrial membrane potential most probably by interfering with the calcium regulation due to the similar ionic

radius (Kajjumba et al., 2021). In the report by Feyerabend et al. (2010), lanthanides are cytotoxic against the human osteosarcoma cell line MG63, but not to the human umbilical cord perivascular (HUCPV) cells, with some of them increasing the levels of the inflammatory factors TNF-α and IL-1a. Lanthanides did not stimulate the growth of HaCaT cells (keratinocytes), while in human dermal fibroblasts they enhanced the proliferation and the production of matrix metalloproteinase-1 (MMP-1) and did not influence the production of type I procollagen (Jenkins et al., 2011). The "Raman fingerprints" of human sperm DNA exposed to CeCl3 demonstrated that Ce can cause DNA damage through oxidative damage and destruction of the antioxidant defense systems of sperm and even lead to damage or death (Chen et al., 2015). This implies that excess REEs exposure may be a risk factor for human infertility. A cytotoxicity study of CeO_2 NPs in six cancers and two normal cell lines was elaborated by Pešic et al. (2015). Only two cancer cell lines were sensitive to CeO_2 NPs, melanoma 518A2 and colorectal adenocarcinoma HT-29, showing a median inhibitory concentration (IC_{50}) of 125 μM and 183 μM, respectively. In this study, human cells also resulted in lower ROS production and higher antioxidant capacity, implying that normal cells are more resistant to CeO_2 NPs versus cancer cells. Ultrafine particles of Y_2O_3 were not cytotoxic against human aortic endothelial cells and resulted in an inflammatory response by increasing the concentration of IL-8, ICAM-1, and MCP-1 (Gojova et al., 2007), but CeO_2 ultrafine particles failed to cause any inflammation on the same cell lines (Gojova et al., 2009). Lanthanum and Ce, alone or in combination, inhibited cell proliferation and altered genes involved in oxidative stress pathways in HepG2 and HT-29 cell lines (Benedetto et al., 2018). Particles enriched with REEs, collected from an REE mining area, showed no cytotoxicity to lung epithelial A549 cells; however, they increased ROS production (Tian et al., 2020). Erbium-laser photoablation was found to cure oligoasthenozoospermia and enhance fertilization (Antinori et al., 1994). Europium selenide nanoparticles synthesized in vivo by recombinant Escherichia coli cells were cytotoxic to the cancer cell lines 293T, HeLa and SKOV-3, and thus could be promising drug carrying agents against cancers (Kim et al., 2016). An Eu complex bearing 8-hydroxyquinoline-N-oxide and 1,10-phenanthroline ligands exhibits low toxicity to normal HL-7702 cells, but high antiproliferative activity against cisplatin-resistant A549/DDP cells by upregulating the expression of LC3 and Beclin1 and downregulating p62 to induce apoptosis which is related to its cell autophagy-inducing properties (Yang et al., 2021). Neodymium-iron-boron magnets are cytotoxic against human oral mucosal fibroblasts (Donohue et al., 1995). Although not causing cell death, the powder of $Nd_2Fe_{14}B$ magnet can cause a dose-dependent ROS production to A549 cells (Rumbo et al., 2021). Gadolinium oxide nanoparticles were found cytotoxic to human umbilical vein endothelial cells, inducing lipid peroxidation, ROS production, mitochondrial dysfunction and autophagic modulation through apoptosis and necrosis (Akhtar et al., 2020). Nanoparticles of Y_2O_3 induced apoptosis and necrosis to human embryonic kidney (HEK293) cells, by elevating the cellular ROS levels, increasing the mitochondrial membrane permeability, and causing DNA damage (Selvaraj et al., 2014). Yttrium aluminum borates nanoparticles are cytotoxic to human bronchial epithelial cells (Cieślik et al., 2019). The study by Perry et al. (2020) was the first to provide in vitro data on the efficacy of radiation therapy with Tm nanoparticles for the management of metastatic cutaneous squamous cell carcinoma (cSCC). REE salts are not skin sensitizers and do not exhibit endocrine disruption to epidermal keratinocytes (Rucki et al., 2021). The chlorides of Ce, La, Eu and Yb are cytotoxic against the embryonal kidney HEK-293 cells (Heller et al., 2019). La citrate induces anoikis (a type of programmed cell death) in HeLa cells by reorganizing actin cytoskeleton and increasing the co-localization of F-actin with mitochondria (Su et al., 2009). La citrate is also cytotoxic against SiHa cells causing a mitochondrial dysfunction that induces apoptosis (Shen et al., 2010). $EuCl_2$ and $EuCl_3$ reduced the viability of the human monocyte (U937) and primary human mononuclear cells (PBMNCs) (Bladen et al., 2013). In the study of L. Wang et al. (2020) a REE-doped up conversion

nanoparticle (UCNP), sodium yttrium fluoride NP, doped with Yb and Er ($NaYF_4$: Yb^{3+}, Er^{3+}), induced cytotoxicity to HepG2 cells after their internalization by promoting ROS generation, and the induced apoptosis was related to the mitochondria mediated pathway after seeing an increase of cleaved caspase-9, cleaved caspase-3 and Bax and a decrease in the anti-apoptotic protein, Bcl-2. They also compared to the cytotoxicity of the UCNP with that of Y^{3+} ions and concluded that the properties of NPs did not play any significant role in the cytotoxicity of the UCNP. In contrast to the above mentioned, $GdCl_3$ increased the survival and the proliferation of HeLa cells by promoting S phase and activating FAK and JPK, but also attenuated the serum deprivation-induced cell loss (Zhang et al., 2009).

10 Conclusion

More than one third of the literature about REE effects on human health regards cytotoxicity. Hair, blood and blood serum are the most biomonitored matrices. In the near future, research should focus on other potential REE targeted tissues and organs. The effects on LREEs are much more studied than for MREEs or HREEs, thus requiring more attention. Cerium is the most investigated among all REEs.

The REEs mining showed to affect human health as they are accumulated in hair, urine or blood, not only of mining workers, who are exposed directly to these elements, but also of residents near the mining areas. Precautionary regulation should be evaluated for their protection—in the perspective of the "prevention is better than cure" paradigm.

Human daily exposure to REEs can occur also due to other factors such as improper management of e-wastes or high traffic volume since they are used for developing technological devices and as additives in diesel fuels. Although REE levels in the environment and food are currently present at low levels and do not possess a huge threat for human health, they should be considered as a potential future risk since REEs concentration is expected to increase along time.

REEs exposure has been associated with several diseases like NTD, anemia or endomyocardial fibrosis. The lifestyle (smoking and drinking) could contribute to increase the exposure to REEs.

A number of studies have shown that Gd used as a contrast media in MRA and MRI can be accumulated in kidney or muscles causing renal failure and fibromyalgia. Through cytotoxicity studies, GBCAs showed to increase the levels of MMP-1 and TIMP-1, possibly interfering in biological processes where collagen is involved.

A regulation should be implemented also in occupational REE exposures since many jobs may lead to adverse effects. To date, most studies have focused on REE miners and workers involved in movie projection. More focus should be given also to other jobs, concerning occupational exposure to REEs, like workers in diesel or technological devices production.

The mechanism of action and the metabolic pathways that REEs activate are still unclear in most cases. GBCAs can activate the pathways related to MPP-1 and TIMP-1. Activation of the PDGF receptor pathway is referred above. REEs can activate the metabolic pathways resulting to ROS production, DNA damage and apoptosis to several cell lines. They seem to be more cytotoxic to cancer cells than normal cells, probably by promoting apoptosis, suggesting their potential protective action against cancer. In some studies, they acted as antioxidants activating pathways related to numerous proteins such as SOD2, GSA, TNF-α, IL-1α, IL-8, ICAM-1, MCP-1, LC3, Beclin1, p62, caspase-9, caspase-3, BAX, Bcl-2, FAK and JPK. They can be uptaken by several cellular

compartments like mitochondria, lysosomes, cytoplasm and nucleus. Attention should be given to the case of mitochondria, since they have been mentioned to cause mitochondrial disruption. REEs have similar ionic radius to calcium and so they may interfere with its regulation. Future cytotoxic studies should focus on the mechanisms of action of REEs to elucidate the metabolic pathways they can activate.

As a general conclusion, REEs seem to constitute a potential risk for human health. Specific human biomonitoring programs should take place especially for occupational exposures (i.e., miners, e-waste workers), evidencing, particularly, how tobacco smoke can change the background exposure level in the population. Further investigations are necessary to highlight stronger cause-effect relationships between pathological status and REEs exposure, looking for their presence in the right target matrix.

Comparative study of two methods for rare earth elements analysis in human urine samples using inductively coupled plasma-mass spectrometry

1 Introduction

REEs have become an essential component of present-day life due to their pervasive applications in several industrial, agricultural, and medical applications. This extensive use of REEs in several technologies is expected to impact human health, including occupational and environmental REE exposures (Pagano et al., 2019; Rim, 2016; Pagano, 2017). Unlike experimental studies, the consequences of REE exposures to human health have been subjected to relatively fewer investigations. The likely environmental threats arising from REE exposures deserve a new line of research efforts (Pagano et al., 2015b). Environmental exposures have been investigated in populations residing in REE mining areas, showing REE bioaccumulation in scalp hair, excess REE urine levels, and defective gene expression (Pagano et al., 2015b, 2015a).

Several studies investigated the bioaccumulation of REEs in human urine matrices. Hao et al. (2015) found elevated levels of REEs in the hair of people living near Baiyun Obo deposit (China), the world's largest REE deposit, compared to the selected control area. Li et al. (2016) found higher levels of La, Ce, Nd, and Gd in the urine of workers manufacturing cerium and lanthanum oxide ultrafine and nano-sized particles. Li et al. (2017) found higher levels of La and Ce in the urine of the same kind of workers. The levels of Y, La, Ce, Pr, Nd, and Sm were higher in the urine of children living near the Bayan Obo mining area (Liang et al., 2018). Liu et al. (2019) concluded that increased maternal urinary Ce and Yb level could be associated to decreased neonatal TSH levels. People living near smelting areas were more exposed to REEs than people living near mining areas since their urine contains higher levels of these metals (Meryem et al., 2016). The urines of e-waste recyclers at Agbogbloshie (Ghana) contain elevated levels of La, Eu, and Tb (Takyi et al., 2021). Cirtiu et al. (2022) investigated the REE levels in urines of residents in Nunavik (Canada) before the beginning of REE exploitation in this area. Allain et al. (1990) investigated REE levels in healthy men and found that their levels were below the related detection limits.

Few innovative methods based on Inductively Coupled Plasma Mass Spectrometry (ICP-MS) have been developed for determination of REEs in urine matrices. The Italian Institute of Health (ISS) described a method for the determination of chemical elements in human biological samples (serum, urine, blood, and similar fluids) by ICP-MS, but no REEs were investigated (Alimonti et al., 2015). A method based on polymer monolithic capillary microextraction combined online with microconcentric nebulization ICP-MS for the determination of REEs in biological samples was developed by Zhang et al. (2013). Li et al. (2016) explored a sensitive and reliable indicator of the exposure level to REEs in urines. Li et al. (2017) identified the occupational exposure to REEs by analyzing urines using ICP-MS based on closed-vessel, microwave-assisted wet digestion. Bettinelli et al. (2002) developed a method with electrothermal vaporization ICP-MS (ETV-ICPMS) for determining REEs in urine, in which the sample was injected into the graphite tube and trifluoromethane (Freon-23) and was used as a chemical modifier to reduce vaporization temperature and the memory effect of most of the lanthanides.

Even if several studies investigated REE levels in human matrices, until today, no standard method has been established for analyzing these elements in human matrices. The sample analysis should be of high quality and the methods should be validated properly to ensure quality of the procedure and traceability of the analytical data. It is essential, therefore, to establish methods for effective tracing of REEs in human matrices, including urines.

In this research, we described a simple sample preparation method by dilution with nitric acid solution (2%, v/v) in a ratio 1:5 (namely, DIL) and compared it to the microwave-assisted-acid digestion (namely, MIN) for the preparation of human urine samples for subsequent determination of REE levels by ICP-MS.

2 Materials and methods

2.1 Reagents and materials

All analyses were conducted at the laboratory of Analytical Chemistry for the Environment of the University of Naples Federico II. High-purity water (resistivity of 18.2 MΩ cm) was obtained from a Milli-Q unit (Millipore, United States) and was used for all solution preparation and sample dilution. Nitric acid (HNO_3, 69% v/v Ultratrace@ ppb-trace analysis grade) was provided by Scharlau (Barcelona, Spain). The multicomponent solution of 16 rare earth elements (50 mg/L each) was of ultrapure grade for ICP, TraceCERT® and was purchased from Merck (Darmstadt, Germany). All glassware used for preparation of samples and standards was washed overnight by immersion in ultrapure HNO_3 solution (10% v/v), while plastic containers used for sampling were washed by HNO_3 diluted solution (2% v/v), following a rinse with deionized water and dryness before use. All the materials have been tested and found free of rare earth elements.

2.2 Ethical statement

All methods were performed in accordance with the guidelines and regulations contained in the Declaration of Helsinki (World Medical Association, 2013). All experimental protocols were approved by the Ethics Committee of the University of Naples Federico II (Italy) (authorization n. 181/21). All the recruited participants provided their written informed consent to participate to the study before the sample collection within the H2020 PANORAMA project (see the acknowledgment for more details).

2.3 Sampling and sample preparation

Urine samples were collected in 100-ml containers and deposited at −18°C and then thawed for preparation prior to ICP-MS analysis. Two different methods of digestion were considered and compared to identify the most adequate method of urine sample preparation for subsequent ICP-MS analysis.

2.3.1 Method 1—simple dilution with nitric acid

In a 10-ml PP test tube, 1 ml of the urine sample was placed and 4 ml of HNO_3 solution (2%, v/v) were added. The mixture was gently stirred with the use of a vortex, and the samples thus prepared were analyzed directly by ICP-MS in the shortest possible time to avoid the possible precipitation of undigested organic compounds.

2.3.2 Method 2—Microwave-assisted-acid decomposition method

In a 10-ml glass vessel provided by CEM Corporation (Charlotte, North Carolina), 2 ml of the urine sample was mixed with 0.5 ml of concentrated HNO3 (69%, v/v). A microwave-assisted-acid decomposition was followed using the automated digestion system Discover SP-D Clinical (CEM

Corporation, Charlotte, North Carolina). After the introduction of a small stirring bar, the vessel was capped and placed in the microwave oven for digestion with the following steps: heating for 2 min up to 120°C, remaining at 120°C for 2 min, and then cooling down for 30 s to room temperature. After the decomposition, the mixture was transferred to a 10-ml PP test tube and diluted with HNO_3 solution (2%, v/v) to a final volume of 10 ml for subsequent analysis by ICP-MS.

2.4 Method validation

A validation program was built up according to Eurachem Guide–The Fitness for Purpose of Analytical Methods (Magnusson and Ornemark, 2014) and UNI CEI EN ISO/IEC 17025 (2018) to ensure the quality of both DIL and MIN methods. The characteristic parameters of the method were evaluated for each element, that is, the limit of detection (LOD) and quantification (LOQ), working and linear ranges, repeatability and reproducibility precision, accuracy, and recovery.

LOD and LOQ were determined according to Eurachem Guide (Magnusson and Ornemark, 2014) with the determination of 10 replicate measurements of blank samples containing only HNO_3 solution (2%, v/v). LOD was calculated as 3s and LOD as 10s, s being the standard deviation of the measured concentrations.

The working range was evaluated by analyzing one blank and six standards at different concentrations, and the linearity was tested verifying the linear regression coefficient (R_2) of the calibration curve. The linearity was acceptable, with R_2 value greater than 0.996.

Precision was evaluated under repeatability conditions with the analysis of 10 replicates of spiked urine matrix carried out by the same analyst, equipment, and laboratory in a short timescale.

Precision was evaluated under reproducibility conditions with the analysis of 10 replicates of the same spiked urine sample carried out by different analysts, equipment, and same laboratory in an extended timescale, over a 2-week period.

Both repeatability and reproducibility precision are generally dependent on analyte concentrations, and so in this study, they were evaluated at three different concentrations of the calibration curve.

By determining the standard deviation of the replicates, the repeatability standard deviation (s_r) and the intra-laboratory reproducibility deviation (s_R) were obtained at each concentration level.

Because at our best knowledge there are no certified reference materials of all the investigated REEs for urine, the accuracy was evaluated by recovery studies. Urine unfortified samples were spiked with a certified REE solution at three different concentrations in the range from 0.05 to 75 μg/L. At least six replicates were executed with both DIL and MIN methods. The recovery is the percentage of fortified concentration, obtained for each element in each sample at the four concentration levels, according to formula presented in the Eurachem Guide (Magnusson and Ornemark, 2014).

2.5 Coupled plasma—mass spectrometry analysis

Multi-elemental analysis was performed by the Inductively Coupled Plasma—Mass Spectrometry (ICP-MS) by using an Aurora M90 ICP-MS instrument (Bruker, Germany). The experimental conditions are given in Table 1. The analysis was performed in the high-sensitivity mode. All standards used for analysis in ICP-MS were prepared in HNO_3 solution (2%, v/v). Calibration curves for determining REEs ranged from 0.005 to 100 μg/L and were constructed daily by analysis of

standard solutions prepared immediately before analysis. Calibration ranges for each REE are presented in Table 2. The internal standard was ^{115}In for both the calibration curve and sample analysis. A blank for reagents and a blank for the digestion method were performed to verify REE contamination of all materials used for each batch and verified in the instrumental sequence every 10 samples. At least two control standards were verified for every 20 samples.

Table 1. Instrumental operating conditions for ICP-MS.

ICP-MS parameter	
Flow parameter (L/min)	**Value**
Plasma flow	16.5
Auxiliary flow	2.00
Sheath gas	0.20
Nebulizer flow	1.00
Torch alignment	
Sampling depth	6.5
Other	
RF power (kW)	1.40
Pump rate (rpm)	4
Stabilization delay (s)	10
Ion optics (volts)	
First extraction lens	−567
Second extraction lens	−770
Third extraction lens	−559
Corner lens	−521
Mirror lens left	88
Mirror lens right	30
Mirror lens bottom	79
Entrance lens	0
Fringe bias	−3.6
Entrance plate	−47
Pole bias	0.0

Table 2. Specific calibration range for the REEs. All values are expressed in µg/L.

	Element	Calibration range
LREEs	^{89}Y	0.010–100
	^{139}La	0.010–100
	^{140}Ce	0.010–100
	^{141}Pr	0.010–100
	^{146}Nd	0.010–100
MREEs	^{149}Sm	0.010–100
	^{153}Eu	0.010–100
	^{157}Gd	0.010–100
	^{159}Tb	0.005–100
	^{163}Dy	0.005–100
	^{165}Ho	0.010–100
HREEs	^{166}Er	0.005–100
	^{169}Tm	0.005–100
	^{172}Yb	0.010–100
	^{175}Lu	0.005–100

3 Results and discussion

3.1 Limit of detection and limit of quantification values

LOD and LOQ values for the ICP-MS determination and for the dilution (DIL) and digestion (MIN) urine sample preparation procedures for each REE are shown in Table 3. For the ICP-MS determination, LOD values ranged from 0.001 to 0.004 µg/L with Tb, Er, and Tm showing the lowest value and Nd the highest value, while LOQ values ranged from 0.005 to 0.013 µg/L, with Tb, Dy, Er, Tm, and Lu showing the lowest and Nd the highest value. For both urine sample preparation procedures, LOD values ranged from 0.007 to 0.019 µg/L, with Tb, Er, and Tm showing the lowest and Nd the highest value, while LOQ values ranged from 0.023 to 0.065 µg/L, with Tb showing the lowest and Nd the highest value. Our findings are in accordance with LOD and LOQ values for determination of REEs from other studies (Hao et al., 2015; Li et al., 2016; Y. Li et al., 2017; Y. Liu et al., 2019). For all elements, the values were normally distributed (Shapiro–Wilk 5% test; $p < 0.05$), and the presence of irregular data was not statistically significant (Dixon 5% single test; $p < 0.05$).

Table 3. Limits of detection (LODs) and limits of quantifications (LOQs) evaluated for the instrument (ICP-MS) and for the preparation methods (dilution, DIL; digestion, MIN). All values are expressed in μg/L.

	Element	LOD		LOQ	
		ICP-MS	DIL—MIN	ICP-MS	DIL—MIN
LREEs	^{89}Y	0.003	0.015	0.010	0.050
	^{139}La	0.003	0.014	0.009	0.046
	^{140}Ce	0.003	0.017	0.011	0.056
	^{141}Pr	0.003	0.015	0.010	0.051
	^{146}Nd	0.004	0.019	0.013	0.065
MREEs	^{149}Sm	0.003	0.013	0.009	0.043
	^{153}Eu	0.002	0.011	0.008	0.038
	^{157}Gd	0.003	0.013	0.009	0.044
	^{159}Tb	0.001	0.007	0.005	0.023
	^{163}Dy	0.002	0.008	0.005	0.025
	^{165}Ho	0.002	0.010	0.006	0.032
HREEs	^{166}Er	0.001	0.007	0.005	0.025
	^{169}Tm	0.001	0.007	0.005	0.025
	^{172}Yb	0.002	0.012	0.008	0.039
	^{175}Lu	0.002	0.008	0.005	0.025

3.2 Precision

The results of the evaluation of repeatability precision and intra-laboratory reproducibility precision were obtained for both DIL and MIN methods at three different concentration levels are presented in Table 4 and Table 5, respectively.

The DIL sample preparation method shows a better level of repeatability than the MIN method. The mean values of relative standard deviation (CV_r%) for the DIL method range from 1.5 to 12% and for the MIN method, they range from 8.4 to 15%. For both methods, as expected, the values are lower with increasing concentrations.

Intra-laboratory reproducibility precision also shows better values of relative standard deviation (CV_R%) for the DIL method for low and high levels of concentrations, with slightly higher values at the medium level than for the MIN method.

However, the CV_R% values were generally similar for both methods ranging from 6.2 to 23% for the DIL method and from 8.6 to 24% for the MIN method.

Table 4. Results of repeatability precision expressed as standard deviation, s_r (μg/L) and relative standard deviation (CV_r%) at three different levels of concentrations for the dilution (DIL) and digestion (MIN) sample preparation procedures.

	LREEs						MREEs					HREEs			
Element	^{89}Y	^{139}La	^{140}Ce	^{141}Pr	^{146}Nd	^{149}Sm	^{153}Eu	^{157}Gd	^{159}Tb	^{163}Dy	^{165}Ho	^{166}Er	^{169}Tm	^{172}Yb	^{175}Lu
DIL— Low level															
Concentration (mean)	0.13	0.17	0.20	0.13	0.13	0.12	0.12	0.09	0.12	0.12	0.11	0.11	0.11	0.11	0.12
Standard deviation, s_r	0.01	0.02	0.02	0.01	0.01	0.01	0.01	0.01	0.01	0.01	0.01	0.01	0.01	0.01	0.01
CV_r%	11	12	9.0	5.2	8.9	9.7	7.1	6.7	9.6	7.2	6.9	8.4	7.0	9.3	8.4
MIN—Low level															
Concentration (mean)	0.25	0.32	0.39	0.20	0.23	0.19	0.20	0.17	0.18	0.17	0.18	0.20	0.20	0.20	0.19
Standard deviation, s_r	0.03	0.05	0.04	0.03	0.03	0.03	0.02	0.02	0.02	0.02	0.02	0.03	0.03	0.03	0.03
CV_r%	11	15	12	13	12	14	13	12	14	12	12	14	14	16	15
DIL—Medium level															
Concentration (mean)	1.4	1.6	2.0	1.3	1.3	1.2	1.2	1.0	1.3	1.2	1.2	1.2	1.2	1.2	1.2
Standard deviation, s_r	0.1	0.1	0.1	0.1	0.1	0.1	0.1	0.1	0.1	0.1	0.1	0.1	0.1	0.1	0.07
CV_r%	4.7	3.6	3.2	4.1	2.8	4.5	6.0	4.6	5.6	6.0	6.1	6.3	6.0	5.2	5.7
MIN—Medium level															
Concentration (mean)	1.9	2.1	2.8	1.8	1.8	1.7	1.7	1.5	1.9	1.8	1.7	1.7	1.7	1.7	1.7
Standard deviation, s_r	0.2	0.3	0.4	0.2	0.2	0.2	0.2	0.2	0.2	0.2	0.2	0.2	0.2	0.2	0.2
CV_r%	13	14	14	13	13	13	13	12	12	13	13	12	14	13	13
DIL—High level															
Concentration (mean)	13.6	15.1	19.6	12.6	12.8	11.5	11.6	10.2	12.9	12.4	11.7	11.7	11.5	11.2	11.9
Standard deviation, s_r	0.4	0.8	0.5	0.4	0.3	0.3	0.3	0.3	0.3	0.2	0.4	0.3	0.3	0.2	0.3
CV_r%	3.1	5.4	2.5	3.3	2.5	2.4	2.5	3.0	2.5	1.5	3.3	2.7	2.6	2.2	2.2
MIN—High level															
Concentration (mean)	18.9	21.0	27.0	18.0	18.6	17.0	17.2	15.7	18.8	18.3	17.4	17.4	17.0	16.9	17.2
Standard deviation, s_r	1.9	1.8	2.8	1.9	1.9	2.0	1.7	1.4	1.9	2.0	1.7	1.9	2.0	1.8	1.7
CV_r%	10	8.4	10	10	10	12	9.7	9.1	10	11	9.7	11	12	11	10

Table 5. Results of reproducibility precision expressed as standard deviation, s_R (μg/L) and relative standard deviation (CV_R%) at three different levels of concentrations (μg/L) for the dilution (DIL) and digestion (MIN) sample preparation procedures.

	LREEs						MREEs					HREEs			
Element	^{89}Y	^{139}La	^{140}Ce	^{141}Pr	^{146}Nd	^{149}Sm	^{153}Eu	^{157}Gd	^{159}Tb	^{163}Dy	^{165}Ho	^{166}Er	^{169}Tm	^{172}Yb	^{175}Lu
DIL—Low level															
Concentration (mean)	0.15	0.10	0.22	0.15	0.14	0.13	0.13	0.11	0.14	0.15	0.14	0.14	0.13	0.13	0.14
Standard deviation, s_r	0.02	0.02	0.03	0.02	0.02	0.02	0.02	0.02	0.02	0.02	0.02	0.02	0.02	0.02	0.02
CV_R%	14	11	14	13	13	15	12	14	12	16	19	16	17	15	14
MIN—Low level															
Concentration (mean)	0.21	0.27	0.43	0.18	0.19	0.16	0.16	0.14	0.17	0.18	0.16	0.17	0.16	0.16	0.17
Standard deviation, s_r	0.04	0.05	0.10	0.03	0.03	0.02	0.02	0.03	0.03	0.03	0.03	0.03	0.03	0.02	0.02
CV_R%	18	18	24	16	17	13	15	18	18	16	16	16	17	14	15
DIL—Medium level															
Concentration (mean)	1.6	1.9	2.3	1.6	1.5	1.4	1.4	1.2	1.5	1.5	1.5	1.4	1.4	1.3	1.5
Standard deviation, s_r	0.3	0.4	0.5	0.3	0.2	0.3	0.2	0.2	0.2	0.3	0.3	0.2	0.3	0.2	0.3
CV_R%	18	20	23	20	17	19	15	14	13	18	20	17	19	14	18
MIN—Medium level															
Concentration (mean)	1.8	2.0	2.5	1.7	1.7	1.6	1.6	1.4	1.7	1.7	1.7	1.6	1.6	1.6	1.7
Standard deviation, s_r	0.2	0.2	0.4	0.2	0.2	0.1	0.2	0.2	0.2	0.2	0.2	0.2	0.2	0.2	0.2
CV_R%	11	11	16	10	11	8.6	11	11	12	10	8.9	8.9	9.3	9.7	9.1
DIL—High level															
Concentration (mean)	14.6	16.1	20.0	14.0	13.6	12.9	12.3	10.6	13.5	13.7	13.3	12.9	12.8	12.2	13.4
Standard deviation, s_r	1.4	1.7	1.2	1.7	1.1	1.6	1.0	0.7	1.1	1.7	1.9	1.4	1.6	1.2	1.8
CV_R%	9.8	11	6.2	12	8.3	12	8.0	6.5	8.2	12	14	11	12	9.8	13
MIN—High level															
Concentration (mean)	17.2	18.8	23.0	16.7	16.5	15.8	15.4	14.0	16.5	16.9	16.3	16.0	15.8	15.4	16.2
Standard deviation, s_r	2.6	3.1	4.8	2.2	2.7	2.0	2.2	2.1	2.7	2.2	1.8	2.1	1.9	2.2	1.7
CV_R%	15	16	21	14	16	12	14	15	16	13	11	13	12	14	11

3.3 Accuracy and recovery

The accuracy of analytical methods was evaluated by analyzing urine samples spiked with known concentrations of REEs at four different levels. The starting unfortified sample was analyzed and shows REE values below the LOQs. The urine sample for the DIL method was fortified with the REE multicomponent solution at concentrations of 0.05, 0.25, 3.0, and 75 μg/L identified as level 1, level 2, level 3, and level 4, respectively. The urine sample for the MIN method was fortified with the same solution at concentrations of 0.05, 0.50, 5.0, and 50 μg/L identified as level 1, level 2, level 3, and level 4, respectively.

In both tested sample preparation methods and at all levels, the recovery values ranged within ±15% in all samples. The results are presented in Table 6.

Table 6. Results of accuracy expressed as recovery (%) based on analysis of spiked samples at four different levels for the dilution (DIL) and digestion (MIN) sample preparation procedures.

Spiked samples

	Element		Recovery (%)			Element		Recovery (%)			Element		Recovery (%)	
			DIL	MIN				DIL	MIN				DIL	MIN
LREEs	^{89}Y	Level 1	88	93	MREEs	^{149}Sm	Level 1	93	91	HREEs	^{166}Er	Level 1	88	87
		Level 2	94	95			Level 2	99	88			Level 2	100	100
		Level 3	100	94			Level 3	96	94			Level 3	99	96
		Level 4	102	107			Level 4	98	105			Level 4	101	108
	^{139}La	Level 1	108	114		^{153}Eu	Level 1	91	86		^{169}Tm	Level 1	96	100
		Level 2	105	100			Level 2	95	98			Level 2	99	99
		Level 3	106	97			Level 3	99	97			Level 3	101	98
		Level 4	108	108			Level 4	102	109			Level 4	102	110
	^{140}Ce	Level 1	95	98		^{157}Gd	Level 1	104	111		^{172}Yb	Level 1	86	83
		Level 2	102	101			Level 2	91	96			Level 2	100	102
		Level 3	106	97			Level 3	92	94			Level 3	101	99
		Level 4	109	110			Level 4	93	105			Level 4	103	111
	^{141}Pr	Level 1	91	94		^{159}Tb	Level 1	87	87		^{175}Lu	Level 1	85	87
		Level 2	101	98			Level 2	97	99			Level 2	102	104
		Level 3	101	96			Level 3	102	97			Level 3	104	101
		Level 4	102	106			Level 4	103	109			Level 4	106	113
	^{146}Nd	Level 1	92	90		^{163}Dy	Level 1	89	94					
		Level 2	98	93			Level 2	95	97					
		Level 3	98	95			Level 3	98	97					
		Level 4	102	106			Level 4	101	108					
						^{165}Ho	Level 1	90	90					
							Level 2	100	101					
							Level 3	102	99					
							Level 4	103	110					

Methods using sample dilution for analyzing REE levels in urine samples have been used in several studies. Allain et al. (1990) also prepared the samples by a simple 6-fold dilution with HNO_3 solution, 10 ml/L. Cirtiu et al. (2022) made a 20-fold dilution with HNO_3 solution, 0.5% (v/v). Hao et al. (2015) made a 10-fold dilution with deionized water. Li et al. (2016) made a 20-fold dilution with HNO_3 solution, 2% (v/v).

In our study, we demonstrated precision, accuracy, and reliability of the simple dilution for urine sample preparation. Use of HNO_3 solution, 2% (v/v) allowed direct analysis to the ICP-MS, and in this way, we did not go beyond a 5-fold dilution, and this allows obtaining lower detection limits.

Similar preparations to our MIN method have been used before. Zhang et al. (2013) also used a microwave digestion method for preparing the urine samples, adding 2.5 ml of concentrated HNO_3 to 1 ml of urine. Li et al. (2017) prepared 1ml of the urine sample with 5 ml of 65% HNO_3, 2 ml of H_2O_2, 30% (v/v), and 2 ml Milli-Q water and used a closed-vessel microwave-assisted wet digestion.

In our study, we decided to leave the dilution ratio between the two methods unchanged for a better comparison of results. We demonstrated precision, accuracy, and reliability of the microwave-assisted urine preparation method with a reduced amount of nitric acid, adding only 0.5 ml of

concentrated HNO_3 to 2 ml of urine. Furthermore, the digested aliquot was brought to a final volume of 10 ml using of HNO_3 solution, 2% (v/v), allowing direct analysis to the ICP-MS. In this way, the dilution ratio 1 to 5 is maintained and, therefore, the possibility of obtaining lower detection limits in urine matrix.

The choice of the methods used in this study was also guided by the possibility of carrying out in the future the analysis of trace metals with the same methods, optimizing the analytical times and the quantity of the sample required.

Several studies in the literature had used acid dilution for urine sample preparation also for the determination of trace elements. Batista et al. (2009) made a 20-fold dilution with a solution containing HNO_3, 0.5% (v/v) and Triton X-100 (0.005%, v/v). Bocca et al. (2019) made a 5-fold dilution with high-purity deionized water. Cui et al. (2005) made a 10-fold dilution with high purity deionized water. De Matos et al. (2022) made a 20-fold dilution with a solution containing HNO_3, 0.4% (v/v) and TritonX-100 (0.005%, v/v). Asante et al. (2012) made a 5-fold dilution with Milli-Q water to determine arsenic. Schmied et al. (2021) made a 10-fold dilution with HNO_3 solution, 2% (v/v) and internal standard solution. Tong et al. (2022) made a 10-fold dilution with HNO_3 solution, 1% (v/v).

In other studies, researchers carried out microwave digestion for preparing urine samples to determine trace elements (Asante et al., 2012; Choe and Gajek, 2016; E. T. Moore et al., 2018; Pham et al., 2017).

A future goal will be to lead a validation study of the two different methods of digestion used in the present work for the determination of trace element levels in human urine samples.

4 Conclusion

The digesting capacity of different sample preparation methods is a crucial step which can affect the accuracy of analytical results.

In this study, we showed the comparison between the validation data obtained from two different digestion procedures for determination of REEs in human urine samples. The analysis was carried out by ICP-MS in high-sensitivity mode, that is, a widely used technique in clinical, forensic, occupational, and environmental fields for determination of metals and metalloids.

We proposed a simple dilution of the sample with diluted nitric acid solution (2%, v/v) and a microwave-assisted-acid digestion.

Both validated methods presented in this work meet the performance criteria and the requirements set out in European regulations for method validation.

Both methods showed adequate precision of repeatability and reproducibility. The mean values of relative repeatability standard deviation (CV_r%) for the DIL method range from 1.5 to 12% and for the MIN method range from 8.4 to 15%. The reproducibility CV_R% values range from 6.2 to 23% for the DIL method and from 8.6 to 24% for the MIN method.

Accuracy of the proposed method was evaluated by spiking the sample matrix, and REE recoveries for both methods were very close to 100% ranging from 91 to 109% for the DIL method and from 88 to 113% for the MIN method.

Therefore, both tested methods of preparation are validated for analyzing REEs in urine samples, according to the method validation and the criteria of the guidelines.

Furthermore, both methods offer satisfactory LOD values ranging from 0.007 to 0.019 μg/L in the urine matrix sample.

Therefore, this allows defining them suitable for the analysis of REEs in environmental health investigations.

Occupational exposure of car mechanics to rare earth elements

1 Introduction

Automotive repair and maintenance workshops have been subjected to investigations on occupational exposures to noxious agents that suggest positive associations between mechanic occupational exposure and several disorders, such as some specific cancers (larynx, lung and bladder cancers) (Ahmed and Eldahshan, 2022; Santos et al., 2020), and oxidative stress biomarker responses (Kamal and Rashid, 2014). The main focus of occupational agents among mechanic workers has been mostly addressed to polycyclic aromatic hydrocarbons (PAH) and NOx content in engine exhaust (Gürü et al., 2002; León-Mejía et al., 2019; Prati et al., 2019), hence to the recommendation of installing devices for exhaust abatement and ventilation; a practice widely adopted by industrial mechanic workshops.

Beyond those well-recognized agents produced as by-products of hydrocarbon combustion, a new emerging contaminant class may be associated with engine exhaust and adverse health effects, the rare earth elements (REEs). REEs have become an integral part of our everyday life over the last years, since they are necessary in several sectors (e.g., agriculture and medicine) and for the production of electronic devices (e.g., TVs, smartphones, electric cars, wind turbines) (Pagano et al., 2015a, 2019). Some of these, cerium and lanthanum, are utilized both in oil refining and as catalytic additives in diesel fuel production . Therefore, there many ways of exposure to these elements and so, the concern about their safety for human health has been increased (Brouziotis et al., 2022a).

REE-associated adverse effects have been reported in a body of literature related to epidemiologic studies focused on residence-based and occupational human REE exposures (Guo et al., 2020; Hao et al., 2015; Henríquez-Hernández et al., 2017; Li et al., 2013, 2016; Y. Li et al., 2017; Liu et al., 2015; H. Liu et al., 2021; Takyi et al., 2021; Tong et al., 2004; B. Wang et al., 2017, 2018; Wei et al., 2013; Zhu et al., 2005). Experimental studies focused on several toxicity endpoints, including oxidative stress, genetic anomalies, developmental toxicity, and organ-targeted effects .

By combining the above summarized knowledge about the necessary presence of REEs in oil-derived fuels and the occupational REE exposure due to engine exhausts, the present study aimed for the first time to evaluate the levels of REEs in urine and scalp hair samples of car mechanics provided with, or lacking, exhaust abatement devices via a no-profit retrospective observational case-control study. We also studied the urine levels of 1-hydroxypyrene (1-OHP) (as a biomarker of exposure to combustion products) and creatinine (as a biomarker of health issues). Furthermore, the effect of the smoking habits on REE levels was evaluated, since previous studies have shown that smoking plays a significant role in the bioaccumulation of REEs in the human body (Marzec-Wróblewska et al., 2015; Rodushkin and Axelsson, 2000; Zhang et al., 2020), as well as the use of hair dye.

2 Materials and methods

2.1 Study design and sample collection

Urine and scalp hair samples of car mechanics were collected from two different types of workshops in collaboration with the local agencies. All donors included in this study were either employed in artisanal workshops located in Avellino province, Campania (southern Italy) or in industrial-shaped workshops located in Como province (northern Italy). The workers in Avellino are lacking means of protection during work-time and so they are referred as ‘exposed’, while the workers in Como are using means of protection so they are called as ‘non-exposed’.

In total, there were 19 donors in Avellino, offering us 19 hair samples and 18 urine samples. In Como there were 82 donors, offering us 40 hair samples and 82 urine samples. The collection of urine and

hair samples were carried out according to the guidelines of the Italian National Health Institute (Pichini and Pacifici, 2013a; Pichini and Pacifici, 2013b).

2.2 Ethical statement

Each donor was informed about the study's background, objectives and procedures, donating on a voluntary basis urine and scalp hair samples. Signed consent was obtained from all subjects involved.

All methods implemented for the analyses were in accordance with the guidelines and regulations included in the Declaration of Helsinki (World Medical Association, 2013). All experimental protocols were approved by the Ethics Committee of the University of Naples Federico II (Italy) (authorization n. 181/ 21). All the recruited participants provided their written informed consent to participate to the study before the sample collection within the H2020 PANORAMA project.

2.3 Analysis of REEs

2.3.1. Reagents and materials

Preparation of all solutions and sample dilution was made with ultrapure water (resistivity of 18.2 MΩ/cm), analytical-grade acetone (Merck) and ultrapure nitric acid (69% v/v, Ultratrace@, Scharlau, Barcelona, Spain). A certified standard solution of 16 rare earth elements (50 mg/L each) was purchased by Merck (Darmstadt, Germany). All glassware and plastic tubes were washed by HNO_3 diluted solution (2% v/v), before analysis. Blanks of all the materials were performed to verify the background levels of REEs.

2.3.2 Analysis of REEs in urines

After collection, all flasks containing urine samples were stored at -20°C. During the day of analysis, the samples were thawed at room temperature, homogenized in a vortex for 10 seconds, and were prepared by a validated method (Brouziotis et al., 2022b). Briefly, aliquots of 1 mL urine were transferred in plastic tubes and 4 mL of HNO_3 2% (v/v) were added. This mixture was vortexed, and the samples thus prepared were analyzed directly by inductively coupled plasma mass spectrometry (ICP-MS).

2.3.3 Analysis of REEs in scalp hair

Hair samples were washed in an ultrasonic cleaning system in 5 steps of 5 minutes each, using the order water-acetone-water-acetone-water according to an established method for washing hair samples (Verrey et al., 2019). The washed hair samples were dried at 80°C overnight, and then were cut into pieces of about 1 cm using ceramic scissors.

Approximately 200 mg of hair samples were mixed with 2 mL HNO_3 69% (v/v) in a 10 mL plastic tube. The plastic tubes closed with a plastic cap were transferred to a water bath for digestion at 80 °C for 3 h. After digestion, the mixture was brought to a final volume of 10 mL by addition of HNO_3 2% (v/v) for the subsequent analysis by ICP-MS.

2.4 ICP-MS

The solutions obtained after the digestion procedures were analyzed by ICP-MS (Aurora M90, Bruker, Germany). Multi-elemental analysis of fifteen REEs was performed in High Sensitivity mode. All standards used for analysis in ICP-MS were prepared in HNO_3 2% (v/v). Ten standards

ranging from 0.005 to 10 µg/L were daily prepared by dilution in HNO_3 2% (v/v) and calibration curves were built before analysis. ^{115}In was used as internal standard for both calibration curve and sample analysis. A blank for reagents and a blank for digestion procedure were performed to verify REE contamination. Two standards were processed for every 20 samples to verify instrumental stability.

2.5 Urine creatinine and 1-hydroxypyrene

The levels of 1-OHP in urine samples were determined by high performance liquid chromatography (HPLC) using a modification of the method described by (Jongeneelen et al., 1987). Briefly, a 10 mL aliquot of urine was adjusted to pH 5.0 with acetate buffer and 50 µL of β-glucuronidase/arylsulfatase (from Helix pomatia) was added. The mixture was incubated overnight at 37°C and further cleaned up with Solid Phase Extraction. The analysis was carried out with a Dionex Ultimate 3000 LC System (Thermo Fisher Scientific, Waltham, MA, USA) with a 20-µL injection loop, fluorescence detector (242 nm excitation wavelength and 389 nm emission wavelength) and Kinetex C18 column (5 µm, 4.6 mm diameter, 250 mm length; Phenomenex). The limit of detection (LOD) was 50 ng/L. The efficiency of the analytical system was verified using urine samples with a known hydroxypyrene content (ClinCheck – Control Recipe, RECIPE Chemicals + Instruments GmbH, München, Germany).

Urine creatinine levels were measured using a modified Jaffe method (Bartels et al., 1972).

2.6 Statistical analysis

Statistical analyses were elaborated in SPSS Statistics v20. Normality of the data groups were tested by the Shapiro-Wilk test. Parametric and nonparametric Levene's tests were used to determine homogeneity of variances. Values of REEs below the limit of detection (LOD) were replaced by LOD/2. Independent Samples t-Test were used to compare the REE-levels between two groups and the REE-levels in scalp hair between smokers and non-smokers. Differences were determined by Welch's t-tests and considered as significant when $p<0.05$.

3 Results and discussion

3.1 Levels of urine 1-OHP and creatinine

As shown in table 1, the levels of both creatinine and 1-OHP were significantly higher in the urines of exposed group. More specifically, the media value of creatinine was 1.676 mg/L in the urines of exposed workers and 1.113 mg/L in the urines of non-exposed. The 1-OHP levels were 0.441 µg/L or 0.283 µg/g creatinine, and 0.145 µg/L or 0.120 µg/g creatinine in the urines of exposed and non-exposed workers, respectively. The elevated levels of 1-OHP and creatinine in the urines of exposed group show a higher exposure to combustion products and a higher probability of health issues, respectively.

Table 1. Mean values and statistical analysis of levels of urine creatinine and 1-OHP between exposed and non-exposed workers.

Group	Creatinine (g/L)	1-OHP (µg/L)	1-OHP (µg/g creatinine)
Exposed	1.676	0.441	0.283
Non-exposed	1.113	0.145	0.120
p value	**0.01**	**0.002**	**0.016**

3.2 REE levels in urines and hair

Analytical results of levels of each REE in urine samples are shown in Tables S1 and S2 of Supplementary materials for exposed and non-exposed workers, respectively.

Table 2 shows the mean value of each REE and Total REEs in the urines of exposed and non-exposed groups, as well as the significant differences between the two groups. In urines of the exposed workers Ce, Sm and Dy were the most abundant elements, while in urine of the non-exposed were Y, Sm and Dy. The levels of La, Ce, Gd, Tb and Total REEs were significantly higher in the urines of exposed workers. On the other hand, the levels of Ho and Er were significantly higher in the urines of the non-exposed workers, although the p value for Er is at the limit of significance (0.05).

Table 2. Mean values (µg/L) of each REE and Total REEs in the urine samples of exposed and non-exposed workers and statistical analysis between the two groups. Significance is considered when $p<0.05$.

REE	Exposed	Non-exposed	p value
Y	0.007	0.013	0.138
La	0.01	0.007	**0.024**
Ce	0.029	0.009	**< 0.001**
Pr	0.007	0.007	0.642
Nd	0.007	0.007	0.512
Sm	0.025	0.033	0.097
Eu	0.007	0.007	0.521
Gd	0.015	0.008	**< 0.001**
Tb	0.012	0.007	**< 0.001**
Dy	0.037	0.027	0.123
Ho	0.004	0.005	**0.029**
Er	0.004	0.007	0.050
Tm	0.004	0.004	0.451
Yb	0.008	0.007	0.390
Lu	0.004	0.004	0.390
Total REEs	0.181	0.153	**0.002**

Previous studies investigated as well the occupational exposure to REEs analyzing urine matrices of two groups. Two similar studies compared the REE levels in urines of exposed and non-exposed

workers. Li et al. (2017) showed that the urines of producers of ultrafine and nano-sized particles containing Ce and La oxide had higher levels of La and Ce. Li et al. (2016) showed that the urines of exposed workers that manufacture cerium and lanthanum oxide ultrafine and nano-sized particles contained significantly elevated levels of La, Ce, Nd and Gd, with respect to the non-exposed group. On the same direction, the urines of e-waste recyclers have been shown to contain significantly higher levels of La, Ce and Eu (Takyi et al., 2021).

Analytical results of levels of each REE on scalp hair samples are shown in Tables S3 and S4 of Supplementary materials for exposed and non-exposed workers, respectively.

Table 3 shows the mean value of each REE and Total REEs in the scalp hair of exposed and non-exposed workers, as well as the significant differences between the two groups. In the hair of both groups, La and Ce were the most abundant elements. All REEs and Total REEs were not significantly different between the two groups.

Table 3. Mean values (ng/g) of each REE and Total REEs in the scalp hair samples of exposed and non-exposed workers and statistical analysis between the two groups. Significance is considered when $p<0.05$.

REE	Exposed	Non-exposed	p value
Y	3.671	3.341	0.751
La	13.901	9.958	0.507
Ce	26.508	14.607	0.293
Pr	0.840	0.916	0.840
Nd	3.175	3.603	0.737
Sm	0.638	0.363	0.148
Eu	0.375	0.337	0.765
Gd	1.051	0.989	0.871
Tb	0.080	0.053	0.400
Dy	0.345	0.387	0.748
Ho	0.093	0.057	0.146
Er	0.244	0.171	0.394
Tm	0.033	0.035	0.854
Yb	0.146	0.249	0.156
Lu	0.050	0.050	-
Total REEs	51.149	35.117	0.418

Previous studies investigated also the occupational bioaccumulation of REEs on hair matrices between two groups of people. In the study of Wei et al. (2013), the hair of miners had much higher levels of light REEs than the non-miners in both mining and control area. Liu et al. (2015) and (H. Liu et al., 2021) found also higher REE levels in the hair of the miners with respect to the control group. REEs in the hair of miners from these studies are higher than REEs in hair of our study, which makes sense since the miners are coming in direct everyday contact with the elements.

In this research we found significantly higher levels of creatinine, 1-OHP and Total REEs in the urines of Avellino workers. The elevated levels of REEs in combination with the elevated levels of 1-OHP indicate a higher exposure of Avellino workers to combustion products which most probably come from the car exhausts, since no means of protection are used in Avellino workshops. In addition, the elevated REE levels in combination with the elevated levels of creatinine indicate a correlation of REEs with the higher possibility of health problems to Avellino workers. REEs in scalp hair were not significantly different between the two groups. This might indicate a non-long-term bioaccumulation of REEs in human body, but could also indicate a possibility of REE-bioaccumulation on other organs besides scalp hair. REEs have been shown to be correlated with several diseases (Brouziotis et al., 2022a) and so, measures to be taken for the mitigation of exposure to these elements should be considered.

In order to investigate also the possible effect of smoking on the bioaccumulation of REEs, a statistical analysis was also elaborated for the REE-levels in hair samples of Como workers between smokers and non-smokers. There were 9 smokers and 31 non-smokers. As shown in Table 1 the levels of La and Ce were statistically significant between the two groups, while there was not significant difference for the other REEs. These results indicate the possibility that the bioaccumulation of La and Ce is due to smoking habits and not due to occupational exposure.

Table 4. Mean values (ng/g) of each REE and Total REEs in the scalp hair samples of smokers and non-smokers of workers from Como workshops and statistical analysis between the two groups. Significance is considered when $p<0.05$.

REE	Smokers	No smokers	p value
Y	2.240	3.661	0.107
La	21.450	6.622	**0.028**
Ce	31.840	9.604	**0.020**
Pr	0.537	1.027	0.273
Nd	2.449	3.938	0.298
Sm	0.361	0.364	0.981
Eu	0.207	0.374	0.319
Gd	0.754	1.058	0.419
Tb	0.037	0.057	0.270
Dy	0.370	0.392	0.881
Ho	0.050	0.060	0.325
Er	0.081	0.198	0.161
Tm	0.036	0.034	0.907
Yb	0.146	0.280	0.092
Lu	0.050	0.050	-
Total REEs	60.607	27.717	0.062

A statistical analysis was also elaborated for the REE-levels in hair samples of Como workers between the ones who use hair dye and those who don't. As shown in Table 2, only the levels of Eu were significant different between the two groups, indicating that the hair dye doesn't affect the bioaccumulative levels of REEs.

Table 5. Mean values (ng/g) of each REE and Total REEs in the scalp hair samples of users and non-users of workers from Como workshops and statistical analysis between the two groups. Significance is considered when $p<0.05$.

REE	Users	No users	p value
Y	4.124	3.229	0.456
La	12.930	9.534	0.690
Ce	21.528	13.618	0.528
Pr	0.991	0.906	0.875
Nd	4.532	3.470	0.653
Sm	0.589	0.331	0.445
Eu	0.672	0.289	0.022
Gd	1.121	0.971	0.788
Tb	0.080	0.049	0.458
Dy	0.418	0.382	0.849
Ho	0.050	0.058	0.324
Er	0.305	0.152	0.410
Tm	0.025	0.036	0.208
Yb	0.334	0.237	0.419
Lu	0.050	0.050	-
Total REEs	47.751	33.313	0.564

4 Conclusions

This is the first study ever concerning REE levels in biological matrices of car mechanics. The significantly higher levels of La, Ce, Gd, Tb and Total REEs in the urines of Avellino workers, together with the higher levels of creatinine and 1-OHP, indicate the potential of REEs to be correlated with a high possibility of health issues and an occupational exposure to combustion products, respectively.

REE levels in scalp hair were not different between the two groups of workers. This might indicate a quick excretion of REEs through urines and a non-long-term bioaccumulation, or could be possible that a significant amount of REEs is bioaccumulated in other organs of the human body before the rest of the amount is excreted through urines.

Smoking has been previously reported that plays a role in the bioaccumulation of REEs in the human body. The statistical analysis in our research indicated as well that smoking might play a role in the elevated levels of La and Ce.

In conclusion this study indicates that measures of safety of Avellino workers should be elaborated so that their exposure to REEs and other hazardous products is lessened. More researches about the occupational exposure to REEs should be elaborated so that we understand better the level of hazard that they can cause on human health during work-time.

Chapter 3: Environmental Toxicology of REEs

In this chapter, the contributions of the PhD project concerning the environmental toxicity of REEs are presented. The first subchapter has been submitted for publication, while the four subchapters following are already published in *Science of the total Environment* (Siciliano et al., 2021a, 2021b), *Frontiers in Environmental Science* (Siciliano et al., 2022) and *Bulletin of Environmental Contamination and Toxicology* (Pagano et al., 2023).

General introduction about chapter 3

Anthropogenic REEs contamination can be a major problem in hot areas, but the altered biogeochemical cycles of these elements point to their potential as pervasive emerging contaminants in agroecosystems as well. REEs are released into the environment in a variety of ways, most notably during the disposal of consumer and industrial products, during the mining and mineral processing process, and through the wastewater produced by REE-using industrial activities (Gwenzi et al., 2018).

Concerns about the potential of anthropogenic activity to cause more significant changes to REEs' biogeochemical cycles are growing. For national and international laws, REEs do not now exhibit any threshold limit values; however, they can be viewed as new emerging pollutants with undetermined impacts (Galdiero et al., 2019).

Particularly in seawater, the biological impacts and toxicity of REEs are poorly understood. Fewer data are available for marine creatures than for freshwater ones from the scant literature on REE toxicity to aquatic organisms (Freitas et al., 2020). For example, no data exist about the toxicity of REEs on *Phaeodactylum tricornutum Bohlin*.

In addition to their negative effects, REEs also exhibit stimulatory effects (Abdelnour et al., 2019; He et al., 2010; Lian et al., 2019). This dual action of REEs can be attributed to the general phenomena of a concentration-related shift from inhibition, or "toxicity," for high agent concentrations to stimulation, also known as hormesis, for lower agent concentrations.

This chapter concerns the second level of research investigation of this PhD, which is the environmental toxicity of REEs. A literature review was elaborated concerning the species sensitivity distribution of REEs. In addition, four published studies are presented that investigated the potential toxicity of REEs on several organisms. The first is about the toxicity of La, Ce, Nd and Gd on three photosynthetic organisms (*R. subcapitata*, *L. sativum*, *V. faba*) on two different pH environments; the second is about the short- and long-term toxicity of La and Ce on *R. subcapitata*; the third is about the toxicity of La, Ce, Nd, Sm, Eu, Gd, Dy and Er on *P. tricornutum*; and the last one about the hormetic action of La, Ce and their combination on the sperm of *S. granularis*.

The main activity of this chapter, which is the elaboration of the ecotoxicological trials, took part in another laboratory by another PhD student that is affiliated on the same H2020 project. The contribution of the PhD student to this part of the project was to determine the real concentration of the REEs, with respect to the nominal concentartions, using ICP-MS. The samples analyzed were either prepared in the lab and were analyzed before the initiation of the trials, or were samples collected on specific times after the initiation.

Species sensitivity distribution of rare earth elements: a full overview

1 Introduction

Rare earth elements (REEs) include the 15 lanthanides [(Lanthanum (La), Cerium (Ce), Praseodymium (Pr), Neodymium (Nd), Promethium (Pm), Samarium (Sm), Europium (Eu), Gadolinium (Gd), Terbium (Tb), Dysprosium (Dy), Holmium (Ho), Erbium (Er), Thulium (Tm), Ytterbium (Yb), and Lutetium (Lu)], also called lanthanoids, together with Yttrium (Y) and Scandium (Sc), which behave rather differently in nature to the other REEs (Wall, 2013). The REEs are metals in silvery-white color and display similar physicochemical properties and small differences in atomic weight across the series (Malhotra et al., 2020). These elements can be divided into three sub-groups (Brown et al., 1990): i) the light rare earths elements (LREEs; with lower atomic numbers and masses) ranging from La to Pm (La, Ce, Pr, Nd, and Pm); ii) middle rare earth elements (MREEs) ranging from Sm to Ho (Sm, Eu, Gd, Tb, Dy, and Ho); and iii) heavy rare earth elements (HREEs; with higher atomic numbers and masses) ranging from Er to Lu (Er, Tm, Yb, and Lu).

The appellation "rare earths" was originally related to the difficulty experienced by chemists in separating these elements from each other and from other elements; also due to the fact that REEs are usually present as stable oxides rather than in zerovalent form (Szabadvary, 1988). Considering the abundance of some of these elements in nature, currently this term is improper, but still widespread in use. In nature, Ce and Y are abundant like tin (Sn) and cobalt (Co); Nd and La occur in similar quantities to lead (Pb), and all the other REEs occur at a level of abundance somewhat above silver (Ag) and cadmium (Cd) (Binnemans and Jones, 2015). Over the past decade, REEs have been used in a variety of activities, such as industrial, agricultural and medical technologies, increasing their presence in the environment (Pagano et al., 2015b). For this reason, REEs have been considered as a new category of potential emerging contaminants for the biota potentially impairing human health as well. REEs toxicity is closely related to their chemical forms that, in turn, depend on pH, salinity, redox conditions, types of clay minerals in surroundings, and complexation with organic and inorganic compounds (Amyot et al., 2017; Migaszewski and Gałuszka, 2015). These elements can exist as free ions, carbonates, halides, and complexes of hydroxyl, sulfate, phosphate, or oxide (Johannesson et al., 1996). Various studies were conducted evaluating their toxicity effects on freshwater, saltwater, terrestrial species and human health (Aashima et al., 2018; Carpenter et al., 2015; Cieślik et al., 2019; Galdiero et al., 2019; Gravina et al., 2018; Laveuf and Cornu, 2009; Loell et al., 2011). Among all REEs, LREEs (especially Ce, La and Y) and Gd (Trapasso et al., 2021b) are the most studied, while HREEs (especially Thulium (Tm), Lu and Yb) are scarcely investigated (Cui et al., 2012; Oral et al., 2017; Zhang et al., 2010).

The aim of this review paper was to provide hazard concentrations at 5% and 50% effect via species sensitivity distributions in order to prioritize the risk of REEs highlighting potential knowledge gaps.

2 Materials and methods

2.1 Toxicity data selection and collection

A stepwise approach to identify papers about REEs toxicity data was used including various sources: Google Scholar, National Center for Biotechnology Information (NCBI), Web of Science (WoS®), and Scopus® (last update April 24, 2022). Only papers reporting original experimental data about freshwater and saltwater invertebrate and vertebrate non-mammal species were used. The following exclusion criteria were adopted: i) papers providing only nominal concentrations of REEs; ii) papers

related only to REEs in the nano-sized form (i.e., the way nanomaterials can interact with the biota can be different from the bulk form).

2.2 Data organization, treatment and management

Toxicity data were processed according to (L. Albarano et al., 2021; Burmaster and Hull, 1997) (Newman et al., 2000; Posthuma et al., 2002).

When toxicity data of REEs were duplicated for the same species and endpoint, their geometric mean was used for the relative evaluations (Kooijman, 1987). This occurred in particular for *P. subcapitata*, *D. magna*, *Hydrocharis dubia*, *Corbicula fluminea*, *T. platyurus*, and *Hydra attenuata*.

All details were reported in Supplementary Materials.

2.3 Species sensitivity distribution determination

The species sensitivity distribution (SSD) approach was used to better understand the taxonomic differences in species sensitivity for each REE. The SSD analysis is based on the cumulative probability distribution of toxicity values for multiple species and the obtained curves can describe the variation in the sensitivity among a set of species towards a contaminant by a statistical or empirical distribution function (Aldenberg and Jaworska, 2000) (Kooijman, 1987; Newman et al., 2000; Posthuma et al., 2002; Wagner and Løkke, 1991; Aldenberg and Slob, 1993). Generally, SSDs are generated from experimentally-derived toxicity data offering protection for the widest range of organisms in the field (Hose and Van Den Brink, 2004). The SSD approach was used to calculate the toxicant concentration at which a specific number of species can be affected identifying the hazardous concentration (HC) impairing the 5% (HC_5) and 50% (HC_{50}) of organisms (Posthuma et al., 2002; Newman et al., 2000).

Toxicity data were estimated using the cumulative SSD of the effective concentration at 10% effect (EC_{10}) according to (Van Vlaardingen PLA, 2007). When EC_{10} data were not available, the EC_{10} value was estimated as $EC_{50/3}$ as suggested by Beiras et al (1997) The EC_{10} data were log-transformed according to (L. Albarano et al., 2021; Burmaster and Hull, 1997) (Newman et al., 2000; Posthuma et al., 2002) using Equation 1:

$$\chi = log_{10}(C) \quad \text{(Equation 1)}$$

where C = toxicity data. When more than one toxicity data were available for the same species, the geometric mean was calculated and used as the estimate for this species according to (Kooijman, 1987).

The associated hazard was visualized as cumulative distribution function as defined in Equation 2:

$$y = \sum_{i=1}^{\kappa} n_i \quad \text{(Equation 2)}$$

where y is the cumulative distribution of species and ni is the absolute frequency of each single TD value.

The distribution model was fitted to toxicity data points obtained for the different species to a log-logistic model, using Equation 3:

$$\text{Cp} = y = \sum_{i=1}^{\kappa} n_i \quad \text{(Equation 3)}$$

where Cp is the cumulative probability of species, defined as (the order of the data point)/(1 + total number of data points). The median hazard concentration (HC_{50}) and the HC affecting the 5% (HC_5) of species were calculated according to (Aldenberg and Slob, 1993), using Equation 4:

$$\text{Log (HCp)} = \mu - Kp * \sigma \qquad \text{(Equation 4)}$$

where HCp is the hazardous concentration for a percentage of the species population, Kp is Aldenberg extrapolation factor that directly depends on the number of the studied species, and μ and σ are the mean and the standard deviation of the distribution, respectively.

3 Results

3.1 Papers collection and analysis

A total of 334 papers were identified and reviewed according to the abovementioned selection criteria. After the pre-revision phase, only 55 papers were shortlisted including toxicity data on invertebrate and vertebrate non-mammal species from freshwater and saltwater environments. The classified papers evidenced data distributed as follows: 17 papers (30.1%) for La, 16 papers (29.1%) papers for Ce, 10 papers (18.2%) for Gd, 6 papers (10.9%) for Y, 6 papers (10.9 %) for Nd, 5 papers (9.1 %) for Er, 4 papers (7.3%) for Pr, 4 papers (7.3%) for Sm, 4 papers (7.3%) for Dy, 3 papers (5.4%) for Lu, 2 papers (3.6%) for Tb, 1 paper (1.8%) for Yb, 1 paper (1.8 %) for Sc, 1 paper (1.8%) for Ho, and 1 paper (1.8%) for Tm.

Highly heterogeneous endpoints were evidenced including mortality, reproduction, growth inhibition, biota-sediment accumulation factor and bioaccumulation reduction, weight gain rate, feed coefficient, bioluminescence reduction, number of offsprings, reactive oxygen species, genotoxicity, swimming velocity, egg production, and hatching inhibition. Being some of these endpoints not directly related to the biological fitness, the paper focused on mortality (M), bioaccumulation (B) and growth inhibition (GI).

The systematic review of the shortlisted papers included the collection of the following information: taxonomy, endpoints (mortality (M), growth inhibition (IG) and bioaccumulation (B)), exposure time, types of compounds (i.e., ion, acetate chloride), effects of REEs (μg/L) (i.e., EC_{50}, EC_{10} and LC_{50}), water quality parameters (i.e., temperature (T), pH, salinity (S), dissolved organic carbon (DOC) and hardness (H)). All units of measure were converted to μg/L to facilitate data management and comparison. All data are summarized in Table S1 in Supplementary Materials.

3.2 Main trends in REEs toxicity data

Focusing on La toxicity, six taxonomic groups were tested (i.e., 17 species in total). Specifically, Macroalgae, Plants, Molluscs, Crustaceans, Cnidaria, and Fishes, were represented with 4, 1, 3, 5, 1 and 3 species, respectively. About Ce, we identified 13 testing species belonging to 6 taxonomic groups (Macroalgae, Crustaceans, Echinoderms, Cnidaria, Rotifers, and Fishes were represented with 3, 4, 2, 1, 1, and 2 species, respectively). About Gd, tested species were 13 belonging to 6 taxonomic groups [Macroalgae, (n = 2), Crustaceans, (n = 3), Echinoderms, (n = 5), Cnidaria, (n = 1), Rotifers (n = 1) and Fish (n = 2)]. About Nd, tested species were 7 belonging to 4 taxonomic groups [Macroalgae, (n = 2), Cnidaria (n = 1), Crustaceans, (n = 3) and Fish (n = 4)]. About Pr, tested species were 6 belonging to 3 taxonomic groups [Macroalgae (n = 2), Cnidaria (n = 1) and Crustaceans (n = 3)]. About Y, we identified 7 testing species belonging to 5 taxonomic groups (Macroalgae, Cnidaria, Molluscs, Crustaceans and Fishes were represented with 1, 1, 1, 1, and 3 species, respectively). About

Er, we identified 6 testing species belonging to four taxonomic groups Crustaceans (n = 1), Fishes (n = 1), Cnidaria (n = 1), and Echinoderms (n = 1). About Lu, tested species were 5 belonging to 5 taxonomic groups [Bacteria, (n = 1), Macroalgae, (n = 1), Cnidaria (n = 1), Rotifers (n = 1), and Echinoderms (n = 1)]. About Dy, we identified 5 testing species belonging to 4 taxonomic groups (Protists, Cnidaria, Echinoderms and Crustaceans were represented with 1, 1, 1, and 2 species, respectively). About Sm, we identified 5 testing species belonging to 4 taxonomic groups (Macroalgae, Cnidaria, Crustaceans, and Fishes were represented with 2, 1, 1 and 1 species, respectively). All information is included in table S1.

As shown in Table S1, toxicity data related to Tb, Yb, Ho, Sc, and Tm was so limited (Tb, n=3; Yb, n = 1; Ho, n = 1; Sc, n = 1; Tm, n = 1) that the related SSDs could not be constructed. About Yb and Ho, only 1 species belonging to 1 taxonomic groups (Echinoderms) were identified. About Sc and Tm, only 1 species belonging to Annelids and Crustaceans, respectively, were identified. About Pm and Eu no work was found meeting the criteria followed in this study.

Considering all REEs, the relative abundance of papers for each group of species was reported in Figure 1. The attention was mainly focused on Crustaceans (30.9 %), Macroalgae (23.6 %) and then on Cnidaria (12.7%), Echinoderms (10.9%), Fishes (10%) and others (≤ 4.5%). Focusing on species, as reported in Figure 2, the most investigated species were: *Hydra attenuata* (12.6%), *Pseudokirchneriella subcapitata* and *Thamnocephalus platyurus* (11.7 %), *Daphnia magna* (8.1 %), *Nitellopsis obtusa* (7.2 %), *Oncorhynchus mykiss* and *Sphaerechinus granularis* (6.3 %), *Heterocypris incongruens* (4.5 %), from *Hyalella azteca* to *Brachionus calyciflorus* (2.7 %), from *Chlorella vulgaris* to *Paracentrotus lividus* (1.8 %), from *Aliivibrio fischeri* to *Caenorhabditis elegans* (0.9 %).

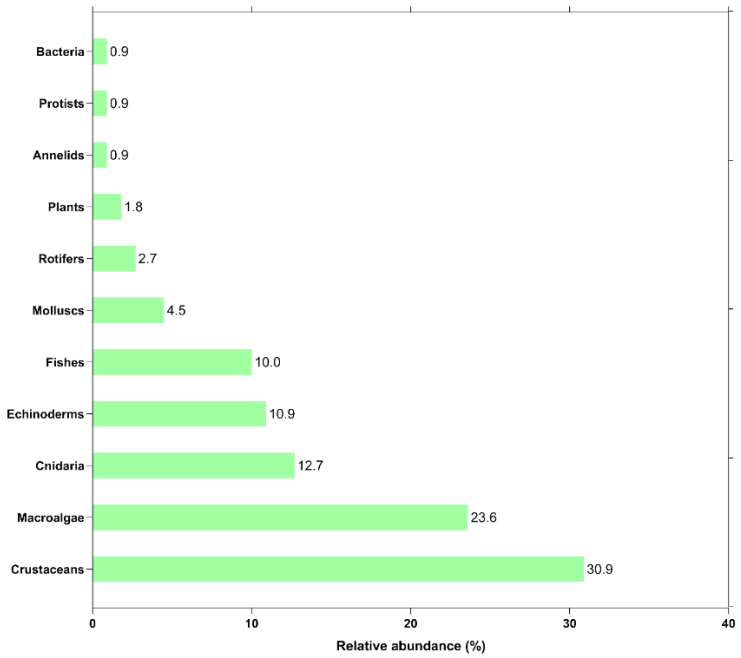

Figure 1. Comparison of the relative abundance (%) of papers for each groups of species studied in response to REEs.

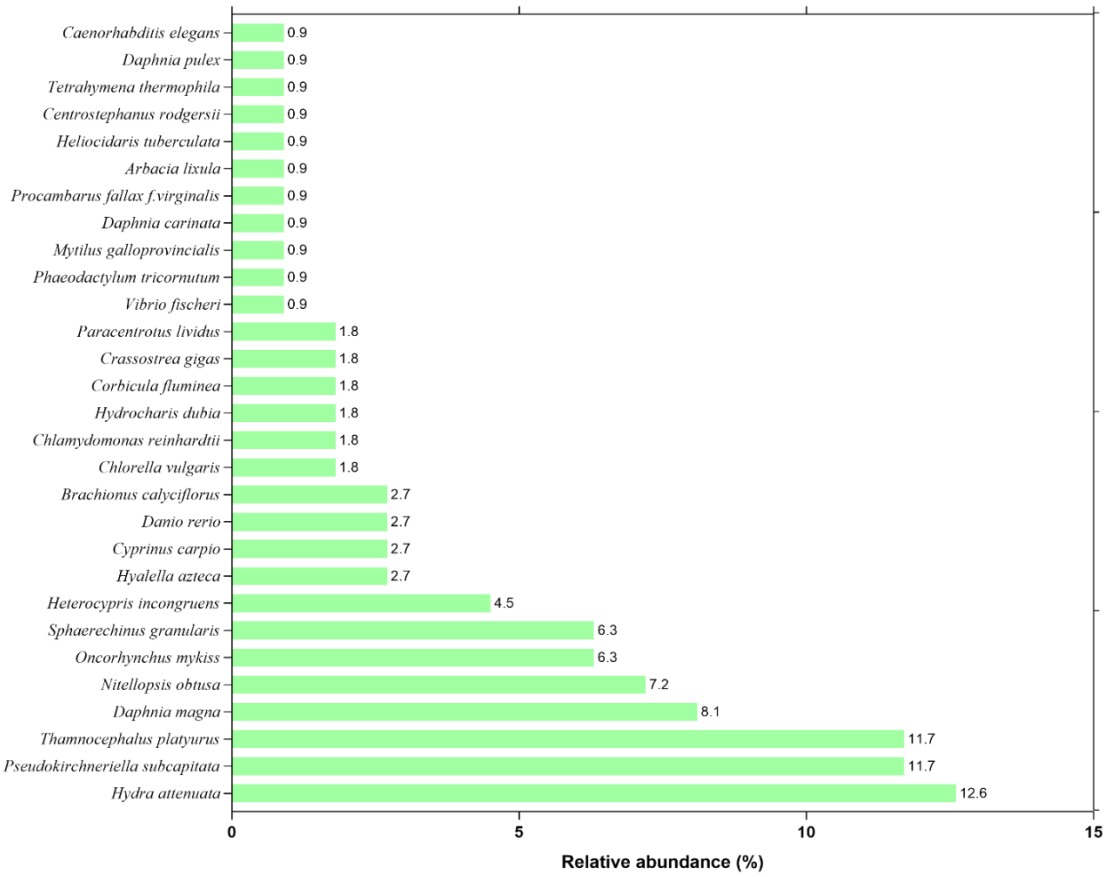

Figure 2. Comparison of the relative abundance (%) of papers for each species towards REEs.

3.3 REEs analyzed

As reported in Table 1, the acute toxicity data sets for La, Ce, Gd, Nd, Y, Pr, Er, Lu, Dy, and Sm were comparable in size, with smaller data sets for the other REEs. Results indicated that the log-logistic distribution fitted most of the groups data points. Data were presented on a species-by-species basis per single REE.

Table 1. Data quantity and goodness-of-fit of total species for ten REEs. p is the significance level.

REEs	Data quantity (n)	Adj-R2	*p*
La	17	99.01	<0.05
Ce	13	99.03	<0.05
Gd	13	99.11	<0.05
Nd	7	99.08	<0.05
Y	7	99.27	<0.05
Pr	6	99.19	<0.05
Er	6	99.20	<0.05
Lu	5	99.18	<0.05
Dy	5	99.00	<0.05
Sm	5	99.00	<0.05

3.4 Toxicity comparison of ten REEs on species-by-species basis

Considering the sensitivity of all groups of species to La, as shown in Figure 3a, the crustacean *Procambarus fallax f. virginalis* and the mollusc *Crassostrea gigas*, exhibited the highest sensitivity compared to all other species. The crustacean *D. magna* and fish *Oncorhynchus mykiss*, exhibited the lowest sensitivity, followed by mollusc *Corbicula fluminea*, and crustacean *Heterocypris incongruens*.

About Ce (Figure 3b), toxicity data of echinoderms *P. lividus* and *H. azteca*, showed the highest sensitivity with respect to all other species, whereas the crustacean *H. incongruens* and fish *O. mykiss*, exhibited the lowest sensitivity.

Considering Gd toxicity data, the fish *Cyprinus carpio* and the group of echinoderms, *especially P. lividus*, *Centrostephanus rodgersii*, *S. granularis* and *Arbacia lixula*, were largely sensitive than other organisms (Figure 3c). Together with *D. magna*, the crustacean *H. incongruens* was found to be the most resistant when exposed to Gd.

Taking into consideration Nd data (Figure 3d), the cnidaria *Hydra attenuata* and the crustacean *D. magna*, showed the highest sensitivity with respect to all other species, whereas the crustacean *H. incongruens* and the fish *O. mykiss* exhibited the lowest sensitivity.

Considering Y (Figure 3e), the fishes *C. carpio* and *Danio rerio* were the most sensitive species, while the macroalgae *Nitellopsis obtuse* and fish O. mykiss exhibited the lowest sensitivity.

As reported Figure 3f, the cnidaria *Hydra attenuata* and the crustacean *D. magna* showed the highest sensitivity, whereas the crustacean *H. incongruens* showed the least sensitivity to Pr.

In Figure 3g, the echinoderm *S. granularis*, followed by the crustacean *D. magna*, was the most sensitive organisms, while together with *T. platyurus*, the fish *O. mykiss* was found to be the most resistant when exposed to Er

Considering Lu toxicity data (Figure 3h), the rotifer *Brachionus calyciflorus*, followed by echinoderm *S. granularis*, showed the highest sensitivity. Bacteria, namely *V. fischeri*, was the least sensitive group of organisms.

Taking into consideration Dy toxicity data (Figure 3i), the crustacean *Daphnia pulex* was the most affected species, whereas the protist *Tetrahymena thermophila* exhibited the lowest sensitivity.

As reported Figure 3l, the macroalgae *Chlamydomonas reinhardtii* and *N. obtusa* were the most and the least sensitive species to Sm, respectively.

Crustaceans and Echinoderms groups seem to be highly sensitive when exposed to REEs. The *D. magna* and *S. granularis* were found to be the most sensitive when exposed to Er. *D. magna* was one of the most sensitive species when exposed to Nd and Pr, while *S. granularis* was the most sensitivity to Lu and Dy. In contrast, the fish group has shown great tolerance to rare earths. In particular, *O. mykiss* was found to be the most resistant when exposed to La, Ce, Nd, Y, Er and Sm. Our results agree with data reported by (Xin et al., 2015) that showed higher susceptibility to heavy metals of marine invertebrate than marine vertebrates. This different sensibility is probably due to the fact that the skin of vertebrates is much more resistant than the skin of invertebrates that are most sensitive to chemicals just after molting (i.e. for example the crustaceans) (Feder and Burggren, 1985; Hanazato, 2001) (Maier et al., 2022). Consequently, aquatic invertebrates accumulate high levels of inorganic

(i.e. heavy metals and REEs) and organic (i.e. for example polycyclic aromatic hydrocarbons) compounds in their tissues and cells where these compounds interact with cellular and molecular components (such as blockage of oxidative phosphorylation and DNA damage) causing high toxic effects (Luisa Albarano et al., 2021a, 2021b; Blaise et al., 2018; Chiarelli and Roccheri, 2014; Kim et al., 2014, 2017; Tamás et al., 2014; Trapasso et al., 2021a).

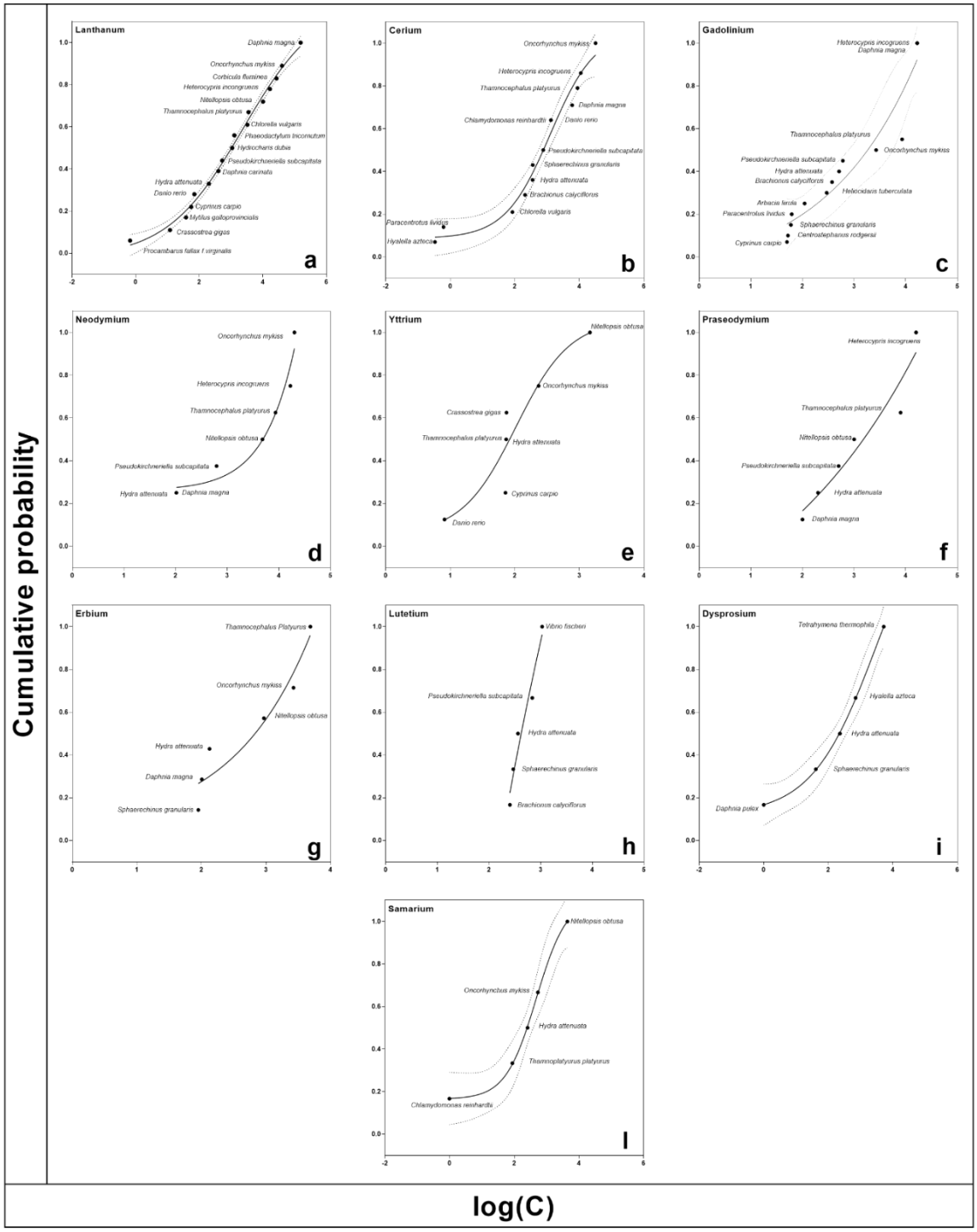

Figure 3. Species sensitivity distribution including all groups of species to a) Lanthanum; b) Cerium; c) Gadolinium; d) Neodynium; e) Yttrium; f) Praseodymium; g) Erbium; h) Lutetium; i) Dysprosium and l) Samarium.

3.5 Overall toxicity comparison of ten REEs

As shown in Figure 4, SSDs of ten rare earths elements based on the total species were constructed and the relationship of sensitivity between total species was investigated for all REEs.

The adverse effect of Lu, Ce and Er was in the middle among all REEs. The curves of La, Gd, Nd and Pr shifted on the right of graph, where at higher concentration the toxicity of La was higher. The toxicity curves of Y, Dy and Sm shifted on the left of other REEs and at lower concentrations, the toxicity of Y was largely higher. When the concentration was below 1 µg/l, there were no differences for the toxicities of Dy, Sm, Y, Ce and La, with Ce and La being slightly more toxic. As the concentration increased to 4 µg/l, the ecological risks of Y, Dy and Sm increased rapidly. The acute HC_5 values were respectively: 0.07 µg/l (CI = 0.002 – 0.98 µg/l) for Ce, 0.27 µg/l (CI = 0.03 – 1.03 µg/l) for Sm, 0.39 µg/l (CI = 0.09 – 0.96 µg/l) for Dy, 0.55 µg/l (CI = 0.47 – 1.25 µg/l) for La, 0.81 µg/l (CI = 0.32 – 1.36 µg/l) for Y, 1.12 µg/l (CI = 0.18 – 1.69 µg/l) for Gd, 1.35 µg/l (CI = 0.15 – 2.02 µg/l) for Er, 1.44 µg/l (CI = 0.32 – 2.23 µg/l) for Pr, 1.55 µg/l (CI = 0.11 – 2.36 µg/l) for Nd and 2.19 µg/l (CI = 1.55 – 2.44 µg/l) for Lu (Table 2). Specifically, the HC_5 value of Lu is 97% higher than HC_5. Similarly, the HC_{50} values were respectively determined to be 1.99 µg/l (CI = 1.49 – 2.48 µg/l) for Y, 2.11 µg/l (CI = 0.77 – 3.45 µg/l) for Dy, 2.14 µg/l (CI = 0.85 – 3.43 µg/l) for Sm, 2.62 µg/l (CI = 1.87 - 3.37 µg/l) for Ce, 2.66 µg/l (CI = 2.41 - 2.91 µg/l) for Lu, 2.69 µg/l (CI = 2.06 - 3.33 µg/l) for Er, 2.72 µg/l (CI = 2.25 - 3.19 µg/l) for Gd, 2.90 µg/l (CI = 2.36 - 3.45 µg/l) for La, 3.02 µg/l (CI = 2.28 - 3.76 µg/l) for Pr and 3.28 µg/l (CI = 2.55 - 4.01 µg/l) for Nd. In particular, the HC_{50} value of Nd (3.28 µg/L) is 40% higher than the HC_{50} of Y. These results manifested that all the considered REEs could represent a potential hazard to freshwater and saltwater organisms. The sensitivity to REEs was as follows: Ce > Sm > Dy > La > Y > Gd > Er > Pr > Nd > Lu for HC5 and Y > Dy > Sm > Ce > Lu > Er > Gd > Pr > La > Nd for HC_{50} (Table 2).

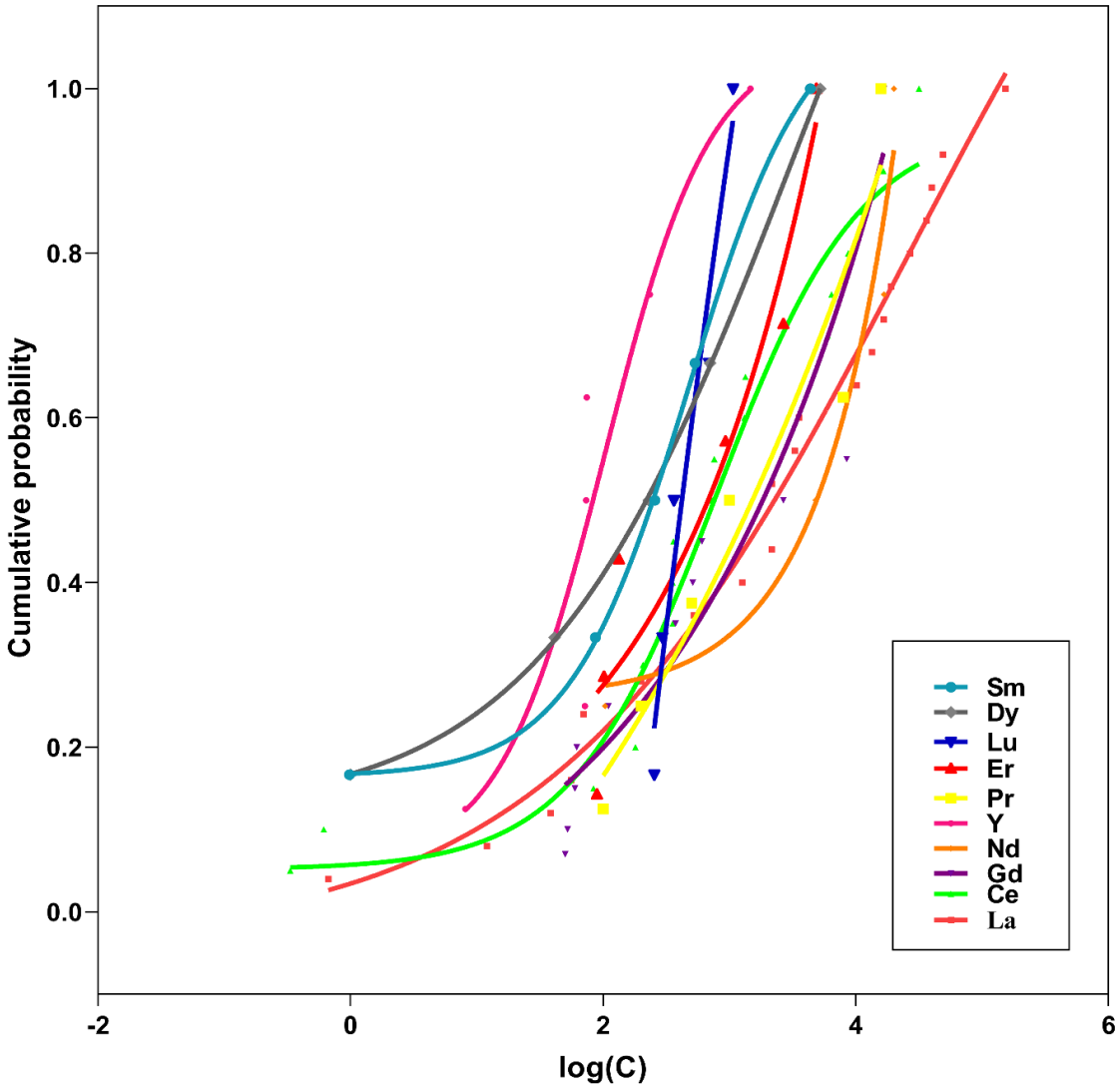

Figure 4. SSD curves for total species exposed to different REEs.

Table 2. The calculated HC_5 and HC_{50} values of total species for ten rare earths elements. The values were expressed in μg/L.

	HC_5	CI	HC_{50}	CI
La	0.55	0.47 - 1.25	2.90	2.36 - 3.45
Ce	0.07	0.002 - 0.98	2.62	1.87 - 3.37
Gd	1.12	0.18 - 1.69	2.72	2.25 - 3.19
Nd	1.55	0.11 - 2.36	3.28	2.55 - 4.01
Y	0.81	0.32 - 1.36	1.99	1.49 - 2.48
Pr	1.44	0.32 - 2.23	3.02	2.28 - 3.76
Er	1.35	0.15 - 2.02	2.69	2.06 - 3.33
Lu	2.19	1.55 - 2.44	2.66	2.41 - 2.91
Dy	0.39	0.09 - 0.96	2.11	0.77 - 3.45
Sm	0.27	0.03 - 1.03	2.14	0.85 - 3.43

Clustering the HC_5 values of REEs according to an order of magnitude range resulted in the following groups (Libralato et al., 2010):

- 0.01- 0.1 µg/L: Ce;

- 0.1-1 µg/L: Sm, Dy, La and Y;

- 1- 10 µg/L: Gd, Er, Pr, Nd, and Lu.

The HC_{50} values felt all in the 1-10 µg/L cluster.

All REEs presented an HC_5 and HC_{50} < 1 mg/L suggesting that all the 10 considered REEs can be of potential concern for the biota according to their background levels (Migaszewski and Gałuszka, 2015). Most HC_5 values were in the 0.01-2 µg/L range (n = 9), while only the HC_5 value of Lu was higher than 2 µg/L.

Moreover, a big gap into the knowledge about Tb, Ho, Sc, Yb, Tb, Eu and Tm biological implications is currently existing.

4 Conclusions

The effects of REEs on the biota have been only partly explored with the current database being still quite incomplete. Cerium, Gd, and La were the most investigated elements, while Ho, Sc, Yb, Tb, Eu and Tm presented just few data being not sufficient to generate the relative SSD curves.

This review paper prioritized the toxicity of 10 REEs (except for Ho, Sc, Yb, Tb, Eu and Tm) according to both HC_{50} and HC_5 values. On the basis of HC_5 value, the most toxic element was Ce (HC_5 = 0.07 µg/l), while Lu was the least toxic (HC_5 = 2.19 µg/l). On the basis of HC_{50} value, the most toxic element was Y (HC_{50} = 1.99 µg/l), while Nd was the least toxic (HC_{50} = 3.28 µg/l).

The to-do-list for the near future research activity can be summarized as follows:

- explore under an experimental viewpoint the potential effects of Ho, Sc, Yb, Tb, Eu and Tm considering measured concentrations on a wide range of biological models and exposure concentrations;

- investigate emerging sources of REEs especially focusing on e-waste and their potential biogeochemical cycles alteration;

- identify on a PEC/PNEC approach the potential environmental risk of REEs considering the current knowledge on their environmental concentrations including natural background levels and anthropogenic conditioned matrices in a one health perspective considering specific target environments.

Supplementary materials

Supplementary Table S1. Group of organisms, species, time of exposure, types of compounds, concentrations, endpoints, effects and references of negative impact of cerium. M = Mortality, B = Bioaccumulation, IG = inhibition growth, T = Temperature, RT = room temperature, DOC = dissolved organic carbon, H = hardness, A = alkalinity, S = salinity, n.a. = not available.

REEs	Group of organisms	Species	Expusure Time (days; *h; +min)	Types of compound	Endpoints	EC_{50} (µg/l)	EC_{10} (µg/l)	Experimental parameters	References
Lanthanum	Macroalgae	*Pseudokirchneriella subcapitata*	3 days	Lanthanum nitrate	IG	1270	423	T =24 ± 1 °C	(Joonas et al., 2017)
Lanthanum	Macroalgae	*Pseudokirchneriella subcapitata*	3 days	Lanthanum ion	IG	751	751	pH=4	(Siciliano et al., 2021a)
Lanthanum	Macroalgae	*Pseudokirchneriella subcapitata*	3 days	Lanthanum ion	IG	400	400	pH=7.8	(Siciliano et al., 2021b)
Lanthanum	Macroalgae	*Chlorella vulgaris*	4 days	Lanthanum nitrate	IG	3271	3271	pH= 8.0, T=23 ±,1 °C	(Sun et al., 2019)
Lanthanum	Macroalgae	*Nitellopsis obtusa*	24 days	Lanthanum ion	M	10600	3533	T = 15-18 °C	(Manusadžianas et al., 2020)
Lanthanum	Macroalgae	*Phaeodactylum tricornutum*	4 days	Lanthanum nitrate	IG	1262	1262	pH= 8.0, T=23 ±1 °C.	(Sun et al., 2019)
Lanthanum	Plants	*Hydrocharis dubia*	7 days	Lanthanum nitrate	B	2.6	1.30	n.a.	(Xu et al., 2012)
Lanthanum	Plants	*Hydrocharis dubia*	7 days	Lanthanum nitrate	IG	6498	2166	n.a.	(Xu et al., 2012)
Lanthanum	Molluscs	*Mytilus galloprovincialis*	28 days	Lanthanum chloride	B	383	38.3	T=18°C ± 1, S = 30± 1, pH=7.8± 1	(Pinto et al., 2019)
Lanthanum	Molluscs	*Corbicula fluminea*	28 days	Lanthanum chloride	B	49000	4900	T= 18.0 °C, DOC= 7.8–8.6 mg L−1, pH=7.9–8.0	(Zhao and Liu, 2018)
Lanthanum	Molluscs	*Corbicula fluminea*	28 days	Lanthanum chloride	M	49000	49000	T= 18.0 °C, DOC= 7.8–8.6 mg L−1, pH=7.9–8.1	(Zhao and Liu, 2018)
Lanthanum	Molluscs	*Crassostrea gigas*	2 days	Lanthanum ion	M	36	12	T = 24 ± 1 °C	(Moreira et al., 2020)
Lanthanum	Crustaceans	*Daphnia magna*	2 days	Lanthanum nitrate	M	50000	16667	T=20°C, pH=7.4	(Blinova et al., 2018)
Lanthanum	Crustaceans	*Daphnia magna*	5 days	Lanthanum nitrate	IG	871000	290333	T=20°C, pH=7.5	(Lürling and Tolman, 2010)
Lanthanum	Crustaceans	*Daphnia carinata*	2 days	Lanthanum ion	M	1200	400	T=20°C	(Barry and Meehan, 2000)

Lanthanum	Crustaceans	*Thamnocephalus platyurus*	24*	Lanthanum nitrate	M	50000	16667	T=20°C, pH=7.4	(Blinova et al., 2018)
Lanthanum	Crustaceans	*Thamnocephalus platyurus*	24*	Lanthanum ion	M	10600	3533	T = 15-18 °C	(Manusadžianas et al., 2020)
Lanthanum	Crustaceans	*Procambarus fallax f.virginalis*	28 days	Lanthanum ion	B	2	0.67	T=20°C, pH=7.4	(Van Oosterhout et al., 2014)
Lanthanum	Crustaceans	*Heterocypris incongruens*	6 days	Lanthanum nitrate	M	50000	16667	T=20°C, pH=7.4	(Blinova et al., 2018)
Lanthanum	Cnidaria	*Hydra attenuata*	4 days	Lanthanum chloride	M	210	70	T=25°C	(Blaise et al., 2018)
Lanthanum	Fishes	*Cyprinus carpio*	45 days	Lanthanum nitrate	B	500	56	T=11-14°C, pH=6	(Qiang et al., 1994)
Lanthanum	Fishes	*Oncorhynchus mykiss*	4 days	Lanthanum chloride	M	120000	40000	T=15 °C	(Dubé et al., 2019)
Lanthanum	Fishes	*Danio rerio*	4 days	Lanthanum chloride	M	603	201	T=25°C	(Cui et al., 2012)
Cerium	Macroalgae	*Pseudokirchneriella subcapitata*	30+	Cerium Chloride	IG	6317	2106	T=25°C	(González et al., 2015)
Cerium	Macroalgae	*Pseudokirchneriella subcapitata*	3 days	Cerium nitrate	IG	1230	410	T=25°C	(Joonas et al., 2017)
Cerium	Macroalgae	*Pseudokirchneriella subcapitata*	3 days	Cerium ion	IG	14	14	pH = 3	(Siciliano et al., 2021a)
Cerium	Macroalgae	*Pseudokirchneriella subcapitata*	3 days	Cerium ion	IG	500	500	pH = 7.8	(Siciliano et al., 2021b)
Cerium	Macroalgae	*Chlorella vulgaris*	24*	Cerium nitrate	M	252	84	T=37 °C	(Evseeva et al., 2010)
Cerium	Macroalgae	*Chlamydomonas reinhardtii*	3 days	Cerium nitrate	IG	4000	1333	n.a.	(Taylor et al., 2016)
Cerium	Crustaceans	*Daphnia magna*	21 days	Cerium Chloride	M	245	82	T = 20°C, pH=7.8, H=160 mg/L, DOC = 6.5 mg/L	(Galdiero et al., 2019)
Cerium	Crustaceans	*Daphnia magna*	2 days	Cerium nitrate	M	50000	16667	T=20°C, pH=7.4-8.0	(Blinova et al., 2018)
Cerium	Crustaceans	*Daphnia magna*	2 days	Cerium nitrate	M	3489	1163	T = 20 ±2 °C	(Ma et al., 2016)
Cerium	Crustaceans	*Thamnocephalus platyurus*	24*	Cerium nitrate	M	50000	16667	T=20°C, pH=7.4-8.0	(Blinova et al. 2018)
Cerium	Crustaceans	*Thamnocephalus platyurus*	24*	Cerium ion	M	2230	743	T = 25 °C	(Manusadžianas et al., 2020)
Cerium	Crustaceans	*Heterocypris incogruens*	6 days	Cerium nitrate	M	33100	11033	T=20°C, pH=7.4-8.0	(Blinova et al. 2018)

Cerium	Crustaceans	*Hyalella azteca*	4 days	Cerium Ion	M	2000	0.61	pH 7.1 ± 0.1 , T=21 ± 1°C	(Vukov, 2015)
Cerium	Echinoderms	*Sphaerechinus granularis*	3 days	Cerium Chloride	IG	1079	360	pH=8.1,T =18°C	(Gravina et al., 2018)
Cerium	Echinoderms	*Paracentrotus lividus*	3 days	Cerium Chloride	IG	1	0.33	pH=8.1,T =18°C	(Pagano et al., 2016)
Cerium	Cnidaria	*Hydra attenuata*	3 days	Cerium Chloride	IG	1797	599	T=25 °C	(Gonzalez et al. 2015)
Cerium	Cnidaria	*Hydra attenuata*	3 days	Cerium Chloride	M	330	110	T=25 °C	(Blaise et al., 2018)
Cerium	Rotifers	*Brachionus calyciflorus*	2 days	Cerium Chloride	IG	620	207	T=25 °C	(González et al., 2015)
Cerium	Fishes	*Oncorhynchus mykiss*	4 days	Cerium Chloride	M	95000	31667	T=15 °C	(Dubé et al., 2019)
Cerium	Fishes	*Danio rerio*	3 days	Cerium ion	M	3940	1313	T = 22-25 °C	(Shahnaz et al., 2022)
Gadolinium	Macroalgae	*Pseudokirchneriella subcapitata*	3 days	Praseodymium nitrate	IG	1210	403	T=25 °C	(Joonas et al., 2017)
Gadolinium	Macroalgae	*Pseudokirchneriella subcapitata*	3 days	Gadolinium chloride	IG	3111	1037	T=25 °C	(González et al., 2015)
Gadolinium	Macroalgae	*Pseudokirchneriella subcapitata*	3 days	Gadolinium ion	IG	1136	379	pH=4	(Siciliano et al., 2021a)
Gadolinium	Macroalgae	*Nitellopsis obtusa*	24 days	Gadolinium ion	M	900	300	T = 15-18 °C	(Manusadžianas et al., 2020)
Gadolinium	Crustaceans	*Daphnia magna*	2 days	Gadolinium nitrate	M	50000	16667	T=20°C, pH=7.4	(Blinova et al., 2018)
Gadolinium	Crustaceans	*Heterocypris incogruens*	6 days	Gadolinium nitrate	M	50000	16667	T=20°C, pH=7.4	(Blinova et al., 2018)
Gadolinium	Crustaceans	*Thamnocephalus platyurus*	24*	Gadolinium nitrate	M	50000	16667	T=20°C, pH=7.4	(Blinova et al., 2018)
Gadolinium	Crustaceans	*Thamnocephalus platyurus*		Gadolinium ion	M	900	300	T = 25 °C	(Manusadžianas et al., 2020)
Gadolinium	Echinoderms	*Sphaerechinus granularis*	3 days	Gadolinium ion	IG	179	60	pH=8.1, T=18°C	(Gravina et al., 2018)
Gadolinium	Echinoderms	*Paracentrotus lividus*	2 days	Gadolinium ion	IG	185	62	T = 18-20 °C	(Martino et al., 2017)
Gadolinium	Echinoderms	*Arbacia lixula*	2 days	Gadolinium ion	IG	330	110	T = 18-20 °C	(Martino et al., 2017)

Gadolinium	Echinoderms	*Heliocidaris tuberculata*	2 days	Gadolinium ion	IG	879	293	T = 18-20 °C	(Martino et al., 2017)
Gadolinium	Echinoderms	*Centrostephanus rodgersii*	2 days	Gadolinium ion	IG	157	52	T = 18-20 °C	(Martino et al., 2017)
Gadolinium	Cnidaria	*Hydra attenuata*	4 days	Gadolinium chloride	M	2549	850	T=23°C	(González et al., 2015)
Gadolinium	Cnidaria	*Hydra attenuata*		Gadolinium chloride	M	520	173	T=20-25°C	(Blaise et al., 2018)
Gadolinium	Rotifers	*Brachionus calyciflorus*	2 days	Gadolinium chloride	IG	1120	373	T=25°C	(González et al., 2015)
Gadolinium	Fishes	*Oncorhynchus mykiss*	4 days	Gadolinium chloride	M	8000	2667	T=15°C	(Dubé et al., 2019)
Gadolinium	Fishes	*Cyprinus carpio*	45 days	Gadolinium nitrate	B	500	50	T=11-14°C, pH=6	(Qiang et al., 1994)
Neodymium	Macroalgae	*Nitellopsis obtusa*	24 days	Neodymium ion	M	14400	4800	T = 15-18 °C	(Manusadžianas et al., 2020)
Neodymium	Macroalgae	*Pseudokirchneriella subcapitata*	3 days	Neodymium ion	IG	1860	620	pH = 4	(Siciliano et al., 2021a)
Neodymium	Cnidaria	*Hydra attenuata*	4 days	Neodymium chloride	M	310	103	T=25°C	(Blaise et al., 2018)
Neodymium	Crustaceans	*Daphnia magna*	2 days	Neodymium nitrate	M	310	103	T=20°C, pH=8.0	(Blinova et al., 2018)
Neodymium	Crustaceans	*Thamnocephalus platyurus*	24*	Neodymium nitrate	M	50000	16667	T=20°C, pH=8.0	(Blinova et al., 2018)
Neodymium	Crustaceans	*Thamnocephalus platyurus*	24*	Neodymium ion	M	1520	507	T = 15-18 °C	(Manusadžianas et al., 2020)
Neodymium	Crustaceans	*Heterocypris incogruens*	6 days	Neodymium nitrate	M	50000	16667	T=20°C, pH=8.0	(Blinova et al., 2018)
Neodymium	Fishes	*Oncorhynchus mykiss*	4 days	Neodymium chloride	M	60000	20000	T=15°C	(Dubé et al., 2019)
Praseodymium	Macroalgae	*Pseudokirchneriella subcapitata*	3 days	Praseodymium nitrate	IG	1360	453	T=25°C	(Joonas et al., 2017)
Praseodymium	Macroalgae	*Nitellopsis obtusa*	24 days	Praseodymium ion	M	3170	1057	T=25°C	(Manusadžianas et al., 2020)
Praseodymium	Cnidaria	*Hydra attenuata*	4 days	Praseodymium chloride	M	560	187	T=25°C	(Blaise et al., 2018)

Praseodymium	Crustaceans	*Daphnia magna*	2 days	Praseodymium nitrate	M	290	97	T=20°C, pH=7.4	(Blinova et al., 2018)
Praseodymium	Crustaceans	*Thamnocephalus platyurus*	24*	Praseodymium nitrate	M	50000	16667	T=20°C, pH=7.	(Blinova et al., 2018)
Praseodymium	Crustaceans		24*	Praseodymium ion	M	1980	660	T=25°C	(Manusadžianas et al., 2020)
Praseodymium	Crustaceans	*Heterocypris incogruens*	6 days	Praseodymium nitrate	M	50000	16667	T=20°C, pH=7.4	(Blinova et al., 2018)
Yttrium	Macroalgae	*Nitellopsis obtusa*	24 days	Yttrium ion	M	4380	1460	T=25°C	(Manusadžianas et al., 2020)
Yttrium	Cnidaria	*Hydra attenuata*	4 days	Yttrium chloride	M	220	73	T=25°C	(Blaise et al., 2018)
Yttrium	Molluscs	*Crassostrea gigas*	2 days	Yttrium ion	M	222	74	T=25°C	(Moreira et al., 2020)
Yttrium	Crustaceans	*Thamnocephalus platyurus*	24*	Yttrium ion	M	220	73	T=25°C	(Manusadžianas et al., 2020)
Yttrium	Fishes	*Danio rerio*	4 days	Yttrium chloride	M	268	8	pH=7.0, H = 65mg/L, T=27°C	(Cui et al., 2012)
Yttrium	Fishes	*Cyprinus carpio*	45 days	Yttrium nitrate	B	500	71	T=11-14°C, pH=6, FW	(Qiang et al., 1994)
Yttrium	Fishes	*Oncorhynchus mykiss*	4 days	Yttrium chloride	M	700	233	T=15°C, FW	(Dubé et al., 2019)
Erbium	Macroalgae	*Nitellopsis obtusa*	24 days	Erbium ion	M	2790	930	T = 15-18 °C	(Manusadžianas et al., 2020)
Erbium	Crustaceans	*Daphnia magna*	21 days	Erbium cloride	M	304	101	T = 20°C, pH=7.8, H =160 mg/L, DOC = 6.5 mg/L	(Galdiero et al., 2019)
Erbium	Crustaceans	*Thamnocephalus Platyurus*	24*	Erbium ion	M	14600	4867	T = 15-18 °C	(Manusadžianas et al., 2020)
Erbium	Fishes	*Oncorhynchus mykiss*	4 days	Erbium cloride	M	8000	2667	T = 15°C	(Dubé et al., 2019)
Erbium	Cnidaria	*Hydra attenuata*	4 days	Erbium cloride	M	400	133	T=20-25°C	(Blaise et al., 2018)
Erbium	Echinoderms	*Sphaerechinus granularis*	3 days	Erbium cloride	IG	268	89	pH=8.1, T=18°C	(Gravina et al., 2018)

Lutetium	Bacteria	*Vibrio fischeri*	30+	Lutetium chloride	IG	3200	1067	T=25°C	(González et al., 2015)
Lutetium	Algae	*Pseudokirchneriella subcapitata*	3 days	Lutetium chloride	IG	2062	687	T=25°C	(González et al., 2015)
Lutetium	Cnidaria	*Hydra attenuata*	4 days	Lutetium chloride	M	1886	629	T=25°C	(González et al., 2015)
Lutetium	Cnidaria	*Hydra attenuata*	5 days	Lutetium chloride	M	290	97	T=25°C	(Blaise et al., 2018)
Lutetium	Rotifers	*Brachionus calyciflorus*	2 days	Lutetium chloride	IG	760	253	T=25°C	(González et al., 2015)
Lutetium	Echinoderms	*Sphaerechinus granularis*	3 days	Lutetium chloride	IG	882	294	pH=8.1, , T=18°C	(Gravina et al., 2018)
Dysprosium	Protists	*Tetrahymena thermophila*	24*	Dysprosium ion	M	15700	5233	T=25°C	(Manusadžianas et al., 2020)
Dysprosium	Cnidaria	*Hydra attenuata*	4 days	Dysprosium chloride	M	690	230.00	T=20-25°C	(Blaise et al., 2018)
Dysprosium	Echinoderms	*Sphaerechinus granularis*	4 days	Dysprosium chloride	IG	123	41	pH=8.1, T=18°C	(Gravina et al. 2018)
Dysprosium	Crustaceans	*Hyalella azteca*	3 days	Dysprosium ion	M	2100	700	pH=7.8, T= 23±1°C	(Vukov et al., 2016)
Dysprosium	Crustaceans	*Daphnia pulex*	2 days	Dysprosium ion	M	3	1	pH=7.8, T= 23±1°C	(Vukov et al., 2016)
Samarium	Macroalgae	*Chlamydomonas reinhardtii*	60+	Samarium ion	B	150360	0.98	T=20°C, pH = 6.0	(Rowell et al., 2018)
Samarium	Macroalgae	*Nitellopsis obtusa*	24 days	Samarium ion	M	13100	4367	T=15°C	(Manusadžianas et al., 2020)
Samarium	Cnidaria	*Hydra attenuata*	4 days	Samarium chloride	M	770	257	T=25°C	(Blaise et al., 2018)
Samarium	Crustaceans	*Thamnoplatyurus platyurus*	24*	Samarium ion	M	260	87	T=25°C	(Manusadžianas et al., 2020)
Samarium	Fishes	*Oncorhynchus mykiss*	4 days	Samarium chloride	M	1600	533	T=15°C	(Dubé et al., 2019)
Terbium	Macroalgae	*Nitellopsis obtusa*	24 days	Terbium ion	M	8670	2890	T = 25°C	(Manusadžianas et al., 2020)

Terbium	Cnidaria	*Hydra attenuata*	4 days	Terbium chloride	M	700	233	T = 25°C	(Blaise et al., 2018)
Terbium	Crustaceans	*Thamnocephalus Platyurus*	24*	Terbium ion	M	510	170	T = 25°C	(Manusadžianas et al., 2020)
Ytterbium	Echinoderms	*Sphaerechinus granularis*	3 days	Ytterbium chloride	IG	2069	690	pH=8.1, T=18°C	(Gravina et al., 2018)
Holmium	Echinoderms	*Sphaerechinus granularis*	3 days	Holmium cloride	M	2299	766	pH=8.1, T=18°C,	(Gravina et al. 2018)
Scandium	Annelids	*Caenorhabditis elegans*	4 days	Scandium chloride	IG	87800	29267	T=20°C	(Xu et al., 2017)
Tulium	Crustaceans	*Hyalella azteca*	5 days	Tulium ion	M	742	247	pH 7.3	(Loveridge et al., 2021)

Cerium, gadolinium, lanthanum, and neodymium effects in simplified acid mine discharges to *Raphidocelis subcapitata*, *Lepidium sativum*, and *Vicia faba*

1 Introduction

Rare earth elements (REEs) are key components of many emerging technologies in industry, agriculture, and medicine due to their unique physical and chemical properties (Gwenzi et al., 2018; Pagano et al., 2015b; Romero-Freire et al., 2018; Takaya et al., 2018). Concerns are rising about the potential increased alterations of REEs biogeochemical cycles due to Anthropocene (Galdiero et al., 2019; Moreira et al., 2020). At present, five REEs are labelled as critical for energy production (neodymium, europium, terbium, dysprosium, and yttrium) and two additional ones as nearly critical (cerium and lanthanum) (Romero-Freire et al., 2018; US DOE, 2012). Currently, REEs do not present any threshold limit values for national and international regulations, but they can be considered as new emerging contaminants with still unknown effects (Galdiero et al., 2019). Two main sources of REEs can be found: 1) direct from active or non-active mining ores activities; 2) indirect from mineral processing and industrial use including the waste cycle (Gwenzi et al., 2018).

REEs can be considered as lithophile elements substituting other cations of comparable radius and charge in several mineral structures like silicates, carbonates, oxides, phosphates, and related oxyhydroxysalts (Migaszewski and Gałuszka, 2015). The principal mineral sources of REEs are bastnaesite, monazite, and loparite and the lateritic ion-adsorption clays (Balaram, 2019). Although REEs are abundant in the earth's crust ("not rare"), the ability for mining tends to make them very scarce (de Boer and Lammertsma, 2013; Thomas et al., 2014). REEs are not individual native metals, but they occur together in numerous ore/accessory minerals as either minor or major constituents. Sites in areas impacted by mining activities, not only related to REEs extraction, and industry have been shown to contain REEs with concentrations up to 100 times higher than normal background levels (Gwenzi et al., 2018). Mining activities such as cutting, drilling, blasting, transportation, stockpiling, and processing have been linked to severe environmental and health damages in countries such as China, United States of America (USA), India, Malaysia, and Brazil (Adeel et al., 2019; Balaram, 2019; Galhardi et al., 2020b; Liang et al., 2014). Acid mine drainage (AMD) has recently raised a great deal of attention as a potential significant source of REEs directly able to affect environmental and human health, if not adequately collected and treated. AMD is composed of acidic wastewater (i.e., approximately pH < 5, but it depends on a site-by-site basis) presenting a generally high amount of sulphate and other metals in a dissolved form including rare earth elements (REEs) ranging from ng/L up to thousands of mg/L and more on a site-specific basis (Migaszewski and Gałuszka, 2015). The median concentration of REEs in European Union stream sediment was 198.9 mg/kg (Salminen, 2005), reaching 457.7 µg/L in USA ore mine effluent and 61.3 µg/L in China coal mine effluent, while in surface water their concentration ranged from 75.03 µg/L up to 518.7 µg/L (Migaszewski and Gałuszka, 2015). Zhao et al. (2007) indicated that the REE-sulphate complexes are the main form of dissolved REEs concentration in acid mine wastewater representing more than 60% of the total amount, followed by free metal species form. The presence of REEs in AMD and its acidic pH can increase their mobility and bioavailability in the various environmental compartments with potential negative effects on a one-health approach, especially in mining areas (i.e., both active or abandoned sites) (Cravotta, 2008; Rim et al., 2013; Stewart et al., 2017; Sun et al., 2017). When the intensity of acidity reaches a baseline ecotoxicity threshold, it can affect organisms through direct acute damage and indirect acidified soil and water (Gonzalez-Gil et al., 2012; Li et al., 2020; Lopes et al., 1999; Xia et al., 2017). Thus, the combined REEs pollution and acid conditions from AMD could adversely affect the structure and function of aquatic ecosystem changing the productivity and

the abundance in biomass or even could lead to the elimination of aquatic species (Bott et al., 2012; Kraus and Pomeranz, 2020).

Relatively scarce information is available to date on REEs-associated biological effects, including bioassays on model organisms, and human health effects (Galdiero et al., 2019; Gravina et al., 2018; Pagano et al., 2015b, 2015a). A recognized mechanism of action in REEs-associated health effects relates to modulating oxidative stress including various endpoints such as growth inhibition, cytogenetic effects, and organ-specific damage (Manier et al., 2013; Tai et al., 2010). Even less is known about the REEs toxicity at low pH levels. Only few papers evidenced that low pHs (i.e., mine wastewater) can modify their biological activity increasing aquatic toxicity (Haferburg et al., 2007; Romero et al., 2010), where a relevant role is also played by organic and inorganic ligands (Thomas et al., 2014). In particular, primary producers can be highly sensitive indicators of toxic effects due to the aquatic exposure to REEs dissolved in AMD. As a parallelism, we must remember that the notorious Itai-Itai disease was caused by the consumption of rice contaminated by cadmium from cultures irrigated with AMD (Inaba et al., 2005). d'Aquino L et al. (2009) stated that few data about REEs effects on macrophytes were available from the scientific literature and, to the best of our knowledge, such scarcity persist today. The need to investigate photosynthetic organisms in relation to AMD contamination (i.e., surface water polluted by uncontrolled and untreated AMD, and direct irrigation with contaminated AMD) pushes ahead the present research topic.

This study evaluated the adverse effects of cerium (Ce), lanthanum (La), gadolinium (Gd), and neodymium (Nd) on *Raphidocelis subcapitata* (green microalgae), and *Lepidium sativum* (macrophyte), and *Vicia faba* (macrophyte) considering a background multi-endpoint approach (i.e., growth inhibition, germination index, and genotoxicity) to check the effect of spiked simplified AMD investigating the role of two pH values (4 and 6) in potential toxicity modification. Graph 1 represents an abstract of the study elaborated.

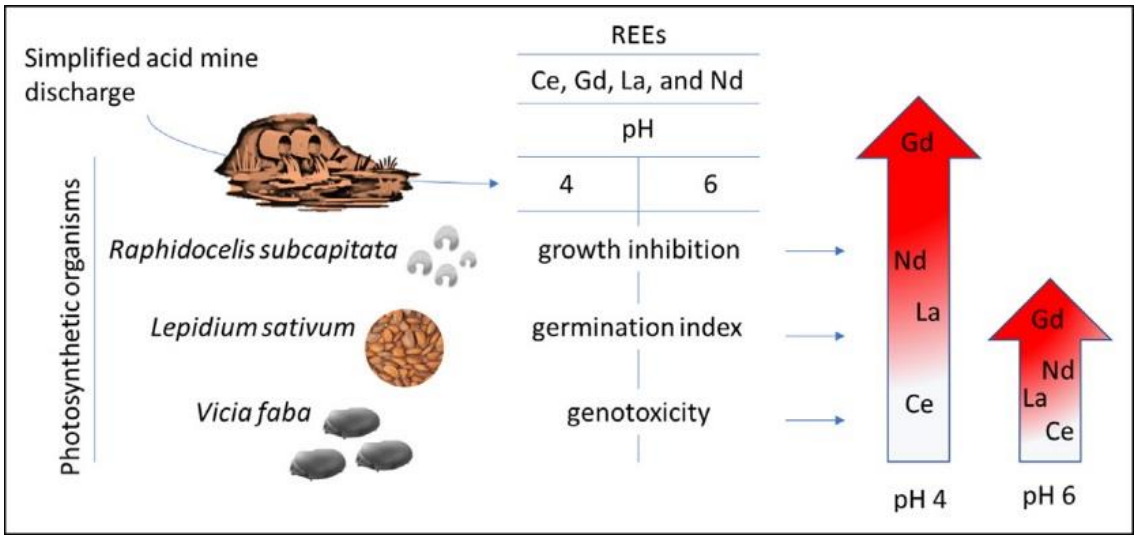

Graph 1. Graphical abstract of the study.

2 Materials and methods

2.1 Analytical methods

Trichloride anhydrous salts of Ce (III), La(III), Gd(III), and Nd(III) were purchased from Sigma-Aldrich (Italy). All chemicals were of analytical grade. Testing solutions were prepared from 1 M stock solutions per element in ultra-pure distilled water stored at 4 °C. Stock solutions were diluted to the final test concentrations using freshwater medium (ISO, 2012a) buffered at pH values 4 and 6. The pH was measured with a pH-meter (Mettler Toledo Five Easy, Milan, Italy). The experimental design included 4 exposure concentrations (i.e., 0.01, 0.1, 1, and 10 mg/L – nominal concentrations). Real concentrations were determined by Inductively Coupled plasma mass spectrometry (ICP-MS, Aurora Bruker M90, Bremen, Germany) following previously established protocols and quality assurance and quality control laboratory procedures according to Pagano et al. (2016). The limits of detection (LOD) and quantification (LOQ) were as follows for Ce, Gd, La, and Nd: 0.0010, 0.0018, 0.0006, and 0.0011 µg/L as LOD; and 0.0035, 0.0058, 0.0021, and 0.0037 µg/L as LOQ. Analyses were carried out in triplicate.

2.2 Algal growth inhibition test

The algal growth inhibition test (72 h) with *R. subcapitata*, formerly known as *Selenastrum capricornutum* and *Pseudokirchneriella subcapitata*, was carried out based on ISO (2012a). The algal density was determined by spectrophotometric analysis (DR5000, Hach Lange GbH, Weinheim, Germany). The percentage inhibition of the cell growth (IG, %) was calculated as the difference between the growth rate of the control and of the sample and expressed as the mean (± standard deviation). Toxicity tests were carried out in triplicate.

2.3 Phytotoxicity test

The *L. sativum* germination and root elongation toxicity tests were performed according to ISO (2012b). Macrophyte seeds (n = 10) were exposed on filter paper Whatman n. 1 imbibed with 3 mL of testing solution in triplicate in Petri dishes. Samples were incubated at 25±1 °C in darkness and the number of seeds germinated and the length of the developing roots were measured after 3 days. Controls were carried out in distilled water. Germination (%), and root elongation inhibition were combined to calculate the germination index (GI, %) (Libralato et al., 2016a).

2.4 Micronucleus test

V. faba was investigated for genotoxicity according to ISO (2013). Macrophyte seeds (n = 5) were exposed on filter paper Whatman n.1 imbibed with 6 mL of testing solution in triplicate in Petri dishes.

After incubating in the dark at 22±2 °C for 96 h, the root tips of germinated seeds were fixed for 24 h in 1:3 acetic acid: ethanol solutions, then were cut, stained in Schiff's Reagent using Feulgens method, and squashed on microscope slides (ISO, 2013). The micronucleus frequency MCN (%) was evaluated in 103 cells from *V. faba* seeds using ImageJ (Schindelin et al., 2015).

2.5 Data analyses

Median effect concentrations (EC_{50}), EC_5 and EC_{10} were calculated as mean values and relative 95% confidence limit values (Galdiero et al., 2019), for *R. subcapitata* and *L. sativum*. Differences between treatments were assessed via one-way analysis of variance (ANOVA) after the verification of normality (Shapiro-Wilk's test) and homoscedasticity (Levene's test). The post-hoc Tukey's test accounted for differences within groups setting the statistical significance at $p < 0.05$. Statistical analysis was carried out via SigmaPlot (Systat Software, San Jose, CA).

3 Results and discussion

All endpoints were calculated on real concentrations summarized in Table S1 (Supplementary Materials). The use of Visual MINTEQ 3.1 (Gustafsson, 2012) allowed to model the speciation of Ce, Gd, La, and Nd considering reconstructed freshwater according to ISO (2012a) and the two fixed pH values (4 and 6). According to the database in Supplementary Materials (Table S2), most of the considered REEs were present in the trivalent dissolved free forms (86–88%) at pH 4 (i.e., Ce 88%, Gd 86%, La 87%, and Nd 87%), which are the most bioavailable ones. At pH 6, the free trivalent forms are still present, but with significant reductions compared to pH 4 like for Ce (75%), Gd (58%), La (81%), and Nd (74%). The lower amount of Ce, Gd, La, and Nd in the free form at pH 6 might have influenced their bioavailability and the subsequent effects in the exposed biological models.

In Figure 1, the results of the IG (%) of *R. subcapitata* were reported at pH 4 and 6, respectively, for Ce (Figures 1 A and B), Gd (Figures 1 C and D), La (Figures 1 E and F), and Nd (Figures 1 G and H). A linear regression model was considered to fit data concentration-response relationships. All equations and the relative standard errors were included in Figure 1 (A–H). These equations allowed the determination of EC_{50}, EC_{10}, and EC_5 that were summarized for both pH values in Table 1.

For Ce, La and Nd, biostimulation effects were detected at the first two lowest exposure concentrations for both pH 4 and 6, and also for Gd at pH 6. Microalgae growth impairment occurred for Ce, La, and Nd at 1 and 10 mg/L (nominal concentrations) at pH 4 and 6, and for Gd at pH 6. For microalgae exposed to Gd at pH 4, all exposure concentrations evidenced a concentration-response significant toxic effect up to 73% at 5.72 mg/L. REEs biostimulation effects in unicellular green algae were already reported for nano-CeO_2 considering photosynthesis inhibition and ROS formation as endpoints (Rodea-Palomares et al., 2012) and $Ce(NO_3)_3$ for growth inhibition (Aharchaou et al., 2020).

The exposure to Ce at pH 4 showed effects not significantly different from the exposure at pH 6 with a correlation coefficient of $R_2 = 0.93$ (Figures 1 A and B). Only, at 0.137 mg/L the effect of pH 6 exposure was still biostimulation and significantly different ($p < 0.001$) from the same concentration at pH 4 treatments being about 25% lower. Ce effects ranged between −10% (0.01 mg/L) and 64% (10.225 mg/L). Indeed, the EC_{50} of Ce at pH 4 was 3.15 (1.36–7.19) mg/L and Ce EC_{50} at pH 6 was 4.75 (0.04–10.99) mg/L (Table 1). These EC_{50} values are not significantly different ($p > 0.05$).

For Gd, a significant difference in the concentration-response curves can be observed in Figure 1 (C and D), at pH 6 the EC_{50} value in the investigated concentration range cannot be detected and only EC_5 and EC_{10} values were calculated (i.e., maximum effect of 23% at 5.72 mg/L). At pH 4 (Figure 1 C), significant differences ($p < 0.001$) between treatments were highlighted. The maximum detected effect was 73% at 5.72 mg/L. Gd EC_{50} at pH 4 was 0.267 (0.01–5.30 mg/L). For Gd exposure at pH 6, only EC_5 and EC_{10} values were calculated (Table 1).

For La, effects ranged between −6% (0.01 mg/L) and 21% (5.32 mg/L) (Figures 1 E and F). At 0.01 mg/L and 0.12 mg/L of La no significant differences ($p > 0.05$) were observed between treatments at pH 4 and pH 6. At 1.207 mg/L, the inhibitory effect of pH 6 exposure was significantly different ($p < 0.01$) from the corresponding concentration at pH 4 treatments being about 8% greater. On the contrary, at 5.321 mg/L, the inhibitory effect of pH 6 exposure was significantly different ($p < 0.001$) from the 5.321 mg/L at pH 4 being about 10% lower. The EC_{50} after 72 h of exposure was not determined in both pH exposure scenarios, while EC_5 and EC_{10} values were summarized in Table 1.

About *R. subcapitata* exposure to Nd, the effects varied between 7.4% and 56.7% for pH 4, and −0.9% and 59.7% for pH 6 (Figures 1 G and H). Significant differences ($p < 0.05$) were evidenced amongst treatments at the first two lowest exposure concentrations, while no significant differences ($p > 0.05$) were observed within treatments at the remaining concentrations. At 0.005 mg/L, the inhibitory effect of pH 6 exposure was significantly different ($p < 0.01$) from the same concentration at pH 4 treatments being about 8% lower. At 0.075 mg/L, the inhibitory effect of pH 6 exposure was significantly different ($p < 0.001$) from the 0.075 mg/L at pH 4 being about 14% lower. The EC_{50} values of Nd at pH 4 and 6 were not significantly different ($p < 0.01$) being 1.860 mg/L and 1.856 mg/L, respectively (Table 1).

These data were partly in agreement with previous studies (Liang and Wang, 2013; Thomas et al., 2014; Wang et al., 2014b). The comparison of the growth inhibition effects at pH 4 and 6 evidenced only limited differences between the two exposure scenarios, except for Gd where low pH values can increase the effect on the targeted species.

REEs were ranked in increasing order of toxicity at pH 4 according to the estimates obtained. For EC_{50}: La < Ce < Gd < Nd; EC_{10}: La < Ce < Nd < Gd and EC_5: La < Ce < Nd < Gd. The toxicity trend evidenced that the most toxic elements at pH 4 were Nd and Gd, while La was the less toxic. At pH 6, the general toxicity decreased and kept similar values compared to pH 4. At both pH, Gd and La EC_{50} values could not be obtained. REEs were ranked in increasing order of toxicity at pH 6, EC_{50}: La ≈ Gd < Ce < Nd; EC_{10}: Gd < La < Nd < Ce and EC_5: Gd < La < Ce < Nd.

In general, the ecotoxicity did not always increase with the increase in the atomic number of the investigated REEs with *R. subcapitata* as reported in previous studies (González et al., 2015; Malhotra et al., 2020; Pagano et al., 2015b), and the general scarcity of experimental data can make it difficult to fully discuss. For example, EC_{50} value of Ce (4.4 mg/L) according to (González et al., 2015) was very similar to both EC_{50}s at pH 4 and 6, but the pH of testing solutions was not displayed, while the Gd EC_{50}s were significantly different compared to González et al. (2015) (1.257 mg/L).

Several authors (Aharchaou et al., 2020; Joonas et al., 2017; Stauber and Binet, 2000) highlighted that the formation of insoluble REEs species in exposure media or of precipitates in the presence of free ion concentration due to the changes in pH levels might be responsible of the differential responses.

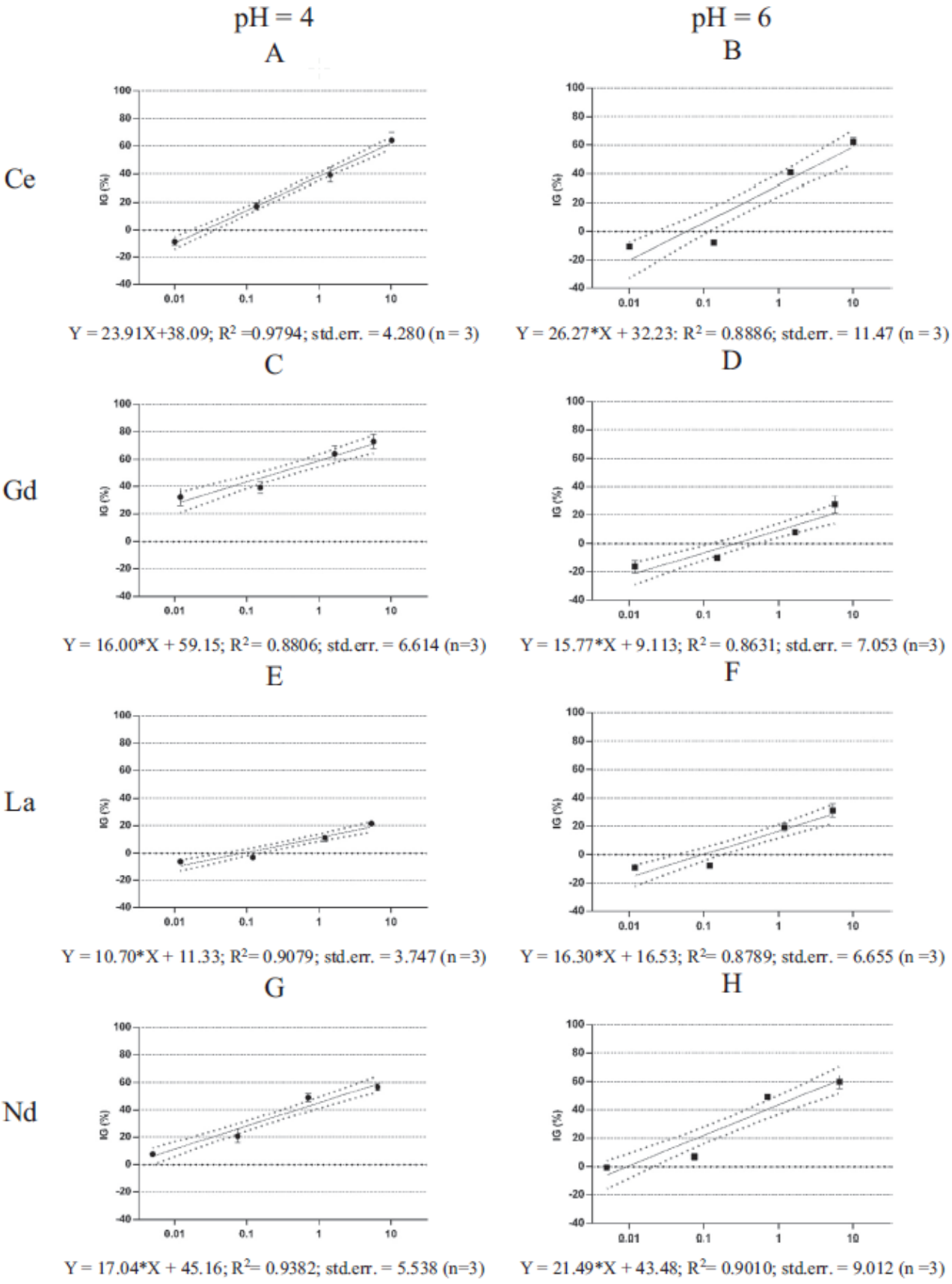

Figure 1. Concentration-response relationship at pH 4 and 6 of Ce (A and B), Gd (C and D), La (E and F), and Nd (G and H) exposed to *R. subcapitata*; concentrations in the x-axis are expressed as mg/L: IG= inhibition of growth.

Table 1. EC_5, EC_{10}, and EC_{50} values for cerium (Ce), gadolinium (Gd), lanthanum (La), and neodymium (Nd) at pH =4 and 6; values are inmg/L; n.a.=not available; REEs=rare earth elements; EC=effective concentration; average EC values are provided ±95% confidence limit values in brackets (n = 3).

pH	REEs	EC5	EC10	EC50
4	Ce	0.04 (0.02–0.10)	0.07 (0.03–0.16)	3.15 (1.36–7.19)
	Gd	0.0004 (0.000009–0.012)	0.0008 (0.00002–0.02)	0.267 (0.009–5.30)
	La	0.256 (0.007–1.15)	0.751 (0.02–3.21)	n.a.
	Nd	0.004 (0.0001–0.096)	0.008 (0.0003–0.187)	1.860 (1.036 to 3.34)
6	Ce	0.09 (0.00–0.25)	0.014 (0.00–0.38)	4.75 (0.04–10.99)
	Gd	0.553 (0.012–0.096)	1.136 (0.023–0.211)	n.a.
	La	0.196 (0.002–0.37)	0.398 (0.005–0.714)	n.a.
	Nd	0.01 (0.001–2.16)	0.0276 (0.002–3.64)	1.856 (0.973–3.54)

In Figure 2, the results about the GI (%) of *L. sativum* were reported at pH 4 and 6, respectively, for Ce (Figures 2 A and B), Gd (Fig. 2 C and D), La (Fig. 2 E and F), and Nd (Figures 2 G and H). All detailed data about seed germination and root elongation were provided in Tables S3 and S4, respectively (Supplementary Materials). GI values between 80% and 120% are considered as acceptable, while, if <80% or > 120% inhibition or biostimulation effects are identified (Libralato et al., 2016a). As a general overview of the obtained results, the GI always evidenced inhibitory effects at the two highest tested concentrations for all the investigated REEs at both pHs. Similarly, all GI values were always >80% and < 120%, so any biostimulation effect was displayed as well.

Considering the exposure of *L. sativum* to Ce (Table S2), the number of *L. sativum* germinated seeds was 100% in the control test, but when Ce solutions at 0.137 mg/L, 1.431 mg/L and 10.225 were used the number of seeds was reduced of about 80% both at pH 4 and 6. At 0.01 mg/L, the number of germinated seeds was not significantly different from the negative control (< 10% effect). No significant differences ($p > 0.05$) were observed at 0.137 mg/L and 10.225 mg/L of Ce for both pH values, while at 0.01 mg/L and 1.431 mg/L statistical differences in the effects were evidenced ($p < 0.05$) within pH 4 and pH 6 treatments (Figures 2 A and B). Ce germination index ranged between 81% (0.010 mg/L) and 54% (10.225 mg/L) at pH 4, and between 90% (0.010 mg/L) and 64% (10.225 mg/L) at pH 6.

The number of *L. sativum* germinated seeds after Gd exposure significantly ($p < 0.05$) decreased from 0.154 mg/L, up to 5.721 mg/L. Effects of Gd at pH 4 were not significantly different from those at

pH 6 with a correlation coefficient of $R^2 = 0.98$ (Figures 2 C and D). The Gd GI ranged between 83% (0.012 mg/L) and 50% (5.721 mg/L) at pH 4, and between 86% (0.012 mg/L) and 60% (5.721 mg/L) at pH 6.

About the exposure to La, the number of germinated seeds was reduced up to 90% at pH 4 and 80% at pH 6. No significant differences ($p > 0.05$) were evidenced between treatments at the different pHs in the considered concentration range (Figures 2 E and F). At pH 4, only the lowest exposure concentration (0.012 mg/L) showed a GI significantly different (90%) than all other treatments (63%–78%) being the only one presenting no effect. At pH 6, the highest concentrations (5.321 mg/L and 1.207 mg/L) showed slight adverse effects ranging between 59% and 66%, while the two lowest treatment presented no effect. In Nd exposure, the number of *L. sativum* germinated seeds was reduced up to 80% at 0.710 and 6.510 mg Nd/L for both pH 4 and 6 (Table S3). Significant differences ($p < 0.05$) were observed only at 6.510 mg/L for both pH values, while at 0.005 mg/L, 0.075 mg/L and 0.710 mg/L no significant difference between treatments was detected ($p > 0.05$) (Table S3). The germination index showed a similar toxicity trend to the previous REEs exposure, but with higher toxicity level (45%) at 6.510 mg/L (pH 4). Indeed, the GI values ranged between 45% and 87% for pH 4, while between 55% and 84% for pH 6.

Currently, few data are available about *L. sativum* exposure to REEs including all endpoints. Wang et al. (2007) reported that Ce^{3+} (14 mg/L), La^{3+} (13.8 mg/L), and Nd^{3+} (14 mg/L) in *Lepidium meyenii* enhanced hyperhydricity and the activities of antioxidative enzymes in adventitious shoots like peroxidase (POD), catalase (CAT), ascorbate peroxidase (APX), superoxide dismutase (SOD), monodehydroascorbate reductase (MDHAR) and glutathione reductase (GR), but most adventitious shoots grew normally. Thomas et al. (2014) highlighted that La and Ce at "high pH" (5.95 ± 0.02 and 6.74 ± 0.03, in that order) had no impact on seed germination in the tested species at any concentration, whereas Ce supplied at "low pH" (4.08 ± 0.02) induced negative effects (i.e., inhibition concentration on 10% exposed population, IC_{10}, mg/kg dry soil (d.s.)) on seed germination in *Asclepias syriaca* (54.6 mg/kg d.s.), *Desmodium canadense* (165.9 mg/kg d.s.), *Panicum virgatum* (166.8 mg/kg d.s.), *Raphanus sativus* (150.4 mg/kg d.s.), and *Solanum lycopersicum* (195.34 mg/kg d.s.).

The frequency distribution of micronuclei in *V. faba* exposed to Ce (0.010 mg/L), Gd (0.012 mg/L), La (0.012 mg/L), and Nd (0.005 mg/L) was reported in Figure 3 for both pH 4 and 6. No significant differences ($p < 0.05$) were evidenced between the negative controls and the treatments at pH 6. At pH 4, effects were significantly different ($p < 0.05$) from negative controls for La, Nd, and Gd being approximately from three- to four-fold compared to negative controls. The MNF confirmed that Gd at pH 4 is significantly toxic like for *R. subcapitata* and *L. sativum*. For Nd, an increased MNF mitotic and chromosomal aberrations in *V. faba* were also evidenced by Jha and Singh (1994), similarly to our findings. For La, Wang et al. (2011) highlighted some hormetic effects in *V. faba*, but the MNF was not investigated. Only Ce presented no mutagenicity effects either at pH 4 or 6. The pH has a significant role in changing the effects of Gd, La, and Nd to *V. faba* inducing mutagenicity at low values (pH 4).

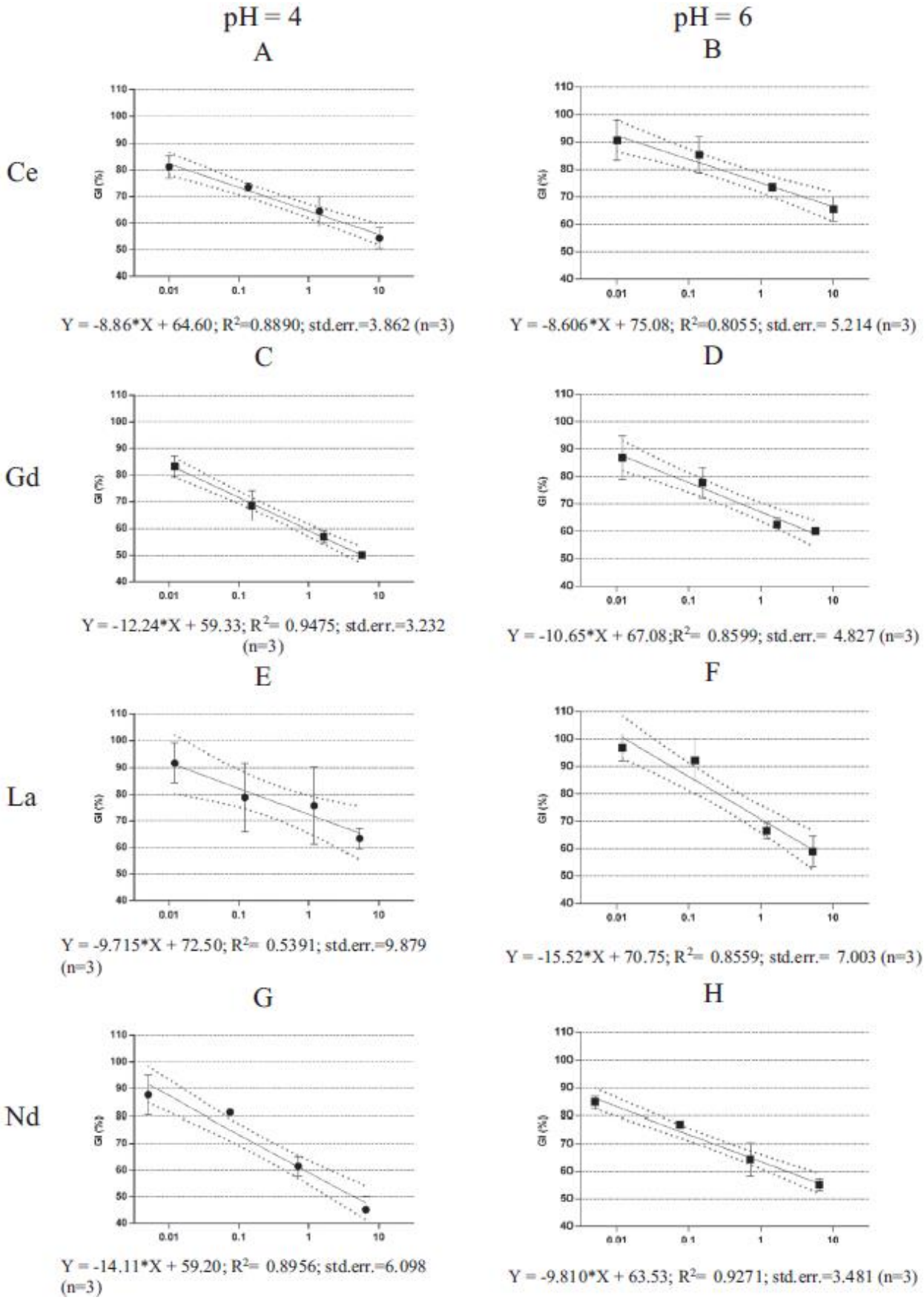

Figure 2. Concentration-response relationship at pH 4 and 6 of Ce (A and B), Gd (C and D), La (E and F), and Nd (G and H) exposed to *L. sativum*; concentrations in the x-axis are expressed as mg/L; GI= germination index.

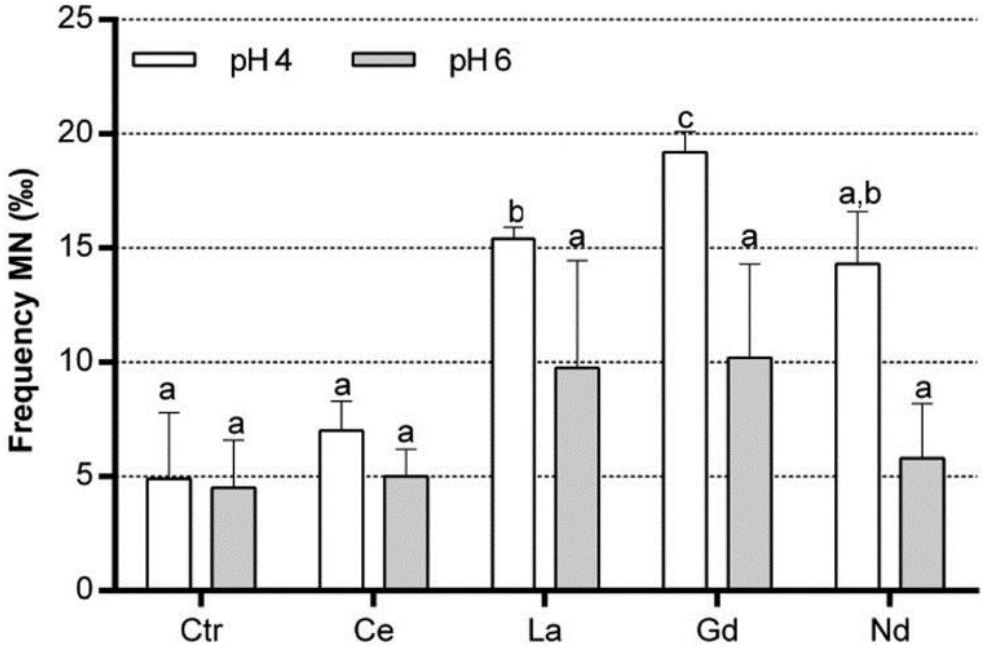

Figure 3. Frequency of micronuclei (MC) in *V. faba* root exposed to Ce (0.010 mg/L), Gd (0.012 mg/L), La (0.012 mg/L), and Nd (0.005 mg/L) at pH = 4 and 6; letters (a-c) correspond to significantly different data (Tukey's test, $p < 0.05$); ctr = negative control; error bars indicate standard errors (n=3).

4 Conclusions

The effects of Ce, Gd, La, and Nd were assessed in a simplified acid mine discharge investigating the role of pH 4 and 6 in changing the toxicity profiles of three photosynthetic organisms. A multiple-endpoint approach (i.e., growth inhibition, germination index, and mutagenicity) was used to investigate real exposure scenarios. Results evidenced that pH 4 can increase the toxicity of the selected REEs increasing the amount of free trivalent ions compared to pH 6. In summary, the toxicity trends were as follows: i) for microalgae (i.e., considering the EC_{50} values): 1) La < Ce < Nd < Gd at pH 4; 2) Nd < Ce < Gd ≈ La at pH 6; ii) for L. sativum (i.e., considering the GI(%) at the highest exposure concentration): 1) La < Ce < Gd < Nd at pH 4; 2) Ce < Gd ≈ La ≈ Nd at pH 6; iii) for V. faba (i.e., MNF): 1) Ce < La ≈ Nd < Gd at pH 4; 2) Ce ≈ La ≈ Nd ≈ Gd at pH 6. The sensitivity of the considered biological models was *R. subcapitata* > *V. faba* > *L. sativum*, suggesting that microalgae can have an important role as well as *V. faba* in the risk assessment of REEs.

Gd was the most toxic element at pH 4, followed by La and Nd, and Ce. At pH 6, their effects significantly decreased, and Nd evidenced the highest toxicity. Gd, La and Nd evidenced at pH 4 their potential mutagenicity, that was not present at pH 6. According to the considered exposure scenarios, potential significant negative effects could be exerted especially by Gd, La, and Nd in acidic aquatic environments to microalgae and macrophytes, but they can be reduced by controlling the pH.

Several gaps into the knowledge still remain about REEs toxicity effects and their potential uptake by aquatic species including the transfer through the food web and potential mechanism of adaptation and detoxification.

Supplementary Materials

Table S1. Nominal and real concentrations (A) of testing solutions of Ce, Gd, La, and Nd at pH 4 and 6 at standard errors (B); N = nominal concentration, R = real concentration; concentrations are in mg/L.

A		pH 4				pH 6			
Ce	N	14.02	1.40	0.14	0.01	14.01	1.40	0.14	0.014
	R	10.22	1.43	0.13	0.01	10.22	1.43	0.13	0.010
Gd	N	15.72	1.57	0.15	0.01	15.72	1.57	0.15	0.015
	R	5.72	1.64	0.16	0.01	5.72	1.66	0.15	0.012
La	N	13.89	1.38	0.13	0.01	13.89	1.38	0.13	0.013
	R	5.32	1.20	0.12	0.01	5.42	1.21	0.12	0.012
Nd	N	14.42	1.44	0.14	0.01	14.42	1.44	0.14	0.014
	R	6.51	0.71	0.07	0.005	6.51	0.71	0.07	0.005

B		pH 4				pH 6			
Ce	R	2.39	0.33	0.03	0.002	2.39	0.33	0.03	0.002
Gd	R	1.34	0.38	0.03	0.003	1.34	0.38	0.03	0.002
La	R	1.24	0.28	0.02	0.002	1.27	0.28	0.02	0.002
Nd	R	1.52	0.16	0.01	0.001	1.52	0.16	0.01	0.001

Table S2. Modelled speciation of Ce, Gd, La, and Nd according to Visual MINTEQ ver. 3.1.

pH 4			pH 6		
Component	% of total concentration	Species name	Component	% of total concentration	Species name
Nd+3	86.817	Nd+3	Nd+3	74.37	Nd+3
	0.252	NdEDTA-		0.423	NdEDTA-
	0.015	Nd(SO4)2-		0.295	NdOH+2
	12.865	NdSO4+		0.013	Nd(SO4)2-
	0.044	NdHCO3+2		11.123	NdSO4+
Mg+2	99.267	Mg+2		2.619	NdHCO3+2
	0.729	MgSO4 (aq)		11.147	NdCO3+
NH4+1	99.949	NH4+1	Mg+2	99.011	Mg+2
	0.051	NH4SO4-		0.737	MgSO4 (aq)

SO4-2	88.058	SO4-2		0.033	MgHPO4 (aq)
	0.685	HSO4-		0.216	MgHCO3+
	0.024	MnSO4 (aq)	NH4+1	99.91	NH4+1
	1.43	MgSO4 (aq)		0.052	NH4SO4-
	0.022	Nd(SO4)2-		0.039	NH3 (aq)
	9.548	NdSO4+	SO4-2	90.012	SO4-2
	0.233	NH4SO4-		0.024	MnSO4 (aq)
PO4-3	0.067	HPO4-2		1.445	MgSO4 (aq)
	98.651	H2PO4-		0.02	Nd(SO4)2-
	1.278	H3PO4		8.255	NdSO4+
Fe+3	99.651	FeEDTA-		0.237	NH4SO4-
	0.314	FeHEDTA (aq)	PO4-3	6.363	HPO4-2
	0.015	FeOHEDTA-2		93.258	H2PO4-
EDTA-4	32.769	NdEDTA-		0.012	H3PO4
	66.858	FeEDTA-		0.339	MgHPO4 (aq)
	0.21	FeHEDTA (aq)		0.025	MnHPO4 (aq)
	0.01	FeOHEDTA-2	Fe+3	0.21	FeOH+2
	0.147	NdHEDTA (aq)		32.672	Fe(OH)2+
H3BO3	99.999	H3BO3		0.014	Fe(OH)3 (aq)
Mn+2	99.294	Mn+2		0.141	FeHPO4+
	0.699	MnSO4 (aq)		65.963	FeEDTA-
Zn+2	99.076	Zn+2		0.998	FeOHEDTA-2
	0.872	ZnSO4 (aq)	EDTA-4	55.064	NdEDTA-
	0.032	ZnEDTA-2		44.255	FeEDTA-
Cu+2	86.49	Cu+2		0.669	FeOHEDTA-2
	0.02	CuOH+	H3BO3	99.945	H3BO3
	0.784	CuSO4 (aq)		0.055	H2BO3-
	0.015	CuHCO3+	Mn+2	98.698	Mn+2
	9.526	CuEDTA-2		0.704	MnSO4 (aq)
	3.12	CuHEDTA-		0.136	MnHPO4 (aq)
	0.037	CuH2EDTA (aq)		0.416	MnHCO3+

MoO4-2	23.327	MoO4-2		0.044	MnCO3 (aq)
	31.81	HMoO4-	Zn+2	98.23	Zn+2
	42.633	MoO3(H2O)3(aq)		0.061	ZnOH+
	2.23	MgMoO4(aq)		0.877	ZnSO4 (aq)
CO3-2	0.426	HCO3-		0.105	ZnHPO4 (aq)
	99.571	H2CO3* (aq)		0.05	ZnCO3 (aq)
				0.61	ZnHCO3+
				0.063	ZnEDTA-2
			Cu+2	75.553	Cu+2
				1.711	CuOH+
				0.694	CuSO4 (aq)
				0.098	CuNH3+2
				0.523	CuHPO4 (aq)
				3.968	CuCO3 (aq)
				0.936	CuHCO3+
				16.46	CuEDTA-2
				0.054	CuHEDTA-
			MoO4-2	90.225	MoO4-2
				1.226	HMoO4-
				0.016	MoO3(H2O)3(aq)
				8.532	MgMoO4(aq)
			CO3-2	29.752	HCO3-
				69.468	H2CO3* (aq)
				0.142	NdHCO3+2
				0.604	NdCO3+
				0.031	MgHCO3+

Table S3. Seed germination of *L. sativum* exposed to Ce, Gd, Ln, and Nd at pH 4 and 6; unit of measure is the number of germinated seed.

		Negative control			**10^{-4} M**			**10^{-5} M**			**10^{-6} M**			**10^{-7} M**		
	pH	R1	R2	R3	R1	R2	R3	R1	R2	R3	R1	R2	R3	R1	R2	R3
Ce	**4**	10	10	10	7	8	7	8	8	8	8	8	8	8	9	9
	6	10	10	10	8	8	8	8	8	8	9	9	9	10	9	8

Gd	**4**	10	10	10	6	7	6	7	9	6	8	8	8	9	9	9
	6	10	10	10	8	6	9	7	7	6	8	8	8	9	9	10
La	**4**	10	10	10	9	8	8	10	9	8	9	9	8	9	10	10
	6	10	10	10	7	8	6	7	8	6	8	10	9	8	9	9
Nd	**4**	10	10	10	6	9	6	7	8	8	9	8	9	10	9	10
	6	10	10	10	7	7	8	8	7	6	9	9	9	8	8	8

Table S4. Root elongation of *L. sativum* exposed to Ce, Gd, Ln, and Nd at pH 4 and 6; length is in centimetres.

		Negative control			**10^{-4} M**			**10^{-5} M**			**10^{-6} M**			**10^{-7} M**		
	pH	R1	R2	R3	R1	R2	R3	R1	R2	R3	R1	R2	R3	R1	R2	R3
Ce	**4**	4.2	4.0	4.5	3.1	3.1	3.2	3.1	3.6	3.6	4.0	3.8	3.9	4.1	3.9	4.0
	6	3.9	4.3	4.2	3.2	3.3	3.6	3.7	3.9	3.8	4.2	3.6	3.9	3.8	4.4	4.2
Gd	**4**	4.2	4.0	4.5	3.5	3.0	3.6	3.6	2.7	3.8	4.0	3.6	3.4	4.1	3.8	3.8
	6	3.9	4.3	4.2	3.1	4.1	2.7	3.7	3.8	4.1	4.3	3.8	3.8	3.7	3.8	3.9
La	**4**	4.2	4.0	4.5	3.2	3.3	3.2	3.8	3.6	3.3	4.3	3.8	3.5	4.0	4.2	4.0
	6	3.9	4.3	4.2	3.5	3.3	3.6	3.9	3.3	4.7	5.0	3.4	4.4	4.7	4.6	4.4
Nd	**4**	4.2	4.0	4.5	3.0	2.4	3.0	3.7	3.5	3.1	3.8	4.3	3.9	4.1	4.0	3.5
	6	3.9	4.3	4.2	3.2	3.4	2.7	3.1	4.2	4.2	3.5	3.5	3.6	4.2	4.4	4.4

Long-term multi-endpoint exposure of the microalga *Raphidocelis subcapitata* to lanthanum and cerium

1 Introduction

Lanthanides are the major family of rare earth elements (REEs) and due to their essential and unique properties are becoming essential in diverse fields of world economy (Charalampides et al., 2015; Gwenzi et al., 2018; Malhotra et al., 2020). Anthropogenic REEs contamination can be of great concern in hot spots (e.g., ore mine tailings and abandoned mines) (Pagano et al., 2015a), but the alteration of their biogeochemical cycles suggests their potential role as widespread emerging contaminants also in agroecosystems (Balaram, 2019; Galdiero et al., 2019; Gravina et al., 2018; Gwenzi et al., 2018; Naccarato et al., 2020; Pagano et al., 2019, 2015a).

About the aquatic environment, their main sources include waste and wastewaters from medical institutions, fertilizers, mining processing, high-technology industries, petroleum refineries, and recycling plants (i.e., e-waste management) (Gwenzi et al., 2018; Minganti and Drava, 2018; Naccarato et al., 2020; Pagano et al., 2015a) (Gwenzi et al., 2021; Pagano, 2016). According to (Migaszewski and Gałuszka, 2015) review paper, La and Ce ranged between 7.7 and 80.4 µg/L and 19.4 and 161 µg/L in wastewater, respectively. In river water, La and Ce concentrations were lower than in wastewater and ranged between 19.7 and 74 ng/L and 9.67 and 212 ng/L, in that order (Migaszewski and Gałuszka, 2015), but on a local basis they can be up to 80–200 µg/L (Uchida et al., 2006).

Recent studies demonstrated that REEs exhibit beneficial effects as well as amoderate to high toxicity towards aquatic biota, including bacteria, microalgae, plants, vertebrates, and invertebrates (Adeel et al., 2019; Balaram, 2019; Blinova et al., 2020, 2018b; Herrmann et al., 2016; Oral et al., 2010; Romero-Freire et al., 2019). Their mechanisms of action and behaviour in biological systems are far from being completely understood, but it seems dependent on their concentration and physico-chemical conditions of the exposure media. Similarities in their mode of action were evidenced, but not univocally (Siciliano et al., 2021a), in relation to their ionic radii and coordination numbers with some essential elements, i.e., Ca,Mn, Mg, Fe, and Zn (Valcheva-Traykova et al., 2014).

Several authors evidenced the potential interactions of REEs with biologically activemolecules resulting in the excess generation of reactive oxygen species (ROS), inhibition of the antioxidant system, and DNA damages of the exposed aquatic organisms or cultured cells (Blinova et al., 2020; Malhotra et al., 2020), potentially altering the stability, permeability, and functioning of cell membranes (Ramos et al., 2016).

Most data on REEs toxicity to aquatic organisms are derived by acute toxicity tests (Blaise et al., 2018; Blinova et al., 2018; González et al., 2015; Trifuoggi et al., 2017). Some data about the chronic toxicity of REEs are present for zooplankton and fish (Blinova et al., 2020), but they are still very limited for unicellular algae (Siciliano et al., 2021a).

Algae are primary producers and key organisms in the food chain allowing the potential biomagnification up to higher trophic levels of REEs with still unknown and unexpected effects on human health (Thomas et al., 2014; Goecke et al., 2015b). Some authors suggested that REEs could be uptaken and concentrated in chloroplasts, where the intracellular lanthanides could cross the internal membrane system until the replacement of magnesium in chlorophyll molecules (Guo et al., 2000; Minqin et al., 2013; Ren et al., 2007; Shen et al., 2002; Kang et al., 2000). Only a few microalgae species have been investigated mainly including *Chlorella vulgaris* and *Raphidocelis*

subcapitata (Evseeva et al., 2010; Fuma et al., 2005; Jin et al., 2009; Tai et al., 2010; Wang et al., 2012; Goecke et al., 2015b; Hu et al., 2001). The median effective concentration (EC_{50}) of lanthanum (La) was >10.1 mg/L for *Desmodesmus quadricauda* (50% inhibition after 22–23 days at 0.01 mg/L) and *Microcystis aeruginosa* (Jin et al., 2009), and >5.42 mg/L for *R. subcapitata* (Siciliano et al., 2021a), and 51.72 (47.29–57.93) mg/L (i.e., nominal concentrations) (Bergsten-Torralba et al., 2020), and 47.13 (45.30–51–56) mg/L (i.e., nominal concentrations) for *C. vulgaris* (Bergsten-Torralba et al., 2020), and 4.38 (4.16–4.62) mg/L (i.e., nominal concentrations) for *Nitellopsis obtusa* (Manusadžianas et al., 2020). The toxicity as EC_{50} of cerium (Ce) as $Ce(NO_3)_3$ was from 3.15 to 6.32 mg/L (i.e., nominal concentrations) for *R. subcapitata* (González et al., 2015) (Siciliano et al., 2021a). Effects of Ce to *Desmodesmus quadricauda* at 0.001 mg/L evidenced biostimulation (16%) after 3 days (Goecke et al., 2015a), while in *Anabaena flosaquae*, after an initial biostimulation (16%, 3 days), showed inhibition (≈33%) at 5–10 mg/L after 17 days (Wang et al., 2012). Most studies lacked environmentally relevant concentrations and REEs uptake (Blinova et al., 2020; Miazek et al., 2015), like the main physiologicalmechanisms underlying REEs induced adaptation phenomena (Wang et al., 2014a).

This research study investigated for the first time the effect of La and Ce considering a long-term exposure to *R. subcapitata* (i.e., 28 days renewal toxicity test). We investigated environmentally relevant concentrations looking at potential generational adaptations in microalgae supporting bioconcentration of La and Ce and hence their possible transfer up to the food web. The multi-endpoint approach included the assessment of algal growth rate, determination of reactive oxygen species (ROS), enzymatic activity, and uptake from exposure media. Graph 1 represents an abstract of the study elaborated.

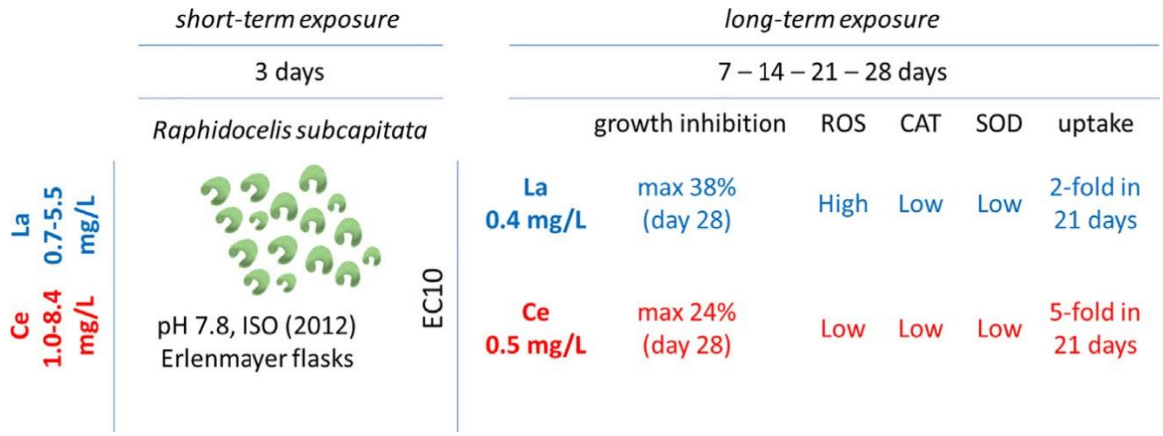

Graph 1. Graphical abstract of the study.

2 Material and methods

2.1 Chemicals, testing solutions, and analytical characterization

The experiments were carried out using commercially available chemicals: i) lanthanum(III) nitrate hexahydrate ($La(NO_3)_3 \cdot 6H_2O$, purity 97%); and ii) cerium(III) nitrate hexahydrate ($Ce(NO_3)_3 \cdot 6H_2O$, purity 97%) purchased from Sigma-Aldrich (Saint Louis, United States of America). Treatment solutions of La and Ce were prepared by adding REEs' solution (1000 mg/L) to artificial freshwater (ISO, 2012a) at least 1 h before the exposure. The pH was measured with a pH-meter (Mettler Toledo Five Easy, Milan, Italy) prior to exposure and samples' collection (day 3, 7, 14, 21, and 28). La and

Ce concentrations were determined by inductively coupled plasma mass spectrometry (ICP-MS NexION 350×, PerkinElmer, Inc., MA, USA). The limits of detection (LOD) and quantification (LOQ) were for La and Ce as follows: 0.0011 and 0.0010 μg/L as LOD; and 0.0037 and 0.0033 μg/L as LOQ. The calibration referred to the following standards: i) Lanthanum Standard for ICP (i.e., standard reference materials (SRM) from NIST $La(NO_3)_3$ in HNO_3 2–3% 1000 mg/L La Certipur®); Cerium Standard for ICP (i.e., SRM from NIST $Ce(NO_3)_3$ in HNO_3 2–3% 1000 mg/L Ce Certipur®). Analyses were carried out in triplicate on samples collected after day 7, 14, 21, and 28. About bioaccumulation experiments (i.e., explained in detail in the below sections), filters and organisms were dried at 65 °C for 24 h and digested in aqua regia (HNO_3/HCl = 1:3, v/v) using a microwave oven (START D, Microwave Digestion System, Milestone S.r.l.) and analyzed via ICP-MS including the relative controls.

2.2 Cell culture conditions and *R. subcapitata* growth inhibition (GI) test

Axenic cultures of *R. subcapitata* were maintained at the Hygiene Laboratory of the Department of Biology of the University of Naples Federico II in artificial freshwater ISO (2012a). Preliminary algal growth inhibition tests (72 h) were performed according to ISO (2012a) in order to reflect the physiological status of algal cells (Piovár et al., 2011).

Treatment solutions were prepared into each volumetric flask and organized in the following experimental design (i.e., nominal concentrations) to calculate the effective inhibition concentration at 10% (EC_{10}) at pH = 7.8: i) from 0.7 mg/L to 5.5 mg/L for La; ii) from 1.0 mg/L to 8.4 mg/L for Ce.

Algae were kept in a climatic growth chamber at constant temperature (24 ± 2 °C) and light conditions (100 ± 10 μE m−2 s−1), and performing continuous shaking during maintenance and testing (50 rpm). After 72 h of exposure, the growth rate relative to the control was calculated by normalizing the final cell density of each replicate to control cultures (incubated in the absence of REEs).

2.3 A multi-endpoint experimental approach with *R. subcapitata*

Modified algal growth inhibition tests (ISO, 2012a) were carried out for 28 days exposing microalgae to La and Ce into 250 mL volumetric flasks including four replicates and an inoculum of *R. subcapitata* of 10^4 cells/mL. Exposure culturing media were spiked with La or Ce in order to obtain the relative EC_{10}. All tested concentrationswere analytically verified. Flasks were incubated for 28 days under the same conditions as the growth inhibition test. On day 3, 7, 14, 21, and 28, effects on microalgae were checked considering the optical density (OD) method (i.e., absorbance at 670 nm by Hach Lange DR5000 spectrophotometer). Algae were sampled after 7, 14, 21, and 28 days of exposure to analyze ROS production and the activation of antioxidant defense (superoxide dismutase (SOD) and catalase (CAT)), and to determine La and Ce concentrations bioaccumulated in the algal biomass. Solutions were partially renewed after each sampling period. Algae collection included two main aliquots: i) 100 mL of algae suspension were filtered (0.45 μm polycarbonate Millipore membrane under vacuum pressure) to check bioaccumulation (i.e., filters were rinsed six times with ultrapure deionized water prior to acid digestion for chemical analysis); ii) 100 mL of algae suspension were centrifuged (1520 g for 20 min, Beckman TJ-6, rotor 5-92, Milan, Italy) and the pellets were rinsed six times with ultra-pure deionized water prior to ROS, SOD, and CAT analysis. The remaining 50 mL of algae suspension were resuspended in freshly spiked La and Ce culturing media at the respective EC_{10} values at concentrations > 10^5 cell/mL.

A high-pressure homogenization method (French press cell, Thermo Electron Co., Waltham, MA, USA) was applied to the algal biomass at 78 atm to disrupt *R. subcapitata* cell wall. The extracts were suspended in potassiumphosphate buffer solution (PBS 1 M at pH 7.4) and centrifuged for 20 min at 15,000g (4 °C). The supernatant was collected, and the protein concentration of each sample was measured using a spectrophotometer (Hach-Lange DR 5000) according to Bradford's method (Bradford, 1976). ROS content was quantified by the ability of free radicals to oxidize the non-fluorescent probe carboxy-H2DFFDA (Sigma Aldrich, Saint Louis, USA) to a fluorescent product that can be measured fluorometrically (Almeida et al., 2019, 2017). SOD and CAT activities were carried out according to Galdiero et al. (2016).

2.4 Statistical analysis

Median effects concentrations (EC_{50}) and effective concentration at 10% inhibition (EC_{10}) were expressed as mean values and the relative 95% confidence limit values for both La and Ce. Growth inhibition data were normalized on negative controls (ISO, 2012). Differences between treatments were assessed via a two-way analysis of variance (ANOVA) after the verification of normality (Shapiro-Wilk (S-W) test) and homoscedasticity (Bartlett's (B) test). If samples are drawn from non-normal populations or do not have equal variances, the nonparametric method Kruskal-Wallis (K-W) ANOVA on ranks was taken into consideration. The post-hoc Tukey's test accounted for differences within groups setting the statistical significance at $\alpha = 0.05$. Pearson correlation coefficients ($\alpha=0.05$) were calculated between the values of biomarkers of stress and La and Ce bioconcentrated in microalgae. Statistical analysis was carried out using SigmaPlot (Systat Software, San Jose, CA) and GraphPad Prism (GraphPad, San Diego, CA, USA).

3 Results and discussion

3.1 72 h GI test

Data about 72 h GI were summarized after their normalization on negative controls in Figure 1. Measured concentrations used to calculate concentration-response curves were highlighted in Table 1. The pH values of solutions ranged between 7.60 and 8.00 (mean pH 7.80) all along the monitoring period. For La, the EC_{50} (±95% confidence limit values) and EC_{10} (±95% confidence limit values) were 1.6 (0.9–2.8) mg/L and 0.4 (0.2–0.8) mg/L, respectively ($Y = 68.72 * X + 37.09$; $r2=0.95$; standard error (std.err.) estimate = 6.98). For Ce, the EC_{50} (±95% confidence limit values) and EC_{10} (±95% confidence limit values) were 1.6 (0.9–2.8) mg/L and 0.5 (0.3–0.7) mg/L, respectively ($Y = 75.34 * X + 35.38$; $r2 = 0.9563$; std.err. estimate = 7.2). Lanthanum and Ce showed comparable growth inhibitory effects, with EC_{50} values of approximately 1.5 mg/L, which is in line with previous findings (González et al., 2015; Joonas et al., 2017; Tai et al., 2010). As a consequence, for the 28 days long-term tests, testing media were spiked with 0.4 mg/L and 0.5 mg/L of La and Ce (i.e., EC_{10} values), respectively, simulating the exposure deriving from ore mine effluents (Verplanck et al., 2004).

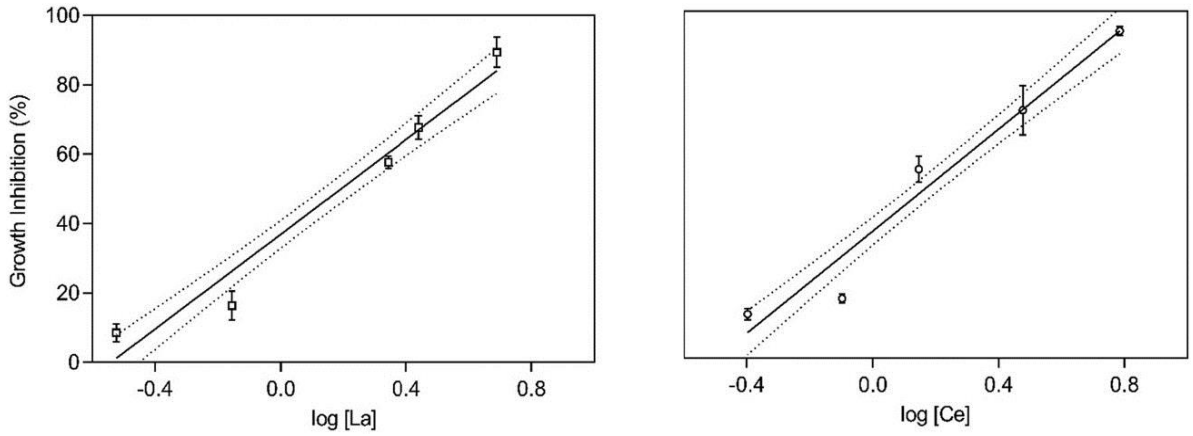

Figure 1. Concentration-response curves for La (Y=68.72 ∗X+37.09, R^2=0.9555 std.err.=6.976) and Ce (Y=75.34 ∗ X+35.38 R^2=0.9563; std.err.=8.350) normalized to negative controls after semi-log regression, including 95% limit values (n= 4).

Table 1. Nominal andmeasured (ICP-MS) La and Ce concentrations (mg/L) and the relative std.err. (n = 3).

La		Ce	
Nominal	Measured	Nominal	Measured
0.7	0.30 ± 0.04	1.0	0.40 ± 0.04
1.4	0.70 ± 0.03	1.4	0.80 ± 0.02
2.2	2.20 ± 0.09	1.7	1.40 ± 0.08
2.8	2.80 ± 0.09	5.6	3.00 ± 0.05
5.5	4.90 ± 0.06	8.4	6.10 ± 0.07

3.2 Long-term exposure effects

Data about La and Ce cumulative growth inhibition after 3, 7, 14, 21, and 28 days were summarized in Figure 2 after data normalization on negative controls. Data were normally distributed (S-W) and presented equal variances (B test). For La, GI increased three times from day 3 (8%) to day 14 (27%), being constant approximately for one week, then increased again at the end of the exposure period (38%). At the end of each week, the GI of Ce tended to slightly increase doubling from 12% (day 3) to 24% (day 28), thus suggesting an increased susceptibility along time. No significant differences (ANOVA, $p > 0.05$) were observed after day 3, 7, 14, and 21 between La and Ce. A statistically significant difference ($p < 0.05$) was found on day 28, where La was more toxic than Ce.

The slow increase of toxic effects during the 28 days exposure period can suggest the presence of nutrient depletion phenomena rather than toxicity per se. It was reported that REEs could sequester essential nutrients such as phosphates producing death by starvation (Lürling and Van Oosterhout, 2013; Yuan et al., 2009). This hypothesis needs further investigations to be confirmed since this effect could influence the EC_{50} of REEs, thus, potentially, environmental decision-making procedures.

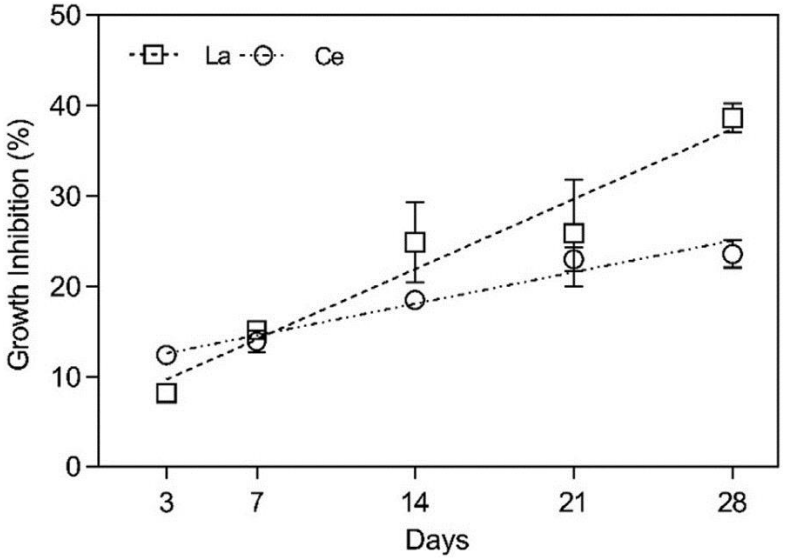

Figure 2. La (0.4 mg/L) and Ce (0.5mg/L) cumulative growth inhibition of *R. subcapitata* after 3, 7, 14, 21, and 28 days of exposure normalized to negative controls (±std.err.; n = 4); La: Y = 0.4991 ∗ X + 11.15, R^2 = 0.7890, std.err. = 2.307; Ce: Y = 1.108 ∗ X + 6.446, R^2 = 0.7714, std.err. = 5.773.

Results about ROS were summarized for La and Ce after data normalization on protein activity in Figure 3. Data were normally distributed (S-W), and presented equal variances (B test). Statistical comparisons between effects due to contact time duration (7, 14, 21 and 28 days) were included in the same figure (post-hoc Tukey's test).

For La, ROS production tended to increase during the 28-days exposure period and after day 14 was greater (days 21 and 28) than the negative control, evidencing the absence of adaptation/detoxification mechanisms. At day 7, La induced less ROS production, while at day 14 no statistical difference was found comparing the ROS value from the control group. At days 21 and 28, ROS production drastically increased.

Cerium exposure did not evidence any specific ROS trend with values substantially comparable between contact times. At 7, 21, and 28 days, Ce induced less, or comparable ROS levels compared to negative controls. Only at day 14, the microalgae exposed to Ce produced more ROS than the negative controls. Compared to La, *R. subcapitata* might follow a different detoxification strategy to contrast and/or clear the oxidative damage caused by ROS.

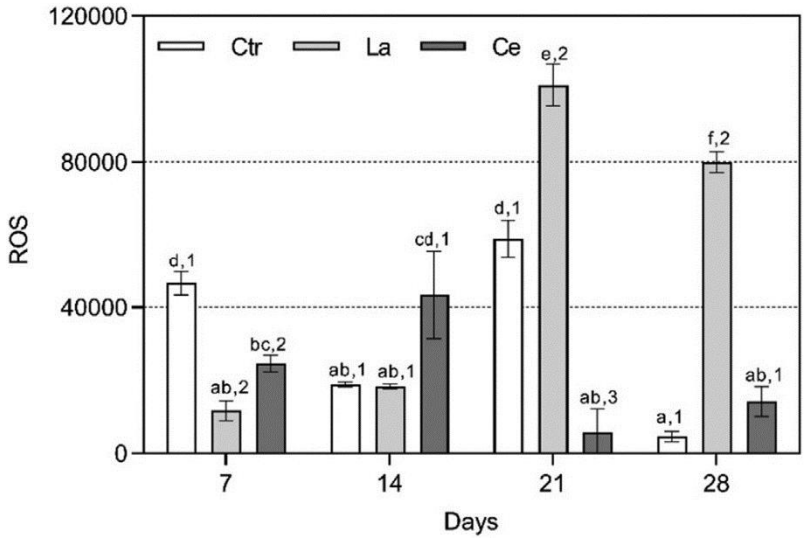

Figure 3. ROS production in *R. subcapitata* exposed to La and Ce lasting 28 days after normalization on protein content. Results are presented as mean ± std.err. (n = 4) in U/mg protein. Letters (a-f) indicate significant differences between exposure times (7, 14, 21, and 28) within treatments (La and Ce), while numbers (1–3) highlighted significant differences within exposure times (7, 14, 21, and 28) between treatments (La and Ce) ($p < 0.05$, Tukey's test).

Data about CAT and SOD were summarized in Figure 4 (A and B, in that order) for both La and Ce after data normalization on protein content. Data were normally distributed (S-W), but they did not present equal variances (B test), so the K-W test was carried out. Generally, La and Ce had different effects on the activities of antioxidant enzymes at most of the considered scenarios compared to negative controls.

The levels of CAT (Figure 4A) and SOD (Figure 4B) activities after La exposure were slightly enhanced after day 7 and remained constant approximately for the entire period of exposure from day 14 to day 28. CAT and SOD contents reached a maximum at day 14 with a value of 170 U/mg protein and 780 U/mg protein, respectively.

About Ce exposure, the contents of CAT (Figure 4A) and SOD (Figure 4B) were at their minimum level. The highest CAT (400 U/mg protein) and SOD (2000 U/mg protein) activities appeared as a consequence of algal exposure to Ce after 14 days. At day 21 and 28, CAT activities were not significantly different ($p > 0.05$). About SOD, at day 21 the activity significantly ($p < 0.05$) decreased compared to day 14, reaching values in day 28 comparable to day 7 (i.e., being similar to negative control value too). Thus after 28 days of exposure, the levels of both CAT and SOD, being not significantly different from the respective negative controls, could suggest the reduction of oxidative stress via other detoxification mechanisms like for example phytochelatins (PCs) production (He et al., 2005) or bioconcentration. He et al. (2005) observed that both calcium and lanthanum can influence the expression of PC synthase gene and cadmium absorption in *Lactuca sativa*. In particular, La (III) was able to enhance the mRNA level of LsPCS1 (i.e., phytochelatin synthase gene) and PCs accumulation. Other causes could be related to inactivation of enzymes by ROS, decrease in synthesis of enzyme, or change in the assembly of its subunits (Cheng et al., 2016). Comparatively, the activities of CAT and SOD in Ce exposure were higher than in La, suggesting that a lower antioxidative capacity was required to eliminate ROS generated by La-based treatments.

Currently, little information about the mechanismof response to environmental stress in microalgae exposed to REEs is known. La and Ce treatments increased the oxidative stress and the activities of antioxidant enzymes (i.e., CAT and SOD) contributing to the elimination of ROS with peak activities at the intermediate monitoring periods (day 14 and 21). At the end of the exposure period (day 28), both La and Ce presented activity values similar or lower than the respective negative controls suggesting the potential development of tolerance to La and Ce due to the generational succession of *R. subcapitata* in 28 days (i.e., the culture was always kept in log-phase). This is something new compared to the existing knowledge about microalgae stress response also to other metals like cadmium, copper, chromium, and lead especially due to the extension of the exposure period from 15 days up to 28 days (Danouche et al., 2020). This is a challenging aspect for microalgae assemblages that could be further investigated considering suitable tolerance genes (i.e., rate of creation of tolerance genes by mutation, fitness cost of tolerance, and size of the population) on which the selection could act as already observed for other metals (e.g., copper from mining sites), but in macrophytes (Macnair, 1993).

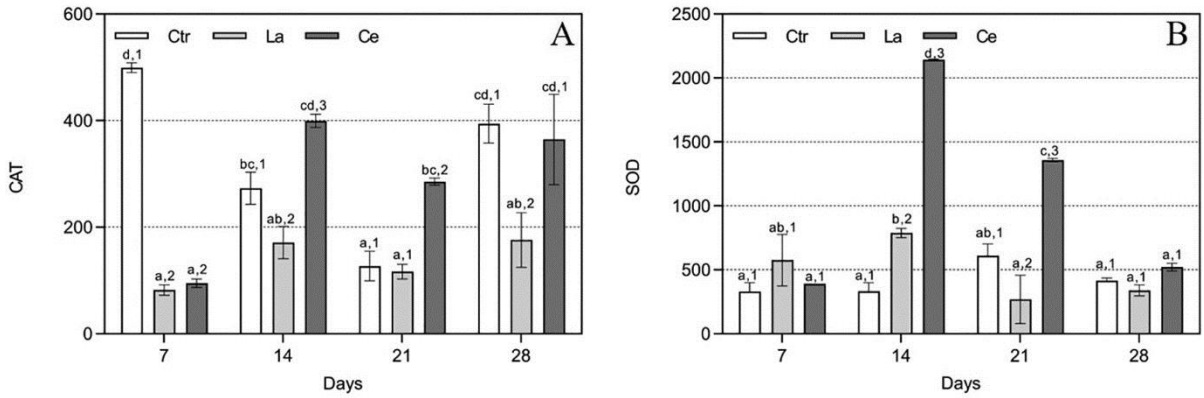

Figure 4. Antioxidant enzyme activities after normalization on protein content; CAT (A) and SOD (B) were expressed as U/mg protein. Results are presented as mean ± std.err. (n = 4). Letters (a–d) indicate significant differences between exposure times (7, 14, 21, and 28) within treatments (La and Ce), while numbers (1–3) highlighted significant differences within exposure times (7, 14, 21, and 28) between treatments (La and Ce) ($p < 0.05$, Tukey's test).

Results about La and Ce uptake in *R. subcapitata* were summarized in Figure 5 after their normalization to negative controls (i.e., 0.210±0.010 µg La/g dry weight (d.w.); 0.368 ± 0.030 µg Ce/g d.w.). Bioconcentration data were best fitted via an exponential growth (3 parameters) curve ($f=y0+a* \exp(b * x)$) (see Supplementary materials for details). The average La content per unitmasswas of 2058 µg/g d.w. (i.e., meanof day 7, 14, 21, and 28 values) ranging from 1442±459, 1684±347, 1947±296, 3157 ± 265 µg/g d.w. at day 7, 14, 21, and 28. The amount of La in microalgae constantly increased from day 7 to day 28, substantially doubling its value in 21 days (day 28).

The average Ce content per unit mass in *R. subcapitata* was of 353 µg/g d.w. ranging from 237±59, 284±35, 442±131, 1232±120 d.w. µg/g at day 7, 14, 21, and 28. Its content in microalgae slightly increased between day 7 and day 21 reaching the highest level in day 28. Cerium was able to bioconcentrate increasing its initial concentration (day 7) in microalgae by 5-fold in 21 days.

No significant Pearson correlations ($p > 0.05$) between the biomarkers of stress and bioconcentrated La and Ce were found. The association between the induction of tolerance and bioconcentration could represent for La and Ce, and potentially for other REEs, the key for bioaccumulation and biomagnification through the food chain. MacMillan et al. (2019) evidenced that freshwater zooplankton can bioconcentrate REEs from several environmental drivers including water column and bottom sediment, especially at higher dissolved organic carbon ratios and lower pH values, as also confirmed in Siciliano et al. (2021a). No information is currently available about trophic transfer of REEs from primary producers to primary consumers (i.e., zooplankton), but we can suspect that the potential convergence of tolerance acquisition and bioconcentration from water of La and Ce in *R. subcapitata* could strongly increase the potential biomagnification through the food chain, also with possible repercussion on food safety and human health.

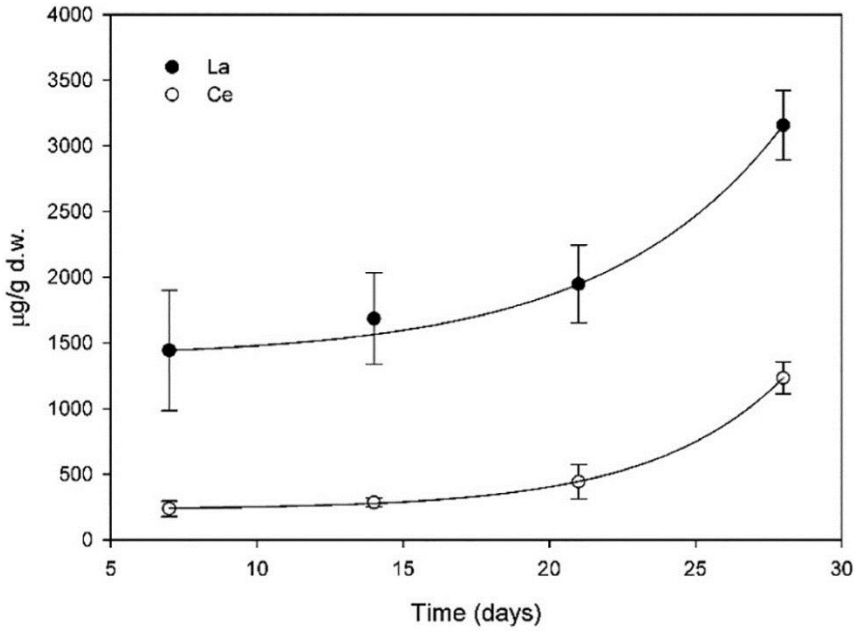

Figure 5. La and Ce uptake (µg/g) in algal biomass at day 7, 14, 21, and 28 after normalization on negative controls; data are in µg/g (±std.err.; n= 3).

4 Conclusions

This research focused on the effects of La and Ce as potential new emerging contaminants as a consequence of the alteration of their natural biogeochemical cycles. Populations of *R. subcapitata* were exposed to La and Ce serial concentrations (3 days) to define their concentration-response curves and the relative EC_{10}. La and Ce EC_{10} values were used to spike the microalgae growth media for the 28-days long-term exposure to monitor their effects on growth inhibition, biomarkers of stress (ROS, SOD, and CAT), and the potential to bioconcentrate. La and Ce are able to slightly increase microalgae growth inhibition in 28 days (i.e., 38% and 28%, in that order), allowing them, at the same time, to bioconcentrate up 3157 and 1232 µg/g dry weight, respectively. CAT and SOD presented relatively low activity levels, like for ROS in the case of Ce. ROS showed higher activities, but without any clear and specific correlations with toxicity data. Microalgae as primary producers showed to bioconcentrate La and Ce from spiked water, suggesting that further investigations on primary consumers (i.e., zooplankton) are necessary in order to verify their potential biomagnification

through the food chain up to human beings. Further studies are also required to investigate the association between the induction of tolerance and bioconcentration in *R. subcapitata*.

Supplementary materials

Bioconcentration data fitting for La

Nonlinear Regression - Dynamic Fitting
Equation: Exponential Growth; Single, 3 Parameter
f=y0+a*exp(b*x)

Dynamic Fit Options:

Total Number of Fits	200
Maximum Number of Iterations	200

Parameter Ranges for Initial Estimates:

	Minimum	Maximum
y0	-1442.045	4326.136
a	-12.865	38.594
b	0.000	0.524

Summary of Fit Results:

Converged	98.0%
Singular Solutions	1.5%
Ill-Conditioned Solutions	1.0%
Iterations Exceeding 200	1.5%
Inner-Loop Failures	0.5%

Results for the Overall Best-Fit Solution:

R	Rsqr	Adj Rsqr	Standard Error of Estimate
1.000	1.000	(+inf)	(+inf)

	Coefficient
y0	1385.773
a	17.822
b	0.164

Analysis of Variance:

Analysis of Variance:

	DF	SS	MS
Regression	3	15836057.735	5278685.912
Residual	0	0.000	(+inf)
Total	3	15836057.735	5278685.912

Corrected for the mean of the observations:

	DF	SS	MS	F	P
Regression	2	1553515.986	776757.993	0.000	(NAN)
Residual	0	0.000	(+inf)		
Total	2	1553515.986	776757.993		

Statistical Tests:

Durbin-Watson Statistic (+inf) Failed

Normality Test (Shapiro-Wilk) Passed (P = <0.0001)

W Statistic= <0.0001 Significance Level = <0.0001

Constant Variance Test Failed (P = <0.0001)

Fit Equation Description:

```
[Variables]
x = col(1)
y = col(2)
reciprocal_y = 1/abs(y)
reciprocal_ysquare = 1/y^2
'Automatic Initial Parameter Estimate Functions
F(q)=ape(x;ln(y-min(y));1;0;1)
[Parameters]
y0 = min(y) "Auto {{previous: 1385.77}}
a = exp(F(0)[1]) "Auto {{previous: 17.8225}}
b = F(0)[2] "Auto {{previous: 0.164249}}
[Equation]
f=y0+a*exp(b*x)
fit f to y
"fit f to y with weight reciprocal_y
"fit f to y with weight reciprocal_ysquare
[Constraints]
b>0
[Options]
tolerance=1e-10
stepsize=1
iterations=200
```

Number of Iterations Performed = 17

The regression produces a perfect fit

Bioconcentration data fitting for Ce

Nonlinear Regression - Dynamic Fitting
Equation: Exponential Growth; Single, 3 Parameter
f=y0+a*exp(b*x)

Dynamic Fit Options:

Total Number of Fits	200
Maximum Number of Iterations	200

Parameter Ranges for Initial Estimates:

	Minimum	Maximum
y0	-236.500	709.501
a	-2.228	6.683
b	0.000	0.652

Summary of Fit Results:

Converged	97.0%
Singular Solutions	3.0%
Ill-Conditioned Solutions	1.5%
Iterations Exceeding 200	2.5%
Inner-Loop Failures	0.5%

Results for the Overall Best-Fit Solution:

R	Rsqr	Adj Rsqr	Standard Error of Estimate
1.000	1.000	1.000	8.791

	Coefficient	Std. Error	t	P
y0	231.705	8.622	26.873	0.0237
a	2.059	0.499	4.124	0.1515
b	0.221	0.008	26.088	0.0244

Analysis of Variance:

Analysis of Variance:

	DF	SS	MS
Regression	3	1851951.450	617317.150
Residual	1	77.277	77.277
Total	4	1852028.727	463007.182

Corrected for the mean of the observations:

	DF	SS	MS	F	P
Regression	2	646577.274	323288.637	4183.516	0.0109
Residual	1	77.277	77.277		
Total	3	646654.551	215551.517		

Statistical Tests:

Durbin-Watson Statistic 2.994 Failed

Normality Test (Shapiro-Wilk) Passed (P = 0.6763)

W Statistic= 0.9436 Significance Level = <0.0001

Constant Variance Test Passed (P = <0.0001)

95% Confidence:

Row	Predicted	95% Pred-L	95% Pred-U
1	241.371	96.036	386.706
2	277.094	146.080	408.108
3	444.836	289.589	600.083
4	1232.490	1074.552	1390.428

Fit Equation Description:

```
[Variables]
x = col(1)
y = col(4)
reciprocal_y = 1/abs(y)
reciprocal_ysquare = 1/y^2
'Automatic Initial Parameter Estimate Functions
F(q)=ape(x;ln(y-min(y));1;0;1)
[Parameters]
y0 = min(y) "Auto {{previous: 231.705}}
a = exp(F(0)[1]) "Auto {{previous: 2.05857}}
b = F(0)[2] "Auto {{previous: 0.220948}}
[Equation]
f=y0+a*exp(b*x)
fit f to y
"fit f to y with weight reciprocal_y
"fit f to y with weight reciprocal_ysquare
[Constraints]
b>0
[Options]
tolerance=1e-10
stepsize=1
iterations=200
```

Number of Iterations Performed = 77

A first attempt to evaluate the toxicity to Phaeodactylum tricornutum Bohlin exposed to rare earth elements

1 Introduction

Rare earth elements (REEs) can have potential harmful effects on environmental and human health, and the related exposure is expected to increase in the near future due to their wide use in technology, medicine, agriculture and industry (Pagano et al., 2019). REEs are considered essential for a large number of applications including the alternative energy sector (Adeel et al., 2019; Cardoso et al., 2019; Hurst, 2010) including permanent catalysis (24%), magnets (23%), polishing (18%), metallurgy (8%), and batteries (8%) (Roskill Information Services Ltd). REEs are strategic resources, but they are not renewable and are considered to be close to "peaking" (Balaram, 2019; Rustad, 2012) with an application boom that would continue also in the near future (Balaram, 2019). The REEs supply chain is still linear and recycling barely reaches 1% of the world production (Rustad, 2012). In this way, REEs enter the environment via many ways, particularly during disposal of consumer and industrial products (e.g., landfills), discharges from mining and mineral processing, and wastewater from industrial processes that use REEs (Balaram, 2019; Gwenzi et al., 2018; Migaszewski and Gałuszka, 2015). Anthropogenic REEs contamination can be of great concern in hot spots (e.g., ore mine tailings and abandoned mines) (Pagano et al., 2015a). The general alteration of their biogeochemical cycles can transform them into potential emerging contaminants (Balaram, 2019; Galdiero et al., 2019; Gravina et al., 2018; Gwenzi et al., 2018; Naccarato et al., 2020; Pagano et al., 2019, 2015a, 2015b). There is still relatively little knowledge of the natural or anthropogenic cycles of REEs in the environment as well as their biological effects compared to cadmium (Cd), mercury (Hg), lead (Pb), chromium (Cr), and nickel (Ni) (Hirano and Suzuki, 1996). However, REEs and heavy metals (HMs) have similar environmental behaviours, can be accumulated by animals and plants and consequently they can pose potential risks in a one-health perspective (Gwenzi et al., 2018; Pagano et al., 2015a). Like HMs, REEs could generate reactive oxygen species (ROS), weaken, or inactivate the antioxidant defence and bind for the high affinity to vital macromolecules (Balali-Mood et al., 2021; Pagano et al., 2015a; Siciliano et al., 2021b; Trapasso et al., 2021a).

The increased mobilisation and concentration of REEs in water systems could have significant impacts primarily to aquatic organisms (Freitas et al., 2020). The REE-content in seawater can be determined by factors relating to different input sources (e.g., terrestrial, hydrothermal) and scavenging processes related to depth, salinity, and oxygen levels (Greaves et al., 1999) (Nozaki, 2001). The distinctive character of the seawater REEs distribution is largely controlled by the uniform trivalent behaviour most REEs (except for Ce and Eu which vary with oxygen levels) and estuarine and oceanic scavenging processes (Nothdurft et al., 2004). In contrast, anthropogenic, strongly chelated, anionic REEs appear to have a conservative behaviour and a long environmental half-life (Kulaksız and Bau, 2013, 2007; Lawrence et al., 2009). REEs anomalies due to anthropogenic activities were observed in seawaters in Plymouth Sound, UK (Karadaş et al., 2011), Ibaraki, Japan (Zhu, 2020) and Western Philippine (Goldstein and Jacobsen, 1988).

The biological effects and the toxicity of REEs is not fully understood, especially in saltwater. From the scarce literature on REE toxicity to aquatic organisms, only few data are available for marine organisms compared to freshwater ones (Freitas et al., 2020; González et al., 2015). Most studies demonstrated the ability of REEs to accumulate in marine species belonging to lower trophic levels, and consequently posing potential ecological risks (Gwenzi et al., 2018; Pagano et al., 2015b; Ponnurangam et al., 2016). Currently, no data about REEs exist about *Phaeodactylum tricornutum*

Bohlin, that is, a cosmopolitan species found in transitional, marine-coastal and marine waters and considered as a reference model in monitoring seawater pollution and assessment of pure organic and inorganic chemicals (Libralato et al., 2016b).

This study investigated the effects of lanthanum (La), cerium (Ce), neodymium (Nd), samarium (Sm), europium (Eu), gadolinium (Gd), dysprosium (Dy), and erbium (Er) on *P. tricornutum* growth explicitly providing the median and 10% effect concentrations (EC_{50} and EC_{10}). The aims of this study were to: 1) generate ecotoxicological information regarding *P. tricornutum* poorly studied for the REE toxicity, 2) compare, if possible, REEs toxicity with HMs, and 3) weigh up the EC_{50} with concentrations already found in the seawater to determine the potential risk associated with these elements.

2 Materials and methods

2.1 Chemicals, testing solutions, and analytical characterization

Nitrate standard solutions of 8 REEs (100 mg/L) provided by Sigma-Aldrich (Saint Louis, United States of America) were used for conducting the toxicity trials [$La(NO_3)_3$ $6H_2O$, purity 97%, $Ce(NO_3)_3$ $6H_2O$, purity 97%; $Nd(NO_3)_3$ $6H_2O$, purity 99.9%], Sm $(NO_3)_3$ $6H_2O$, purity 99.9%, $Eu(NO_3)_3$ $5H_2O$, purity 99.9%, $Gd(NO_3)_3$ $6H_2O$, purity 99.9%, $Dy(NO_3)_3$ xH_2O, purity 99.9% and $Er(NO_3)_3$ $6H_2O$, purity 99.9%. Treatment REE solutions were prepared by diluting REE standard solutions into artificial seawater (ISO, 2016) at least 1 h prior to the exposure followed by the pH measurement (Mettler Toledo Five Easy, Milan, Italy).

Rare earth elements analytical concentrations were determined by inductively coupled plasma mass spectrometry (ICP-MS, Aurora M90 Bruker Daltonics Inc.). High-purity water (resistivity of 18.2 MΩ cm) was obtained from a Milli-Q unit (Millipore, United States). Nitric acid (HNO_3, 69% v/v Ultratrace@ ppb-trace analysis grade) was provided by Scharlau (Barcelona, Spain). All samples analyzed in ICP-MS were prepared in HNO_3 solution (2% v/v). The analysis was performed in Normal Sensitivity mode. Calibration curves for determining REEs ranged from 0.5 to 1,000 µg/L and were constructed daily by analysis of standard solutions prepared immediately before analysis. The internal standard was ^{115}In for both calibration curve and sample analysis.

2.2 *Phaeodactylum tricornutum* bioassay

Axenic cultures of *P. tricornutum* microalgae were cultured at Hygiene Laboratory, Department of Biology at the University of Naples Federico II. Culture of *P. tricornutum* were routinely maintained in axenic artificial seawater medium supplemented with nutrients (ISO, 2016) at 22 ± 1°C and 4,800 lux on a 16:8 h light-dark cycle. Algal growth inhibition test (72 h) was performed according to ISO (2016) by using multiwell plates. For each concentrations four wells were filled with 2,250 µL of the respective solution ($K_2Cr_2O_7$ positive control, spiked REE solution, sinthetic sea water as negative control), 125 µL of the 20-fold culture media and 125 µL of inocula of exponentially growing microalgae. One of the four replicates served as blanks the prepared well plates were then placed on a horizontal shaker with 50 rpm for 72 h at 22 ± 1°C under continuous light of 6,700 lux. Solutions spiked with REEs ranged between 0.3 mg/L and 5.0 mg/L (nominal concentrations).

After a 72 h of exposure, spectrophotometric measurement of samples at 670 nm (DR 5000 sc, Hach) allowed to determine algal cell density through linear regression equation that described the

relationship between optical density and cell density. The growth rate compared to negative control was calculated according to ISO (2016).

2.3 Data analysis

After screening assays, testing concentrations were set up in order to allow the calculation of median, 20, 10 and 5% effect concentrations (EC_{50}, EC_{20}, EC_{10}, and EC_5) which were determined using linear and nonlinear regression. For each REE, the best-fitting model was selected based on the mean corrected coefficient of determination (R^2) and by graphical interpretation of the model fit. Differences between treatments were assessed via one-way analysis of variance (ANOVA) after the verification of normality (Shapiro-Wilk's test) and homoscedasticity (Levene's test). Moreover, to further evaluate the risk of REEs, the estimated concentration causing an effect (EC_{50}) was divided by an assessment factor (AF) to estimate a predicted no-effect concentration (PNEC). The ratio of measured environmental concentration (MEC) listed in Table 3 to the PNEC was calculated to estimate the risk quotient (RQ).

3 Results

3.1 REE nominal vs. analytical concentrations

Analytical concentrations used to calculate concentration-response curves are highlighted in Table 1. The ratio between analytical and nominal concentrations in most samples ranged from 0.8 to 1.2. Results are in accordance with previous studies (Oral et al., 2017; Pagano et al., 2016).

Table 1. Nominal and measured concentrations of rare earth elements and the relative standard deviations; NC = nominal concentrations; MC = measured concentrations (mg/L).

NC	MC							
	La	Eu	Ce	Gd	Nd	Dy	Sm	Er
0.3	0.33 ± 0.01	0.24 ± 0.01	0.27 ± 0.01	0.38 ± 0.02	0.30 ± 0.013	0.27 ± 0.01	0.31 ± 0.02	0.29 ± 0.14
0.6	0.70 ± 0.03	0.81 ± 0.04	0.63 ± 0.01	0.58 ± 0.03	0.55 ± 0.024	0.56 ± 0.03	0.51 ± 0.03	0.52 ± 0.02
1.2	1.24 ± 0.05	1.59 ± 0.08	1.13 ± 0.03	1.01 ± 0.05	1.42 ± 0.062	1.40 ± 0.08	1.11 ± 0.06	1.28 ± 0.06
2.5	2.03 ± 0.09	2.95 ± 0.12	2.19 ± 0.06	2.06 ± 0.11	2.84 ± 0.124	2.74 ± 0.15	2.28 ± 0.11	2.08 ± 0.09
5	6.00 ± 0.26	5.82 ± 0.28	5.04 ± 0.15	4.08 ± 0.22	6.05 ± 0.26	6.21 ± 0.34	4.26 ± 0.21	4.28 ± 0.20

3.2 REE toxicity on *P. tricornutum*

In Figure 1, the results about the growth inhibition of *P. tricornutum* are reported for Ce, Dy, Eu, La, Er, Gd, Sm, and Nd. All equations and the relative standard errors are provided in Figure 1 and the determination of EC_{50}, EC_{20}, EC_{10}, and EC_5 are summarized in Table 2.

As a general overview, the algal growth always evidenced inhibitory effects at all the tested concentrations, except for La and Dy, which displayed biostimulation effect at the two lowest tested concentrations. Cells of *P. tricornutum* exposed to La and Dy concentrations between 0.3 and 0.7 mg/L after 72 h showed greater cell density than the control group. The elements that caused the highest growth inhibition at the lowest concentrations were Gd and Ce (27 and 24%, respectively).

Cell density of *P. tricornutum* at the highest concentrations exposed of Ce, La, Gd and Er showed the highest inhibition of growth with inhibitions of 88, 91, 98, and 96% respectively (Figure 1). In contrast, the highest concentrations of Eu, Nd, Dy, and Sm showed the lowest growth inhibition 72, 62, 71, and 53%, respectively (Figure 1).

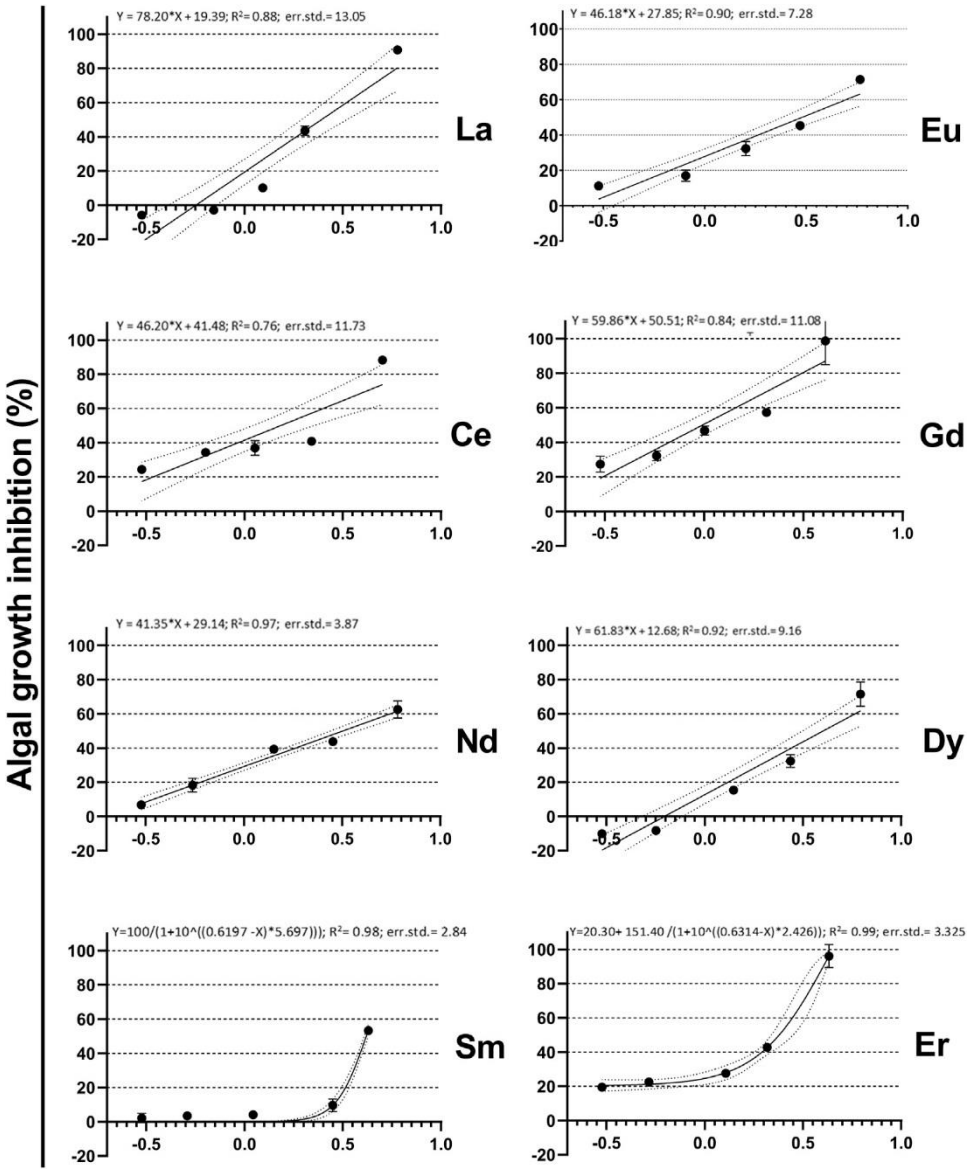

Figure 1. Concentration-response relationship of La, Eu, Ce, Gd, Nd, Dy, Sm, and Er exposed to *P. tricornutum*; x-axis log scaled concentrations are in mg/L. Solid line indicates the line of best fit, the dashed lines represent the 95% confidence intervals for linear regression (La, Eu, Ce, Gd, Nd, and Dy) and for nonlinear regression (Sm, and Er).

The toxicity always showed a dose-response relationship. Both Dy and La displayed biostimulation at low concentrations, while the highest relative inhibition was observed at the highest concentration.

The EC_{50} values (±95% confidence limit values) obtained for all the tested elements were summarised in Table 2 including EC_5, EC_{10} and E_{20}. Based on the calculated EC_{50} values, the following toxicity relationship was established: Gd > Ce > Er > La > Eu > Nd > Dy > Sm.

Table 2. EC_5, EC_{10}, EC_{20}, and EC_{50} values for Ce, Dy, Eu; La and Nd on *P. tricornutum*; values are in mg/L; n.a. = not available; REEs = rare earth elements; EC = effective concentration; average EC values are provided ±95% confidence limit values in brackets (n = 3).

REEs	EC_5	EC_{10}	EC_{20}	EC_{50}
La	0.65 (0.24–1.89)	0.76 (0.28–2.19)	1.02 (0.37–2.97)	2.46 (0.87–7.34)
Eu	0.32 (0.11–0.84)	0.41 (0.15–1.07)	0.68 (0.25–1.74)	3.02 (1.16–7.41)
Ce	0.16 (0.04–0.78)	0.21 (0.05–1.01)	0.34 (0.08–1.68)	1.53 (0.32–7.75)
Gd	0.17 (0.07–0.46)	0.21 (0.08–0.56)	0.31 (0.12–0.83)	0.98 (0.37–2.67)
Nd	0.26 (0.17–0.40)	0.34 (0.23–0.53)	0.60 (0.39–0.92)	3.19 (2.09–4.88)
Dy	0.75 (0.31–1.81)	0.90 (0.38–2.18)	1.31 (0.55–3.16)	4.01 (1.67–9.70)
Sm	0.60 (0.06–8.18)	0.85 (0.08–11.20)	1.68 (0.16–20.99)	13.21 (1.03–138.28)
Er	0.27 (0.05–1.44)	0.33 (0.06–1.75)	0.48 (0.09–2.57)	1.55 (0.28–8.20)

3.3 Comparative risk assessment

About risk assessment, RQs for each REEs were estimated using values of MEC considering three different scenarios from the literature (coastal seawater, open seawater and estuarine seawater) (Wysocka and Vassileva, 2017; Zhu, 2020) and PNEC (Table 3). Wennmalm and Gunnarsson (2009) and Verlicchi et al. (2012) classified the environmental risk into different levels according to the RQs obtained. The classification follows: if RQ < 0.1 the environmental risk level is considered insignificant, an RQ from 0.1–1.0 is considered low, an RQ from 1.0–10 is considered moderate, and an RQ > 10 is considered high risk. For groups of relatively unknown sensitivity such as saltwater species and for acute laboratory studies, the assessment factor is between the range of 10–1,000 (Fairbrother, 2008). Because of the scarce data available about the toxicity of REEs to marine species, the factor of this study was set at 1,000.

In all scenarios, RQs were below 1 and none of the investigated REEs were classified as high risk. The estimated RQs varied from 0.0006 to 0.1803 with a mean value of 0.0346 in the coastal seawaters, from 0.0008 to 0.0403 in the open seawaters with a mean value of 0.0135 and from 0.0196 to 0.4606 in the estuarine waters with a mean value of 0.2154, indicating, in the latter case, a potential low risk posed by the REEs on the marine organisms. Only Ce posed low risks to aquatic organisms in the coastal seawaters, while all the other elements resulted in insignificant risk. Moreover, for open seawaters, all the REEs resulted in insignificant risks, including Ce, La and Nd, which are considered the most abundant REEs in the environment (Adeel et al., 2019; Freitas et al., 2020). Overall, of the 8 REEs, more than 60% exhibited potential ecotoxicological risks in the estuarine waters due to their relative high concentrations and/or toxicities. The results agreed with the previous study of (González et al., 2015) that REEs in the different exposure environmental conditions had ecological risks limited to some hotspots.

Table 3. Calculated risk quotients for REEs in seawater.

REE	PNEC [ng/L]	MEC [ng/L]			RQ		
		Open seawater (Zhu, 2020)	Coastal seawater (Zhu, 2020)	Estuarine water (Wysocka and Vassileva, 2017)	Open sea water	Coastal seawater	Estuarine
La	2,460	99.30	166.00	794.83	0.0404	0.0675	0.3231
Eu	3,020	2.50	2.07	59.06	0.0008	0.0007	0.0196
Ce	1,530	33.50	276.00	704.75	0.0219	0.1804	0.4606
Gd	980	13.90	10.10	311.32	0.0142	0.0103	0.3177
Nd	3,190	58.80	31.00	855.91	0.0184	0.0097	0.2683
Dy	4,010	14.60	10.80	356.38	0.0036	0.0027	0.0889
Sm	13210	10.80	7.50	778.84	0.0008	0.0006	0.0590
Er	1,550	12.50	8.20	288.31	0.0081	0.0053	0.1860

4 Discussion

To the best of our knowledge, this is the first study reporting a large set of REEs toxicity data towards *P. tricornutum*. Previous data are available only from Sun et al. (2019) on La but considering only nominal concentrations. The EC_{50} of La from this study (2.46 mg/L) is more than 4 times lower than that obtained by (Sun et al., 2019) (10.08 mg/L), being such difference attributable to the use in our paper of measured concentrations. However, the values obtained in both studies do not differ greatly and can therefore still be comparable in the effects on the growth. Moreover, to further evaluate the data obtained and interpret the toxicological relations for tested REEs, the results obtained were compared to those obtained by (Tai et al., 2010) on diatom *Skeletonema costatum*. From this study, the EC_{50} of Ce (1.53 mg/L) was lower than those obtained by Tai et al. (2010) (4.2 mg/L) and the Dy values obtained were very similar in value (4.01 and 4.6 mg/L).

Moreover, to understand better the sensitivity of *P. tricornutum* to metals, the EC_{50} values obtained were also compared to data available on the toxicity of heavymetals (Table 4). The ecotoxicity of HMs (e.g., Cd, Pb) is higher than that of REEs, when compared under similar experimental conditions and species. From the results presented in this study compared to those obtained by (Horvatić and Peršić, 2007), the element with the highest toxicity was Gd (0.98 mg/L), which differed around 4 orders of magnitude with the element with the highest toxicity mercury chloride ($1.16 \cdot 10{-}5$ mg/L), had a similar toxicity to cobalt chloride (1.19 mg/L) and had a higher toxicity than cadmium nitrate (5.37 mg/L). Moreover, (Horvatić and Peršić, 2007), also found that low concentrations of Cd and Co had a stimulatory effect on the growth rate from concentrations between 0.02 and 1.25 mg/L for Co and 0.16–0.31 mg/L for Cd, which are in a similar range to those obtained for Dy and La, which presented a biostimulation effect from concentrations between 0.3 and 0.7 mg/L. Results displayed, indicate that HMs such as copper and mercury are more toxic than the tested REEs, nevertheless, the results obtained are in a similar range to the remaining HMs presented. Elements such as Hg, Pb, Co and Cr have shown to be themost toxic elements affecting the growth of *P. tricornutum* (Cabrita et al., 2016), this might be explained by the fact that the cells incorporate these elements and the internalization causes damages in terms of cell division and growth (Cabrita et al., 2016, 2014; Deng et al., 2013).

Table 4. Toxicity response of *P. tricornutum* to metals in 72-h growth inhibition bioassays. *Measured, #Nominal Concentrations.

Element	72-h EC_{50}	References
Cadmium ($Cd(NO_3)_2$.$4H_2O$)	5.37#	Horvatić and Peršić, (2007)
Cobalt ($Co(NO_3)_2$)	19.57#	
Cobalt ($CoCl_2$)	1.19#	
Zinc ($ZnSO_4 \cdot 7H_2O$)	41.85#	
Mercury ($HgSO_4$)	0.03#	
Mercury ($HgCl_2$)	1.16×10^{-5}#	
Nickel ($NiSO_4 \cdot 6H_2O$)	7.28#	
Copper ($CuSO_4 \cdot 5H_2O$)	0.035	Moreno-Garrido et al., (2000)
	0.008*	Levy et al., (2007)
	0.010#	Franklin et al., (2001)
	0.565*	Liping and Zheng, (2008)

The outcome of the environmental risk assessment of investigated REEs was different depending on the MECs of coastal, oceanic, and estuarine waters used to calculate the RQs. The evaluation results showed that RQ values were gradually increasing from ocean to estuary. The RQs were less than 0.1 in coastal and oceanic waters, except for Ce, which meant ecological environmental risk of REEs to marine species was not of concern. While for coastal and oceanic scenarios, hydrodynamics and significant dilution could explain the lower REE concentrations, it was notable that REEs concentrations were higher at estuarine waters, which could be attributed to the local sewage discharge and anthropic activities.

Either way, the RQs in the estuarine waters for REEs were always higher than 0.1. In this scenario, based on the RQ approach, the REEs assessed herein appear to be of raising marine concern, especially with regard to La and Ce, which could be explained based on the more frequent use of Ce and La that can promote their occurrence in environment as well as seawater. This work reinforces the urgent need for more data embracing other REEs and other species, in order to avoid under- or over-estimation when assessing the environmental risks of these metals.

5 Conclusion

Rare earth elements (Ce, La, Eu, Sm, Gd, Dy, Er, and Lu) effects to *P. tricornutum* growth inhibition were investigate. Results showed similar toxicity levels between light, medium and heavy REEs.

Toxicity can be compared to the effect of heavy metals on *P. tricornutum*. Although the differences in orders of magnitude between some elements, it can be observed that both groups of elements can have a bio-stimulatory effect but an inhibitory effect at higher concentrations. Further studies to evaluate the effects of low and constant exposure is suggested.

Further, this study presents a first insight on the effect of several REEs on the unicellular species *P. tricornutum*, which can be considered as a potential candidate to further study the effect of REEs on more complex matrices such as artificial sea water.

Based on *P. tricornutum* toxicity results, the presence of REEs in the marine environment does not seem to represent a widespread environmental risk except at some hotspots which may become more severe with the increase of REE application.

This approach could be used to further investigate more relevant endpoints, which could lead to indirect effects on the food chain and to study predictable patterns in bioavailability, bioaccumulation and ecotoxicity, as well as studies addressing the combined effect of several stressors such as REEs mixtures.

Hormetic Effects of Cerium, Lanthanum and Their Combination at Sub-micromolar Concentrations in Sea Urchin Sperm

1 Introduction

Rare earth elements (REEs) include a group of elements, the lanthanoids [lanthanum (La) to lutetium (Lu)] and two closely related elements, yttrium (Y) and scandium (Sc) which are recognized to be indispensable in the present world, due to their extensive roles in a number of technologies (Du and Graedel, 2013; González et al., 2015; Pagano et al., 2015a). REE-associated adverse effects have been assessed in a vast body of literature encompassing several biota, with implications also in human health, so that REEs have raised extensive health concern and are viewed as emergent contaminants (Brouziotis et al., 2022a; Gravina et al., 2018; Thomas et al., 2014; Trifuoggi et al., 2017).

Apart from their adverse effects, REEs also display recognized stimulatory effects, as reported in a body of literature on their use as components of fertilizers improving crop yields and in livestock feed additives (Abdelnour et al., 2019; Agathokleous et al., 2019; Bölükbaşı et al., 2016; He et al., 2010; Lian et al., 2019; Tommasi et al., 2021; Yin et al., 2021; Zhong et al., 2018.). This duplicity of REE-associated effects is not specific for REEs, but may be ascribed to a general phenomenon of a concentration-related shift from inhibition, or "toxicity" for high agent concentrations to stimulation for lower agent concentrations, also termed hormesis, and previously tagged as "Arndt-Schulz effect" (Agathokleous et al., 2020; Calabrese, 2016; Cedergreen et al., 2007; Pagano et al., 1982; Técher et al., 2020; Stebbing, 1982). The multiple implications of hormesis have been reported in an extensive body of basic and applied disciplines (e.g. Agathokleous et al., 2022; Calabrese et al., 2022; Jalal et al., 2021; Katsnelson et al., 2021; Lee and Lee, 2019; Nitti et al., 2022; Schirrmacher, 2021; Shibamoto and Nakamura, 2018).

Within the frame of REE-associated hormetic effects, the present study was aimed at verifying the effects of micromolar and sub-micromolar levels of two REEs, Ce and La, and their combination on sea urchin sperm fertilization success and offspring embryogenesis. The results confirmed a shift from inhibition to stimulation of tested events by comparing 10^{-5} M vs. < 10^{-6} M.

2 Materials and Methods

Cerium nitrate, lanthanum nitrate and their equimolar combinations were tested for their effects on *Sphaerechinus granularis* sea urchin sperm in changing fertilization success and the frequency of developmental defects in the offspring of exposed sperm. A preliminary assay tested a duration of control sperm suspension (10 to 60 min), allowing to either assess inhibition or stimulation of fertilization rate, leading to an intermediate (~50%) fertilization rate, and was found as 30-min sperm exposure (Pagano et al., 2017).

Sperm suspension was carried out by 1% dilution of "dry" sperm (as released by testes from two males) in agent solutions at concentrations ranging from 10^{-8} to 10^{-5} M. These duplicate sperm suspensions, in turn, fertilized eggs from three females, thus providing six-replicate embryo cultures that were observed for fertilization rate (FR, % fertilized eggs) and then for offspring quality. FR was measured starting from the appearance of fertilization membrane and of early cleavage (2-cell stage) for approximately 3 h post-fertilization. Subsequent observation of offspring was performed 3 days post-fertilization allowing detection of % prepared immediately before analysis developmental defects (DD) as larval malformations or pre-larval arrest and of mortality. This observation was

carried out after immobilizing larvae and embryos by adding a 10^{-4} M chromium sulfate, which allowed screening of bottom-laying embryos/larvae in an inverted microscope, ×10 magnification.

Analytical concentrations of Ce and La in the samples were determined by inductively coupled plasma mass spectrometry (ICP-MS, Aurora M90 Bruker, Germany). A Milli-Q unit (Millipore, United States) was used to obtain high-purity water (resistivity = 18.2 MΩ cm) was obtained from a Milli-Q unit (Millipore, United States). Nitric acid (HNO_3, 69% v/v Ultratrace@ ppb-trace analysis grade) was purchased from Scharlau (Barcelona, Spain). All samples analyzed in ICP-MS were prepared in HNO_3 solution (2% v/v). The analysis was performed in High Sensitivity mode. Calibration curves for determining REEs ranged from 0.5 to 1,000 μg/L for Normal and from 0.005 to 10 μg/L for High Sensitivity and were constructed daily by analysis of standard solutions prepared immediately before analysis. The internal standard was ^{115}In for both calibration curve and sample analysis.

The uniform and minimal weight concentration of sperm cells was not measured.

Datasets were analyzed in IBM SPSS v20 and Microsoft® Excel 2013/XLSTAT©-Pro (Version 7.2, 2003, Addinsoft, Inc., Brooklyn, NY, USA). Homogeneity of variances was checked by Levene's test. Differences between each concentration group and the controls were determined by two-tailed Independent Samples t-test. A normality test was performed and the significance of the difference among the groups was evaluated by One-way Analysis of Variance (ANOVA). Differences were considered significant when $p < 0.05$.

3 Results and Discussion

The correspondence between nominal and analytical concentrations of the tested samples, measured by ICP-MS, is shown in Table 1. The analytical/nominal ratios mostly ranged from 0.889 to 1.283; thus nominal concentration values were considered as reliable for concentration-related trends.

Table 1. Ratios of analytically checked concentrations of tested REEs (by ICP-MS, as μg/L) vs. nominal concentrations.

Nominal concentrations	10^{-4} M	10^{-5} M	10^{-6} M	10^{-7} M	10^{-8} M
Ce	1.095	1.008	1.102	1.277	1.021
La	0.92	0.883	1.238	1.053	1.224

As shown in Figure 1, fertilization rate (FR) of *S. granularis* sperm exposed for 30 min to $Ce(NO_3)_3$, or $La(NO_3)_3$, or their equimolar combination at concentrations ranging from 10^{-8} to 10^{-5} M showed the expected spermiotoxicity following 10^{-5} M pretreatment as reported previously (Trifuoggi et al., 2017). No significant effect was detected following sperm exposure to 10^{-6} M $Ce(NO_3)_3$ or $La(NO_3)_3$ level, with a significant FR decrease was observed following sperm exposure to 10^{-6} M Ce + La combination. Lower agent levels, as 10^{-7} and 10^{-8} M Ce, La and Ce + La combination resulted in significant FR increase.

The opposite concentration-related trend was found for the frequency of developmental defects (DD) and mortality (M) in the offspring of Ce-, La- and (Ce + La)-exposed sperm, which was significantly increased following sperm exposure to 10^{-5} M agents and to Ce 10^{-6} M, whereas lower agent concentrations (10^{-7} and 10^{-8} M Ce, or La or their combination) in sperm exposure resulted in significantly decreased offspring DD and M, as shown in Figure 2.

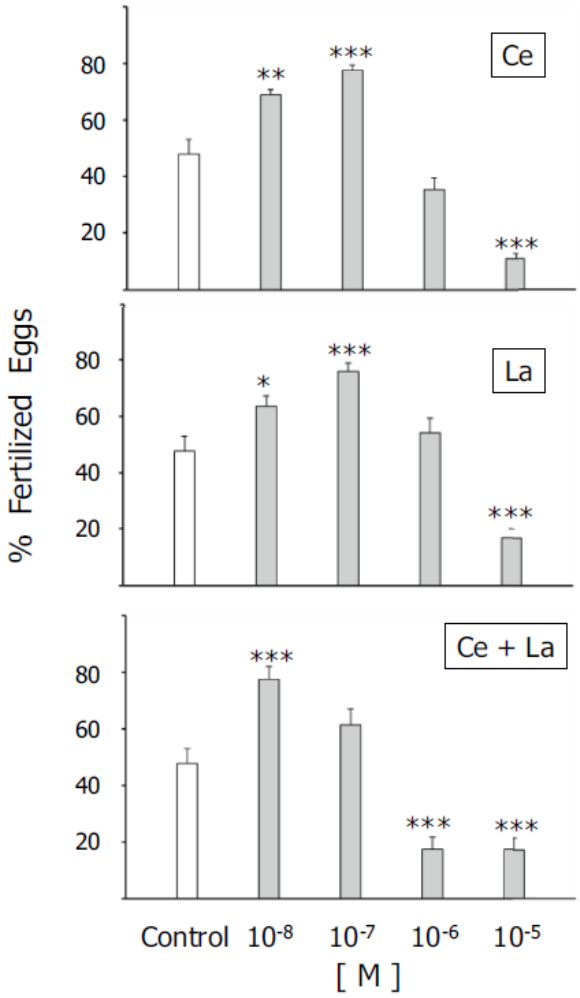

Figure 1. Percent fertilization rate of *S. granularis* sperm exposed 30 min to $Ce(NO_3)$, or $La(NO_3)$, or their combination atconcentrations ranging from 10^{-8} to 10^{-5} M.

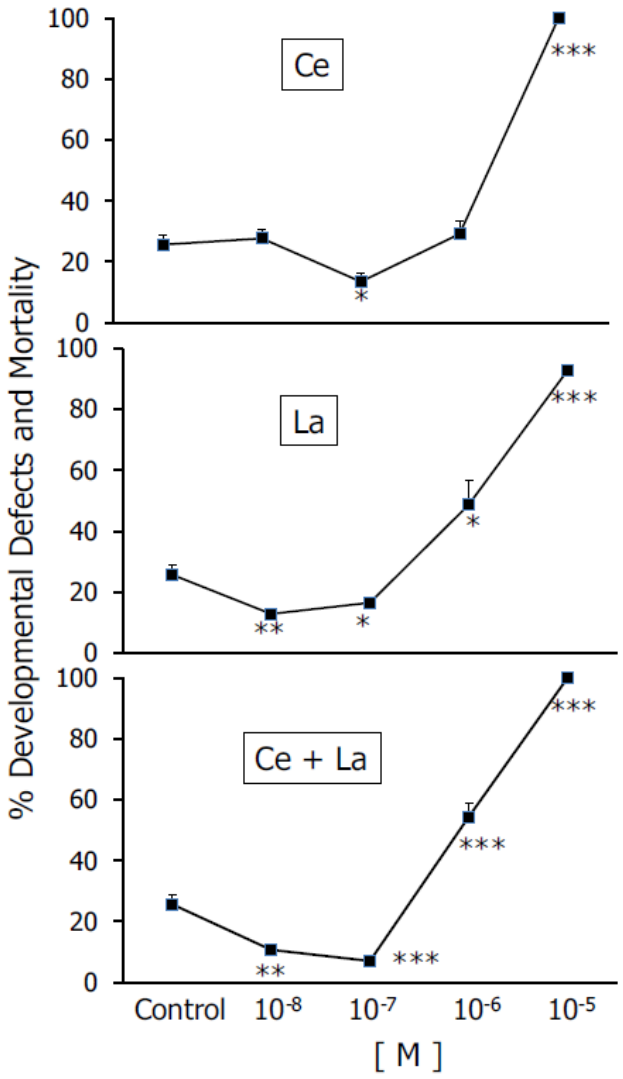

Figure 2. Percent developmental defects and mortality inthe offspring of *S. granularis* spermexposed 30 min to Ce(NO_3), or La(NO_3), or theircombination at concentrations ranging from 10^{-8} to 10^{-5} M.

The present results confirm the established database of REE-associated spermiotoxicity and induction of offspring damage following sperm exposure to Ce and La at concentrations ≥ 10^{-5} M (Trifuoggi et al., 2017). On the other hand, this study provides evidence for a hormetic shift of these REEs and of their combination at sub-micromolar concentrations that were found to significantly increase fertilization success and to decrease offspring anomalies vs. controls. Trans-generational hormetic effects were reported by Agathokleous et al., 2022. These results are new, though they could be anticipated on the grounds of the established use of REEs in supporting animal growth (Abdelnour et al., 2019; Bölükbaşı et al., 2016; He et al., 2010). Should these results be further confirmed in other bioassay models, they provide the grounds toward REE utilization in safely promoting animal growth.

Chapter 4: Environmental Chemistry of REEs

In this chapter, the contributions of the PhD project concerning the environmental chemistry of REEs are presented. The first of the two following subchapters is already published in *Molecules* (Saviano et al., 2023), while the second has been submitted for publication.

General introduction about chapter 4

Conventional wastewater treatment facilities have demonstrated poor efficacy in eliminating contaminants of recent concern over the past few decades (Lofrano et al., 2018). There is an urgent need for improvements in wastewater treatment technology since the persistent discharge of these compounds into water bodies poses a major hazard to ecosystems and human health (Pedrazzani et al., 2019). Advanced oxidation Processess (AOPs) have shown the possibility of ground-breaking advancements in the design of integrated systems for the treatment of contaminated wastewater (Lofrano et al., 2018).

The efficiency of the process can be increased by adding catalysts, such as heavy metals (Kuang et al., 2014). Rare earth element (REE) use in AOPs has recently attracted increasing interest (Zhang et al., 2019). REE ions are becoming increasingly important in green chemistry because they can be used in aqueous solvents without any deactivation, can be easily recovered from the reaction medium by extraction, and can be used multiple times without losing activity (Oliverio et al., 2018; Zhang et al., 2019).

Tha mining of REEs has increased concerns for both human and environmental health, especially on the areas near the mining sites. Previous studies have investigated the environmental levels of REEs on environmental samples near active or abandoned mining sites sites (Atibu et al., 2016; Medas et al., 2013), while others have evaluated their risk assessment on the populations living near them (Hao et al., 2015; Liang et al., 2018).

In addition to the potential adverse effects of REEs, the demand for these elements is continuously increasing globally, since their utilization is necessary for the production of electronic devices (Pagano et al., 2019). Therefore, the discovery of new sites for a potential REE exctraction in the future is on demand.

This chapter concerns the third level of investigation of this PhD project which is the Environmental Chemistry of REEs. A literature review was elaborated and published concerning the catalytic activity of REEs on AOPs for a more efficient removal of organic pollutants (pharmaceuticals, dyes and other targets) from aqueous solutions, like wastewaters. In addition, the environmental levels of REEs on three abandoned mining sites of bauxite in the region of Puglia (Gargano, Otranto and Spinazzola) were determined. Environmental samples from these sites were collected, digested and analyzed by two different techniques, TXRF and ICP-MS.

Catalytic activity of rare earth elements (REEs) in advanced oxidation processes of wastewater pollutants: A review

1 Introduction

Over the past few decades, conventional wastewater treatment plants (WWTPs) showed low efficiencies in removing contaminants of emerging concern (CECs) (Lofrano et al., 2018; Priya et al., 2022; Rout et al., 2021). CECs encompass a wide range of substances, including pharmaceuticals, personal care products, and dyes (Lofrano et al., 2018, 2016; Priya et al., 2022; Rout et al., 2021).

The chronic release of these substances in water bodies represents a serious threat to human health and ecosystems and requires urgent advancements in wastewater treatment technologies (Pedrazzani et al., 2019; Ugwu et al., 2022; Karri et al., 2021) focusing also on the perspective of treated wastewater reuse.

Advanced oxidation processes (AOPs) evidenced potential revolutionary solutions in the development of integrated systems for the treatment of contaminated wastewater (Lofrano et al., 2018, 2016; Pedrazzani et al., 2019; Priya et al., 2022; Rout et al., 2021; Ugwu et al., 2022; Karri et al., 2021; Werkneh et al., 2019). The mechanism of action of AOPs relies on the generation of reactive oxygen species (ROS) with strong oxidation capabilities, such as hydroxyl (OH•), sulfate (SO_4^{2-}•), and superoxide ion radicals (O^{2-}•), which quickly degrade a wide range of organic compounds in CO_2, H_2O, and inorganic acids (Andreozzi, 1999; Lofrano et al., 2009; Spasiano et al., 2016). The addition of catalysts, such as heavy metals, can promote the development of such radicals and improve the process efficiency (Kuang, 2014; Wang et al., 2016; Wang, 2008).

AOPs, particularly Fenton oxidation, are commonly carried out under acidic conditions, leading to the consumption of significant amounts of acid and base reagents (Acharya et al., 2011; Atalay and Ersöz, 2016). The effectiveness of AOPs relies on the proper dosage of reactive hydroxyl (HO) radicals, ensuring the desired level of treatment is achieved (Oturan and Aaron, 2014; Kumar and Shah, 2021). A major limitation of AOPs is their relatively high cost, primarily due to the use of expensive chemicals and increased energy consumption (Kumar and Shah, 2021). Additionally, AOPs can result in the formation of unknown recalcitrant by-products, which may be more nephrotoxic than the original compounds, posing unresolved challenges (Lofrano et al., 2018, 2016; Pedrazzani et al., 2019; Priya et al., 2022; Rout et al., 2021; Ugwu et al., 2022; Karri et al., 2021). While AOPs are effective in scavenging reactive radicals from non-target substances, they may not be suitable for certain categories of toxic compounds that resist degradation by HO radicals.

Recently, the application of rare earth elements (REEs) in the advanced oxidation process (AOP) has gained growing interest (Zhang et al., 2019). The REEs are a group of seventeen chemical elements in the periodic table, the 15 lanthanides from lanthanum (La) to lutetium (Lu), to which scandium (Sc) and yttrium (Y) are added since the latter tend to occur in the same mineral deposits with lanthanides and exhibit similar chemical properties. REE ions have a particular electronic structure compared to transition metal ions and are gaining great importance as Lewis acids in Green Chemistry because they can be used in aqueous solvents or water without any deactivation; they can be easily recovered from the reaction medium by extraction and can be used several times without loss of activity (Oliverio et al., 2018; Zhang et al., 2019). The redox properties of REEs depend on the arrangement of the surfaces and the shape and size of their crystals, and, for this reason, they can be improved by checking the nanostructure (Zinatloo-Ajabshir et al., 2022).

REEs exhibit unique physicochemical properties, such as high surface area, reactivity, and redox potential (Ambaye et al., 2020). These properties make REEs suitable to be used in AOPs, where they can enhance the performance of the processes (Bokare and Choi, 2014; Chan et al., 2011). REEs can be used as catalysts to promote the generation of reactive oxygen species (ROS) when exposed to UV radiation in photocatalysis processes (Onozuka et al., 2012), to catalyze Fenton-like processes (Assila et al., 2023), and to enhance the efficiency of ozonation by increasing the production of hydroxyl radicals (Song et al., 2022).

To date, most applications are still at lab scale and an increasing number of studies are being performed to fill the existing gaps in the usage of REEs for polluted water treatment. The main limitations to full-scale applications deal with high energy and capital cost.

This review focuses on the use of REEs as catalysts for the degradation of CECs from wastewater, since their use, which is currently in place for wastewater treatment, lacks processing and economic sustainability.

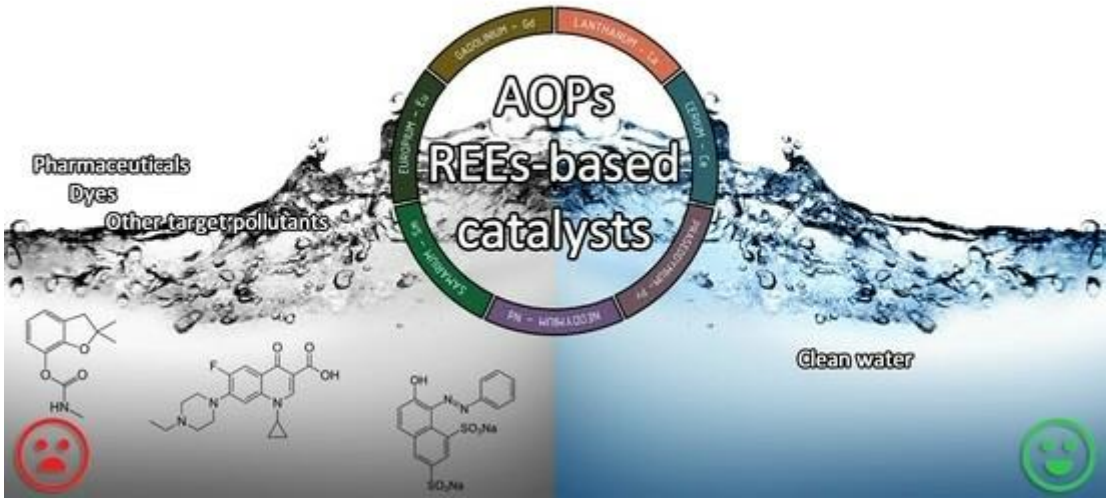

Graph 1. Graphical abstract of the study.

2 Methodology of Data Collection

The REE-assisted catalytic removal of CECs has substantially grown in recent decades, as retrieved in a Scopus search (keywords: rare earth elements, catalyst, and wastewater) updated on 20 December 2022.

We have collected 60 papers dealing with the degradation of different CECs from wastewater using REEs in AOPs. As shown in Figure 1a where the number of papers issued each year on catalytic removal of contaminants in wastewater treatment using REEs have been reported, the first publication was made in 1995 (Tokunaga et al., 1995), which means that the field is quite new. Since 2015, the number of publications has been increasing each year. Figure 1b shows the cumulative number of publications for each REE over the period of 1995–2022. Most processes were carried out by using Ce and La. Cerium has received by far most of the attention (148 publications), followed by La (44), Y (10), and Nd (10). Five REEs (Sc, Ho, Tm, Lu, and Pm) and their possible effective role in this field have never been explored.

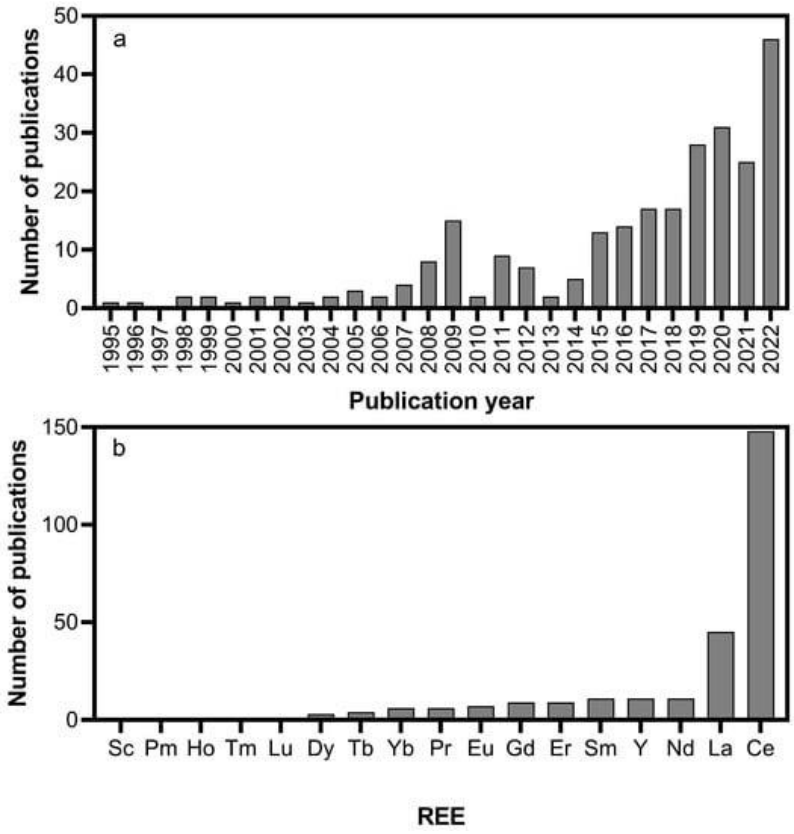

Figure 1. (a) The number of papers issued each year on catalytic removal of contaminants in wastewater treatment using REEs over the period of 1995–2022; (b) a cumulative number of publications for each REE over the period of 1995–2022.

Figure 2 presents the distribution of research papers that focused on the utilization of REE catalysts for the degradation of various types of contaminants. According to the data, pharmaceutical compounds and dyes accounted for the highest percentage of research papers, with approximately 33% and 42%, respectively. Alkaloids, herbicides, phenols, organic acids, cyanides, and other contaminants were also investigated to a lesser extent, each representing 3–8% of the papers. This distribution highlighted the varying levels of research emphasis on different categories of contaminants in relation to REE catalysts in the past.

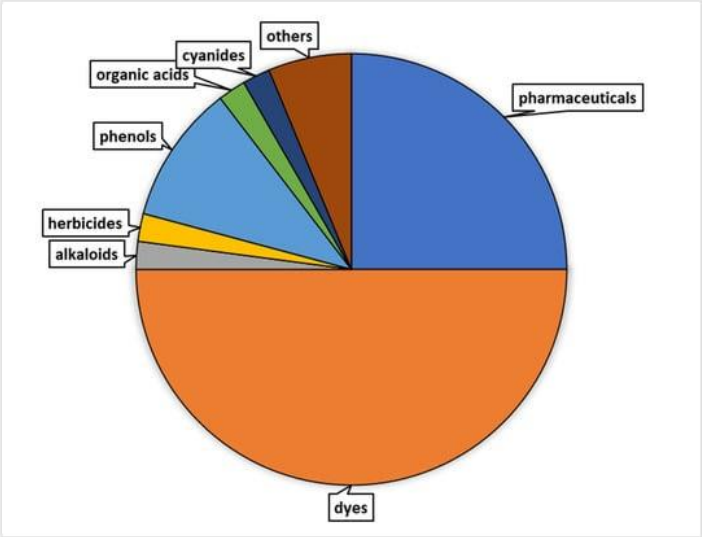

Figure 2. Percentage distribution of research papers on the utilization of REE catalysts for the degradation of different contaminant types.

The chemical, metallurgical, and physical properties of the REEs are governed by their electron configuration. In contrast to element Y, the lanthanides are characterized by the progressive filling of the 4f orbital (Liu, 1978). Due to the low energy of these electrons, they do not directly participate in the bonding when forming compounds with other elements. As a consequence, this leads to a significant similarity in the chemical reactivity of the lanthanides. This uniform reactivity pattern is evident consistently throughout geochemical processes, rather than being unique to each individual element (Been et al., 2021; Liu, 1978).

In Table 1, the essential details encompassing the atomic numbers and intricate valence shell electronic configurations pertaining to the distinctive set of REEs are provided.

Table 1. Atomic Number and Valence Shell Electronic Configuration of the Rare Earth Elements.

Element	Atomic Number	Valence Shell Electronic Configuration
Y	39	[Ar] 3d1 4s2
La	57	[Ar] 4d1 5s3
Ce	58	[Xe] 4f1 5d1 6s2
Pr	59	[Xe] 4f3 5d0 6s2
Nd	60	[Xe] 4f4 5d0 6s2
Pm	61	[Xe] 4f5 5d0 6s2
Sm	62	[Xe] 4f6 5d0 6s2
Eu	63	[Xe] 4f7 5d0 6s2
Gd	64	[Xe] 4f7 5d1 6s2
Tb	65	[Xe] 4f9 5d0 6s2
Dy	66	[Xe] 4f10 5d0 6s2
Ho	67	[Xe] 4f11 5d0 6s2
Er	68	[Xe] 4f12 5d0 6s2
Tm	69	[Xe] 4f13 5d0 6s2
Yb	70	[Xe] 4f14 5d0 6s2
Lu	71	[Xe] 4f14 5d1 6s2

3 AOP-Based REEs for CECs Removal

3.1 Pharmaceutical Degradation

Pharmaceutical toxic compounds can end up in wastewater via many routes, such as via their consumption by humans or their use in agriculture. Therefore, it is essential to discover effective ways for decomposing these hazardous compounds in wastewater. The use of REEs has been shown by several studies to be potentially useful. Numerous researchers utilized REEs in various forms as heterogeneous catalysts in AOPs (Table 3).

Nie et al. (Nie et al., 2015) carried out a Fenton-like reaction, at 30°C, to take complete degradation of the antibiotic sulfamethoxazole (SMX), in the simultaneous presence of $LaFeO_3$ and H_2O_2 at pH values ranging between 5.5 and 7.14. It was found that the SMX removal efficiency increased with the increase of the catalyst load and then reached a constant value when the $LaFeO_3$ concentration was above 1.4 g/L. Furthermore, it was investigated that the $LaFeO_3$ could be reused for at least 10 cycles and the reused catalyst kept the catalytic activity nearly as efficient as the fresh one. Ref. (Younes et al., 2023) investigated the photocatalytic activity for degradation of carbamazepine and caffeine using MIL-125-NH_2, $LaFeO_3$, and $LaFeO_3$/MIL-125-NH_2 photocatalysts under solar simulator at ambient temperatures. $LaFeO_3$/MIL-125-NH_2 composite exhibited higher carbamazepine and caffeine degradation than MIL-125-NH_2 MOF and $LaFeO_3$ perovskite and this is highlighted through the calculation of pseudo-first-order kinetics equation. $LaFeO_3$/MIL-125-NH_2 composite photocatalysts prepared by the self-assembly method have shown excellent and promising results in the degradation of pharmaceutical compounds.

Chen et al. (2022) used $LaFeO_3$/lignin-biochar (LFO/LG) catalysts prepared by a sol–gel pyrolysis to evaluate the degradation of ofloxacin (OFX) under visible light irradiation. The pure $LaFeO_3$ (LFO) and the pure lignin-biochar (LG) were tested and prepared under the same conditions to compare which one had the best performance. The whole process was operated at a constant temperature in the presence of H_2O_2 (30 wt%) and all experiments were carried out under different initial pH, revealing later an optimal photodegradation efficiency at pH values above 6. In addition, the morphology, microstructure, energy band structure, and photoelectrochemical behavior of the composite catalysts were characterized and the relationship with catalytic performance was explained. Pure LFO has almost no adsorption of OFX when the system was left in the dark to reach a saturation adsorption state and the degradation efficiency for LFO is only 53.4% after a 75-min degradation reaction. Instead, LFO-LG samples showed a significant adsorption effect on OFX, and the degradation efficiency was also improved up to 95.6%.

In the study of (Assumpção et al., 2013), the electrochemical degradation of dipyrone using cerium catalysts was not effective during a two-hour electrolysis. However, the use of a CeO_2/C gas diffusion electrode degraded all of the dipyrone in 20 min with 26% mineralization at −1.3 V, and after only 5 min with 57% mineralization at −1.1 V when the Fenton process was employed. The authors declared that ceria acts as an oxygen buffer leading to an increase in the local oxygen concentration, facilitating H_2O_2 formation and consequently improving the dipyrone degradation. $FeCeO_x$ can remove 83% of diclofenac in a heterogenous Fenton process and can be reused due to its chemical stability (Chong et al., 2016).

A heterogeneous Fenton catalyst, Ce^0-Fe^0-reduced graphene oxide (Ce–Fe–RGO), showed good catalytic performance and adsorption of sulfamethazine (Wang et al., 2016). Ferrum-doped CeO_2 nanosheets with various Fe/Ce ratios were evaluated for the Fenton-like degradation of salicylic acid (SA). The 2% Fe-doped CeO_2 nanosheets showed the highest concentration of surface oxygen vacancies and catalytic activity under the optimum reaction conditions due to the complex adsorption of SA and H_2O_2 on the surface Ce^{3+}. The catalytic activity of the nanosheets could be recovered, and so they could be reused in new cycles (W. Wang et al., 2018). A surface of graphite felt loaded with CeO_x accelerated the mineralization of carbamazepine via an E-peroxone process (Wang et al., 2021).

The Fe^0/CeO_2 nanocomposite enhanced the removal of tetracycline (TC) in the Fenton oxidation process and could be reused for further cycles. The authors suggested a synergistic effect between nanoscale Fe^0 and CeO_2 (Zhang et al., 2019).

Hu et al. (2021) tried out for the first time the use of cobalt (Co) and REE gadolinium (Gd) to investigate the removal of two antibiotics from wastewater, ciprofloxacin (CIP) and tetracycline. In particular, the sponge-like structure of Co- and Gd-modified biochar (MBC) was conducive to studying its adsorption capacity due to the presence of metal oxides and functional groups. Furthermore, the influence of pH on the absorption of antibiotics was studied by varying the pH between 3 and 11. It was observed that at pH 9, the antibiotic adsorption capacity of MBC was greatly increased. These data suggested that MBC is an innovative and effective adsorbent for the removal of antibiotics from complex contaminated water.

Luan et al. (2022) synthesized photocatalysts Er_2FeSbO_7, $BiTiSbO_6$, or N-TO by solid-state method to degrade enrofloxacin (ENR), a common antibiotic able to effectively kill Gram-positive and Gram-negative bacteria and mycoplasma under visible light irradiation. A new photocatalyst provided by $Er_2FeSbO_7/BiTiSbO_6$ heterojunction (EBH) was prepared for the first time by the thermal solvent method and tested. It was observed that the photocatalytic activity among the four photocatalysts was

as follows: EBHP > Er_2FeSbO_7 > $BiTiSbO_6$ > N-TO. Therefore, it can be concluded that the EBHP process can be a potent method for treating pharmaceutical wastewater that is polluted by ENR.

In general, the studies highlighted the use of diverse catalysts to improve the efficiency of removing pharmaceutical compounds. Each study focused on targeting specific pharmaceutical compounds; this targeted approach allowed for a more accurate evaluation of the catalyst's performance against particular contaminants. Among the studies conducted on CIP removal, the highest removal percentage (>99%) within a timeframe of 180 min was achieved by the study utilizing the MBC catalyst (Hu et al., 2021).

The pH can play a significant role in the reactivity and adsorption behavior of both the catalyst and the target compound. The studies reported a range of pH values, including pH 4, 5, 6.48, and 9, indicating that different pH levels can be effective depending on the specific catalyst and target compound.

Furthermore, the temperature of the reaction can influence the reaction kinetics and the stability of the catalyst. It was generally observed that moderate temperatures (20–25°C) were preferred to strike a balance between reaction rates and energy consumption.

The pharmaceutical degradation studies highlighted the potential of Fenton-based processes for wastewater treatment, showcasing the reusability of $FeCeO_x$ (Chen et al., 2022), the catalytic performance and adsorption properties of Ce-Fe-RGO (Wang et al., 2016), and the degradation capabilities of ferrum-doped CeO_2 nanosheets (Zhang et al., 2019). The results emphasize the versatility and effectiveness of Fenton processes in removing pharmaceutical compounds, offering promising solutions for the treatment of wastewater contaminated with these contaminants.

3.2 Dye Degradation

Wastewater from the textile industry contains residual dyes which are hardly biodegradable. Advanced Oxidation Processes (AOPs) are alternative techniques for the destruction of dyes and many other organic products in wastewater and effluents. In Table 4, the degradation efficiency of various dyes using REE catalysts is highlighted, including the type of contaminant, initial concentration, reaction conditions, and the corresponding degradation percentage achieved by the REE catalysts.

The presence of La in the La–Fe montmorillonite (La–Fe MMT) composite enhanced the degradation efficiency of the organic dyes Rhodamine B (RhB) and methylene blue (MB) and resulted in a little iron leaching, consequently increasing the lifetime of the system. Due to its low cost, efficient reactivity, high stability, and low metal leaching, it seems a great potential as a green catalyst for the heterogeneous Fenton-like degradation of hazardous dyes (Fida et al., 2017). FeOCl doped with Y or La showed efficient Fenton catalytic activity for ibuprofen degradation under simulated solar light (Shi et al., 2019). Tungsten oxide composites (WO_3) doped with La, Gd, or Er showed an enhanced photocatalytic degradation of organic dyes compared to the pure composites (Bilal Tahir and Sagir, 2019).

Huang et al. (2014) doped hydroxyl FeAl intercalated montmorillonite with La or Ce and saw an improvement in the photo-Fenton catalytic oxidation of Reactive Blue 19 under natural sunlight irradiation. The photo-Fenton activity of pristine $CoFe_2O_4$ on the oxidation of five organic dyes was enhanced by inserting a very small quantity of La or Ce cations into its spinel structure in the presence of two different oxidants (Sharma et al., 2016).

Divya and Renuka (2015) doped nanoceria with five different elements (Cu, Fe, Zr, Dy, and La) and investigated the heterogenous Fenton-like oxidation of MB. CuO showed the highest catalytic activity, which is attributed to the synergistic effect between copper and ceria. The Cu–Mn/CeO_2/SBA-15 catalysts can efficiently degrade (>99%) high-concentration dye pollutants. The excellent catalytic performance could be attributed to the well-dispersed catalytic nanoparticles inside the mesopores and the catalytic synergic effect of CeO_2 (Fan et al., 2014). Xie and Yuan (2003) showed that Ce^{4+}-TiO_2 sol and nanocrystallites can photodegrade the reactive brilliant red dye (X-3B) with the dye/Ce^{4+}-TiO_2/visible-light reaction system.

Singh et al. (2016) prepared several Cu/zeolite Y catalysts to test the decolorization, degradation, and mineralization of recalcitrant diazo dye (Congo red) in a heterogeneous Fenton-like process. The catalyst with 7.5 wt% Cu showed the maximum degradation, decolorization, and mineralization of 93.58%, 95.34%, and 79.52% after 2.5, 2, and 4 h, respectively, along with reproducible activity for three cycles. The addition of Y on the surface of BiW_2O_6 composites enhanced the degradation of RhB compared to the individual composites under visible light illumination, by producing holes (h^+) and superoxide radicals (Cao et al., 2015).

Seroglazova and Popkov (2022) showed that Praseodymium orthoferrite ($PrFeO_3$) nanopowders can achieve 100% efficiency of photo-Fenton-like degradation of methyl violet. The $PrFeO_3$/CeO_2-based nanocomposites can degrade methyl violet (MV) under the presence of visible light via a photocatalytic Fenton-like activity. These nanoparticles can be reused due to their stability and be separated from the reaction solution (Seroglazova et al., 2023). In the study of (Ahmadi et al., 2020), Pr-$CdWO_4$ nanoparticles could degrade the toxic synthetic azo dye Remazol Black B by 93.9% at optimal conditions.

Nd-doped ZnO nanoneedles can degrade MB under UV light. Especially 1% Nd can degrade 2.5 times more with respect to undoped ZnO (Yayapao et al., 2013). The $LaFeO_3$ perovskites exhibit better photocatalytic activity towards the oxidative degradation of dye molecules when doped with Nd, Eu, Gd, or Dy (Dhiman and Singhal, 2019).

Keerthana et al. (2021) showed that zinc ferrite ($ZnFe_2O_4$) nanoparticles doped with 2% Samarium (Sm) can remove 65% of MB dye with the help of visible light irradiation within 1 h and, due to their stability, could be reused for more than three cycles. In the study of (Chahal et al., 2020), Sm-doped CeO_2 nanoparticles demonstrated a very efficient photodegradation of UV-irradiated rose bengal dye. M. Wang et al. (2017) showed that Sm-doped Bi_2MoO_6 photocatalysts could degrade more effectively RhB with respect to the individual particles.

The europium-nitrogen (EueN) co-doped TiO_2/Sepiolite nanocomposites, prepared through microwave-hydrothermal treatment, can be used to effectively eliminate dyestuff in real wastewater treatment. In particular, in order to evaluate the degradation of an anionic dye, Orange G, the photocatalytic activities were conducted under solar irradiation. The Eu-N co-doped TiO_2/Sep NCs, with various amounts of EuIII, photocatalysts exhibited improved photoactivity as compared to mono-doped and undoped samples (Zhou et al., 2020). In other studies, europium, in the +2 and +3 oxidation state, has been used as a dopant in VOC degradation over metal oxide catalysts such as TiO_2 for photocatalytic oxidation of RhB and MB (Vargas Hernández et al., 2017; Zhang et al., 2003) and $BiVO_4$ for photocatalytic oxidation of methyl orange (Zhang and Zhang, 2010). $EuFeO_3$ nanoparticles have photo-Fenton-like catalytic activity, as indicated by the efficient decolorization of RhB aqueous solution under visible-light irradiation, and they can be recovered and reused due to their excellent photocatalytic stability (Ju et al., 2011). Xu et al., (2014) showed that the addition of

Eu^{3+} ions on the surface of Bi_2WO_6 composites enhances the photocatalytic degradation of RhB under visible light irradiation by producing hydroxyl radicals.

Sharmin and Basith (2022) synthesized 10% Gd-doped $BiFeO_3$ nanoparticles (BGFO) via a simple and cost-effective hydrothermal technique at a lower reaction temperature of 160 °C. Following this approach, the synthesized nanoparticles exhibited photocatalytic activity towards the degradation of hazardous industrial pollutants, such as RhB and MB pharmaceutical pollutants such as ciprofloxacin (CIP) and levofloxacin (LFX) under simulated solar irradiation. The photocatalyst BGFO demonstrated 96% and 97% degradation of RhB and MB within 240 and 180 min of solar irradiation, respectively, and about 80% and 79% degradation of CIP and LFX were obtained within 240 min in the same conditions. Similarly, through the hydrothermal method, Sn-Gd_2O_3 nanomaterial was prepared and mixed with a hot aqueous solution (T > 60°C) of gelatin polymer, followed by cross-linking, for the efficient reduction of water pollutants (Marwani et al., 2022). The catalytic activity of Sn-Gd_2O_3 NPs was analyzed against different dyes, such as 4-nitrophenol (4-NP), 2,6-dinitrophenol (2,6-DNP), 2-nitrophenol (2-NP), MB, methyl orange (MO) and congo red, the presence of a strong reducing agent, $NaBH_4$. These latter two anionic azo dyes are used as indicators as well as in the food, textile, paper and pulp, cotton, silk, plastic, cosmetic, pharmaceutical, rubber, printing, and wool industries (Ismail et al., 2019). Therefore, this scientific approach has led to the fabrication of a new hydrogel nanocomposite for the removal of water pollutants, especially in the reduction of the activity of industrial dyes. Composites of Bi_2MoO_6 showed an enhanced photodegradation of RhB and TC when doped with Gd and Pt ions, by producing hydroxyl radicals, holes in the valence band (h^+), and superoxide radicals (Li et al., 2018). Yu et al. (2016) showed that Bi_2MoO_6 nanoplate crystals perform a better photocatalytic degradation of RhB when doped with Gd^{3+} ions, with the production of hydroxyl radicals as a proposed mechanism of action. Wu et al. (2019) showed that the TiO_2 NPs demonstrated an enhanced photocatalytic degradation of MB and RhB when doped with Gd^{3+} ion or Gd_2O_3.

Vinosha et al. (2022) showed that zinc ferrite ($ZnFe_2O_4$) nanocrystals doped with dysprosium (Dy) exhibit a photo-Fenton activity against MB with an efficiency of 97.3% within 45 min. This ferrite can act as a magnetic recyclable catalyst even after five cycles with an insignificant lessening of elements.

Liang et al. (2006) showed that Er^{3+}-TiO_2 catalysts had higher adsorption equilibrium constants and better adsorption capacity than pure TiO_2, and the degradation and mineralization of orange I under both UV radiation and visible light were more efficient with Er^{3+}-TiO_2 catalyst than with pure TiO_2.

Tikhanova et al. (2021) showed that the heterojunction h-$YbFeO_3$/o-$YbFeO_3$ photocatalyst demonstrates an enhanced photo-Fenton decolorization of MV under visible light compared to pure o-$YbFeO_3$. A novel developed 2.0%Yb/2.0%Er/2.0%Pr-BiW_2O_6 catalyst could degrade the Congo red dye, TC, RhB, and MB by 90.2%, 52.3%, 95.5%, and 64.6%, respectively, under visible light illumination. The proposed mechanism of action was the promoted reactive oxide species production and photocarrier separation (Li et al., 2022).

The addition of Ln_2O_3 (Ln = Sm, Eu or Tb) on the surface of $BiVO_4$ composites enhanced the degradation of RhB with respect to the individual composites, by producing superoxide radicals, holes (h^+), and hydroxyl radicals (Gu et al., 2016). In the study of (H. Li et al., 2017), the Bi_2WO_6 photocatalyst showed enhanced performance in the degradation of RhD when doped with the combination of Tb/Eu, Dy/Sm, or Er/Nd. The proposed mechanism of action was the production of hydroxyl radicals, holes (h^+), and superoxide radicals.

Among the catalysts discussed, the most promising results for the removal of dyes were obtained with nanoceria doped with Cu, Fe, Zr, Dy, or La, which achieved a remarkable removal efficiency of over 99% MB (Divya and Renuka, 2015). These catalysts demonstrated a high level of effectiveness in degrading and eliminating MB from wastewater, showcasing their potential for applications in water treatment. However, it is important to consider that the performance of catalysts can be influenced by various factors, such as reaction conditions and the specific dye compound being targeted. Optimal results may vary depending on these factors and further exploration and optimization are necessary to discover even more efficient catalysts for MB removal. By improving catalyst design, fine-tuning reaction conditions, and exploring novel materials, it may be possible to achieve even higher removal efficiencies and enhance the overall sustainability and efficiency of water treatment processes.

3.3 Degradation of Other Target Pollutants

With the rapid development of industrialization, wastewater has increasingly enriched itself with various substances which often include, in addition to those already extensively discussed above, alkaloids, herbicides, phenols, etc. Unconventional wastewater treatment methods are presented below based on photocatalysis and Fenton-like reaction using REEs for the abatement of these molecules. In the first-ever study using REEs for removing pollutants from aqueous solutions, Tokunaga et al. (1995) studied the use of solid compounds of Y(III), La(III), Ce(III), Nd(III), Sm(III), Gd(III), and Ce(IV) in the form of oxides, hydrous oxides and basic carbonates for the removal of fluoride ions, and only Ce(IV) was capable of removing them effectively without a significant dissolution even at pH 2.

Fouad et al. (2021) tried to modify the $LaFeO_3$ catalyst with Ti (Ti-$LaFeO_3$) by developing photocatalysis and photo-Fenton processes under UV and visible light for the degradation of carbofuran (CBF). It was observed that about 20% of CBF was degraded by H_2O_2 without catalyst loading under UV irradiation. In the presence of UV light and the absence of H_2O_2, the CBF degradation was 59%, which was mainly due to the photocatalysis process induced by the illumination of Ti-$LaFeO_3$. The degradation of CBF was 73% under metal-halide lamp irradiation in the system of Ti-$LaFeO_3$/H_2O_2, which confirms the activity of the catalyst under visible light. Moreover, the degradation was improved to 89.5% when this lamp was replaced by UV light. Heterogeneous catalytic wet peroxide oxidation (CWPO) was proposed in this work, aiming to obtain degradation rates and faster mineralization of recalcitrant pollutants like CBF (Garcia-Muñoz et al., 2019). The results showed that the efficiency of the CWPO process by Ti-$LaFeO_3$ is higher than other photocatalytic processes used in the literature for the degradation of CBF. Furthermore, the catalyst could maintain its catalytic activity for five consecutive cycles. In the study of (Ho et al., 2019), the La-doped TiO_2 photocatalyst could degrade acetone and NO under visible light by 38% and 98%, respectively.

Gogoi et al. (2017) used Fe_3O_4-CeO_2 nanocomposite materials as a Fenton-like heterogeneous catalyst for the degradation of catechol. Fe_3O_4-CeO_2 (15 wt%) showed the maximum degradation of catechol compared to the other prepared catalysts. The catalyst could also be recovered and used for five consecutive cycles with excellent catalytic activity. Cerium chloride exhibited radical production in the presence of hydrogen peroxide, as assessed by relaxation of supercoiled plasmid DNA and the production of radical cation of 2,2′-azinobis-(3-ethylbenzthiazoline-6-sulfonic acid), and so it is proposed that cerium is capable of redox-cycling with peroxide to generate damaging oxygen radicals (Heckert et al., 2008). Orge et al. (2012) tested ceria and Ce-based mixed oxides (Ce-Sm, Ce-La, and Ce-Zr with different compositions) as catalysts in the ozonation of oxalic acid, aniline, and the textile

dye C. I. Reactive Blue 5. CeO_2-ZrO_2 catalyst with higher than 25 wt.% of ZrO_2 presented the best catalytic oxidation of oxalic acid, which may be related to the larger percentage of the Ce (III) species on their surfaces. On the other hand, the ozonation catalyzed by 25 wt.% of Zr, Sm, or La oxides with Ce oxide or by Ce oxide did not present significant differences. In addition, the association of O_3 and all mentioned catalysts leads to an improved TOC removal from the dye and almost complete mineralization in all cases after about two hours. The highest mineralization rate of aniline was achieved by CeO_2 and $Ce_{0.75}Zr_{0.25}O_2$ with the latter being the sample with the largest amount of oxygen vacancies number in its structure. Cerium nanotubes catalysts (CeNTs) doped with different amounts of Nb_2O_5 (0–10 wt.%) were used for the catalytic reduction of NO_x with NH_3 (NH_3-SCR) in the presence of CH_2Cl_2. The 10 wt.% Nb-CeNTs catalyst presented the best oxidation of NH_3-SCR and degradation efficiency of CH_2Cl_2 among the prepared catalysts, due to its abundant surface oxygen species and acid sites, superior redox capability, the interaction between Nb and Ce, higher ratio of $Nb^{4+}/(Nb^{5++}\ Nb^{4+})$ and $Ce^{3+}/(Ce^{3++}\ Ce^{4+})$, and the special tubular structure of the Ce nanotube (Ouyang et al., 2022).

A magnetic nanoscaled Fe_3O_4/CeO_2 composite can degrade 4-chlorophenol and be reused for six successive cycles (Xu and Wang, 2012).

A ZnO nanoparticle doped with 2% Ce can catalyze the oxidation of cyanide and subsequently of cyanate as well under UV-A light or natural sunlight (Karunakaran et al., 2010).

Sharma et al. (2016) doped cobalt ferrite ($CoFe_2O_4$) with La or Ce and observed an enhancement in its photo-Fenton degradation properties of various organic pollutants using two different inorganic oxidants: hydrogen peroxide (H_2O_2) and potassium peroxymonosulphate ($KHSO_5$), with respect to pure cobalt ferrite. The doped catalyst could also be reused in wastewater treatment without a decline in its catalytic activity due to its chemical stability.

Samarium-doped ZnO nanorods (Sm/ZNRs) can exhibit a higher photocatalytic degradation of phenol aqueous solution under visible light irradiation than that of the pure ZNRs due to their high charge separation efficiency and OH• generation ability. These nanorods could also be reused for more cycles (Sin et al., 2013).

Cymes et al. (2020) doped cryptomelane with europium via either co-precipitation or ion exchange in order to promote the catalytic oxidation of ethanol. Eu-doping by co-precipitation generally improves catalytically advantageous physical and chemical properties whereas Eu-doping by ion exchange shows deleterious effects.

Composites of Bi_2MoO_6 showed an enhanced photodegradation of 4-Chlorophenol when doped with Gd and Pt ions, by producing hydroxyl radicals, holes in the valence band (h^+), and superoxide radicals (Cao et al., 2015). In the study of (Xu et al., 2014), the Bi_2WO_6 photocatalyst showed enhanced performance in the degradation of phenol when doped with the combination of Tb/Eu, Dy/Sm, or Er/Nd. The proposed mechanism of action was the production of hydroxyl radicals, holes (h^+), and superoxide radicals.

Table 2 shows which REEs have been studied for photocatalysis and which for Fenton-like catalysis.

Table 3, Table 4 and Table 5 below summarize all the catalyst-doped REEs divided and ordered according to publication date.

Table 2. REEs studied for simple photocatalysis and Fenton-like photocatalysis.

Type of Reaction	REEs Studied
Photocatalysis	Y, La, Ce, Nd, Sm, Eu, Gd, Tb, Dy, Er, Yb
Fenton-like catalysis	Y, La, Ce, Pr, Nd, Eu, Gd, Dy, Yb

Table 3. REE catalysts used for pharmaceutical degradation.

Catalyst Doped REE	Target	Dose of Catalyst	Dose of Target	Time (min)	Conditions	Proposed Mechanism	Removal (%)	Reference
$LaFeO_3$	Sulfamethoxazole	1.4 g/L	3 mg/L	120	pH = 6.48, T = 30 °C	Production of •OH and superoxide radicals (O_2^-/HOO)	100%	[31]
$LaFeO_3$/MIL-125-NH_2	Carbamazepine (CBZ) and Caffeine (CAF)	250 mg/L	5 mg/L CBZ and 1 mg/L CAF	60	Visible light	Production of •OH and O_2^-	74% CBZ 87% CAF	[32]
$LaFeO_3$/lignin-biochar (LFO/LG)	Ofloxacin (OFX)	250 mg/L	30 mg/L	75	Visible light, addition of H_2O_2	Production of •OH	95.60%	[33]
CeO_2/C gas diffusion electrode (GDE)	Dipyrone	-	100 mg/L	20	-	Production of •OH	100%	[34]
$FeCeO_x$	Diclofenac	0.5 g/L	20 mg/L	40	pH = 5, addition of H_2O_2, ambient temperature	Production of •OH	83%	[35]
CeO_2 nanosheets doped with Fe	Salicylic acid	250 mg/L	50 mg/L	120	Addition of H_2O_2, pH = 4, T = 55 °C	Production of superoxide radicals (O_2^-/HOO)	96% by 2wt% Fe-CeO_2	[36]
CeO_x modified graphite felt	Carbamazepine	-	10 mg/L	60	pH = 5, T = 25 °C	Production of •OH	69.40%	[37]
Sponge-like structure of Co- and Gd-modified biochar (MBC)	Ciprofloxacin (CIP)/Tetracycline (TC)	1.1 g/L	20 mg/L	180	pH = 9	-	99% of CIP or TC	[38]
Er_2FeSbO_7/$BiTiSbO_6$ heterojunction (EBH) catalyst	Enrofloxacin (ENR)	0.75 g/L	0.025 mM	150	Visible light, T = 20 °C,	Production of •OH	99,16%	[39]
FeOCl doped with Y or LA	Ibuprofen	0.5 g/L	5 mg/L	20	Neutral pH, addition of H_2O_2, room temperature, dark	Production of •OH	84–82% by 0.9wt% FeOCl/La and 1.2wt% FeOCl/Y, respectively	[40]
Gd doped $BiFeO_3$ nanoparticles (BGFO)	Ciprofloxacin (CIP)/Levofloxacin (LFX)	-	-	240	Solar illumination	Production of O_2^-	80%/79%	[64]

Table 4. REE catalysts used for dyes degradation.

Catalyst Doped REE	Target	Dose of Catalyst	Dose of Target	Time (min)	Conditions	Proposed Mechanism	Removal (%)	Reference
La–Fe MMT	Rhodamine B (RhB)/Methylene Blue (MB)	1 g/L	100 mg/L	60	Neutral pH, addition of H_2O_2	Production of •OH	97% MB 96% RhB	[40]
Tungsten oxide composites (WO_3) doped with La, Gd, or Er	Organic dyes	300 mg/L	-	90	Visible light,	Production of O_2^-	98% for MB and >90% for MT, MO, TC and CV by 2% Gd-doped WO_3	[42]
FeAl/Ce-Mts and FeAl/La-Mts	Reactive Blue 19	0.5 g/L	0.12 mM	180	Sunlight, addition of H_2O_2, pH = 3.0	Production of •OH	100% by FeAl/Ce1.0-Mt and 99.7% with FeAl/La1.0-Mt	[43]
$CoFe_2O_4$ doped with La or Ce	Remazol black 5, remazol brilliant yellow, *o*-nitrophenol, *m*-nitrophenol (MNP) and *p*-nitrophenol	0.5 g/L	-	ott-30	Visible light, room temperature, pH = 2.5, addition of H_2O_2	Production of •OH	-	[44]
Nanoceria doped with Cu, Fe, Zr, Dy or La	MB	80 mg/L	55.2 mg/L	420	pH = 9.6, T = 27 °C, UV light	Production of •OH	>99% by CuO/CeO_2	[45]
Cu-Mn/CeO_2/SBA-15	RhB	200 mg/L	2 g/L	210	pH = 7.0, addition of H_2O_2, atmospheric pressure and constant temperature	Production of •OH	0.99	[46]
Ce_4+-TiO_2 sol and nanocrystallites	Brilliant red dye (X-3B)	1 g/L	100 mg/L	120	Visible light	Production of •OH and O_2^-	83.1% by Ce_4+-TiO_2 nanocrystallines and 99.9% by Ce_4+-TiO_2 sol	[47]
Cu/zeolite Y	Congo red (CR)	1 g/L	0.143 mM	150	Addition of H_2O_2, pH = 7.0	Production of •OH	93.58% by 7.5wt% Cu	[48]
$PrFeO_3$	Methyl violet (MV)	250 mg/L	23.2 mg/L	60	Addition of H_2O_2, visible light	Production of •OH	-	[50]
$PrFeO_3$/CeO_2-based nanocomposites	MV	250 mg/L	23.2 mg/L	30	Visible light, addition of H_2O_2	Production of •OH	80.1% by 9 wt% CeO_2	[51]
Pr-$CdWO_4$ NPs	Remazol Black B	350 mg/L	100 mg/L	100	pH = 3.0, T = 25 °C, addition of enhancers	Production of •OH	93.90%	[52]
ZnO nanoneedles doped with Nd	MB	5 g/L	10^{-5} M	300	UV light	Production of O_2^-	92% by 1% Nd-doped ZnO	[53]
$LaFeO_3$ perovskites doped with Eu, Gd, Dy, or Nd	Safranine-O and remazol brilliant yellow	0.5 g/L	15 mg/L SO and 60 mg/L RBY	20, 35, 35, 20	Visible light, pH = 2.0, adding H_2O_2	Production of •OH	More than 90%	[54]
$ZnFe_2O_4$ nanocrystals doped with Sm	MB	0.1 g/L	1 mg/L	60	Visible light	Production of •OH	65% by 2 wt% Sm	[55]
Sm doped CeO_2 nanoparticles	Rose bengal dye	1 g/L	5 mg/L	90	UV light	Production of •OH	84% by 4 wt% Sm and 89% by 6 wt% Sm	[56]
Eu-N co-doped TiO_2/Sepiolite NCs	Orange G	0.8 g/L	10 mg/L	540	Visible light, pH = 3.0	Production of •OH	More than 98% by 0.6 wt% Eu	[58]
Eu^{3+}–TiO_2	RhB	2 g/L	10^{-5} M	30	UV light	Formation of a complex between the doped lanthanide ions and substrates	96%	[59]

Eu^{2+}–TiO_3	MB	0.125 M	2×10^{-5} M	60	UV light, pH = 8.3	Induced surface plasmon resonances	-	[60]
$Eu^{2+,3+}$–$BiVO_4$	Methyl orange (MO)	2 g/L	10 mg/L	180	Visible light	Trapping of photogenerated electrons in the catalyst by Eu dopant	93.6% by 1.46 wt% Eu	[61]
$EuFeO_3$ NPs	RhB	1 g/L	5 mg/L	180	Visible light, room temperature, addition of H_2O_2	Production of •OH	71%	[62]
Gd doped $BiFeO_3$ NPs (BGFO)	RhB/MB	-		240/180	Solar illumination	Production of O_2^-	96%/97%	[64]
Sn-Gd_2O_3 NPs	4-NP, 2,6-DNP, 2-NP, MB, MO and CR	8 g/L	0.07 mM	18	Addition of $NaBH_4$	Electron transfer from the catalyst to the dye	-	[65]
$ZnFe_2O_4$ nanocrystals doped with Dy	MB	1 g/L	20 mg/L	45	Visible light, addition of H_2O_2	Production of •OH	97.30%	[66]
Er^{3+}–TiO_2	Orange I	1 g/L	6×10^{-5} M	60	T = 25 °C, UV light or visible light, pH = 7.0	Production of •OH	About 100% under UV and about 80% under visible light by 1.5 wt% Er	[70]
Heterojunction h-$YbFeO_3$/o-$YbFeO_3$	MV	125 mg/L	0.25 mM	180	Visible light, addition of H_2O_2	Production of •OH	64%	[72]
Yb/Er/Pr-Bi2WO6 catalyst	CR/TC/RhB/MB	1 g/L	-	60	Visible light	Reactive oxide species production and photocarrier separation	90.2%/52.3%/95.5%/64.6%	[73]
BiVO4 composites doped with Ln2O3 (Ln = Sm, Eu, or Tb)	RhB	1 g/L	10 mmol/L	210	Visible light, 25 °C	Production of $•O_2^-$, holes in the valence band (h^+), and •OH	55.1%, 51.8%, and 57.3% by 2% Sm2O3/BiVO4, 2% Eu2O3/BiVO4, and 10% Tb2O3/BiVO4, respetively	[74]
Y-Bi2WO6 photocatalyst	RhB	1 g/L	0.01 mM	240	Visible light	Production of holes (h^+) and O_2^-	85% by 1% Y-Bi2WO6	[49]
Gd/Pt-Bi_2MoO_6 composites	RhB/TCs	1 g/L	12 mg/L RhB/20 mg/L TCs	80 for RhB and 90 for TCs	UV visible light	Production of $•O_2^-$, holes in the valence band (h^+), and •OH	95% of RhB and 77.6% of TCs by 2%Gd/2%Pt-Bi_2MoO_6	[67]
Eu-doped Bi_2WO_6 composites	RhB	1 g/L	10 mg/L	60	Visible light, 25 °C, addition of H_2O_2	Production of OH radicals	98%	[63]
Ln1/Ln2 co-doped Bi_2MoO_6 photocatalysts (Ln1/Ln2 = Tb/Eu, Dy/Sm, Er/Nd)	RhB	1 g/L	12 mg/L	240	UV visible light	Production of OH, holes (h^+) and superoxide radicals O_2^-	95.9% by 3%Tb/3%Eu, 98.5% by 3%Dy/3%Sm and 91.6% by 2%Er/2%Nd	[75]
Gd^{3+} doped Bi_2MoO_6 nanoplate crystals	RhB	0.5 g/L	20 mg/L	10	Visible light, 20 °C	Production of OH and holes (h^+)	84% by 6%Gd/Bi_2MoO_6	[68]
Gd^{3+}/TiO_2 and Gd_2O_3/TiO_2 NPs	MV/RhB	0.2 g/L for MV and 0.1 mg/L for RhB	25 mg/L/30 mg/L	60	UV visible light	Production of $•O_2^-$, holes in the valence band (h^+), and •OH	97.9% by 2.5% Gd^{3+}/TiO_2	[69]
Sm-doped Bi_2MoO_6 photocatalyts	RhB	0.2 g/L	5 mg/L	50	Visible light	Production of $•O^{2-}$ and holes (h^+)	89% by 0.8% Sm-doped Bi_2MoO_6	[57]

Table 5. REE catalysts used for herbicide, alkaloid, cyanide, organic acid, and phenol degradation.

Catalyst Doped REE	Target	Dose of Catalyst	Dose of Target	Time (min)	Conditions	Proposed Mechanism	Removal (%)	Reference
Ti-$LaFeO_3$	Carbofuran	700 mg/L	7 mg/L	180	Adding H_2O_2, pH = 3.0	Production of •OH	91%	[76]
Ti-substituted $LaFeO_3$	4-Chlorophenol	0.5 g/L	25 mg/L	-	Circumneutral pH, ambient atmospheric pressure and temperature, UV-A light, addition of H_2O_2	Production of •OH	100% by 3.2% Ti	[77]
Fe_3O_4-CeO_2	Catechol	1 g/L	10 mg/L	60	Adding H_2O_2, room temperature, pH = 2.4	Production of ROS	100% by Fe_3O_4-CeO_2 (15 wt%)	[79]
Ce-Sm, Ce-La, Ce-Zr	Oxalic acid/Aniline/C.I. Reactive Blue 5	-	C0,oxalic acid = C0,aniline = 1 mM, C0,dye = 50 mg L^{-1}	180/30/15	pH0,oxalic acid ≈ 3.0, pH0,aniline ≈ 6.5, pH0,dye ≈ 5.5, constant gas (oxygen + ozone) flow rate and constant inlet ozone concentration, 25 °C	Production of •OH	100% of oxalic acid with more than 25% of Sm, La or Zr/100% of aniline by $Ce0.75Zr0.25O_2$/100% by $Ce0.75Zr0.25O_2$	[80]
Fe_3O_4/CeO_2 composite	4-Chlorophenol	2 g/L	0.78 mM	90	Addition of H_2O_2, T = 30 °C, pH = 3.0	Production of •OH	100%	[81]
ZnO nanoparticles doped with Ce	Cyanide	4 g/L	-	60	UV-A light or natural sunlight, pH = 12.5	Production of •OH	-	[84]
Sm/ZNRs	Phenol	1 g/L	20 mg/L	480	Visible light, room temperature	Production of •OH radicals	89.5% by 1 wt% Sm/ZNRs	[85]
Cryptomelane doped with Eu	Ethanol	50 mg	-	-	Dark, T = 175–200 °C	Production of O_2^-	100%	[86]
Cerium nanotubes catalysts (CeNTs)	NOx	-	600 mg/L	600	Addition of CH_2Cl, 200 °C	Production of •OH	100% by 10% Nb-CeNTs	[82]
Gd/Pt-Bi_2MoO_6 composites	4-Chlorophenol	1 g/L	15 mg/L	300	UV visible light	Production of $•O_2^-$, holes in the valence band (h^+), and •OH	80% by 2%Gd/2%Pt-Bi_2MoO_6	[49]
Ln1/Ln2 co-doped Bi_2MoO_6 photocatalysts (Ln1/Ln2 = Tb/Eu, Dy/Sm, Er/Nd)	Phenol	1 g/L	15 mg/L	300	UV visible light	Production of $•O_2^-$, holes in the valence band (h^+), and •OH	76.2%, 79.1% and 70.7% by 3%Tb/3%Eu, 3%Dy/3%Sm and 2%Er/2%Nd, respectively	[75]
La-doped TiO_2 photocatalyst	Acetone/NO	-	1000 ppb/500 ppb	30	UV visible light	Production of $•O_2^-$ and •OH	38% of acetone and 98% of NO by 0.5%La-TiO_2	[78]

4 Potential Environmental Impacts of REE Catalysts

As for the use of REEs in AOPs, different perspectives are to be considered. Further improvement needs to be implemented in water treatments; as of now, several methods have been adopted that increase efficiency and provide better handling of waste, such as Fenton-like oxidation processes (Chong et al., 2010). Studies focused on the use of lanthanides have demonstrated an improvement in wastewater treatments, as their use can produce on average 30% less sludge compared to other alternatives such as iron and aluminum (Kajjumba and Marti, 2022). The use of REEs could represent an alternative for reducing wastelands generated by sludge (Kajjumba and Marti, 2022) and improving the removal of organic pollutants by enhancing photocatalytic activity (Chan et al., 2011).

Moreover, care should be taken to avoid the loss and transfer of particles into the environment, contributing to the anthropogenic input of REEs. Kajjumba et al., (2021) found that the mixture of lanthanides used in wastewater treatment had an antagonistic behavior, which could reduce their environmental impact. However, up to now, the knowledge of the toxicity of REEs is very limited, as the environmental fate is highly dependent on the system, such as the presence of organic matter, pH, and presence of cations (Gonzalez et al., 2014) which influence the speciation, which, by extension influences the bioaccumulation and bioavailability. Because of the lack of knowledge regarding the potential effects of REEs, the regulation for the discharge of REEs is still lacking. In contrast, many restrictions regarding the presence of organic pollutants have been applied globally (Ghadiri et al., 2013).

5 Conclusions

The study of REEs for their potential use in removing toxic organic compounds from aqueous solutions is a relatively recent field, with the first publication on this topic occurring only 28 years ago. Among the REEs, cerium has been extensively studied for its photo Fenton-like catalytic activity against organic pollutants, followed by lanthanum. However, the remaining REEs have received little attention, with five of them having never been studied in this context.

REEs have been shown to be promising for removing hazardous organic compounds from aqueous solutions, such as wastewater. The effectiveness of REEs in this regard depends mainly on the presence of oxygen vacancies and the concentration of REE ions in the catalysts. Specifically, the metal oxide surfaces promote the decomposition of hydrogen peroxide, which leads to the formation of hydroxide species responsible for the degradation of organic compounds.

Moreover, AOPs, which include REE-combined catalysts and other parameters, should be chosen based on the nature of the contaminants and the acid-base properties of the wastewater to be treated.

Due to their exceptional properties, REEs have the potential to revolutionize wastewater treatment. However, achieving the production of clean water without generating traces of persistent toxins remains a challenging goal.

Levels of rare earth elements on three abandoned mining sites in Southern Italy: A comparison between TXRF and ICP-MS

1 Introduction

The rare earth elements (REEs) is a group of metals consisting of the 15 lanthanides [Lanthanum (La), Cerium (Ce), Praseodymium (Pr), Neodymium (Nd), Promethium (Pm), Samarium (Sm), Europium (Eu), Gadolinium (Gd), Terbium (Tb), Dysprosium (Dy), Holmium (Ho), Erbium (Er), Thulium (Tm), Ytterbium (Yb), and Lutetium (Lu)] plus Scandium (Sc) and Yttrium (Y) (Wall, 2013). REEs are used in several technological applications since the manufacturing of many devices relies on their utilization (Du and Graedel, 2013, 2011; Pagano et al., 2019). Due to this extensive use of REEs, concerns about their safety have been raised, not only for human (Brouziotis et al., 2022a; Pagano et al., 2015b) but also for the environmental health (Chen et al., 2020; Malhotra et al., 2020).

Previous studies investigated the REE content on environmental matrices on mining sites that are either active or abandoned or on the areas near these sites. REE levels were found to be higher in a mine tailing composed by sludge and gravimetric waste (Azizi et al., 2022), in a coal mine drainage (Lefticariu et al., 2020), in acid mine drainages (Li and Wu, 2017; Olías et al., 2018; Soyol-Erdene et al., 2018; Vass et al., 2019), in a rare earth mining area (W.-S. Liu et al., 2019), in an U-REE mining site (Nkrumah et al., 2021), in stream waters of a Cu–Pb–Zn mining area (Protano and Riccobono, 2002), in an inactive Zn–Pb mine (Romero et al., 2010) in coal mine drainages (Silva et al., 2020; Stewart et al., 2017), or the areas close to abandoned mining sites (Atibu et al., 2016; Fernández-Caliani et al., 2009; González et al., 2020; Medas et al., 2013; Purwadi et al., 2019).

Except for the elevated levels of REEs on areas near the mining sites, several studies evaluated the environmental risk of REEs and showed that they can be transferred from soil to plants (Galhardi et al., 2020b, 2020a; Nkrumah et al., 2021; Zhao et al., 2019) or from water to clams (Wang et al., 2022). Other studies showed that REEs can be very hazardous to several living organisms (Pagano et al., 2023; Siciliano et al., 2022, 2021a, 2021b).

In this research, environmental samples were collected from three abandoned mining sites in the region of Puglia, Southern Italy. Each site is in the region of Gargano, Otranto and Spinazzola. Samples of soil, sediment, rock, water and biota were collected and the REE content in them was analyzed by two different techniques, Total Reflection X-Ray Fluorescence (TXRF) and Inductively Coupled Plasma – Mass Spectrometry (ICP-MS). The methods were compared for determining which one is the most ideal for the analysis of the REE-content on such environmental samples. Thus, the advantages and disadvantages of the two methods were elaborated upon for practical application in the measurement of such environmental samples.

2 Materials and methods

2.1 Sampling campaign

For determining the REE background levels, samples of soil, sediment, rock, water and biota were collected from three abandoned mining sites, each one in the areas of Gargano, Otranto and Spinazzola in the Puglia region, Southern Italy (Figure 1).

Each area of sampling was tracked on Google maps on the scale of 50 meters and was divided into 20 smaller areas. Ten of these areas were selected randomly for sample collection. Supplementary

materials 1 includes the figures (Figuers S1-S3) showing how each sampling site was divided and the coordinates of each point chosen for sample collection.

In total, 78 samples were collected; in Gargano 9 soil, 3 sediment, 4 rock and 5 biota; in Otranto 8 soil, 4 sediment, 5 rock, 9 biota and 1 water; in Spinazzola 10 soil, 9 rock, 9 sediment and 2 water samples. The temperature, pH, dissolved oxygen, % of O_2 saturation and conductivity of the water samples were calculated at the time of the sampling (Table 1).

Table 1. Characteristics of the water samples collected.

Region	**Otranto**	**Spinazzola**	
Sampling point	**D3**	**B3**	**E2**
Temperature (^{o}C)	22.3	20.3	19.1
pH	7.88	8.01	7.80
Disolved oxygen (mg/L)	8.71	7.20	6.21
% O_2 saturation	104	91	70
Conductivity (mS/cm)	1157	303	284

The reason that we didn't collect 10 samples of each type from each area is that not all the types of samples existed in all points selected for sampling, and also some points were not possible to be reached.

Sub-surface soil and sediment samples were collected using a small shovel for removing the surface part. Rock, water and biota samples were collected on the surface of the areas. All samples were collected in sterilized plastic bags except for the water samples which were collected in plastic bottles. Biota samples were stored at -20^{o}C until further digestion and analysis, while the rest of the samples were stored at 4^{o}C.

Figure 1. Map of Italy and location points of the three abandoned mining sites in the region of Puglia.

2.2 Sites of sampling

The Apenninic (NW-SE trending) and anti-Apenninic (NE-SW trending) tectonic deformation, which divided the region into three main structural blocks: Gargano promontory, Murge area, and Salento Peninsula, has an impact on the structure of the Apulia region (Mongelli et al., 2017). Typically referred to as the "Apulian foreland" or the "Southern Apennine foreland," this area is a vast foreland domain of the Apenninic and Dinaric orogens. Ephemeral sub-aerial exposures regularly interrupted carbonate accumulation. Albian-Cenomanian and Turonian are two important regional intra-Cretaceous unconformities that were created as a result of early tectonic deformation of the carbonate platform in this region.

The Late Cretaceous exposure events resulted in the formation of the Gargano karst bauxite deposits. On the karstified limestone, the Gargano promontory bauxite (Cenomanian-Senonian) is found as lenticular, irregular bodies. Up to the 1970s of the previous century, this deposit was mined underground (Figures 2 A and B).

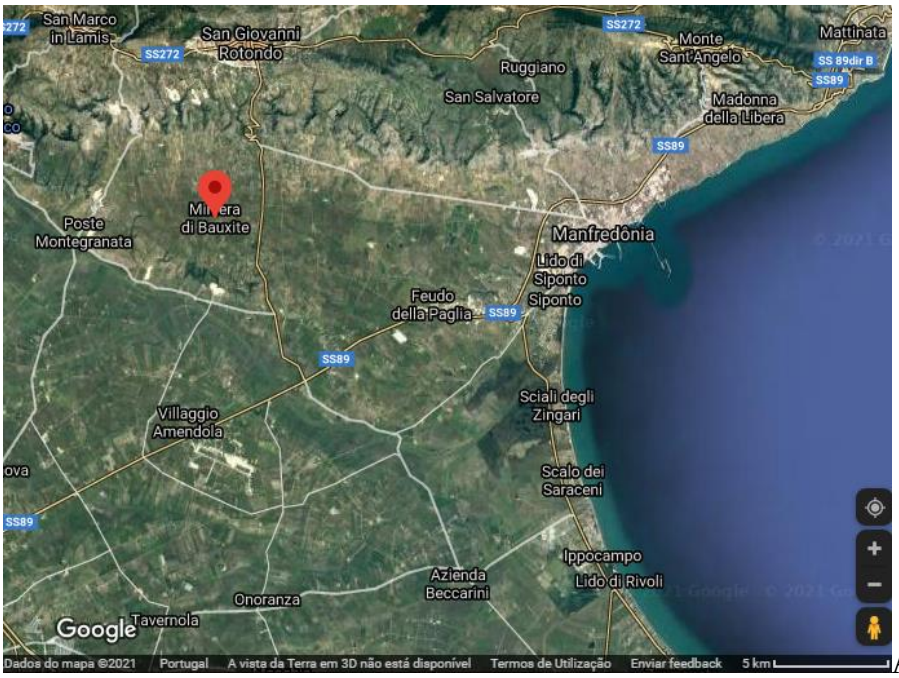

A

B

Figures 2 A and B. Location and image of Miniera di Bauxite (underground), "Gargano site", 71013 Foggia, Italy.

Allochthonous bauxite, also known as Salento or Terra d'Otranto, is a mineral that grows in the southern Apulian Foreland (Mongelli et al., 2015). According to the stratigraphical classification of Bosellini and Parente (1994), the Melissano Limestone beneath the Campanian-lower Maastrichtian Santa Cesarea Limestone is the lowest unit of the late Cretaceous in this area. The Ciolo Limestone, which is the topmost unit in the succession, has a latest Maastrichtian age at its type section. Schlüter et al. (2008) discovered that the Ciolo Limestone has an age range from the middle Campanian to the latest Maastrichtian based on the $^{87}Sr/^{86}Sr$ dating of rudist shells. The Melissano Limestone Formation in the southeast of the ACP is comparable to the Altamura Limestone Formation (Alfonso Bosellini, Michele Morsilli, 1999).

The bauxite of the Salento-type deposits is made up of bauxitic fragments that resulted from previous deposits' weathering and erosion (Bárdossy, 1982). The late Oligocene succession, which developed in alternating freshwater, lagoonal, and emergent habitats at the Otranto site, was sandwiched between the underlying, severely weathered late Cretaceous limestone and the detritus. A debris layer several meters thick makes up the bauxite deposit, which today faces a small lake (Fig. 3 A and B). The debris has a reddish-yellow hue and is filled with several sizable bauxite pebbles that were once part of a healthy bauxite deposit.

Figures 3 A and B. Location and image of Cava de Bauxite, "Otranto site", Puglia Region, Italy.

The Spinazzola group of bauxite deposits are situated in the northern portion of the Murge district of Apulia, in southern Italy (40.986812762416804, 16.181751378099847) (Mongelli et al., 2014). A 3-km-thick succession of Cretaceous shallow-water limestones and dolomites dominate this region, which is a portion of the southern Apennines foreland. These rocks form a monocline that dips from southwest to southeast and is gently deformed by folds and crosscut by subvertical normal and trans-tensional faults. In the interior of the Mesozoic Apulia Carbonate Platform (ACP), a shallow-water

environment with limited energy development is where the carbonate succession was formed. The ACP suffered deformation brought on by the propagation of intraplate stress during the early stages of the Alpine Orogeny as a result of the beginning of the collision between Africa and Eurasian in the middle to late Cretaceous. Two significant regional intra-Cretaceous unconformities that show evidence of prolonged subaerial exposures during the Albian-Cenomanian and Turonian are the result of the carbonate platform's tectonic deformation. According to a new plate tectonic model put out by (Schettino and Turco, 2011), the ACP was located between tropical latitudes between 20° and 30° during the Cretaceous. The ACP only documents the Turonian exposure event, and in the Murge region, bauxite formed as vertical masses filling large voids that resembled canyons and were surrounded by steep walls. Most of these are small, karstification-related sliding planes. But the majority of the bauxite deposits in the Murge area's sub-parallel east-west arrangement points to a structural control and the existence of a fault system that supports the development of karst cavities. The bedrock that has been karstified is made of Valanginian-Cenomanian limestone (Calcare di Bari Formation), which has been severely distorted by the Cenomanian tectonism that has elevated the entire region. Using biostratigraphic and chronostratigraphic data, uplift has been dated to 4 Ma (early Turonian-Santonian). The Valanginian-Cenomanian carbonate footwall and the transgression, shallow-water Coniacian-Campanian limestones (Calcare di Altamura Formation) at the hanging wall are both preserved in the 20-m-thick bauxite deposit at the Spinazzola sampling site. Just below the hanging wall separating the bauxite from the underlying carbonate, there is also a conglomerate level with a clay matrix and carbonate clastics. A distinct normal fault clearly borders the right and left sides of the bauxite deposit's typical canyon-like structure (Figures 4 A, B, and C).

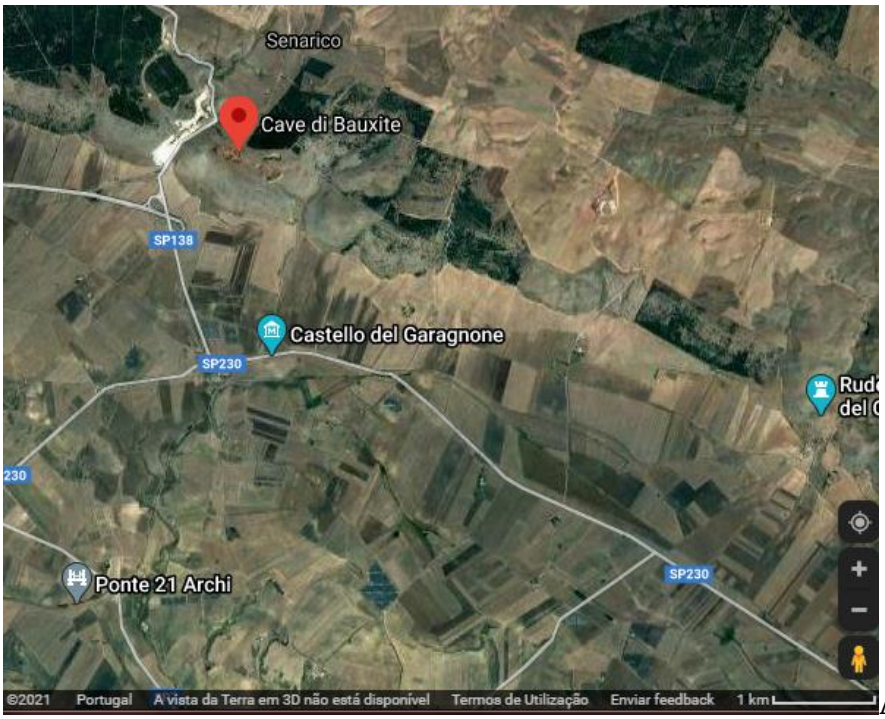

A

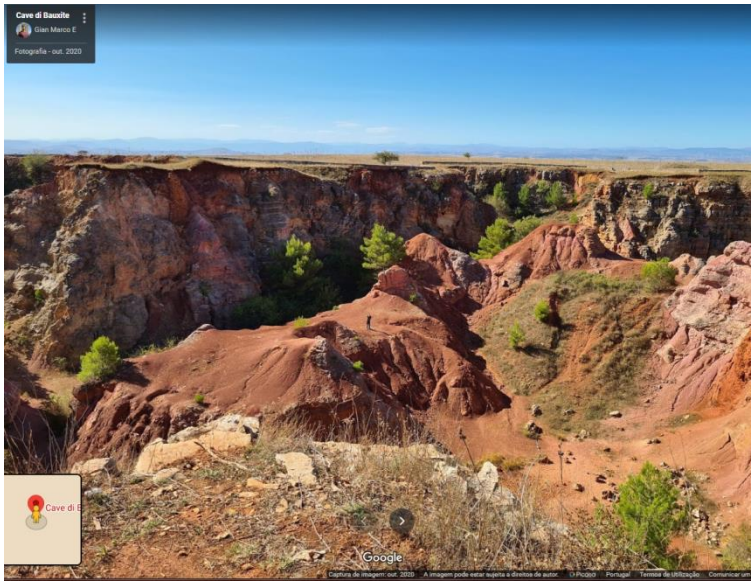

B

C

Figures 4 A, B and C. Location and images of "Spinazzola site", Cave di Bauxite, Puglia Region, Italy.

2.3 Digestion of samples

Rock samples were rinsed with ultra-pure water, dried overnight, at 70°C, and then pulverized by FastPrep-24 5G (MP Biomedicals, Germany). Soil and sediment samples were dried overnight at 70°C and then pulverized with the use of a mortar. All three types of sample were digested by a microwave digestion system (MARS 6, CEM) using the US EPA method 3051a. Briefly, about 0.5g of dry sample was weighted, followed by the addition of 9ml HNO_3 (69%, v/v) and 3ml HCl (37%, v/v). The digestion protocol was as follows: Heating for 5:30 minutes up to 175°C, remaining at 175°C for 4:30 minutes, and then cooling down to room temperature. The samples were then

transferred to 50ml falcon, filtrated by Fisherbrand™ Grade 600 cellulose general purpose filter paper and ultrapure water was added up to a final volume of 20ml.

Biota samples were rinsed with ultrapure water, dried overnight at 70°C, and digested following the method of (Donohue and Friedricks, 1984). Briefly, about 4g of dry sample were weighted and incinerated at 550ºC overnight. The next day, the ash was dissolved by the addition of 1.5ml HCl (37% v/v), was let stand for 30 minutes, and then 15ml of ultrapure water were added. The samples were then filtrated using Millipore Millex syringe filter, pore size 0.22μm by Merck.

Water samples were digested by MARS6 by CEM (Bruker, Gemrnay) using the method US EPA 3015a. Briefly, 5ml of HNO_3 (69%, v/v) were added in 45ml of water sample. The properties of the digestion period were the following: heating for 10 minutes up to 170°C, remaining at 170°C for 10 minutes, and then cooling down to room temperature. The samples were then transferred on 50ml falcon, filtrated by Fisherbrand™ Grade 600 cellulose general purpose filter paper.

2.4 Analysis by TXRF

Multielement analysis by TXRF were performed with a benchtop Total Reflection X-ray Fluorescence (TXRF) spectrometer (Picofox S2,Bruker, Germany) operating with a molybdenum X-ray source at 50 kV. The experimental conditions are given in Table 2. Reusable quartz sample carriers (4 × 30 mm) were employed for all measurements. The sequence of the sample preparation was the following: The digested samples were prepared in a 2 ml reaction caps (Eppendorf) containing 10 mg/L of Gallium as internal standard and were homogenized on a vortex for 10 seconds. A drop of 10μl of the sample was pipetted on the center of the surface of the carrier and dried at 60 °C on a hot scale.

A gain correction was performed before each series of measurements. Samples were measured for 1000 seconds. All volumes were controlled gravimetrically by weighing. Spectra were analyzed with the Bruker Spectra Picofox V 6.2.0.0 software. Corrections were made for the escape peak and for pile ups. The background was corrected by a maximum of 1000 stripping cycles with a step width of 50.

Table 2. Instrumental operating conditions for TXRF.

TXRF PARAMETERS	
Measuring system	
Maximum impulse density	300 kcps
Signal shaping	0.46μs
Pulse throughput	130 kcps
Energy resolution	< 150 eV FWHM at 100000 cps
Detector temperature	-20ºC
Peltier current adjust	0.8 A (Cool max)
Mechanical data	
Endcap	58.7 mm/mod.
Window	13μm, Dura Be
Electrical data	
Preamp. Supply	24 V DC
Power rating	ca. 20 W
Environment conditions	
Pressure range	0 - 1.5 bar
Pressure change	< 0.5 bar/s
Surrounding temperature	0 - 30oC
Humidity	< 85% RH at 20ºC

2.5 Analysis by ICP-MS

Multi-elemental analysis by ICP-MS was performed by ICP-MS Aurora M90 (Bruker, Germany). The experimental conditions are given in Table 3. The analysis was performed in high-sensitivity mode. All standards and samples were prepared in HNO_3 solution (2%, v/v). Calibration curves for determining REEs ranged from 0.005 to 100 μg/L and were constructed daily by analysis of standard solutions prepared immediately before analysis. The internal standard was ^{115}In for both the calibration curve and sample analysis. To confirm REE contamination of all materials utilized for each batch, a blank for reagents and a blank for the digestion procedure were carried out, and the instrumental sequence was validated every 10 samples. For every 20 samples, at least two control standards were confirmed.

The working range was evaluated by analyzing one blank and six standards at different concentrations, and the linearity was tested verifying the linear regression coefficient (R_2) of the calibration curve. The linearity was acceptable, with R_2 value equal or greater than 0.996.

Table 3. Instrumental operating conditions for ICP-MS.

ICP-MS PARAMETERS	
Flow parameters (L/min)	**Value**
Plasma flow	16.5
Auxiliary flow	2.00
Sheath Gas	0.20
Nebulizer flow	1.00
Torch alignment	
Sampling Depth	6.5
Other	
RF power (kW)	1.40
Pump rate (rpm)	4
Stabilization delay (s)	10
Ion optics (volts)	
First extraction lens	-567
Second extraction lens	-770
Third extraction lens	-559
Corner lens	-521
Mirror lens left	88
Mirror lens right	30
Mirror lens bottom	79
Entrance lens	0
Fringe bias	-3.6
Entrance plate	-47
Pole bias	0.0
CRI (mL/min)	
Skimmer gas source	Off
Sampler gas source	Off
Skimmer flow	0
Sampler flow	0

2.6 Limits of Detection (LOD)

LOD values on ICP-MS Aurora M90 were determined according to Eurachem Guide (Magnusson and Ornemark, 2014) with the determination of 10 replicate measurements of blank samples containing only HNO_3 solution (2%, v/v). LOD was calculated as 3s, s being the standard deviation of the measured concentrations.

On Picofox S2, every time that a sample is analyzed on Picofox S2, a LOD value is also received depending on several parameters (Riaño et al., 2016). According to (Espinoza-Quiñones et al., 2018) the LOD value of a specific element in TXRF is proportional to at least three times the square root of the integrated area of background or three-sigma background fluctuation. Within such a statistical estimation, the concept of 3σ detection limits conveys an exploitation of the minimum concentration in TXRF analysis through the true confirmation of a detectable X-ray when its peak area is at least three times the background signal fluctuation.

2.7 Statistical analysis

Statistical analysis was elaborated in SPSS Statistics v20. Values of REEs below the limit of detection (LOD) were replaced by 0, due to the different LOD values between TXRF and ICP-MS. Independent samples t-test was used to compare REE concentrations analyzed by the two different methods. Significant differences between the results from the two methods were determined by Welch's t-test. Differences were considered significant when $p < 0.05$.

Correlation of matrix was used to investigate the correlation of REE levels between soil and biota sample from the same sampling point. Existence of correlation was considered when Pearson $r > 0.7$.

Percentage (%) of the bioconcentration factor (BCF) was calculated by dividing the REE concentration in biota to this in soil from the same sampling point, multiplied by 100.

3 Results and Discussion

3.1 LOD values

Table 4 shows the LOD values received from TXRF and ICP-MS, respectively. LOD values of ICP-MS were about 1000 times lower than the LOD values of TXRF. LOD values on TXRF ranged from 2 μg/L to 16 μg/L, while LOD values of ICP-MS ranged from 0.001 μg/L to 0.004 μg/L.

As described also above, LOD values in ICP-MS were determined by analyzing 10 blank samples, while in TXRF the LOD values were already determined from the manufacturer. On TXRF, only LOD values of the 6 elements detected at least once (Y, La, Ce, Nd, Yb and Lu) could be acquired for our samples. LOD values of the other 9 REEs (Pr, Sm, Eu, Gd, Tb, Dy, Ho, Er and Tm) couldn't be received, since these elements were not detected at all, because their spectra was covered by the spectra of other heavy metals that were included in higher concentrations in the samples.

Table 4. Limits of detection (LOD) values for the ICP-MS determination. All values are expressed in μg/L.

Element	LOD TXRF	LOD ICP-MS
^{89}Y	2	0.003
^{139}La	16	0.003
^{140}Ce	16	0.003
^{141}Pr	-	0.003
^{146}Nd	16	0.004
^{149}Sm	-	0.003
^{153}Eu	-	0.002
^{157}Gd	-	0.003
^{159}Tb	-	0.001
^{163}Dy	-	0.002
^{165}Ho	-	0.002
^{166}Er	-	0.001
^{169}Tm	-	0.001
^{172}Yb	12	0.002
^{175}Lu	3	0.002

3.2 Analysis by TXRF and ICP-MS

Supplementary materials 2 includes all the results concerning the concentrations of each REE, on each type of sample, from each sampling point, and analyzed by which technique (Tables S1-S24).

3.2.1 Analysis by TXRF

No REE was detected in any of the three water samples when analyzed by TXRF.

Tables 5, 6 and 7 show the mean concentrations of each REE in each type of sample collected from the regions of Gargano, Otranto and Spinazzola, respectively, after elemental analysis by TXRF.

In the region of Gargano, Y, La and Ce were detected in all types of samples; Nd was detected in rocks and biota, Lu was detected in sediments and rocks, and Yb only in rocks. The most abundant REE was Ce in soil, sediments and biota, and Yb in rocks.

Table 5. Mean values of each REE in each type of sample from Gargano region, after analysis by TXRF. Values are given in mg/kg.

Sample type	Y	La	Ce	Pr	Nd	Sm	Eu	Gd	Tb	Dy	Ho	Er	Tm	Yb	Lu
SOIL	13.5	66.1	111	< LOD	< LOD	< LOD	< LOD	< LOD	< LOD	< LOD	< LOD	< LOD	< LOD	< LOD	< LOD
SEDIMENTS	8.80	40.1	75.1	< LOD	< LOD	< LOD	< LOD	< LOD	< LOD	< LOD	< LOD	< LOD	< LOD	< LOD	2.18
ROCKS	3.13	5.16	15.4	< LOD	0.37	< LOD	< LOD	< LOD	< LOD	< LOD	< LOD	< LOD	< LOD	19.1	6.51
BIOTA	5.87	3.60	12.1	< LOD	1.21	< LOD	< LOD	< LOD	< LOD	< LOD	< LOD	< LOD	< LOD	< LOD	< LOD

In the region of Otranto, Y, La and Ce were detected in all types of samples collected; Nd was detected in rocks and biota, and Yb and Lu were detected in sediments and rocks. The most abundant REE was Ce in soil, sediments and biota, and Y in rocks.

Table 6. Mean values of each REE in each type of sample from Otranto region, after analysis by TXRF. Values are given in mg/kg.

Sample type	Y	La	Ce	Pr	Nd	Sm	Eu	Gd	Tb	Dy	Ho	Er	Tm	Yb	Lu
SOIL	17.7	69.6	117	< LOD	< LOD	< LOD	< LOD	< LOD	< LOD	< LOD	< LOD	< LOD	< LOD	< LOD	< LOD
SEDIMENTS	14.6	51.5	93.4	< LOD	< LOD	< LOD	< LOD	< LOD	< LOD	< LOD	< LOD	< LOD	< LOD	1.57	12.6
ROCKS	8.71	5.11	7.47	< LOD	0.31	< LOD	< LOD	< LOD	< LOD	< LOD	< LOD	< LOD	< LOD	6.65	4.41
BIOTA	3.83	4.43	8.02	< LOD	0.45	< LOD	< LOD	< LOD	< LOD	< LOD	< LOD	< LOD	< LOD	< LOD	< LOD

In the region of Spinazzola, Y, La Ce and Nd were detected in all types of samples collected, while Lu was detected only in soil. The most abundant REE was La in all three types of samples.

Table 7. Mean values of each REE in each type of sample from Spinazzola region, after analysis by TXRF. Values are given in mg/kg.

Sample type	Y	La	Ce	Pr	Nd	Sm	Eu	Gd	Tb	Dy	Ho	Er	Tm	Yb	Lu
SOIL	34.1	159	155.97	< LOD	42.4	< LOD	< LOD	< LOD	< LOD	< LOD	< LOD	< LOD	< LOD	< LOD	3.40
ROCKS	15.1	59.8	31.83	< LOD	12.61	< LOD	< LOD	< LOD	< LOD	< LOD	< LOD	< LOD	< LOD	< LOD	< LOD
BIOTA	8.42	8.78	5.18	< LOD	7.60	< LOD	< LOD	< LOD	< LOD	< LOD	< LOD	< LOD	< LOD	< LOD	< LOD

3.2.2 Analysis by ICP-MS

Tables 8, 9 and 10 show the mean concentrations of each REE in each type of sample collected from the regions of Gargano, Otranto and Spinazzola, respectively, after elemental analysis by ICP-MS.

All REEs were detected by ICP-MS in all types of samples collected from all three regions. The most abundant REE was Ce, followed by La, in all types of samples from all regions. The only exception were the biota samples from Spinazzola region, where La was the most abundant REE, followed by Nd.

Table 8. Mean values of each REE in each type of sample from Gargano region, after analysis by ICP-MS. Values are given in mg/kg.

Sample type	Y	La	Ce	Pr	Nd	Sm	Eu	Gd	Tb	Dy	Ho	Er	Tm	Yb	Lu
SOIL	35.1	78.0	309	20.7	74.1	13.7	2.97	14.0	1.78	7.62	1.31	3.96	0.43	3.27	0.40
SEDIMENTS	20.4	52.8	120	12.4	41.7	7.65	1.45	7.61	0.93	3.87	0.64	2.11	0.23	1.66	0.22
ROCKS	20.6	38.1	98.7	9.93	34.7	6.57	1.62	6.57	0.91	4.11	0.76	2.25	0.25	1.84	0.23
BIOTA	4.89	10.7	21.7	2.59	9.67	1.85	0.40	1.59	0.21	1.07	0.19	0.51	0.07	0.43	0.06

Table 9. Mean values of each REE in each type of sample from Otranto region, after analysis by ICP-MS. Values are given in mg/kg.

Sample type	Y	La	Ce	Pr	Nd	Sm	Eu	Gd	Tb	Dy	Ho	Er	Tm	Yb	Lu
SOIL	36.0	66.3	188	15.8	55.5	10.9	2.45	11.2	1.58	6.99	1.28	3.91	0.46	3.61	0.45
SEDIMENTS	36.6	45.0	163	11.3	41.7	8.22	1.91	9.09	1.27	6.09	1.16	3.53	0.44	3.18	0.43
ROCKS	21.8	28.8	33.6	4.96	17.0	3.72	0.86	3.67	0.64	3.25	0.67	1.96	0.25	1.87	0.24
BIOTA	3.21	7.22	13.9	1.41	5.04	0.97	0.21	0.87	0.12	0.64	0.12	0.33	0.04	0.28	0.04
WATER	0.28	0.25	0.60	0.05	0.17	0.04	0.02	0.10	0.01	0.06	0.01	0.02	< 0.01	0.02	< 0.01

Table 10. Mean values of each REE in each type of sample from Spinazzola region, after analysis by ICP-MS. Values are given in mg/kg.

Sample type	Y	La	Ce	Pr	Nd	Sm	Eu	Gd	Tb	Dy	Ho	Er	Tm	Yb	Lu
SOIL	125	247	366	63.7	236	42.1	10.0	42.1	5.46	23.1	4.36	12.60	1.37	8.94	1.18
ROCKS	47.6	66.0	115	17.7	65.9	12.4	3.10	13.2	1.84	8.67	1.68	4.75	0.51	3.35	0.43
BIOTA	7.75	254	130	63.9	253	46.3	11.1	40.3	4.67	21.7	3.34	7.83	0.89	5.26	0.72
WATER	19.8	37.0	46.1	10.3	32.4	6.72	1.51	7.48	0.74	2.65	0.51	1.49	0.16	0.93	0.13

3.2.3 Comparison of the two techniques

Supplementary materials 3 includes the statistical analysis elaborated for comparing the results obtained from the two techniques.

An independent sample t-test (Welch) was elaborated for the investigation of significant differences ($p < 0.05$) between the REE-levels obtained by TXRF and ICP-MS (Table S25). Only Y, La and Ce were compared since they were the only elements detected in all samples by TXRF. Significant differences were observed for Y in the soil samples of Gargano and Otranto and in the rock samples of Spinazzola, and for Ce in the soil samples of Spinazzola. No statistically significant difference was observed for La in any type of sample. Figures S4, S5, S6, S7 and S8 show the differences of the levels of Y, La and Ce after analysis by TXRF and ICP-MS, respectively.

Our results are in accordance with the study of Towett et al. (2013) in which they found similar or lower levels of REEs in soil samples when analyzed by TXRF Picofox S2, compared to ICP-MS. They referred as well to errors occurred during analysis by TXRF due to the line inerferences by other elements, depending on the concentration of the interfering element. Only systematic errors, such as fluorescence radiation adsorption for the light elements, can be corrected in TXRF.

Previous studies investigated also the REE levels in soil samples from abandoned mining sites around the world, using different techniques of analysis. Purwadi et al. (2019) analyzed the REE-contents in tailing samples from two abandoned tin mine tailings in Indonesia using inductively coupled plasma optical emission spectrometry (ICP-OES). Except for the very elevated Er levels found in their samples, their results are similar to our results from soil samples from Spinazzola region, after analysis by ICP-MS. Medas et al. (2013) analyzed the REE levels in solid materials from an abandoned mining in Sardenia using ICP-OES, while Atibu et al. (2016) analyzed the REE-content in soil samples near an abandoned mining site in Congo using ICP-MS. All REE levels in the samples from both studies were much lower than the REE levels in our soil samples from all three regions, after analysis by ICP-MS. Fernández-Caliani et al. (2009) analyzed the REE-content in soil samples from Tharsis abandoned mines in Spain using XRF. The levels of La and Ce in their soil samples were lower than in our soil samples, in all three regions, after analyzed by TXRF. All in all, compared to other studies, it seems that the REE-content in the soil samples from the abandoned mining sites in the region of Puglia are at higher levels, making them ideal spots for a possible REE extraction.

Table 11 demonstrates a summary of the advantages and disadvantages using each technique for the analysis of REEs in environmental samples.

Table 11. Comparison of the advantages and disadvantages between TXRF and ICP-MS.

Parameter	**TXRF**	**ICP-MS**
Matrix effects	Yes	Yes
Time-consuming	Less	More
LOD values	Higher	Lower
Precision and accuracy	Less	More
Cost	Less	More
Use of one internal standard	Yes	Yes
Multi-elemental analysis	Yes	Yes
Spectral interferences	Yes	No
Possible sample contamination and lose of elements due to digestion	Yes	Yes

The ICP-MS seems to be a more suitable technique for the analysis of REEs on such environmental samples. The analysis of the REE levels in these samples by TXRF compared to ICP-MS has two main disadvantages. The first is the much higher LOD values, about 1000 times, which means that by ICP-MS we can determine REEs in much lower concentrations with respect to TXRF. The second is the spectra interferences of some REEs by the spectra of other elements that exist in higher concentrations in the samples. While ICP-MS functions with a quadrupole and the ions can be separated according to their mass per ratio and been detected separately without any interferences, in TXRF the spectra of the whole sample has to be analyzed (Figure 5). After a sample is analyzed by Picofox S2, a fit has to be made in the computer program for the whole spectra between the spectra received from the instrument and the spectra given from the program. Only by this way someone can be sure about the concentrations of the elements that are included in the sample analyzed. While analyzing the spectra of a sample by TXRF, some REEs are in the same range with other heavy metals that are in higher concentrations and so, the spectra of the latter covers the spectra of these REEs, making them impossible for determination. For example, as shown in figure 6, the main spectra of Gd, Tb, Dy, Ho, Er and Tm are covered by the spectra of Fe, and so, these elements are not able to be determined by TXRF.

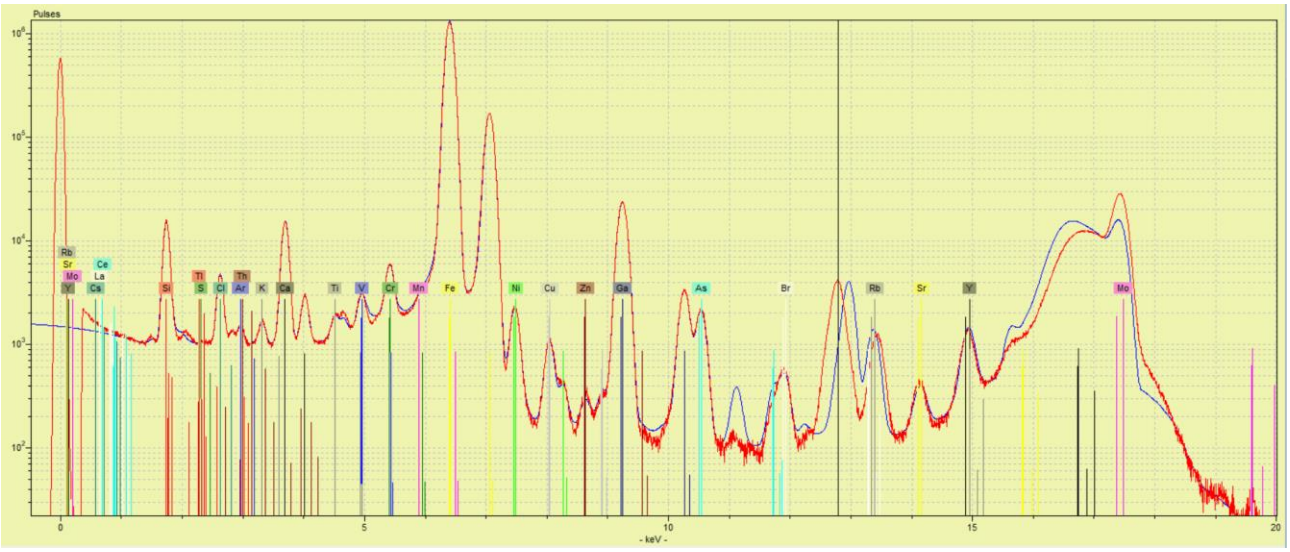

Figure 5. An example of the whole spectra of a soil sample analyzed by Picofox S2.

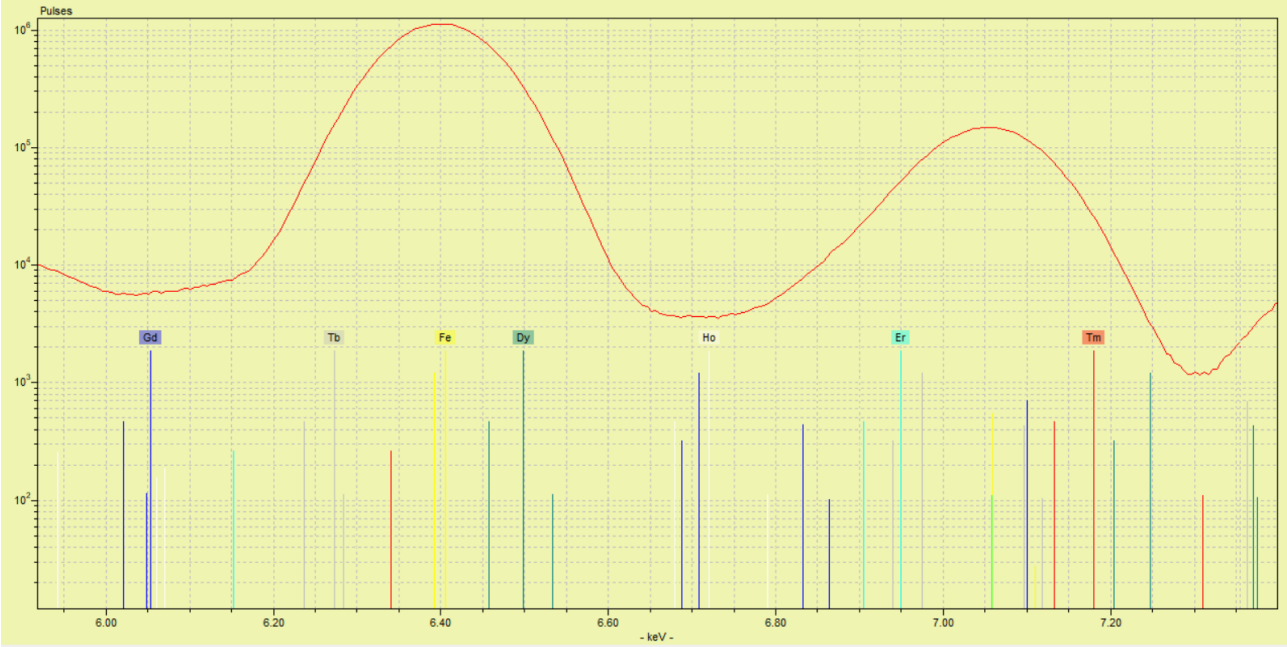

Figure 6. The spectra of Fe after analysis of a soil sample by Picofox S2. This spectra is covering the spectra of Gd, Tb, Dy, Ho, Er, and Tm, making them impossible to be detected by this technique.

3.3 Comparison of REE levels between the three sites after analysis by ICP-MS

Figures S10, S11 and S12 on Supplementary materials 3 show the concentrations of each REE on soil, biota and rock samples, respectively, from the three abandoned mining sites, after analysis by ICP-MS.

Among all three sites, Spinazzola seems to be the richest site, containing higher concentrations of REEs with respect to Gargano and Otranto. As mentioned also above, Ce is the most abundant REE,

followed by La, in all types of samples from all regions, except for the biota samples from Spinazzola region, where La was the most abundant REE, followed by Nd.

Soil, rock and biota samples from Spinazzola seem to contain a high amount of REEs, especially La and Ce. The mean concentration of Ce in soil samples is at 366.37 mg/kg, while in biota is at 130.04 mg/kg, and 115.81 mg/kg in rocks. On the same hand, the mean concentration of La is at 247.37 mg/kg, 65.99 mg/kg and 254.30 mg/kg in soil, biota and rock samples respectively. Therefore, the environmental samples from the abandoned mining site from Spinazzola region, seem to be exclusively ideal for extraction of REEs.

The correlation analysis between the REE-levels in the soil and biota samples from the same sampling point of each area after analysis by ICP-MS (Table S26), showed that there is correlation (Pearson r > 0.7) of the REE-levels between the two types of sample for 13 REEs in Gargano, 11 in Otranto and 9 in Spinazzola.

The calculation of the Bioconcentration factor (BCF) of the biota and soil samples from each sampling point (Tables S27, S28 and S29) revealed that no REE is bioaccumulative at any sampling point (> 1000 L/kg).

The bioaccumulation of metals in biota from soil, depend on several factors, such as the soil properties, the types of extractants and the metals (Xu et al., 2022). According to (Cataldo and Wildung, 1978), the major factor governing metal availability to plants in soils is the solubility of the metal associated with the solid phase, since in order for root uptake to occur, a soluble species must exist adjacent to the root membrane for some finite period.

We have to highlight that the small number of soil (9 from Gargano, 8 from Otranto and 10 from Spinazzola) and biota samples (5 from Gargano, 8 from Otranto and 9 from Spinazzola) obtained for this research makes the results having a big bias. Therefore, we can only have some first indications about the REE-levels and the correlation between soil and biota samples.

4 Conclusions

By analyzing environmental samples collected from the three abandoned mining sites, it can be concluded that REEs are not only present in traceable levels, but in levels that could be suitable for a possible extraction.

The analysis of the REE levels in these samples by TXRF compared to ICP-MS has two main disadvantages. The very higher LOD values, and the covering of the spectra of some REEs by the spectra of other elements. Instead, in ICP-MS there are no interferences for the analysis of REEs. This makes ICP-MS a more suitable technique for determining the whole range of REEs in environmental samples, even from areas with past mining activity.

However, other parameters of each technique should be also determined in the future, such as accuracy and precision. With that way, we can be more sure of which technique is more suitable for the analysis of REE levels in environmental samples.

Cerium is the most abundant REE in all environmental samples from all three regions, except for the biota from Spinazzola, where La is the most abundant.

The correlation analysis revealed that REE levels are correlated between the biota and soil samples, while the calculation of BCF showed that REEs are not bioaccumulative at all.

Comparing REE-levels between the three regions after analysis by ICP-MS, Spinazzola is the site containing higher levels of these elements making it the most interesting among all for a possible REE extraction.

REEs in environmental samples from abandoned mining sites in Southern Italy are still in traceable levels. Since several previous studies have shown that they might consist a threat for human and environmental health, more investigations should be elaborated about their concentrations either near or further from mining sites.

Supplementary materials

Supplementary materials 1

On this supplementary material are presented the three abandoned mining sites followed by the coordinations of each sampling point. Each site is divided in twenty areas, ten of which (marked with x) were selected randomly for the sample collection.

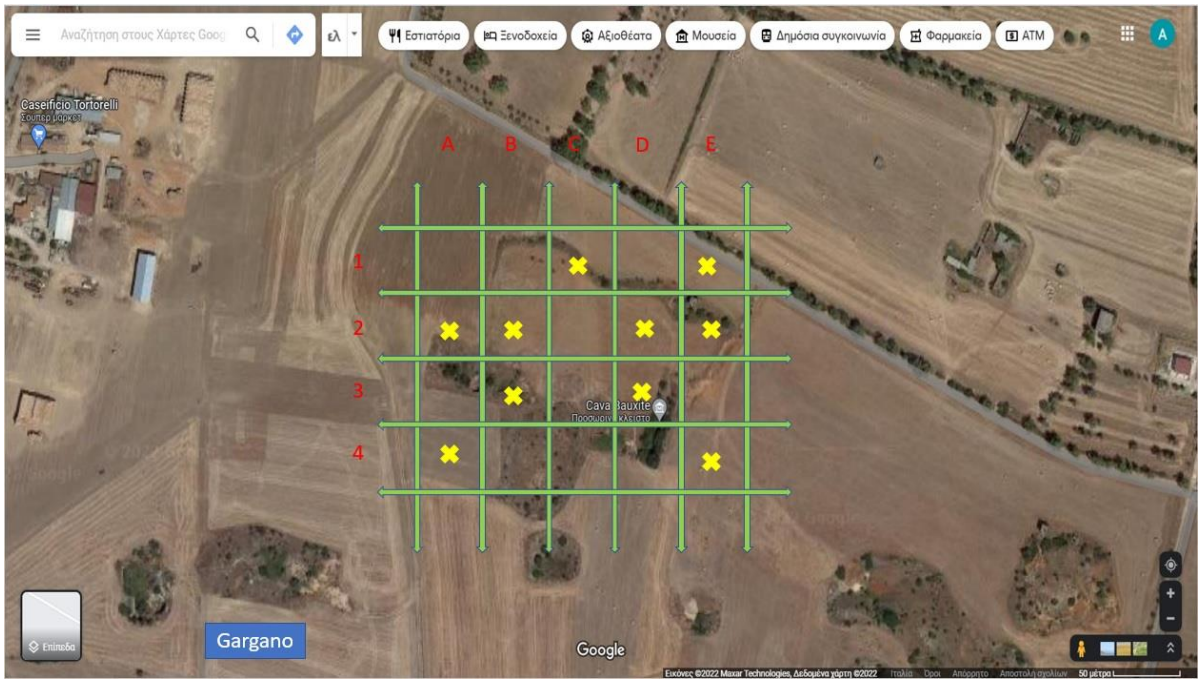

Figure S1. Location of Miniera di Bauxite (underground), "Gargano site", 71013 Foggia, Italy.

Coordinations of each sampling point on the site of Gargano:

A2: 41.637875, 15.713630

A4: 41.637221, 15.713750

B2: 41.637891, 15.714280

B3: 41.637569, 15.714273

C1: 41.638255, 15.714837

D2: 41.637954, 15.715465

D3: 41.637548, 15.715395

E1: 41.638260, 15.716094

E2: 41.637933, 15.716065

E4: 41.637131, 15.715995

Figure S2. Location and of Cava de Bauxite, "Otranto site", Puglia Region, Italy.

Coordinations for each sampling point on the site of Otranto:

A2: 40.132281, 18.499606

A4: 40.131613, 18.499581

B2: 40.132233, 18.500149

B3: 40.131901, 18.500114

C1: 40.132617, 18.500638

D2: 40.132282, 18.501225

D3: 40.131939, 18.501269

E1: 40.132607, 18.501799

E2: 40.132249, 18.501843

E4: 40.131543, 18.501737

Figure S3. Location of "Spinazzola site", Cave di Bauxite, Puglia Region, Italy.

Coordinations of each sampling point on the site of Spinazzola:

A2: 40.987293, 16.179972

A4: 40.986569, 16.179992

B2: 40.987308, 16.180603

B3: 40.986888, 16.180590

C1: 40.987683, 16.181173

D2: 40.987298, 16.181885

D3: 40.986923, 16.181811

E1: 40.987718, 16.182381

E2: 40.987232, 16.182454

E4: 40.986538, 16.182435

Supplementary materials 2

On this supplementary material are presented the concentrations of each REE in each type of sample and from each sampling point. First are presented the results after analysis by TXRF and then the results after analysis by ICP-MS.

Analyses by TXRF

Table S1. Concentrations of REEs in the soil samples from the region of Gargano after analysis by TXRF. Values are expressed in mg/kg.

Sample Label	Y	La	Ce	Pr	Nd	Sm	Eu	Gd	Tb	Dy	Ho	Er	Tm	Yb	Lu
A2	16.97	32.46	114.79	< LOD	< LOD	< LOD	< LOD	< LOD	< LOD	< LOD	< LOD	< LOD	< LOD	< LOD	< LOD
A4	14.61	26.11	106.56	< LOD	< LOD	< LOD	< LOD	< LOD	< LOD	< LOD	< LOD	< LOD	< LOD	< LOD	< LOD
B2	12.65	67.42	131.31	< LOD	< LOD	< LOD	< LOD	< LOD	< LOD	< LOD	< LOD	< LOD	< LOD	< LOD	< LOD
B3	10.32	50.54	52.38	< LOD	< LOD	< LOD	< LOD	< LOD	< LOD	< LOD	< LOD	< LOD	< LOD	< LOD	< LOD
C1	10.19	69.18	100.91	< LOD	< LOD	< LOD	< LOD	< LOD	< LOD	< LOD	< LOD	< LOD	< LOD	< LOD	< LOD
D2	4.61	148.72	153.88	< LOD	< LOD	< LOD	< LOD	< LOD	< LOD	< LOD	< LOD	< LOD	< LOD	< LOD	< LOD
D3	20.81	19.35	41.15	< LOD	< LOD	< LOD	< LOD	< LOD	< LOD	< LOD	< LOD	< LOD	< LOD	< LOD	< LOD
E2	13.16	92.48	110.04	< LOD	< LOD	< LOD	< LOD	< LOD	< LOD	< LOD	< LOD	< LOD	< LOD	< LOD	< LOD
E4	18.24	88.79	188.71	< LOD	< LOD	< LOD	< LOD	< LOD	< LOD	< LOD	< LOD	< LOD	< LOD	< LOD	< LOD

Table S2. Concentrations of REEs in the soil samples from the region of Otranto after analysis by TXRF. Values are expressed in mg/kg.

Sample Label	Y	La	Ce	Pr	Nd	Sm	Eu	Gd	Tb	Dy	Ho	Er	Tm	Yb	Lu
A2	4.22	65.36	44.10	< LOD	< LOD	< LOD	< LOD	< LOD	< LOD	< LOD	< LOD	< LOD	< LOD	< LOD	< LOD
A4	1.68	58.39	63.66	< LOD	< LOD	< LOD	< LOD	< LOD	< LOD	< LOD	< LOD	< LOD	< LOD	< LOD	< LOD
C1	20.12	81.81	84.76	< LOD	< LOD	< LOD	< LOD	< LOD	< LOD	< LOD	< LOD	< LOD	< LOD	< LOD	< LOD
D2	27.21	55.80	411.89	< LOD	< LOD	< LOD	< LOD	< LOD	< LOD	< LOD	< LOD	< LOD	< LOD	< LOD	< LOD
D3	38.02	104.98	156.56	< LOD	< LOD	< LOD	< LOD	< LOD	< LOD	< LOD	< LOD	< LOD	< LOD	< LOD	< LOD
E1	14.48	85.71	74.80	< LOD	< LOD	< LOD	< LOD	< LOD	< LOD	< LOD	< LOD	< LOD	< LOD	< LOD	< LOD
E2	7.28	46.60	26.76	< LOD	< LOD	< LOD	< LOD	< LOD	< LOD	< LOD	< LOD	< LOD	< LOD	< LOD	< LOD
E4	28.17	58.32	76.36	< LOD	< LOD	< LOD	< LOD	< LOD	< LOD	< LOD	< LOD	< LOD	< LOD	< LOD	< LOD

Table S3. Concentrations of REEs in the soil samples from the region of Spinazzola after analysis by TXRF. Values are expressed in mg/kg.

Sample Label	Y	La	Ce	Pr	Nd	Sm	Eu	Gd	Tb	Dy	Ho	Er	Tm	Yb	Lu
A2	8.65	101.03	66.04	< LOD	< LOD	< LOD	< LOD	< LOD	< LOD	< LOD	< LOD	< LOD	< LOD	< LOD	0.59
A4	21.02	110.73	191.12	< LOD	2.57	< LOD	< LOD	< LOD	< LOD	< LOD	< LOD	< LOD	< LOD	< LOD	< LOD
B2	14.78	194.87	223.02	< LOD	< LOD	< LOD	< LOD	< LOD	< LOD	< LOD	< LOD	< LOD	< LOD	< LOD	3.36
B3	133.79	180.13	131.56	< LOD	19.64	< LOD	< LOD	< LOD	< LOD	< LOD	< LOD	< LOD	< LOD	< LOD	8.69
C1	6.47	89.17	139.05	< LOD	< LOD	< LOD	< LOD	< LOD	< LOD	< LOD	< LOD	< LOD	< LOD	< LOD	< LOD
D2	24.19	220.26	108.58	< LOD	98.14	< LOD	< LOD	< LOD	< LOD	< LOD	< LOD	< LOD	< LOD	< LOD	< LOD
D3	47.30	321.30	203.62	< LOD	235.14	< LOD	< LOD	< LOD	< LOD	< LOD	< LOD	< LOD	< LOD	< LOD	7.87
E1	13.31	122.51	225.44	< LOD	3.05	< LOD	< LOD	< LOD	< LOD	< LOD	< LOD	< LOD	< LOD	< LOD	< LOD
E2	42.91	142.71	189.93	< LOD	44.64	< LOD	< LOD	< LOD	< LOD	< LOD	< LOD	< LOD	< LOD	< LOD	11.74
E4	28.98	107.23	81.33	< LOD	21.04	< LOD	< LOD	< LOD	< LOD	< LOD	< LOD	< LOD	< LOD	< LOD	1.74

Table S4. Concentrations of REEs in the sediment samples from the region of Gargano after analysis by TXRF. Values are expressed in mg/kg.

Sample Label	Y	La	Ce	Pr	Nd	Sm	Eu	Gd	Tb	Dy	Ho	Er	Tm	Yb	Lu
B3	11.21	4.82	52.00	< LOD	< LOD	< LOD	< LOD	< LOD	< LOD	< LOD	< LOD	< LOD	< LOD	< LOD	6.54
D3	14.68	22.39	96.44	< LOD	< LOD	< LOD	< LOD	< LOD	< LOD	< LOD	< LOD	< LOD	< LOD	< LOD	< LOD
E2	0.50	93.04	76.98	< LOD	< LOD	< LOD	< LOD	< LOD	< LOD	< LOD	< LOD	< LOD	< LOD	< LOD	< LOD

Table S5. Concentrations of REEs in the sediment samples from the region of Otranto after analysis by TXRF. Values are expressed in mg/kg.

Sample Label	Y	La	Ce	Pr	Nd	Sm	Eu	Gd	Tb	Dy	Ho	Er	Tm	Yb	Lu
A2	13.89	81.84	201.42	< LOD	< LOD	< LOD	< LOD	< LOD	< LOD	< LOD	< LOD	< LOD	< LOD	< LOD	< LOD
D2	9.88	53.19	26.80	< LOD	< LOD	< LOD	< LOD	< LOD	< LOD	< LOD	< LOD	< LOD	< LOD	6.27	< LOD
D3 acquatic	23.77	43.56	145.53	< LOD	< LOD	< LOD	< LOD	< LOD	< LOD	< LOD	< LOD	< LOD	< LOD	< LOD	< LOD
E1	11.01	27.41	< LOD	< LOD	< LOD	< LOD	< LOD	< LOD	< LOD	< LOD	< LOD	< LOD	< LOD	< LOD	50.49

Table S6. Concentrations of REEs in the rock samples from the region of Gargano after analysis by TXRF. Values are expressed in mg/kg.

Sample Label	Y	La	Ce	Pr	Nd	Sm	Eu	Gd	Tb	Dy	Ho	Er	Tm	Yb	Lu
B2	0.38	5.75	4.18	< LOD	< LOD	< LOD	< LOD	< LOD	< LOD	< LOD	< LOD	< LOD	< LOD	< LOD	0.63
B3	< LOD	< LOD	< LOD	< LOD	< LOD	< LOD	< LOD	< LOD	< LOD	< LOD	< LOD	< LOD	< LOD	< LOD	< LOD
D2	12.13	14.87	57.57	< LOD	1.46	< LOD	< LOD	< LOD	< LOD	< LOD	< LOD	< LOD	< LOD	16.66	3.24
D3	< LOD	< LOD	< LOD	< LOD	< LOD	< LOD	< LOD	< LOD	< LOD	< LOD	< LOD	< LOD	< LOD	59.75	22.17

Table S7. Concentrations of REEs in the rock samples from the region of Otranto after analysis by TXRF. Values are expressed in mg/kg.

Sample Label	Y	La	Ce	Pr	Nd	Sm	Eu	Gd	Tb	Dy	Ho	Er	Tm	Yb	Lu
A2	7.68	< LOD	29.88	< LOD	< LOD	< LOD	< LOD	< LOD	< LOD	< LOD	< LOD	< LOD	< LOD	< LOD	11.42
A4	< LOD	< LOD	< LOD	< LOD	< LOD	< LOD	< LOD	< LOD	< LOD	< LOD	< LOD	< LOD	< LOD	< LOD	< LOD
C1	4.17	0.71	2.85	< LOD	< LOD	< LOD	< LOD	< LOD	< LOD	< LOD	< LOD	< LOD	< LOD	< LOD	< LOD
D2	26.27	14.81	< LOD	< LOD	< LOD	< LOD	< LOD	< LOD	< LOD	< LOD	< LOD	< LOD	< LOD	33.27	10.60
E4	5.44	10.05	4.64	< LOD	1.55	< LOD	< LOD	< LOD	< LOD	< LOD	< LOD	< LOD	< LOD	< LOD	< LOD

Table S8. Concentrations of REEs in the rock samples from the region of Spinazzola after analysis by TXRF. Values are expressed in mg/kg.

Sample Label	Y	La	Ce	Pr	Nd	Sm	Eu	Gd	Tb	Dy	Ho	Er	Tm	Yb	Lu
A2	13.30	92.60	109.90	< LOD	< LOD	< LOD	< LOD	< LOD	< LOD	< LOD	< LOD	< LOD	< LOD	< LOD	< LOD
A4	13.40	62.69	7.31	< LOD	< LOD	< LOD	< LOD	< LOD	< LOD	< LOD	< LOD	< LOD	< LOD	< LOD	< LOD
B2	0.94	55.75	47.58	< LOD	< LOD	< LOD	< LOD	< LOD	< LOD	< LOD	< LOD	< LOD	< LOD	< LOD	< LOD
B3	38.26	38.54	47.87	< LOD	33.77	< LOD	< LOD	< LOD	< LOD	< LOD	< LOD	< LOD	< LOD	< LOD	< LOD
C1	5.53	40.74	8.14	< LOD	11.57	< LOD	< LOD	< LOD	< LOD	< LOD	< LOD	< LOD	< LOD	< LOD	< LOD
D2	9.56	68.94	11.95	< LOD	< LOD	< LOD	< LOD	< LOD	< LOD	< LOD	< LOD	< LOD	< LOD	< LOD	< LOD
D3	34.58	63.09	< LOD	< LOD	23.73	< LOD	< LOD	< LOD	< LOD	< LOD	< LOD	< LOD	< LOD	< LOD	< LOD
E1	6.87	37.42	< LOD	< LOD	< LOD	< LOD	< LOD	< LOD	< LOD	< LOD	< LOD	< LOD	< LOD	< LOD	< LOD
E4	13.67	77.98	53.73	< LOD	44.44	< LOD	< LOD	< LOD	< LOD	< LOD	< LOD	< LOD	< LOD	< LOD	< LOD

Table S9. Concentrations of REEs in the biota samples from the region of Gargano after analysis by TXRF. Values are expressed in mg/kg.

Sample Label	Y	La	Ce	Pr	Nd	Sm	Eu	Gd	Tb	Dy	Ho	Er	Tm	Yb	Lu
A2	11.27	7.88	21.37	< LOD	1.86	< LOD	< LOD	< LOD	< LOD	< LOD	< LOD	< LOD	< LOD	< LOD	< LOD
B3	3.10	4.47	13.70	< LOD	2.13	< LOD	< LOD	< LOD	< LOD	< LOD	< LOD	< LOD	< LOD	< LOD	< LOD
D3	2.89	< LOD	7.25	< LOD	< LOD	< LOD	< LOD	< LOD	< LOD	< LOD	< LOD	< LOD	< LOD	< LOD	< LOD
E2	1.22	1.63	2.80	< LOD	< LOD	< LOD	< LOD	< LOD	< LOD	< LOD	< LOD	< LOD	< LOD	< LOD	< LOD
E4	10.87	4.03	15.43	< LOD	2.05	< LOD	< LOD	< LOD	< LOD	< LOD	< LOD	< LOD	< LOD	< LOD	< LOD

Table S10. Concentrations of REEs in the biota samples from the region of Otranto after analysis by TXRF. Values are expressed in mg/kg.

Sample Label	Y	La	Ce	Pr	Nd	Sm	Eu	Gd	Tb	Dy	Ho	Er	Tm	Yb	Lu
A2	1.05	7.36	13.75	< LOD	0.65	< LOD	< LOD	< LOD	< LOD	< LOD	< LOD	< LOD	< LOD	< LOD	< LOD
A4	0.57	2.83	5.57	< LOD	< LOD	< LOD	< LOD	< LOD	< LOD	< LOD	< LOD	< LOD	< LOD	< LOD	< LOD
C1	8.78	3.86	4.24	< LOD	< LOD	< LOD	< LOD	< LOD	< LOD	< LOD	< LOD	< LOD	< LOD	< LOD	< LOD
D2	1.93	3.44	4.97	< LOD	< LOD	< LOD	< LOD	< LOD	< LOD	< LOD	< LOD	< LOD	< LOD	< LOD	< LOD
D3	8.94	7.59	11.41	< LOD	< LOD	< LOD	< LOD	< LOD	< LOD	< LOD	< LOD	< LOD	< LOD	< LOD	< LOD
D3 acquatic	3.70	4.92	13.49	< LOD	3.39	< LOD	< LOD	< LOD	< LOD	< LOD	< LOD	< LOD	< LOD	< LOD	< LOD
E1	4.49	5.29	9.64	< LOD	< LOD	< LOD	< LOD	< LOD	< LOD	< LOD	< LOD	< LOD	< LOD	< LOD	< LOD
E2	0.38	2.04	3.44	< LOD	< LOD	< LOD	< LOD	< LOD	< LOD	< LOD	< LOD	< LOD	< LOD	< LOD	< LOD
E4	4.63	2.49	5.69	< LOD	< LOD	< LOD	< LOD	< LOD	< LOD	< LOD	< LOD	< LOD	< LOD	< LOD	< LOD

Table S11. Concentrations of REEs in the biota samples from the region of Spinazzola after analysis by TXRF. Values are expressed in mg/kg.

Sample Label	Y	La	Ce	Pr	Nd	Sm	Eu	Gd	Tb	Dy	Ho	Er	Tm	Yb	Lu
A2	2.15	1.13	3.26	< LOD	1.84	< LOD	< LOD	< LOD	< LOD	< LOD	< LOD	< LOD	< LOD	< LOD	< LOD
A4	6.12	0.76	1.42	< LOD	< LOD	< LOD	< LOD	< LOD	< LOD	< LOD	< LOD	< LOD	< LOD	< LOD	< LOD
B2	4.97	7.38	1.25	< LOD	8.66	< LOD	< LOD	< LOD	< LOD	< LOD	< LOD	< LOD	< LOD	< LOD	< LOD
B3	8.34	4.49	4.09	< LOD	4.60	< LOD	< LOD	< LOD	< LOD	< LOD	< LOD	< LOD	< LOD	< LOD	< LOD
C1	3.80	12.45	17.73	< LOD	2.73	< LOD	< LOD	< LOD	< LOD	< LOD	< LOD	< LOD	< LOD	< LOD	< LOD
D2	2.74	5.39	3.24	< LOD	4.55	< LOD	< LOD	< LOD	< LOD	< LOD	< LOD	< LOD	< LOD	< LOD	< LOD
D3	34.77	34.94	< LOD	< LOD	40.46	< LOD	< LOD	< LOD	< LOD	< LOD	< LOD	< LOD	< LOD	< LOD	< LOD
E2	2.52	4.57	10.14	< LOD	1.17	< LOD	< LOD	< LOD	< LOD	< LOD	< LOD	< LOD	< LOD	< LOD	< LOD
E4	10.41	7.91	5.48	< LOD	4.39	< LOD	< LOD	< LOD	< LOD	< LOD	< LOD	< LOD	< LOD	< LOD	< LOD

Analyses by ICP-MS

Table S12. Concentrations of REEs in the soil samples from the region of Gargano after analysis by ICP-MS. Values are expressed in mg/kg.

Sample Label	Y	La	Ce	Pr	Nd	Sm	Eu	Gd	Tb	Dy	Ho	Er	Tm	Yb	Lu
A2	30.15	84.79	185.86	19.57	68.82	12.12	2.56	13.19	1.54	6.17	1.14	3.20	0.36	3.03	0.35
A4	27.01	71.71	145.63	15.73	51.09	8.96	2.05	8.91	1.21	5.22	0.85	2.75	0.31	2.63	0.30
B2	50.10	143.48	505.11	35.54	129.53	22.18	5.22	23.06	2.93	13.19	2.24	6.07	0.63	4.91	0.58
B3	41.44	98.49	274.55	24.72	85.31	15.84	3.33	15.42	2.06	8.83	1.51	4.70	0.53	3.90	0.49
C1	19.66	67.42	166.79	17.68	62.14	11.07	2.56	10.77	1.26	5.88	0.81	2.51	0.29	2.28	0.26
D2	20.87	33.85	97.71	7.62	26.89	5.30	1.30	5.67	0.81	3.91	0.70	2.04	0.27	1.83	0.26
D3	33.36	94.27	289.45	23.22	79.45	14.16	3.17	13.86	1.84	7.66	1.32	4.41	0.45	3.46	0.42
E2	69.40	50.20	968.36	27.38	111.01	23.80	4.58	24.79	3.10	12.74	2.41	7.16	0.73	5.07	0.67
E4	23.48	58.17	152.98	15.22	52.84	10.08	1.95	9.94	1.29	5.00	0.86	2.77	0.31	2.32	0.29

Table S13. Concentrations of REEs in the soil samples from the region of Otranto after analysis by ICP-MS. Values are expressed in mg/kg.

Sample Label	Y	La	Ce	Pr	Nd	Sm	Eu	Gd	Tb	Dy	Ho	Er	Tm	Yb	Lu
A2	31.41	67.63	195.05	14.12	49.65	11.02	2.18	9.50	1.59	7.53	1.56	4.31	0.53	4.95	0.55
A4	17.65	69.82	186.71	9.63	29.49	5.78	1.41	6.39	0.73	3.22	0.58	1.92	0.24	2.22	0.24
C1	32.76	53.10	121.80	11.38	40.24	7.93	1.78	8.35	1.23	5.41	1.04	3.34	0.41	3.37	0.39
D2	33.98	81.29	128.90	24.27	85.50	13.47	3.35	14.39	1.73	7.31	1.14	3.57	0.37	2.66	0.33
D3	72.35	86.74	340.85	24.21	89.28	18.29	4.16	19.20	2.84	12.40	2.40	7.09	0.91	6.12	0.91
E1	23.25	57.19	239.49	16.58	53.68	11.64	2.38	11.58	1.64	6.55	0.99	3.20	0.39	2.91	0.37
E2	26.80	46.24	147.91	10.78	38.89	8.29	1.74	8.25	1.19	5.62	1.02	3.14	0.35	3.02	0.34
E4	49.64	68.66	150.30	15.62	57.49	11.01	2.60	11.88	1.70	7.85	1.55	4.71	0.51	3.60	0.48

Table S14. Concentrations of REEs in the soil samples from the region of Spinazzola after analysis by ICP-MS. Values are expressed in mg/kg.

Sample Label	Y	La	Ce	Pr	Nd	Sm	Eu	Gd	Tb	Dy	Ho	Er	Tm	Yb	Lu
A2	31.64	96.71	73.62	23.26	87.39	14.00	3.08	13.25	1.65	6.79	1.29	3.49	0.29	2.74	0.25
A4	61.94	196.34	472.53	40.69	142.30	24.04	5.62	27.22	3.13	13.04	2.25	6.53	0.61	4.31	0.53
B2	45.84	190.42	381.24	51.32	189.75	34.00	8.02	31.97	4.07	16.83	3.36	8.22	0.76	5.86	0.64
B3	513.22	295.86	404.19	68.99	257.86	46.60	12.00	50.13	7.35	33.60	7.32	31.06	4.28	26.73	3.51
C1	42.75	155.26	485.44	40.60	140.58	26.38	6.11	24.16	3.41	16.65	3.01	8.70	0.76	5.67	0.63
D2	44.87	133.53	205.30	38.06	142.25	25.84	6.12	27.47	3.56	15.84	2.76	7.72	0.72	5.21	0.61
D3	206.33	798.88	596.32	215.35	822.91	140.91	33.83	139.19	16.82	66.51	12.39	29.43	2.91	16.33	2.34
E1	45.42	157.79	516.20	44.14	160.97	28.03	6.49	28.55	3.56	15.05	2.39	7.18	0.60	5.63	0.53
E2	147.57	258.57	341.32	66.98	248.05	49.60	11.48	46.91	6.78	28.85	5.41	14.29	1.61	9.30	1.58
E4	113.36	190.38	187.51	47.09	173.00	31.20	7.63	32.15	4.29	17.31	3.38	9.35	1.12	7.62	1.12

Table S15. Concentrations of REEs in the sediment samples from the region of Gargano after analysis by ICP-MS. Values are expressed in mg/kg.

Sample Label	Y	La	Ce	Pr	Nd	Sm	Eu	Gd	Tb	Dy	Ho	Er	Tm	Yb	Lu
B3	30.54	72.48	152.10	16.00	53.01	9.63	1.77	9.25	1.22	5.66	0.91	2.92	0.34	2.25	0.31
D3	19.46	46.69	96.47	11.22	36.86	6.96	1.34	6.67	0.90	3.42	0.65	2.26	0.24	1.75	0.23
E2	11.20	39.10	112.97	10.02	35.31	6.37	1.22	6.90	0.65	2.53	0.37	1.16	0.12	0.99	0.11

Table S16. Concentrations of REEs in the sediment samples from the region of Otranto after analysis by ICP-MS. Values are expressed in mg/kg.

Sample Label	Y	La	Ce	Pr	Nd	Sm	Eu	Gd	Tb	Dy	Ho	Er	Tm	Yb	Lu
A2	13.52	24.85	35.33	4.80	17.96	3.80	1.02	4.37	0.54	2.69	0.48	1.38	0.18	1.18	0.16
D2	85.69	102.96	497.44	28.05	101.52	20.31	4.55	22.51	3.09	14.67	2.77	8.14	0.99	7.25	1.01
D3 acquatic	31.59	27.24	60.10	6.34	23.04	4.29	1.07	4.84	0.78	4.12	0.83	2.60	0.36	2.44	0.37
E1	15.72	24.74	58.84	6.15	24.07	4.46	0.99	4.63	0.66	2.90	0.55	1.99	0.21	1.86	0.20

Table S17. Concentrations of REEs in the rock samples from the region of Gargano after analysis by ICP-MS. Values are expressed in mg/kg.

Sample Label	Y	La	Ce	Pr	Nd	Sm	Eu	Gd	Tb	Dy	Ho	Er	Tm	Yb	Lu
B2	12.60	18.10	42.08	4.00	13.56	2.93	0.73	3.00	0.47	1.54	0.41	1.04	0.15	1.01	0.14
B3	3.00	1.45	1.62	0.44	1.69	0.42	0.13	0.44	0.08	0.45	0.09	0.26	0.04	0.24	0.03
D2	49.36	122.05	336.28	32.83	113.90	20.65	5.02	20.10	2.63	11.96	2.11	6.49	0.69	5.24	0.63
D3	17.30	10.95	14.80	2.44	9.53	2.28	0.62	2.75	0.45	2.49	0.45	1.21	0.14	0.86	0.12

Table S18. Concentrations of REEs in the rock samples from the region of Otranto after analysis by ICP-MS. Values are expressed in mg/kg.

Sample Label	Y	La	Ce	Pr	Nd	Sm	Eu	Gd	Tb	Dy	Ho	Er	Tm	Yb	Lu
A2	35.70	80.66	87.35	12.21	39.72	7.89	1.56	7.31	1.10	5.30	1.03	3.46	0.37	3.15	0.39
A4	0.35	1.04	2.08	0.15	0.50	0.11	0.09	0.11	0.01	0.05	0.01	0.03	0.00	0.03	0.00
C1	21.77	23.91	48.38	5.69	19.04	4.55	1.05	4.15	0.76	3.74	0.71	1.95	0.28	1.86	0.25
D2	43.76	36.04	26.02	6.08	22.99	5.39	1.41	5.95	1.19	6.47	1.44	3.93	0.52	4.01	0.53
E4	7.21	2.33	4.00	0.69	2.57	0.68	0.21	0.84	0.14	0.71	0.15	0.42	0.05	0.30	0.04

Table S19. Concentrations of REEs in the rock samples from the region of Spinazzola after analysis by ICP-MS. Values are expressed in mg/kg.

Sample Label	Y	La	Ce	Pr	Nd	Sm	Eu	Gd	Tb	Dy	Ho	Er	Tm	Yb	Lu
A2	14.82	20.48	26.09	4.39	15.84	2.67	0.53	3.06	0.42	2.76	0.47	1.67	0.19	1.60	0.18
A4	78.72	117.61	50.83	33.56	122.29	22.25	5.18	20.48	2.81	12.30	2.28	7.28	0.73	5.19	0.61
B2	18.03	83.81	321.67	21.19	71.04	12.55	2.63	12.11	1.33	4.66	0.70	2.28	0.26	2.30	0.26
B3	80.43	83.84	30.86	19.24	74.48	13.69	4.00	17.26	2.51	11.99	2.50	6.74	0.66	4.67	0.56
C1	37.55	95.40	526.37	34.91	123.56	24.58	5.88	23.53	2.92	11.69	2.30	6.55	0.68	5.01	0.56
D2	22.91	30.56	23.20	7.20	25.99	5.03	1.45	5.78	0.77	4.63	0.85	2.54	0.30	2.19	0.27
D3	67.39	94.80	23.01	21.82	88.17	16.88	4.16	18.28	2.48	11.12	2.15	5.62	0.59	3.12	0.48
E1	21.42	41.42	16.12	11.19	43.91	7.92	1.78	7.47	1.01	4.69	0.84	2.18	0.27	1.78	0.24
E4	87.50	25.99	24.17	6.14	28.01	6.37	2.26	10.85	2.32	14.18	3.05	7.91	0.91	4.30	0.67

Table S20. Concentrations of REEs in the biota samples from the region of Gargano after analysis by ICP-MS. Values are expressed in mg/kg.

Sample Label	Y	La	Ce	Pr	Nd	Sm	Eu	Gd	Tb	Dy	Ho	Er	Tm	Yb	Lu
A2	9.20	21.47	45.61	5.03	18.39	3.43	0.71	2.99	0.38	1.95	0.34	0.94	0.12	0.77	0.11
B3	3.43	8.91	14.80	2.09	7.68	1.43	0.32	1.20	0.16	0.81	0.14	0.39	0.05	0.32	0.05
D3	3.07	7.11	15.23	1.64	5.98	1.15	0.25	0.97	0.13	0.71	0.12	0.35	0.05	0.31	0.04
E2	1.35	3.47	6.71	0.84	3.09	0.57	0.13	0.49	0.06	0.33	0.06	0.15	0.02	0.13	0.02
E4	7.40	12.51	26.03	3.38	13.19	2.65	0.58	2.32	0.30	1.54	0.27	0.74	0.10	0.61	0.09

Table S21. Concentrations of REEs in the biota samples from the region of Otranto after analysis by ICP-MS. Values are expressed in mg/kg.

Sample Label	Y	La	Ce	Pr	Nd	Sm	Eu	Gd	Tb	Dy	Ho	Er	Tm	Yb	Lu
A2	1.18	5.89	12.11	0.99	3.27	0.60	0.12	0.47	0.06	0.31	0.05	0.15	0.02	0.13	0.02
A4	0.75	4.98	9.17	0.72	2.28	0.41	0.08	0.31	0.04	0.20	0.03	0.09	0.01	0.08	0.01
C1	4.94	10.47	18.83	2.08	7.45	1.42	0.30	1.28	0.17	0.96	0.17	0.50	0.07	0.42	0.06
D2	2.22	4.99	9.34	1.03	3.73	0.76	0.16	0.68	0.09	0.50	0.09	0.26	0.04	0.22	0.03
D3	8.31	13.96	28.67	3.02	11.12	2.21	0.48	2.05	0.29	1.58	0.30	0.85	0.11	0.72	0.10
D3 acquatic	3.40	6.26	14.53	1.34	4.97	0.98	0.21	0.92	0.12	0.67	0.12	0.34	0.05	0.30	0.04
E1	3.58	9.82	17.80	1.85	6.44	1.20	0.25	1.02	0.13	0.73	0.13	0.37	0.05	0.32	0.05
E2	0.55	2.56	4.78	0.42	1.37	0.25	0.05	0.20	0.03	0.13	0.02	0.06	0.01	0.06	0.01
E4	3.97	6.02	9.91	1.27	4.75	0.94	0.21	0.90	0.12	0.67	0.13	0.36	0.05	0.30	0.04

Table S22. Concentrations of REEs in the biota samples from the region of Spinazzola after analysis by ICP-MS. Values are expressed in mg/kg.

Sample Label	Y	La	Ce	Pr	Nd	Sm	Eu	Gd	Tb	Dy	Ho	Er	Tm	Yb	Lu
A2	1.94	41.75	42.61	10.03	39.72	7.17	1.69	6.47	0.76	3.61	0.62	1.61	0.19	1.18	0.17
A4	3.24	42.11	33.33	10.11	40.44	7.77	1.91	7.60	0.91	4.57	0.80	2.10	0.25	1.53	0.22
B2	20.88	129.12	56.80	32.91	126.50	22.25	5.23	18.92	2.23	10.25	1.56	3.55	0.38	2.16	0.29
B3	6.68	46.76	24.06	10.11	40.09	7.29	1.80	7.26	0.87	4.41	0.84	2.67	0.35	2.03	0.28
C1	3.57	176.52	152.06	46.78	175.86	32.54	7.57	26.68	3.42	17.43	2.86	6.80	0.76	4.60	0.62
D2	2.48	85.55	50.28	21.98	82.94	15.41	3.55	13.24	1.65	8.04	1.33	3.25	0.38	2.30	0.32
D3	21.13	1631.40	650.65	409.92	1647.51	299.46	71.87	260.52	29.40	132.90	19.80	44.52	4.98	28.95	3.92
E2	2.39	60.02	99.89	15.24	58.98	11.25	2.63	9.68	1.23	6.21	1.04	2.71	0.34	2.09	0.28
E4	7.42	75.48	60.67	17.95	71.12	13.32	3.27	12.58	1.52	7.49	1.26	3.27	0.41	2.45	0.34

Table S23. Concentrations of REEs in the water sample from the region of Otranto after analysis by ICP-MS. Values are expressed in μg/L.

Sample Label	Y	La	Ce	Pr	Nd	Sm	Eu	Gd	Tb	Dy	Ho	Er	Tm	Yb	Lu
D3	0.34	0.29	0.88	0.07	0.24	0.07	0.03	0.10	0.01	0.05	0.01	0.03	0.00	0.03	0.00

Table S24. Concentrations of REEs in the water samples from the region of Spinazzola after analysis by ICP-MS. Values are expressed in μg/L.

Sample Label	Y	La	Ce	Pr	Nd	Sm	Eu	Gd	Tb	Dy	Ho	Er	Tm	Yb	Lu
B3	21.52	52.70	60.69	14.23	44.42	9.58	2.07	10.34	1.01	3.46	0.65	1.91	0.19	1.11	0.15
E2	18.01	21.20	31.45	6.35	20.46	3.86	0.94	4.72	0.47	1.83	0.37	1.07	0.13	0.74	0.11

Supplementary materials 3

On this supplementary materials are presented the results of the statistical analysis concerning the comparison of the results between TXRF and ICP-MS, followed by the box plots. In addition, are presented the results of the correlation analysis of each REE between soil and biota samples of the same region, as well as the calculation of the bioconcentration factor of each REE between biota and soil samples of the same sampling point.

Table S25. Statistical analysis (t-test welch) between the REE concentrations after analysis by TXRF and ICP-MS. Only Y, La and Ce were taken into account since they were the only REEs detected in all samples by TXRF. Significance is considered when $p < 0.05$.

		GARGANO				OTRANTO				SPINAZZOLA		
Sample type		**Y**	**La**	**Ce**		**Y**	**La**	**Ce**		**Y**	**La**	**Ce**
SOIL		0.004	0.5	0.064		0.033	0.703	0.189		0.087	0.219	0.003
SEDIMENTS		0.18	0.694	0.1		0.284	0.783	0.597		-	-	-
ROCKS		0.181	0.327	0.375		0.212	0.181	0.182		0.013	0.655	0.21
BIOTA		0.717	0.083	0.249		0.656	0.06	0.051		0.877	0.193	0.097
WATER		-	-	-		0.121	0.101	0.278		0.056	0.257	0.196

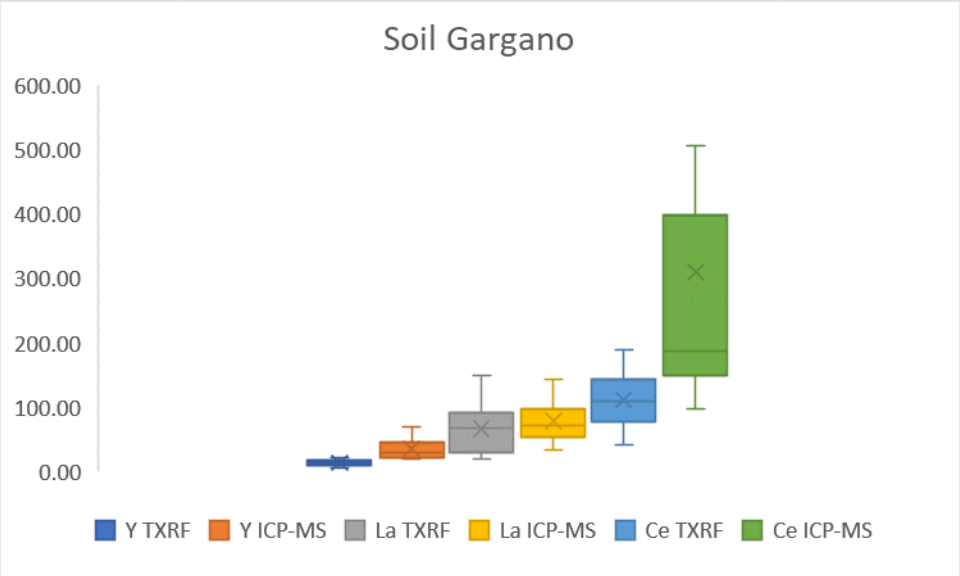

Figure S4. Comparison of concentrations (mg/kg) of Y, La and Ce between TXRF and ICP-MS in soil samples from Gargano region.

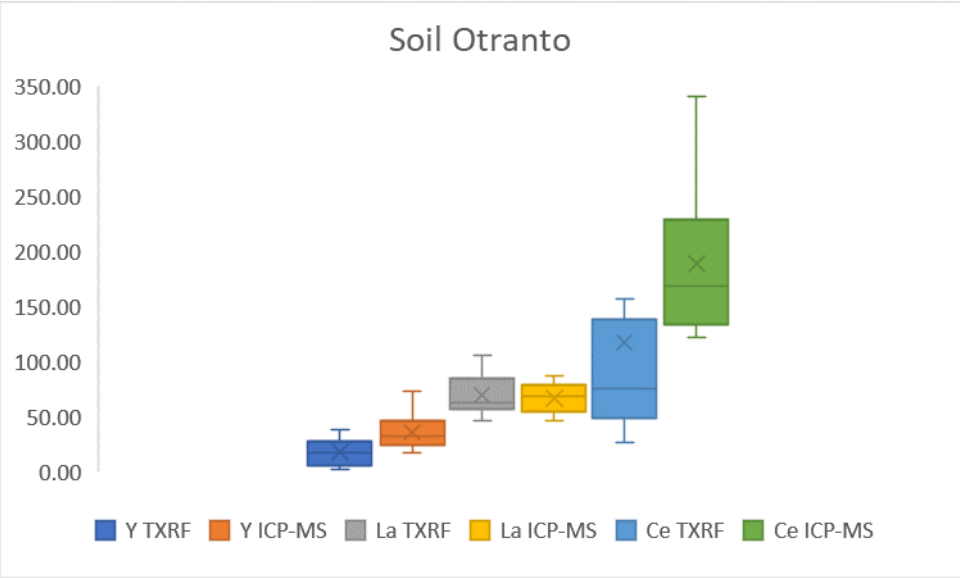

Figure S5. Comparison of concentrations (mg/kg) of Y, La and Ce between TXRF and ICP-MS in soil samples from Otranto region.

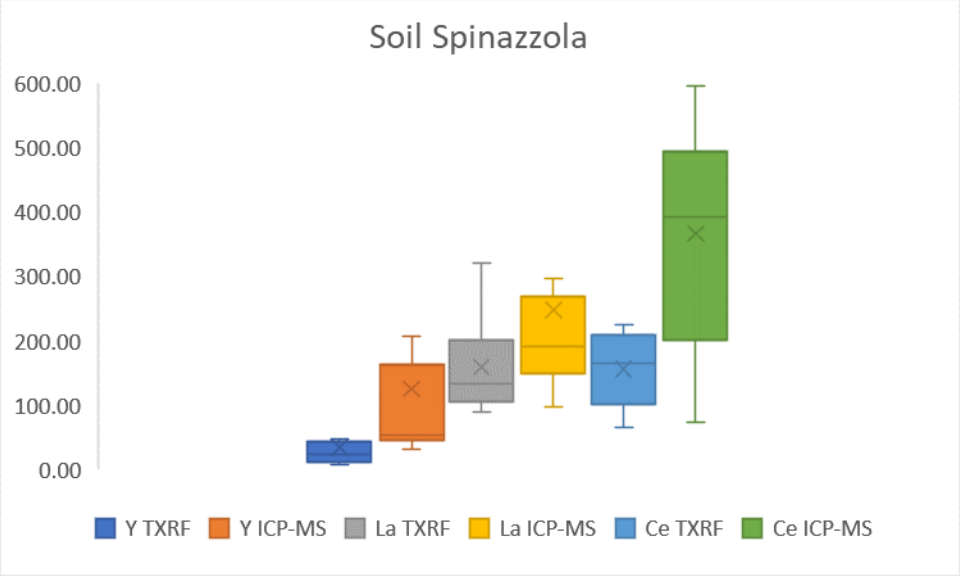

Figure S6. Comparison of concentrations (mg/kg) of Y, La and Ce between TXRF and ICP-MS in soil samples from Spinazzola region.

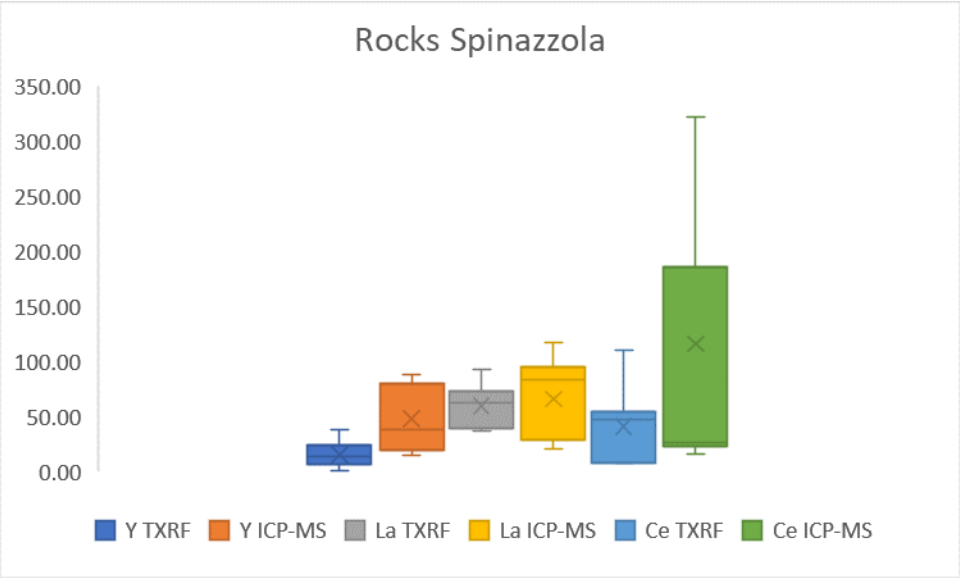

Figure S7. Comparison of concentrations (mg/kg) of Y, La and Ce between TXRF and ICP-MS in rock samples from Spinazzola region.

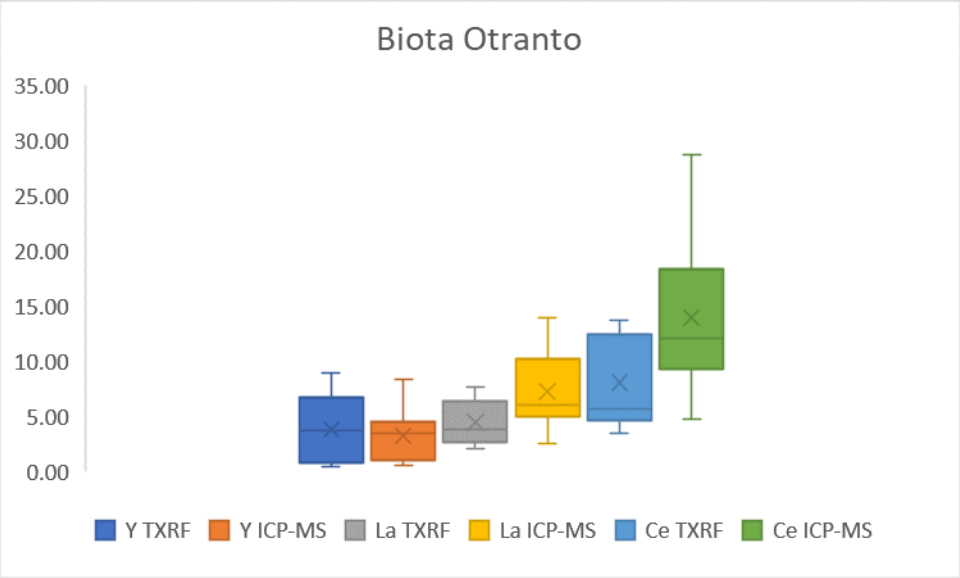

Figure S8. Comparison of concentrations (mg/kg) of Y, La and Ce between TXRF and ICP-MS in biota samples from Otranto region.

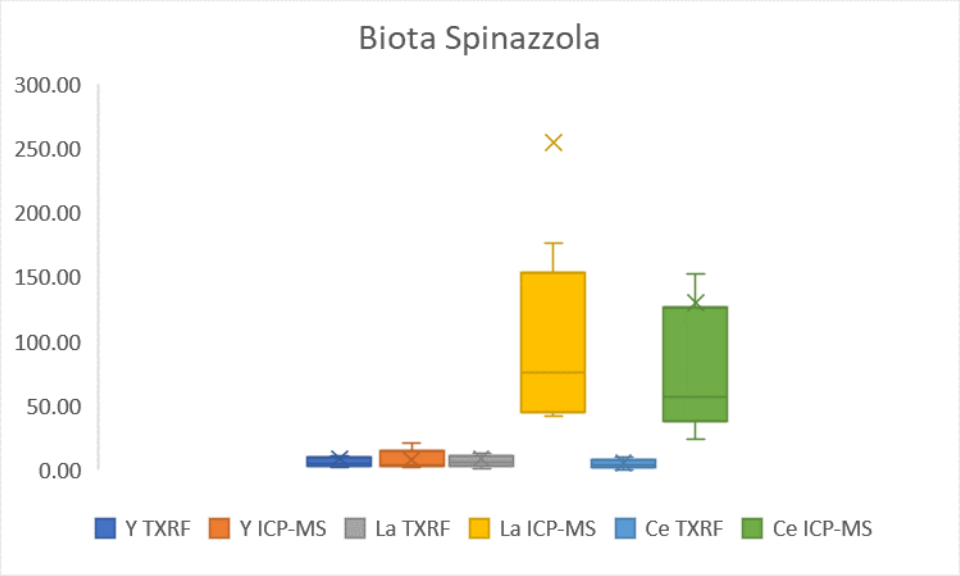

Figure S9. Comparison of concentrations (mg/kg) of Y, La and Ce between TXRF and ICP-MS in biota samples from Spinazzola region.

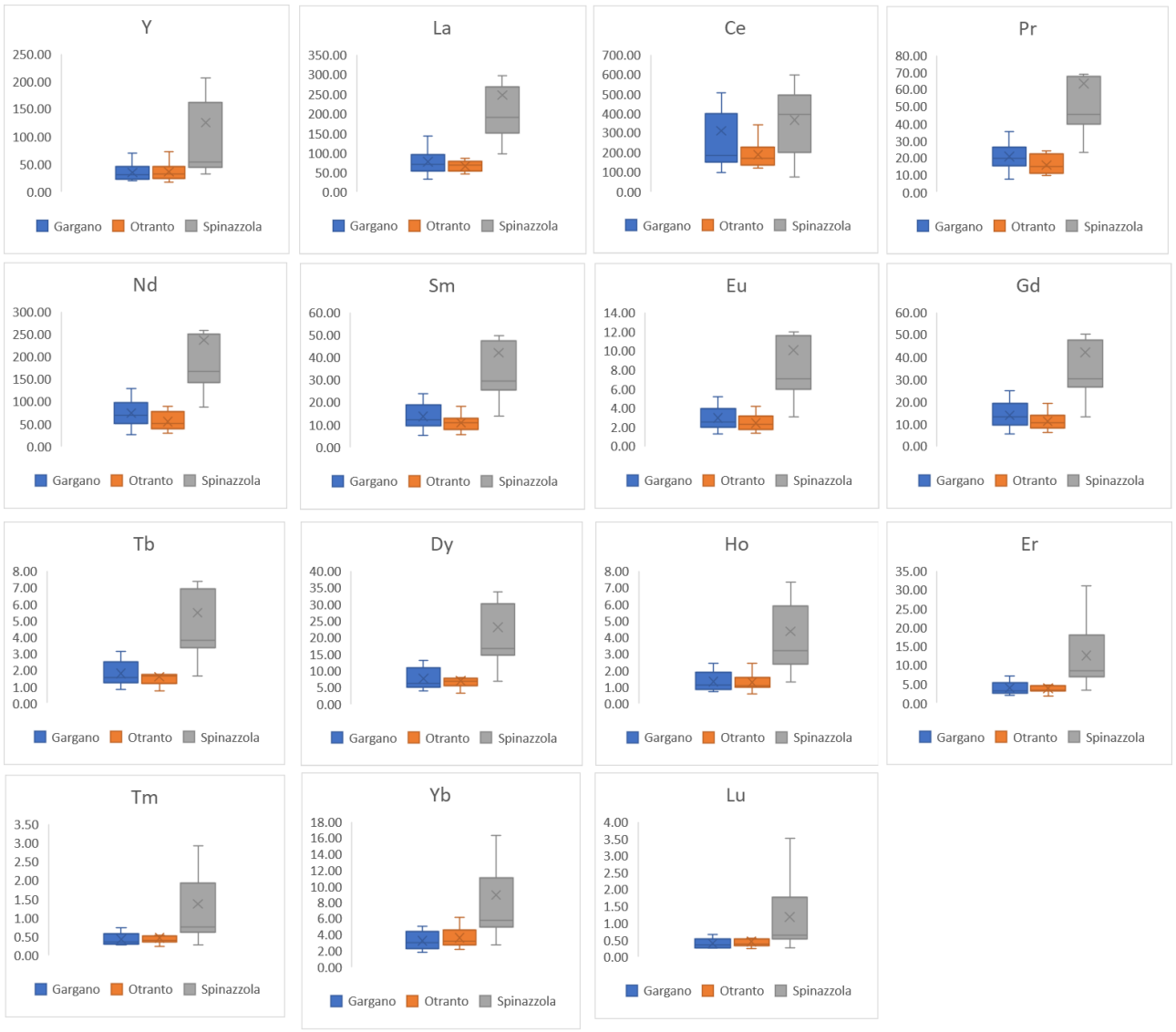

Figure S10. Comparison of the levels (mg/kg) of each REE between the soil samples of the three abandoned mining sites, after analysis by ICP-MS.

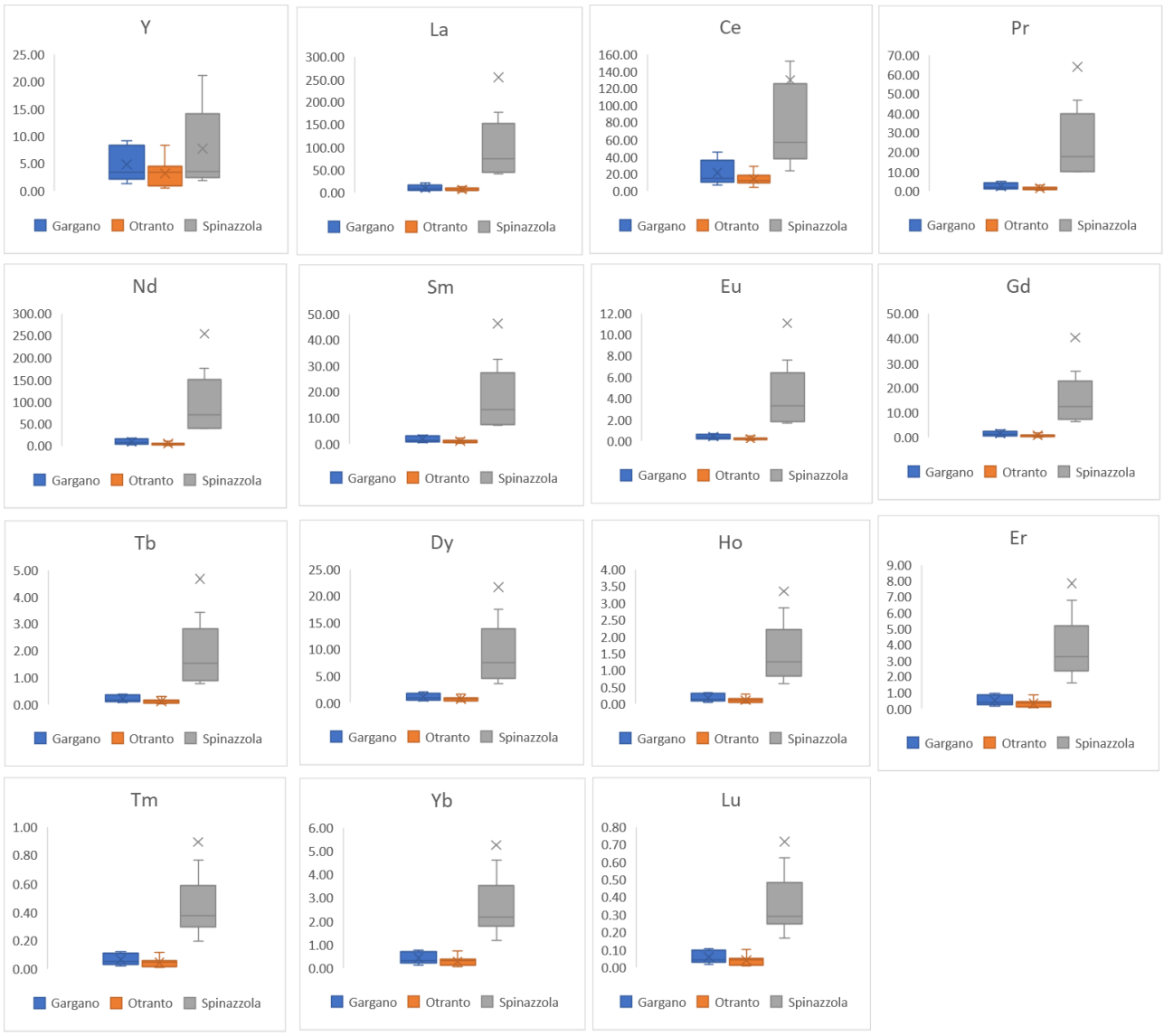

Figure S11. Comparison of the levels (mg/kg) of each REE between the biota samples of the three abandoned mining sites, after analysis by ICP-MS.

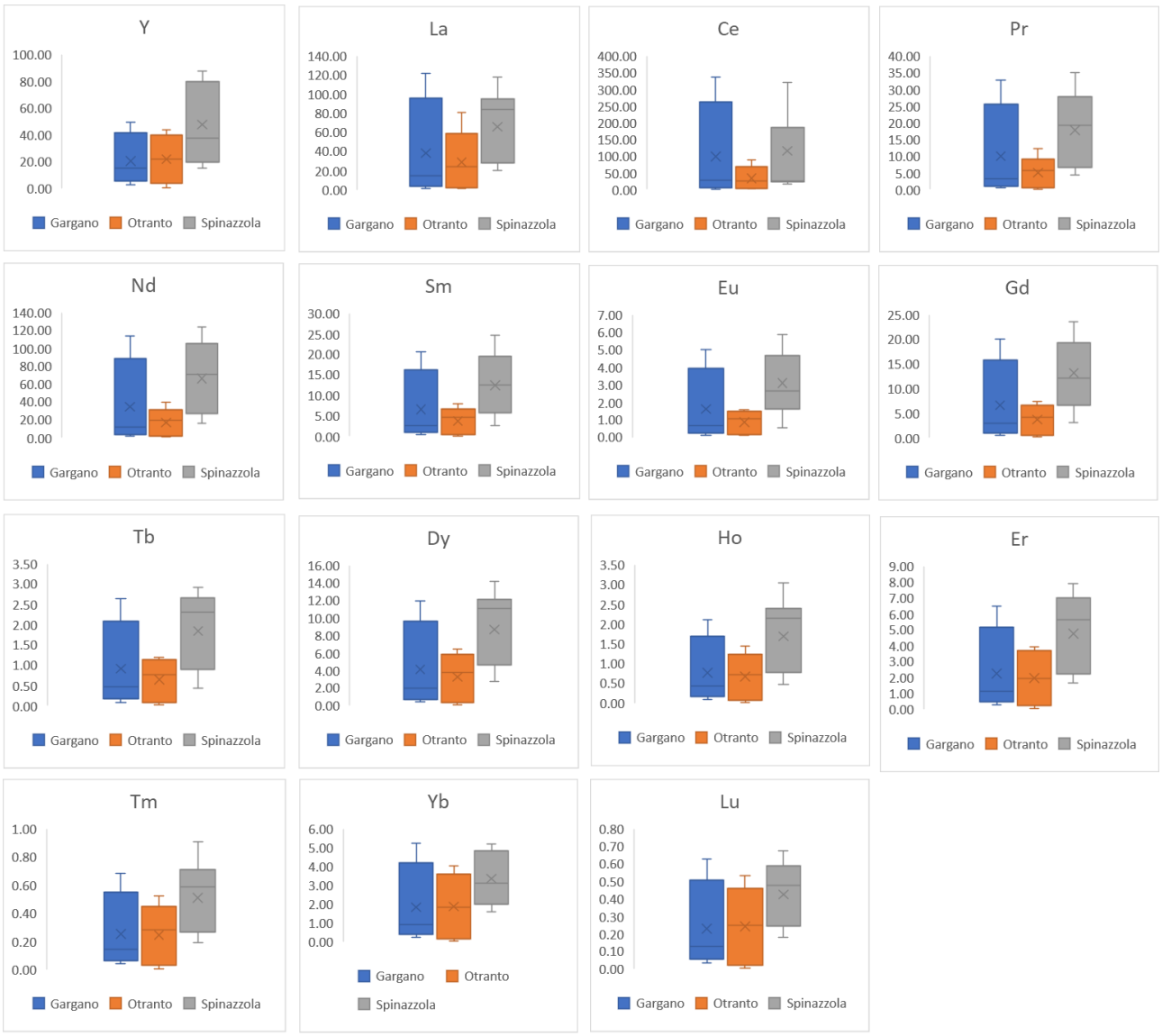

Figure S12. Comparison of the levels (mg/kg) of each REE between the rock samples of the three abandoned mining sites, after analysis by ICP-MS.

Table S26. Correlation analysis of each REE levels between soil and biota samples from each sampling area after analysis by ICP-MS. Correlation is considered when Pearson r > 0.7.

		Y	La	Ce	Pr	Nd	Sm	Eu	Gd	Tb	Dy	Ho	Er	Tm	Yb	Lu
Gargano	**Pearson r**	-0.760	0.240	-0.648	-0.746	-0.772	-0.793	-0.851	-0.714	-0.817	-0.841	-0.783	-0.877	-0.890	-0.834	-0.843
Otranto	**Pearson r**	0.834	0.331	0.754	0.521	0.560	0.713	0.703	0.757	0.812	0.761	0.745	0.789	0.798	0.662	0.781
Spinazzola	**Pearson r**	0.116	0.949	0.598	0.962	0.964	0.951	0.946	0.947	0.911	0.885	0.844	0.596	0.412	0.340	0.377

Table S27. Bioconcentration factors for each sampling point and each REE between biota and soil samples from the region of Gargano, after analysis by ICP-MS.

Sample Label	Y	La	Ce	Pr	Nd	Sm	Eu	Gd	Tb	Dy	Ho	Er	Tm	Yb	Lu
A2	30.5	25.3	24.5	25.7	26.7	28.3	27.9	22.7	24.9	31.7	30.0	29.2	33.6	25.4	31.5
B3	8.3	9.1	5.4	8.4	9.0	9.0	9.6	7.8	7.7	9.2	9.4	8.2	9.7	8.3	9.3
D3	9.2	7.5	5.3	7.0	7.5	8.1	7.8	7.0	7.2	9.3	9.3	7.9	10.6	8.9	10.6
E2	1.9	6.9	0.7	3.1	2.8	2.4	2.9	2.0	2.0	2.6	2.3	2.1	2.8	2.6	2.8
E4	31.5	21.5	17.0	22.2	25.0	26.3	29.8	23.4	23.5	30.8	31.5	26.8	31.1	26.3	30.5

Table S28. Bioconcentration factors for each sampling point and each REE between biota and soil samples from the region of Otranto, after analysis by ICP-MS. Results are given as %.

Sample Label	Y	La	Ce	Pr	Nd	Sm	Eu	Gd	Tb	Dy	Ho	Er	Tm	Yb	Lu
A2	3.7	8.7	6.2	7.0	6.6	5.4	5.6	4.9	3.9	4.1	3.3	3.4	3.7	2.7	3.4
A4	4.2	7.1	4.9	7.5	7.7	7.1	5.8	4.8	5.5	6.1	5.6	4.7	5.2	3.8	5.0
C1	15.1	19.7	15.5	18.3	18.5	18.0	17.0	15.3	14.2	17.7	16.8	14.9	16.2	12.6	15.5
D2	6.5	6.1	7.2	4.2	4.4	5.6	4.9	4.7	5.4	6.9	8.0	7.2	9.7	8.4	9.6
D3	11.5	16.1	8.4	12.5	12.5	12.1	11.6	10.7	10.1	12.7	12.3	11.9	12.5	11.8	11.6
E1	15.4	17.2	7.4	11.1	12.0	10.3	10.5	8.8	8.2	11.2	13.4	11.6	12.9	10.9	12.4
E2	2.1	5.5	3.2	3.9	3.5	3.0	2.9	2.4	2.1	2.4	2.2	2.0	2.5	1.9	2.5
E4	8.0	8.8	6.6	8.2	8.3	8.6	7.9	7.6	7.1	8.6	8.1	7.6	9.1	8.4	9.2

Table S29. Bioconcentration factors for each sampling point and each REE between biota and soil samples from the region of Spinazzola, after analysis by ICP-MS. Results are given as %.

Sample Label	Y	La	Ce	Pr	Nd	Sm	Eu	Gd	Tb	Dy	Ho	Er	Tm	Yb	Lu
A2	6.1	43.2	57.9	43.1	45.4	51.2	54.9	48.8	46.2	53.2	47.6	46.0	67.7	42.9	65.1
A4	5.2	21.4	7.1	24.9	28.4	32.3	34.0	27.9	29.0	35.1	35.7	32.1	41.2	35.6	40.6
B2	45.5	67.8	14.9	64.1	66.7	65.4	65.3	59.2	54.7	60.9	46.3	43.2	50.4	36.8	45.8
B3	1.3	15.8	6.0	14.7	15.5	15.6	15.0	14.5	11.8	13.1	11.4	8.6	8.3	7.6	8.0
C1	8.4	113.7	31.3	115.2	125.1	123.4	123.9	110.4	100.2	104.7	95.2	78.1	101.1	81.2	98.2
D2	5.5	64.1	24.5	57.8	58.3	59.6	58.1	48.2	46.5	50.8	47.9	42.1	52.1	44.2	51.9
D3	10.2	204.2	109.1	190.4	200.2	212.5	212.4	187.2	174.9	199.8	159.8	151.3	170.7	177.3	167.5
E2	1.6	23.2	29.3	22.7	23.8	22.7	22.9	20.6	18.2	21.5	19.2	19.0	21.3	22.5	18.0
E4	6.5	39.6	32.4	38.1	41.1	42.7	42.9	39.1	35.4	43.3	37.2	34.9	36.1	32.1	30.8

Chapter 5: Conclusions

5.1 Human toxicology

For examining the human toxicology of REEs, a literature review was elaborated at first place, gathering all the information concerning their toxicity on human health. According to this, Ce is the most studied REE; hair, blood and blood serum the most studied matrices; and cytotoxicity the field of toxicity with the most studies. The human exposure to REEs could occur via several ways, such as environmental exposure, through the food chain or due to lifestyle. REEs have been associated with human diseases like neura tube defects, anemia or endomyordical fibrosis. GBCAs could be accumulated in kidney or muscles causing renal failure and fibromyalgia. REEs have been shown to affect a number of metabolic pathways, like those of MPP-1, TIMP-1 and PDGF. REEs could activate metabolic pathways resulting to ROS production, DNA damage and apoptosis; however, they could be potential anticancer agents, since they are more cytotoxic on cancer compared to normal cells. REEs could be uptaken by cellular compartmnets, like mitochondria, and may be interfere to the regulation of calcium. The mining of REEs does not affect only the mining workers, but also residents near the mining areas. Focus should be given also other jobs, like workers in diesel or technological devices production.

Due to the implementation of REEs in diesel fuels as additives, concerns have increased about the potential exposure to them through the car exhausts. For that reason, urine and scalp hair samples were collected from car mechanics employed in two different types of workshops. The car mechanics in the workshops of Avellino are lacking the use of means of protection, while those of Como are using them properly.

Before determining the REE levels in the human samples, it was essential to validate the methods of preparation before procceding to the analysis with ICP-MS. We validated two different methods of preparation of the urines. Both methods showed adequate precision of repeatability and reproducibility, and REE recoveries for both methods were very close to 100%. Therefore, both tested methods of preparation are validated for analyzing REEs in urine samples, according to the method validation and the criteria of the guidelines.

After validating two different methods for preparing human urines, the focus was on the determination of REE levels in the human samples. The levels of some REEs together with creatinine and 1-OHP were significantly higher in he urines of Avellino workers, while no significant difference was found for REE levels in the hair samples between the two groups. These results indicate a quick excretion of REEs through urines and a non-long-term bioaccumulation, as well as a potential of REEs to be correlated with a high possibility of health issues and an occupational exposure to combustion products. Smoking might contribute to the bioaccumulation of La and Ce.

This study indicates that measures of safety of Avellino workers should be elaborated so that their exposure to REEs and other hazardous products is lessened. More researches about the occupational exposure to REEs should be elaborated so that we understand better the level of hazard that they can cause on human health during work-time. Although REE levels in the environment and food are currently present at low levels and do not possess a huge threat for human health, they should be considered as a potential future risk since REEs concentration is expected to increase along time.

5.2 Environmental toxicology

For determining the toxicity of REEs on the environmental level, several models were used in the lab (i.e. *R. subcapitata*, *V. faba*, *P. tricornutum*), preparing samples containing a specific concentration of REEs. Everytime samples for elaborating an ecotoxicity trial were prepared, the real concentration, with respect to the nominal concentration, was determine by ICP-MS.

Cerium, Gd, La and Nd were proved more toxic against three photosynthetic organisms in a more acidic environment. These results indicate a mitigation of the toxic effects of REEs due to the increase of the pH. La and Ce were proved to provoke adverse efetcs against R. subcapitata even at low concentrations, as well as against the sperm of *S. granularis*. In addition, REEs were toxic also against *P. tricornutum*.

In a general conclusion REEs have been found to be potentially hazardous for the environmental health. Several gaps into the knowledge still remain about REEs toxicity effects and their potential uptake by aquatic species including the transfer through the food web and potential mechanism of adaptation and detoxification. Furthermore, the risk threat due to REE presence could be increased in some areas of the marine environment, leading to a higher possibility of bioaccumulation and ecotoxicity of these elements.

5.3 Environmental chemistry

According to the literature review elaborated, several REEs could be used as catalysts on AOPs for a more efficient removal of toxic pollutant from wastewaters and other aquatic environmental solutions. Cerium is the most studied REE on this field followed by La. Focus should be given on the rest of the REEs since they have been little studied or not studied at all. In a few words, AOPs which include REE-combined catalysts and other parameters, should be chosen based on the nature of the contaminants and the acid-base properties of the wastewater to be treated.

REEs seem to be not only in traceable, but in levels ideal for a possible extraction in the future in all three abandoned mining sites in Puglia, especialy Spinazolla which contains the highest amount of these elements. Cerium is the most abundant REE in all sites. There is a correlation between REE levels of biota and soil samples, but these elements are not bioaccumulative.

There are two main disadvantages on TXRF compared to ICP-MS considering the determination of REEs in environmental samples; this makes TXRF a more ideal technique for analyzing the whole spectra of the REE content, while ICP-MS the ideal technique for determining their levels in the samples.

Since several previous studies have shown that REEs might consist a threat for human and environmental health, more investigations should be elaborated about their concentrations either near or further from mining sites.

References

Aashima, Pandey, S.K., Singh, S., Mehta, S.K., 2018. Biocompatible gadolinium oxide nanoparticles as efficient agent against pathogenic bacteria. J. Colloid Interface Sci. 529, 496–504. https://doi.org/10.1016/j.jcis.2018.06.030

Abdelnour, S.A., Abd El-Hack, M.E., Khafaga, A.F., Noreldin, A.E., Arif, M., Chaudhry, M.T., Losacco, C., Abdeen, A., Abdel-Daim, M.M., 2019. Impacts of rare earth elements on animal health and production: Highlights of cerium and lanthanum. Sci. Total Environ. 672, 1021–1032. https://doi.org/10.1016/j.scitotenv.2019.02.270

Acharya, B.K., Pathak, H., Mohana, S., Shouche, Y., Singh, V., Madamwar, D., 2011. Kinetic modelling and microbial community assessment of anaerobic biphasic fixed film bioreactor treating distillery spent wash. Water Res. 45, 4248–4259. https://doi.org/10.1016/j.watres.2011.05.048

Adams, F., Gijbels, R., Van Grieken, R., 1988. Inorganic Mass Spectrometry. John Wiley and Sons, New York

Adeel, M., Lee, J.Y., Zain, M., Rizwan, M., Nawab, A., Ahmad, M.A., Shafiq, M., Yi, H., Jilani, G., Javed, R., Horton, R., Rui, Y., Tsang, D.C.W., Xing, B., 2019. Cryptic footprints of rare earth elements on natural resources and living organisms. Environ. Int. 127, 785–800. https://doi.org/10.1016/j.envint.2019.03.022

Agathokleous, E., Kitao, M., Calabrese, E.J., 2020. Hormesis: Highly Generalizable and Beyond Laboratory. Trends Plant Sci. 25, 1076–1086. https://doi.org/10.1016/j.tplants.2020.05.006

Agathokleous, E., Kitao, M., Calabrese, E.J., 2019. Hormetic dose responses induced by lanthanum in plants. Environ. Pollut. 244, 332–341. https://doi.org/10.1016/j.envpol.2018.10.007

Agathokleous, E., Zhou, B., Geng, C., Xu, J., Saitanis, C.J., Feng, Z., Tack, F.M.G., Rinklebe, J., 2022. Mechanisms of cerium-induced stress in plants: A meta-analysis. Sci. Total Environ. 852, 158352. https://doi.org/10.1016/j.scitotenv.2022.158352

Aharchaou, I., Beaubien, C., Campbell, P.G.C., Fortin, C., 2020. Lanthanum and Cerium Toxicity to the Freshwater Green Alga *Chlorella fusca* : Applicability of the Biotic Ligand Model. Environ. Toxicol. Chem. 39, 996–1005. https://doi.org/10.1002/etc.4707

Ahmadi, S., Rahdar, A., Igwegbe, C.A., Mortazavi-Derazkola, S., Banach, A.M., Rahdar, S., Singh, A.K., Rodriguez-Couto, S., Kyzas, G.Z., 2020. Praseodymium-doped cadmium tungstate (CdWO4) nanoparticles for dye degradation with sonocatalytic process. Polyhedron 190, 114792. https://doi.org/10.1016/j.poly.2020.114792

Ahmed, A.S., Eldahshan, R.M., 2022. Occupational dermatoses: knowledge, attitudes and perceptions among motor vehicle repair workers. Int. J. Occup. Saf. Ergon. 28, 2112–2118. https://doi.org/10.1080/10803548.2021.1962640

Akhtar, M.J., Ahamed, M., Alhadlaq, H., 2020. Gadolinium Oxide Nanoparticles Induce Toxicity in Human Endothelial HUVECs via Lipid Peroxidation, Mitochondrial Dysfunction and Autophagy Modulation. Nanomaterials 10, 1675. https://doi.org/10.3390/nano10091675

Albarano, L., Guida, M., Tommasi, F., Lofrano, G., Padilla Suarez, E., Gjata, I., et al., 2022. Species sensitivity distribution of rare Earth elements: A full overview. Sci. Total Environ.

Albarano, L., Lofrano, G., Costantini, M., Zupo, V., Carraturo, F., Guida, M., Libralato, G., 2021. Comparison of in situ sediment remediation amendments: Risk perspectives from species sensitivity distribution. Environ. Pollut. 272, 115995. https://doi.org/10.1016/j.envpol.2020.115995

Albarano, L., Zupo, V., Caramiello, D., Toscanesi, M., Trifuoggi, M., Guida, M., Libralato, G., Costantini, M., 2021a. Sub-Chronic Effects of Slight PAH- and PCB-Contaminated Mesocosms in Paracentrotus lividus Lmk: A Multi-Endpoint Approach and De Novo Transcriptomic. Int. J. Mol. Sci. 22, 6674. https://doi.org/10.3390/ijms22136674

Albarano, L., Zupo, V., Guida, M., Libralato, G., Caramiello, D., Ruocco, N., Costantini, M., 2021b. PAHs and PCBs Affect Functionally Intercorrelated Genes in the Sea Urchin Paracentrotus lividus Embryos. Int. J. Mol. Sci. 22, 12498. https://doi.org/10.3390/ijms222212498

Aldenberg, T., Jaworska, J.S., 2000. Uncertainty of the Hazardous Concentration and Fraction Affected for Normal Species Sensitivity Distributions. Ecotoxicol. Environ. Saf. 46, 1–18. https://doi.org/10.1006/eesa.1999.1869

Aldenberg, T., Slob, J., 1993. Confidence limits for Hazardous Concentrations based on logistically distributed NOEC toxicity data. Ecotoxicol. Environ. Saf. 25, 48/63.

Alfonso Bosellini, Michele Morsilli, 1999. Long-Term Event Stratigraphy of the Apulia Platform Margin (Upper Jurassic To Eocene, Gargano, Southern Italy). SEPM J. Sediment. Res. Vol. 69 (1999),. https://doi.org/10.1306/D4268B4E-2B26-11D7-8648000102C1865D

Alimonti, A., Bocca, B., and Ruggieri, F., 2015. Reference method for the determination of chemical elements in human biological matrices: analytical performances and uncertainty of data. Rapporti ISTISAN 15/30. Roma: Istituto Superiore di Sanità. Available at: https://www.iss.it/documents/20126/45616/15_30_web.pdf/4f95e0d8-38eb-82cd-0ccc-3336d29cfac1?t=1581099105455

Allain, P., Berre, S., Premel-Cabic, A., Mauras, Y., and Delaporte, T., 1990. Concentrations of rare Earth elements in plasma and urine of healthy subjects determined by inductively coupled plasma mass spectrometry. Clin. Chem. 36, 2011–2012. https://doi.org/10.1093/clinchem/36.11.2011b

Almeida, A.C., Gomes, T., Langford, K., Thomas, K.V., Tollefsen, K.E., 2019. Oxidative stress potential of the herbicides bifenox and metribuzin in the microalgae Chlamydomonas reinhardtii. Aquat. Toxicol. 210, 117–128. https://doi.org/10.1016/j.aquatox.2019.02.021

Almeida, A.C., Gomes, T., Langford, K., Thomas, K.V., Tollefsen, K.E., 2017. Oxidative stress in the algae Chlamydomonas reinhardtii exposed to biocides. Aquat. Toxicol. 189, 50–59. https://doi.org/10.1016/j.aquatox.2017.05.014

Alpaslan, E., Yazici, H., Golshan, N.H., Ziemer, K.S., Webster, T.J., 2015. pH-Dependent Activity of Dextran-Coated Cerium Oxide Nanoparticles on Prohibiting Osteosarcoma Cell Proliferation. ACS Biomater. Sci. Eng. 1, 1096–1103. https://doi.org/10.1021/acsbiomaterials.5b00194

Ambaye, T.G., Vaccari, M., Castro, F.D., Prasad, S., Rtimi, S., 2020. Emerging technologies for the recovery of rare earth elements (REEs) from the end-of-life electronic wastes: a review on progress, challenges, and perspectives. Environ. Sci. Pollut. Res. 27, 36052–36074. https://doi.org/10.1007/s11356-020-09630-2

Amyot, M., Clayden, M.G., MacMillan, G.A., Perron, T., Arscott-Gauvin, A., 2017. Fate and Trophic Transfer of Rare Earth Elements in Temperate Lake Food Webs. Environ. Sci. Technol. 51, 6009–6017. https://doi.org/10.1021/acs.est.7b00739

Andreozzi, R., 1999. Advanced oxidation processes (AOP) for water purification and recovery. Catal. Today 53, 51–59. https://doi.org/10.1016/S0920-5861(99)00102-9

Antinori, S., Versaci, C., Fuhrberg, P., Panci, C., Caffa, B., Gholami, G.H., n.d. Seventeen live births after the use of an erbium—yytrium aluminium garnet laser in the treatment of male factor infertility.

Asante, K.A., Agusa, T., Biney, C.A., Agyekum, W.A., Bello, M., Otsuka, M., Itai, T., Takahashi, S., Tanabe, S., 2012. Multi-trace element levels and arsenic speciation in urine of e-waste recycling workers from Agbogbloshie, Accra in Ghana. Sci. Total Environ. 424, 63–73. https://doi.org/10.1016/j.scitotenv.2012.02.072

Assila, O., Barros, Ó., Fonseca, A.M.F., Parpot, P., Soares, O.S.G.P., Pereira, M.F.R., Zerrouq, F., Kherbeche, A., Rombi, E., Tavares, T., Neves, I.C., 2023. Degradation of pollutants in water by Fenton-like oxidation over LaFe-catalysts: Optimization by experimental design. Microporous Mesoporous Mater. 349, 112422. https://doi.org/10.1016/j.micromeso.2022.112422

Assumpção, M.H.M.T., Moraes, A., De Souza, R.F.B., Reis, R.M., Rocha, R.S., Gaubeur, I., Calegaro, M.L., Hammer, P., Lanza, M.R.V., Santos, M.C., 2013. Degradation of dipyrone via advanced oxidation processes using a cerium nanostructured electrocatalyst material. Appl. Catal. Gen. 462–463, 256–261. https://doi.org/10.1016/j.apcata.2013.04.008

Atalay, S., Ersöz, G., 2016. Novel Catalysts in Advanced Oxidation of Organic Pollutants, SpringerBriefs in Molecular Science. Springer International Publishing, Cham. https://doi.org/10.1007/978-3-319-28950-2

Atibu, E.K., Devarajan, N., Laffite, A., Giuliani, G., Salumu, J.A., Muteb, R.C., Mulaji, C.K., Otamonga, J.-P., Elongo, V., Mpiana, P.T., Poté, J., 2016. Assessment of trace metal and rare earth elements contamination in rivers around abandoned and active mine areas. The case of Lubumbashi River and Tshamilemba Canal, Katanga, Democratic Republic of the Congo. Geochemistry 76, 353–362. https://doi.org/10.1016/j.chemer.2016.08.004

Azizi, M., Faz, A., Zornoza, R., Martínez-Martínez, S., Shahrokh, V., Acosta, J.A., 2022. Environmental pollution and depth distribution of metal(loid)s and rare earth elements in mine tailing. J. Environ. Chem. Eng. 10, 107526. https://doi.org/10.1016/j.jece.2022.107526

Badea, M., Luzardo, O.P., González-Antuña, A., Zumbado, M., Rogozea, L., Floroian, L., Alexandrescu, D., Moga, M., Gaman, L., Radoi, M., Boada, L.D., Henríquez-Hernández, L.A., 2018. Body burden of toxic metals and rare earth elements in non-smokers, cigarette smokers and electronic cigarette users. Environ. Res. 166, 269–275. https://doi.org/10.1016/j.envres.2018.06.007

Bai, Y., Long, C., Hu, G., Zhou, D., Gao, X., Chen, Z., Wang, T., Yu, S., Han, Y., Yan, L., 2019. Association of blood chromium and rare earth elements with the risk of DNA damage in chromate exposed population. Environ. Toxicol. Pharmacol. 72, 103237. https://doi.org/10.1016/j.etap.2019.103237

Baird R.B., Eaton, A.D., Rice, E.W. (Ed.), 2017. Standard methods for the examination of water and wastewater (23rd edition), American Water Works Association

Balali-Mood, M., Naseri, K., Tahergorabi, Z., Khazdair, M.R., Sadeghi, M., 2021. Toxic Mechanisms of Five Heavy Metals: Mercury, Lead, Chromium, Cadmium, and Arsenic. Front. Pharmacol. 12, 643972. https://doi.org/10.3389/fphar.2021.643972

Balaram, V., 2019. Rare earth elements: A review of applications, occurrence, exploration, analysis, recycling, and environmental impact. Geosci. Front. 10, 1285–1303. https://doi.org/10.1016/j.gsf.2018.12.005

Bárdossy, G., 1982. Karst bauxites. Bauxite deposits on carbonate rocks. Elsevier, Amsterdam.

Barry, M.J., Meehan, B.J., 2000. The acute and chronic toxicity of lanthanum to Daphnia carinata. Chemosphere 41, 1669–1674. https://doi.org/10.1016/S0045-6535(00)00091-6

Bartels, H., Böhmer, M., Heierli, C. (1972). Serum creatinine determination without protein precipitation. Clin Chim Acta. 37, 193–197. httpss://doi.org/10.1016/0009-8981(72)90432-9

Batista, B.L., Rodrigues, J.L., Tormen, L., Curtius, A.J., Barbosa Jr, F., 2009. Reference concentrations for trace elements in urine for the Brazilian population based on q-ICP-MS with a simple dilute-and-shoot procedure. J. Braz. Chem. Soc. 20, 1406–1413. https://doi.org/10.1590/S0103-50532009000800004

Becker, J.S., 2008. Inorganic mass spectrometry: Principles and applications. Wiley Interscience, malden, Mass

Been, E., Lee, W.-S., Hwang, H.Y., Cui, Y., Zaanen, J., Devereaux, T., Moritz, B., Jia, C., 2021. Electronic Structure Trends Across the Rare-Earth Series in Superconducting Infinite-Layer Nickelates. Phys. Rev. X 11, 011050. https://doi.org/10.1103/PhysRevX.11.011050

Bellin, M.-F., Van Der Molen, A.J., 2008. Extracellular gadolinium-based contrast media: An overview. Eur. J. Radiol. 66, 160–167. https://doi.org/10.1016/j.ejrad.2008.01.023

Benedetto, A., Bocca, C., Brizio, P., Cannito, S., Abete, M.C., Squadrone, S., 2018. Effects of the rare elements lanthanum and cerium on the growth of colorectal and hepatic cancer cell lines. Toxicol. In Vitro 46, 9–18. https://doi.org/10.1016/j.tiv.2017.09.024

Beres, S.A., Bruckner, P.H., Denoyer, E.R., 1994. Performance evaluation of a cyclonic spray chamber for ICP-MS. Atomic Spectroscopy 15(2), 96–99

Bergsten-Torralba, L.R., Magalhães, D.P., Giese, E.C., Nascimento, C.R.S., Pinho, J.V.A., Buss, D.F., 2020. Toxicity of three rare earth elements, and their combinations to algae, microcrustaceans, and fungi. Ecotoxicol. Environ. Saf. 201, 110795. https://doi.org/10.1016/j.ecoenv.2020.110795

Bettinelli, M., Spezia, S., Terni, C., Ronchi, A., Balducci, C., Minoia, C., 2002. Determination of rare earth elements in urine by electrothermal vaporization inductively coupled plasma mass spectrometry. Rapid Commun. Mass Spectrom. 16, 579–584. https://doi.org/10.1002/rcm.609

Bhagavathula, N., Dame, M.K., DaSilva, M., Jenkins, W., Aslam, M.N., Perone, P., Varani, J., 2010. Fibroblast Response to Gadolinium: Role for Platelet-Derived Growth Factor Receptor. Invest. Radiol. 45, 769–777. https://doi.org/10.1097/RLI.0b013e3181e943d2

Bhagavathula, N., DaSilva, M., Aslam, M.N., Dame, M.K., Warner, R.L., Xu, Y., Fisher, G.J., Johnson, K.J., Swartz, R., Varani, J., 2009. Regulation of Collagen Turnover in Human Skin Fibroblasts Exposed to a Gadolinium-Based Contrast Agent: Invest. Radiol. 44, 433–439. https://doi.org/10.1097/RLI.0b013e3181a4d7e9

Bilal Tahir, M., Sagir, M., 2019. Carbon nanodots and rare metals (RM = La, Gd, Er) doped tungsten oxide nanostructures for photocatalytic dyes degradation and hydrogen production. Sep. Purif. Technol. 209, 94–102. https://doi.org/10.1016/j.seppur.2018.07.029

Binnemans, K., Jones, P.T., 2015. Rare Earths and the Balance Problem. J. Sustain. Metall. 1, 29–38. https://doi.org/10.1007/s40831-014-0005-1

Bladen, C.L., Tzu- Yin, L., Fisher, J., Tipper, J.L., 2013. *In vitro* analysis of the cytotoxic and anti-inflammatory effects of antioxidant compounds used as additives in ultra high- molecular weight polyethylene in total joint replacement components. J. Biomed. Mater. Res. B Appl. Biomater. 101B, 407–413. https://doi.org/10.1002/jbm.b.32798

Blaise, C., Gagné, F., Harwood, M., Quinn, B., Hanana, H., 2018. Ecotoxicity responses of the freshwater cnidarian Hydra attenuata to 11 rare earth elements. Ecotoxicol. Environ. Saf. 163, 486–491. https://doi.org/10.1016/j.ecoenv.2018.07.033

Blinova, I., Lukjanova, A., Muna, M., Vija, H., Kahru, A., 2018. Evaluation of the potential hazard of lanthanides to freshwater microcrustaceans. Sci. Total Environ. 642, 1100–1107. https://doi.org/10.1016/j.scitotenv.2018.06.155

Blinova, I., Muna, M., Heinlaan, M., Lukjanova, A., Kahru, A., 2020. Potential Hazard of Lanthanides and Lanthanide-Based Nanoparticles to Aquatic Ecosystems: Data Gaps, Challenges and Future Research Needs Derived from Bibliometric Analysis. Nanomaterials 10, 328. https://doi.org/10.3390/nano10020328

Bocca, B., Ruggieri, F., Pino, A., Rovira, J., Calamandrei, G., Martínez, M.Á., Domingo, J.L., Alimonti, A., Schuhmacher, M., 2019. Human biomonitoring to evaluate exposure to toxic and essential trace elements during pregnancy. Part A. concentrations in maternal blood, urine and cord blood. Environ. Res. 177, 108599. https://doi.org/10.1016/j.envres.2019.108599

Böhlandt, A., Schierl, R., Diemer, J., Koch, C., Bolte, G., Kiranoglu, M., Fromme, H., Nowak, D., 2012. High concentrations of cadmium, cerium and lanthanum in indoor air due to environmental tobacco smoke. Sci. Total Environ. 414, 738–741. https://doi.org/10.1016/j.scitotenv.2011.11.017

Bokare, A.D., Choi, W., 2014. Review of iron-free Fenton-like systems for activating H2O2 in advanced oxidation processes. J. Hazard. Mater. 275, 121–135. https://doi.org/10.1016/j.jhazmat.2014.04.054

Bölükbaşı, S.C., Al-sagan, A.A., Ürüşan, H., Erhan, M.K., Durmuş, O., Kurt, N., 2016. Effects of cerium oxide supplementation to laying hen diets on performance, egg quality, some antioxidant enzymes in serum and lipid oxidation in egg yolk. J. Anim. Physiol. Anim. Nutr. 100, 686–693. https://doi.org/10.1111/jpn.12429

Bosellini, A., Parente, M., 1994. The Apulia Platform margin in the Salento Peninsula (southern Italy). Giornale di Geologia 56, 167–177.

Bott, T.L., Jackson, J.K., McTammany, M.E., Newbold, J.D., Rier, S.T., Sweeney, B.W., Battle, J.M., 2012. Abandoned coal mine drainage and its remediation: impacts on stream ecosystem structure and function. Ecol. Appl. 22, 2144–2163. https://doi.org/10.1890/11-1735.1

Brouziotis, A.A., Giarra, A., Libralato, G., Pagano, G., Guida, M., Trifuoggi, M., 2022a. Toxicity of rare earth elements: An overview on human health impact. Front. Environ. Sci. 10, 948041. https://doi.org/10.3389/fenvs.2022.948041

Brouziotis, A.A., Giarra, A., Marano, A., Di Nunzio, A., Lombardo, F., Guida, M., Libralato, G., Trifuoggi, M., 2022b. Comparative study of two methods for rare earth elements analysis in human urine samples using inductively coupled plasma-mass spectrometry. Front. Environ. Sci. 10, 942441. https://doi.org/10.3389/fenvs.2022.942441

Brown, C.J., Chenery, S.R.N., Smith, B., Mason, C., Tomkins, A., Roberts, G.J., Sserunjogi, L., Tiberindwa, J.V., 2004. Environmental influences on the trace element content of teeth—implications for disease and nutritional status. Arch. Oral Biol. 49, 705–717. https://doi.org/10.1016/j.archoralbio.2004.04.008

Brown, P.H., Rathjen, A.H., Graham, R.D., Tribe, D.E., 1990. Chapter 92 Rare earth elements in biological systems, in: Handbook on the Physics and Chemistry of Rare Earths. Elsevier, pp. 423–452. https://doi.org/10.1016/S0168-1273(05)80135-7

Burmaster, D.E., Hull, D.A., 1997. Using lognormal distributions and lognormal probability plots in probabilistic risk assessments. Hum. Ecol. Risk Assess. Int. J. 3, 235–255. https://doi.org/10.1080/10807039709383683

Cabrita, M.T., Gameiro, C., Utkin, A.B., Duarte, B., Caçador, I., Cartaxana, P., 2016. Photosynthetic pigment laser-induced fluorescence indicators for the detection of changes associated with trace element stress in the diatom model species Phaeodactylum tricornutum. Environ. Monit. Assess. 188, 285. https://doi.org/10.1007/s10661-016-5293-4

Cabrita, M.T., Raimundo, J., Pereira, P., Vale, C., 2014. Immobilised Phaeodactylum tricornutum as biomonitor of trace element availability in the water column during dredging. Environ. Sci. Pollut. Res. 21, 3572–3581. https://doi.org/10.1007/s11356-013-2362-x

Calabrese, E., 2016. The Emergence of the Dose–Response Concept in Biology and Medicine. Int. J. Mol. Sci. 17, 2034. https://doi.org/10.3390/ijms17122034

Calabrese, E.J., Dhawan, G., Kapoor, R., Agathokleous, E., Calabrese, V., 2022. Hormesis: wound healing and fibroblasts. Pharmacol. Res. 184, 106449. https://doi.org/10.1016/j.phrs.2022.106449

Cao, R., Huang, H., Tian, N., Zhang, Y., Guo, Y., Zhang, T., 2015. Novel Y doped Bi2WO6 photocatalyst: Hydrothermal fabrication, characterization and enhanced visible-light-driven photocatalytic activity for Rhodamine B degradation and photocurrent generation. Mater. Charact. 101, 166–172. https://doi.org/10.1016/j.matchar.2015.01.016

Cardoso, C.E.D., Almeida, J.C., Lopes, C.B., Trindade, T., Vale, C., Pereira, E., 2019. Recovery of Rare Earth Elements by Carbon-Based Nanomaterials—A Review. Nanomaterials 9, 814. https://doi.org/10.3390/nano9060814

Carpenter, D., Boutin, C., Allison, J.E., Parsons, J.L., Ellis, D.M., 2015. Uptake and Effects of Six Rare Earth Elements (REEs) on Selected Native and Crop Species Growing in Contaminated Soils. PLOS ONE 10, e0129936. https://doi.org/10.1371/journal.pone.0129936

Carr, D., Brown, J., Bydder, G., Steiner, R., Weinmann, H., Speck, U., Hall, A., Young, I., 1984. Gadolinium-DTPA as a contrast agent in MRI: initial clinical experience in 20 patients. Am. J. Roentgenol. 143, 215–224. https://doi.org/10.2214/ajr.143.2.215

Cassee, F.R., van Balen, E.C., Singh, C., Green, D., Muijser, H., Weinstein, J., Dreher, K., 2011. Exposure, Health and Ecological Effects Review of Engineered Nanoscale Cerium and Cerium Oxide

Associated with its Use as a Fuel Additive. Crit. Rev. Toxicol. 41, 213–229. https://doi.org/10.3109/10408444.2010.529105

Cataldo, D.A., Wildung, R.E., 1978. Soil and plant factors influencing the accumulation of heavy metals by plants. Environ. Health Perspect.

Cedergreen, N., Streibig, J.C., Kudsk, P., Mathiassen, S.K., Duke, S.O., 2007. The Occurrence of Hormesis in Plants and Algae. Dose-Response 5, dose-response.0. https://doi.org/10.2203/dose-response.06-008.Cedergreen

Celardo, I., De Nicola, M., Mandoli, C., Pedersen, J.Z., Traversa, E., Ghibelli, L., 2011a. Ce^{3+} Ions Determine Redox-Dependent Anti-apoptotic Effect of Cerium Oxide Nanoparticles. ACS Nano 5, 4537–4549. https://doi.org/10.1021/nn200126a

Celardo, I., Pedersen, J.Z., Traversa, E., Ghibelli, L., 2011b. Pharmacological potential of cerium oxide nanoparticles. Nanoscale 3, 1411. https://doi.org/10.1039/c0nr00875c

Chahal, S., Rani, N., Kumar, A., Kumar, P., 2020. Electronic structure and photocatalytic activity of samarium doped cerium oxide nanoparticles for hazardous rose bengal dye degradation. Vacuum 172, 109075. https://doi.org/10.1016/j.vacuum.2019.109075

Chan, S.H.S., Yeong Wu, T., Juan, J.C., Teh, C.Y., 2011. Recent developments of metal oxide semiconductors as photocatalysts in advanced oxidation processes (AOPs) for treatment of dye waste-water. J. Chem. Technol. Biotechnol. 86, 1130–1158. https://doi.org/10.1002/jctb.2636

Charalampides, G., Vatalis, K.I., Apostoplos, B., Ploutarch-Nikolas, B., 2015. Rare Earth Elements: Industrial Applications and Economic Dependency of Europe. Procedia Econ. Finance 24, 126–135. https://doi.org/10.1016/S2212-5671(15)00630-9

Chen, H., Chen, Zhibiao, Chen, Zhiqiang, Ou, X., Chen, J., 2020. Calculation of Toxicity Coefficient of Potential Ecological Risk Assessment of Rare Earth Elements. Bull. Environ. Contam. Toxicol. 104, 582–587. https://doi.org/10.1007/s00128-020-02840-x

Chen, J., Xiao, H., Qi, T., Chen, D., Long, H., Liu, S., 2015. Rare earths exposure and male infertility: the injury mechanism study of rare earths on male mice and human sperm. Environ. Sci. Pollut. Res. 22, 2076–2086. https://doi.org/10.1007/s11356-014-3499-y

Chen, X., Zhang, M., Qin, H., Zhou, J., Shen, Q., Wang, K., Chen, W., Liu, M., Li, N., 2022. Synergy effect between adsorption and heterogeneous photo-Fenton-like catalysis on LaFeO3/lignin-biochar composites for high efficiency degradation of ofloxacin under visible light. Sep. Purif. Technol. 280, 119751. https://doi.org/10.1016/j.seppur.2021.119751

Cheng, J., Qiu, H., Chang, Z., Jiang, Z., Yin, W., 2016. The effect of cadmium on the growth and antioxidant response for freshwater algae Chlorella vulgaris. SpringerPlus 5, 1290. https://doi.org/10.1186/s40064-016-2963-1

Chiarelli, R., Roccheri, M.C., 2014. Marine Invertebrates as Bioindicators of Heavy Metal Pollution. Open J. Met. 04, 93–106. https://doi.org/10.4236/ojmetal.2014.44011

Chien, C.-C., Wang, H.-Y., Wang, J.-J., Kan, W.-C., Chien, T.-W., Lin, C.-Y., Su, S.-B., 2011. Risk of Acute Kidney Injury after Exposure to Gadolinium-Based Contrast in Patients with Renal Impairment. Ren. Fail. 33, 758–764. https://doi.org/10.3109/0886022X.2011.599911

Chigurupati, S., Mughal, M.R., Okun, E., Das, S., Kumar, A., McCaffery, M., Seal, S., Mattson, M.P., 2013. Effects of cerium oxide nanoparticles on the growth of keratinocytes, fibroblasts and vascular endothelial cells in cutaneous wound healing. Biomaterials 34, 2194–2201. https://doi.org/10.1016/j.biomaterials.2012.11.061

Choe, K.-Y., Gajek, R., 2016. Determination of trace elements in human urine by ICP-MS using sodium chloride as a matrix-matching component in calibration. Anal. Methods 8, 6754–6763. https://doi.org/10.1039/C6AY01877G

Chong, M.N., Jin, B., Chow, C.W.K., Saint, C., 2010. Recent developments in photocatalytic water treatment technology: A review. Water Res. 44, 2997–3027. https://doi.org/10.1016/j.watres.2010.02.039

Chong, S., Zhang, G., Zhang, N., Liu, Y., Zhu, J., Huang, T., Fang, S., 2016. Preparation of FeCeO by ultrasonic impregnation method for heterogeneous Fenton degradation of diclofenac. Ultrason. Sonochem. 32, 231–240. https://doi.org/10.1016/j.ultsonch.2016.03.019

Cieślik, I., Płocińska, M., Płociński, T., Zdunek, J., Woźniak, M.J., Bil, M., Hirano, S., 2019. Influence of polymeric precursors on the viability of human cells of yttrium aluminum borates nanoparticles doped with ytterbium ions. Appl. Surf. Sci. 488, 874–886. https://doi.org/10.1016/j.apsusc.2019.05.001

Cirtiu, C.M., Valcke, M., Gagné, M., Bourgault, M.-H., Narame, C., Gadio, S., Poulin, P., Ayotte, P., 2022. Biological monitoring of exposure to rare earth elements and selected metals in the Inuit population of Nunavik, Canada. Chemosphere 289, 133142. https://doi.org/10.1016/j.chemosphere.2021.133142

Colon, J., Hsieh, N., Ferguson, A., Kupelian, P., Seal, S., Jenkins, D.W., Baker, C.H., 2010. Cerium oxide nanoparticles protect gastrointestinal epithelium from radiation-induced damage by reduction of reactive oxygen species and upregulation of superoxide dismutase 2. Nanomedicine Nanotechnol. Biol. Med. 6, 698–705. https://doi.org/10.1016/j.nano.2010.01.010

Conesa, JoséC., 1995. Computer modeling of surfaces and defects on cerium dioxide. Surf. Sci. 339, 337–352. https://doi.org/10.1016/0039-6028(95)00595-1

Corma, A., Atienzar, P., García, H., Chane-Ching, J.-Y., 2004. Hierarchically mesostructured doped CeO2 with potential for solar-cell use. Nat. Mater. 3, 394–397. https://doi.org/10.1038/nmat1129

Cravotta, C.A., 2008. Dissolved metals and associated constituents in abandoned coal-mine discharges, Pennsylvania, USA. Part 1: Constituent quantities and correlations. Appl. Geochem. 23, 166–202. https://doi.org/10.1016/j.apgeochem.2007.10.011

Cui, J., Zhang, Z., Bai, W., Zhang, L., He, X., Ma, Y., Liu, Y., Chai, Z., 2012. Effects of rare earth elements La and Yb on the morphological and functional development of zebrafish embryos. J. Environ. Sci. 24, 209–213. https://doi.org/10.1016/S1001-0742(11)60755-9

Cui, Y., Zhu, Y.-G., Zhai, R., Huang, Y., Qiu, Y., Liang, J., 2005. Exposure to metal mixtures and human health impacts in a contaminated area in Nanning, China. Environ. Int. 31, 784–790. https://doi.org/10.1016/j.envint.2005.05.025

Cymes, B.A., Almquist, C.B., Krekeler, M.P.S., 2020. Europium-doped cryptomelane: Multi-pathway synthesis, characterization, and evaluation for the gas phase catalytic oxidation of ethanol. Appl. Catal. Gen. 589, 117310. https://doi.org/10.1016/j.apcata.2019.117310

d'Aquino, L., De Pinto, M.C., Nardi, L., Morgana, M., Tommasi, F., 2009. Effect of some light rare earth elements on seed germination, seedling growth and antioxidant metabolism in Triticum durum. Chemosphere 75, 900–905. https://doi.org/10.1016/j.chemosphere.2009.01.026

Da F. Iwahara, L.K., De Oliveira, M.S., De Alencar, M.A.V., 2019. Evaluation of the effect of three constituent metals of monazita on the radiosensibility of human osteoblasts. J. Environ. Radioact. 208–209, 106011. https://doi.org/10.1016/j.jenvrad.2019.106011

Dai, Y., Li, Jian, Li, Jie, Yu, L., Dai, G., Hu, A., Yuan, L., Wen, Z., 2002. EFFECTS OF RARE EARTH COMPOUNDS ON GROWTH AND APOPTOSIS OF LEUKEMIC CELL LINES. Vitro Cell. Dev. Biol. - Anim. 38, 373. https://doi.org/10.1290/1071-2690(2002)038<0373:EORECO>2.0.CO;2

Dai, Y., Sun, S., Li, Y., Yang, J., Zhang, C., Cao, R., Zhang, H., Chen, J., Geng, N., 2022. Residual levels and health risk assessment of rare earth elements in Chinese resident diet: A market-based investigation. Sci. Total Environ. 828, 154119. https://doi.org/10.1016/j.scitotenv.2022.154119

Danouche, M., El Ghachtouli, N., El Baouchi, A., El Arroussi, H., 2020. Heavy metals phycoremediation using tolerant green microalgae: Enzymatic and non-enzymatic antioxidant systems for the management of oxidative stress. J. Environ. Chem. Eng. 8, 104460. https://doi.org/10.1016/j.jece.2020.104460

Date, A.R., Gray, A.L., 1989. Applications of inductively coupled plasma mass spectrometry. Blackie & Son, Ltd., Glasgow, U.K.

Dawson, P.H., 1995. Quadrupole Mass Spectrometry and its Applications. ed. Elsevier, Amsterdam, 1976; reissued by AIP Press, Woodbury, NY

De Marzi, L., Monaco, A., De Lapuente, J., Ramos, D., Borras, M., Di Gioacchino, M., Santucci, S., Poma, A., 2013. Cytotoxicity and Genotoxicity of Ceria Nanoparticles on Different Cell Lines in Vitro. Int. J. Mol. Sci. 14, 3065–3077. https://doi.org/10.3390/ijms14023065

de Vathaire, F., Challeton de Vathaire, C., Ropers, J., Mollié, A., 1998. Cancer mortality in the commune of Pargny sur Saulx in France. J. Radiol. Prot. 18, 23–27. https://doi.org/10.1088/0952-4746/18/1/004

de Boer, M.A., Lammertsma, K., 2013. Scarcity of Rare Earth Elements. ChemSusChem 6, 2045–2055. https://doi.org/10.1002/cssc.201200794

Deng, C., Zhang, D., Pan, X., Chang, F., Wang, S., 2013. Toxic effects of mercury on PSI and PSII activities, membrane potential and transthylakoid proton gradient in Microsorium pteropus. J. Photochem. Photobiol. B 127, 1–7. https://doi.org/10.1016/j.jphotobiol.2013.07.012

Denoyer, E.R., Jacques, D., Debrah, E., Tanner, S.D., 1995. Determination of trace elements in uranium: Practical benefits of a new ICP-MS lens system. Atomic Spectroscopy 16(1), 1-6

Denoyer, E.R., Thomas, R.J., Cousins, L., 1997. Design Forum: A New Approach to Extending the Dynamic Range in ICP Mass Spectrometry. Spectroscopy 12(2), 56–61

Dhiman, M., Singhal, S., 2019. Effect of doping of different rare earth (europium, gadolinium, dysprosium and neodymium) metal ions on structural, optical and photocatalytic properties of LaFeO3 perovskites. J. Rare Earths 37, 1279–1287. https://doi.org/10.1016/j.jre.2018.12.015

Diatloff, E., Asher, C. J., Smith, F. W., 1996. Concentrations of rare earth elements in some Australian soils. Aust. J. Soil Res. 34, 735–747. https://doi.org/10.1071/SR9960735

Ding, S.-M., Liang, T., Zhang, C.-S., Wang, L.-J., Sun, Q., 2006. Accumulation and Fractionation of Rare Earth Elements in a Soil-Wheat System. Pedosphere 16, 82–90. https://doi.org/10.1016/S1002-0160(06)60029-5

Divya, T., Renuka, N.K., 2015. Modulated heterogeneous Fenton-like activity of 'M' doped nanoceria systems (M = Cu, Fe, Zr, Dy, La): Influence of reduction potential of doped cations. J. Mol. Catal. Chem. 408, 41–47. https://doi.org/10.1016/j.molcata.2015.07.018

Donohue, S.J., Friedericks, J.B., 1984. Laboratory Procedures. Soil Testing and Plant Analysis Laboratory, Virginia Technical Publication, pp. 452-881.

Donohue, V.E., McDonald, F., Evans, R., 1995. In vitro cytotoxicity testing of neodymium-iron-boron magnets. J. Appl. Biomater. 6, 69–74. https://doi.org/10.1002/jab.770060110

Douglas, D.J., French, J.B., 1986. An improved interface for inductively coupled plasma-mass spectrometry (ICP-MS). Spectrochim. Acta 41(3), 197-204. https://doi.org/10.1016/0584-8547(86)80159-8

Drago, G., Perrino, C., Canepari, S., Ruggieri, S., L'Abbate, L., Longo, V., Colombo, P., Frasca, D., Balzan, M., Cuttitta, G., Scaccianoce, G., Piva, G., Bucchieri, S., Melis, M., Viegi, G., Cibella, F., Balzan, M., Bilocca, D., Borg, C., Montefort, S., Zammit, C., Bucchieri, S., Cibella, F., Colombo, P., Cuttitta, G., Drago, G., Ferrante, G., L'Abbate, L., Grutta, S.L., Longo, V., Melis, M.R., Ruggieri, S., Viegi, G., Minardi, R., Piva, G., Ristagno, R., Rizzo, G., Scaccianoce, G., 2018. Relationship between domestic smoking and metals and rare earth elements concentration in indoor PM2.5. Environ. Res. 165, 71–80. https://doi.org/10.1016/j.envres.2018.03.026

Du, X., Graedel, T.E., 2013. Uncovering the end uses of the rare earth elements. Sci. Total Environ. 461–462, 781–784. https://doi.org/10.1016/j.scitotenv.2013.02.099

Du, X., Graedel, T.E., 2011. Uncovering the Global Life Cycles of the Rare Earth Elements. Sci. Rep. 1, 145. https://doi.org/10.1038/srep00145

Dubé, M., Auclair, J., Hanana, H., Turcotte, P., Gagnon, C., Gagné, F., 2019. Gene expression changes and toxicity of selected rare earth elements in rainbow trout juveniles. Comp. Biochem. Physiol. Part - C Toxicol. Pharmacol. 223, 88–95. https://doi.org/10.1016/j.cbpc.2019.05.009

Dufresne, A., Krier, G., Muller, J.F., Case, B., Perrault, G., 1994. Lanthanide particles in the lung of a printer. Sci. Total Environ. 151, 249–252. https://doi.org/10.1016/0048-9697(94)90474-X

E. T. Moore, R., Rehkämper, M., Kreissig, K., Strekopytov, S., Larner, F., 2018. Determination of major and trace element variability in healthy human urine by ICP-QMS and specific gravity normalisation. RSC Adv. 8, 38022–38035. https://doi.org/10.1039/C8RA06794E

Edward, M., Quinn, J.A., Burden, A.D., Newton, B.B., Jardine, A.G., 2010. Effect of Different Classes of Gadolinium-based Contrast Agents on Control and Nephrogenic Systemic Fibrosis–derived Fibroblast Proliferation. Radiology 256, 735–743. https://doi.org/10.1148/radiol.10091131

Ergün, I., Keven, K., Uruç, I., Ekmekçi, Y., Canbakan, B., Erden, I., Karatan, O., 2006. The safety of gadolinium in patients with stage 3 and 4 renal failure. Nephrol. Dial. Transplant. 21, 697–700. https://doi.org/10.1093/ndt/gfi304

Espinoza-Quiñones, F.R., Módenes, A.N., Dos Santos, J., Obregón, P.L., De Pauli, A.R., 2018. Insights on limits of detection, precision and accuracy in TXRF analysis of trace and major elements in environmental solid suspensions. Appl. Radiat. Isot. 137, 80–90. https://doi.org/10.1016/j.apradiso.2018.03.016

Evseeva, T., Geras'kin, S., Majstrenko, T., Brown, J., Belykh, E., 2010. Comparative estimation of 232Th and stable Ce (III) toxicity and detoxification pathways in freshwater alga Chlorella vulgaris. Chemosphere 81, 1320–1327. https://doi.org/10.1016/j.chemosphere.2010.08.028

Fairbrother, A., 2008. Risk Management Safety Factor, in: Encyclopedia of Ecology. Elsevier, pp. 3062–3068. https://doi.org/10.1016/B978-008045405-4.00426-2

Fan, J., Jiang, X., Min, H., Li, D., Ran, X., Zou, L., Sun, Y., Li, W., Yang, J., Teng, W., Li, G., Zhao, D., 2014. Facile preparation of Cu–Mn/CeO2/SBA-15 catalysts using ceria as an auxiliary for advanced oxidation processes. J. Mater. Chem. A 2, 10654. https://doi.org/10.1039/c4ta01355g

Feder, M.E., Burggren, W.W., 1985. Skin Breathing in Vertebrates. Sci. Am. 253, 126–142. https://doi.org/10.1038/scientificamerican1185-126

Fernández-Caliani, J.C., Barba-Brioso, C., De La Rosa, J.D., 2009. Mobility and speciation of rare earth elements in acid minesoils and geochemical implications for river waters in the southwestern Iberian margin. Geoderma 149, 393–401. https://doi.org/10.1016/j.geoderma.2009.01.004

Ferreira, M. da S., Fontes, M.P.F., Lima, M.T.W.D.C., Cordeiro, S.G., Wyatt, N.L.P., Lima, H.N., Fendorf, S., 2022. Human health risk assessment and geochemical mobility of rare earth elements in Amazon soils. Sci. Total Environ. 806, 151191. https://doi.org/10.1016/j.scitotenv.2021.151191

Feyerabend, F., Fischer, J., Holtz, J., Witte, F., Willumeit, R., Drücker, H., Vogt, C., Hort, N., 2010. Evaluation of short-term effects of rare earth and other elements used in magnesium alloys on primary cells and cell lines☆. Acta Biomater. 6, 1834–1842. https://doi.org/10.1016/j.actbio.2009.09.024

Fida, H., Zhang, G., Guo, S., Naeem, A., 2017. Heterogeneous Fenton degradation of organic dyes in batch and fixed bed using La-Fe montmorillonite as catalyst. J. Colloid Interface Sci. 490, 859–868. https://doi.org/10.1016/j.jcis.2016.11.085

Fouad, K., Gar Alalm, M., Bassyouni, M., Saleh, M.Y., 2021. Optimization of catalytic wet peroxide oxidation of carbofuran by Ti-LaFeO 3 dual photocatalyst. Environ. Technol. Innov. 23, 101778. https://doi.org/10.1016/j.eti.2021.101778

Freitas, R., Costa, S., D Cardoso, C.E., Morais, T., Moleiro, P., Matias, A.C., Pereira, A.F., Machado, J., Correia, B., Pinheiro, D., Rodrigues, A., Colónia, J., Soares, A.M.V.M., Pereira, E., 2020. Toxicological effects of the rare earth element neodymium in Mytilus galloprovincialis. Chemosphere 244, 125457. https://doi.org/10.1016/j.chemosphere.2019.125457

Fuma, S., Takeda, H., Takaku, Y., Hisamatsu, S., Kawabata, Z., 2005. Effects of Dysprosium on the Species-Defined Microbial Microcosm. Bull. Environ. Contam. Toxicol. 74, 263–272. https://doi.org/10.1007/s00128-004-0579-6

Galdiero, E., Carotenuto, R., Siciliano, A., Libralato, G., Race, M., Lofrano, G., Fabbricino, M., Guida, M., 2019. Cerium and erbium effects on Daphnia magna generations: A multiple endpoints approach. Environ. Pollut. 254, 112985. https://doi.org/10.1016/j.envpol.2019.112985

Galdiero, E., Siciliano, A., Maselli, V., Gesuele, R., Guida, M., Fulgione, D., Galdiero, S., Lombardi, L., Falanga, A., 2016. An integrated study on antimicrobial activity and ecotoxicity of quantum dots and quantum dots coated with the antimicrobial peptide indolicidin. Int. J. Nanomedicine Volume 11, 4199–4211. https://doi.org/10.2147/IJN.S107752

Galhardi, J.A., De Mello, J.W.V., Wilkinson, K.J., 2020a. Bioaccumulation of potentially toxic elements from the soils surrounding a legacy uranium mine in Brazil. Chemosphere 261, 127679. https://doi.org/10.1016/j.chemosphere.2020.127679

Galhardi, J.A., Leles, B.P., De Mello, J.W.V., Wilkinson, K.J., 2020b. Bioavailability of trace metals and rare earth elements (REE) from the tropical soils of a coal mining area. Sci. Total Environ. 717, 134484. https://doi.org/10.1016/j.scitotenv.2019.134484

Garcia-Muñoz, P., Lefevre, C., Robert, D., Keller, N., 2019. Ti-substituted LaFeO3 perovskite as photoassisted CWPO catalyst for water treatment. Appl. Catal. B Environ. 248, 120–128. https://doi.org/10.1016/j.apcatb.2019.02.030

Geraets, L., Oomen, A.G., Schroeter, J.D., Coleman, V.A., Cassee, F.R., 2012. Tissue Distribution of Inhaled Micro- and Nano-sized Cerium Oxide Particles in Rats: Results From a 28-Day Exposure Study. Toxicol. Sci. 127, 463–473. https://doi.org/10.1093/toxsci/kfs113

Gerhardsson, L., Nordberg, G.F., n.d. Lung cancer in smelter workers — interactions of metals as indicated by tissue levels 6.

Ghadiri, M., Ghasemi Darehnaei, M., Sabbaghian, S., Shirazian, S., 2013. Computational Simulation for Transport of Priority Organic Pollutants through Nanoporous Membranes. Chem. Eng. Technol. 36, 507–512. https://doi.org/10.1002/ceat.201200513

Gibby, Wendell A., Gibby, K.A., Gibby, W Andrew, 2004. Comparison of Gd DTPA-BMA (Omniscan) versus Gd HP-DO3A (ProHance) Retention in Human Bone Tissue by Inductively Coupled Plasma Atomic Emission Spectroscopy. Invest. Radiol. 39, 138–142. https://doi.org/10.1097/01.rli.0000112789.57341.01

Goecke, F., Jerez, C.G., Zachleder, V., Figueroa, F.L., BiÅ¡ovÃ¡, K., Å˜ezanka, T., VÃ-tovÃ¡, M., 2015a. Use of lanthanides to alleviate the effects of metal ion-deficiency in Desmodesmus quadricauda (Sphaeropleales, Chlorophyta). Front. Microbiol. 6. https://doi.org/10.3389/fmicb.2015.00002

Goecke, F., Zachleder, V., Vítová, M., 2015b. Rare earth elements and algae: physiological effects, biorefinery and recycling. Algal Biorefineries. 339–363. https://doi.org/10.1007/978-3-319-20200-6_10

Gogoi, A., Navgire, M., Sarma, K.C., Gogoi, P., 2017. Fe 3 O 4 -CeO 2 metal oxide nanocomposite as a Fenton-like heterogeneous catalyst for degradation of catechol. Chem. Eng. J. 311, 153–162. https://doi.org/10.1016/j.cej.2016.11.086

Gojova, A., Guo, B., Kota, R.S., Rutledge, J.C., Kennedy, I.M., Barakat, A.I., 2007. Induction of Inflammation in Vascular Endothelial Cells by Metal Oxide Nanoparticles: Effect of Particle Composition. Environ. Health Perspect. 115, 403–409. https://doi.org/10.1289/ehp.8497

Gojova, A., Lee, J.-T., Jung, H.S., Guo, B., Barakat, A.I., Kennedy, I.M., 2009. Effect of cerium oxide nanoparticles on inflammation in vascular endothelial cells. Inhal. Toxicol. 21, 123–130. https://doi.org/10.1080/08958370902942582

Goldstein, S.J., Jacobsen, S.B., 1988. Rare earth elements in river waters. Earth Planet. Sci. Lett. 89, 35–47. https://doi.org/10.1016/0012-821X(88)90031-3

Gómez-Aracena, J., Riemersma, R.A., Gutiérrez-Bedmar, M., Bode, P., Kark, J.D., Garcia-Rodríguez, A., Gorgojo, L., Veer, P. van't, Fernández-Crehuet, J., Kok, F.J., Martin-Moreno, J.M., 2006. Toenail cerium levels and risk of a first acute myocardial infarction: The EURAMIC and heavy metals study. Chemosphere 64, 112–120. https://doi.org/10.1016/j.chemosphere.2005.10.062

González, R.M., Cánovas, C.R., Olías, M., Macías, F., 2020. Rare earth elements in a historical mining district (south-west Spain): Hydrogeochemical behaviour and seasonal variability. Chemosphere 253, 126742. https://doi.org/10.1016/j.chemosphere.2020.126742

Gonzalez, V., Vignati, D.A.L., Leyval, C., Giamberini, L., 2014. Environmental fate and ecotoxicity of lanthanides: Are they a uniform group beyond chemistry? Environ. Int. 71, 148–157. https://doi.org/10.1016/j.envint.2014.06.019

González, V., Vignati, D.A.L., Pons, M.-N., Montarges-Pelletier, E., Bojic, C., Giamberini, L., 2015. Lanthanide ecotoxicity: First attempt to measure environmental risk for aquatic organisms. Environ. Pollut. 199, 139–147. https://doi.org/10.1016/j.envpol.2015.01.020

Gonzalez-Gil, G., Lopes, S.I.C., Saikaly, P.E., Lens, P.N.L., 2012. Leaching and accumulation of trace elements in sulfate reducing granular sludge under concomitant thermophilic and low pH conditions. Bioresour. Technol. 126, 238–246. https://doi.org/10.1016/j.biortech.2012.09.044

Gravina, M., Pagano, G., Oral, R., Guida, M., Toscanesi, M., Siciliano, A., Di Nunzio, A., Burić, P., Lyons, D.M., Thomas, P.J., Trifuoggi, M., 2018. Heavy Rare Earth Elements Affect Sphaerechinus granularis Sea Urchin Early Life Stages by Multiple Toxicity Endpoints. Bull. Environ. Contam. Toxicol. 100, 641–646. https://doi.org/10.1007/s00128-018-2309-5

Gray, A.L. Date, A.R., 1983. Inductively coupled plasma source mass spectrometry using continuum flow ion extraction. Analyst 108, 1033. https://doi.org/10.1039/AN9830801033

Greaves, M.J., Elderfield, H., Sholkovitz, E.R., 1999. Aeolian sources of rare earth elements to the Western Pacific Ocean. Mar. Chem. 68, 31–38. https://doi.org/10.1016/S0304-4203(99)00063-8

Grobner, T., 2006. Gadolinium – a specific trigger for the development of nephrogenic fibrosing dermopathy and nephrogenic systemic fibrosis? Nephrol. Dial. Transplant. 21, 1104–1108. https://doi.org/10.1093/ndt/gfk062

Gu, S., Li, W., Bian, Y., Wang, F., Li, H., Liu, X., 2016. Highly-Visible-Light Photocatalytic Performance Derived from a Lanthanide Self-Redox Cycle in Ln_2O_3/$BiVO_4$ (Ln: Sm, Eu, Tb) Redox Heterojunction. J. Phys. Chem. C 120, 19242–19251. https://doi.org/10.1021/acs.jpcc.6b06436

Guo, C., Wei, Y., Yan, L., Li, Zhigang, Qian, Y., Liu, H., Li, Zhipeng, Li, X., Wang, Z., Wang, J., 2020. Rare earth elements exposure and the alteration of the hormones in the hypothalamic-pituitary-thyroid (HPT) axis of the residents in an e-waste site: A cross-sectional study. Chemosphere 252, 126488. https://doi.org/10.1016/j.chemosphere.2020.126488

Guo, P., Wang, J., Li, X., Zhu, J., Reinert, T., Heitmann, J., Spemann, D., Vogt, J., Flagmeyer, R.-H., Butz, T., 2000. Study of metal bioaccumulation by nuclear microprobe analysis of algae fossils and living algae cells. Nucl. Instrum. Methods Phys. Res. Sect. B Beam Interact. Mater. At. 161–163, 801–807. https://doi.org/10.1016/S0168-583X(99)00933-7

Guo, Y., Zhang, S., Lai, L., Wang, G., 2015. Rare earth elements in Oolong tea and their human health risks associated with drinking tea. J. Food Compos. Anal. 44, 122–127. https://doi.org/10.1016/j.jfca.2015.08.001

Gürü, M., Karakaya, U., Altıparmak, D., Alıcılar, A., 2002. Improvement of Diesel fuel properties by using additives. Energy Convers. Manag. 43, 1021–1025. https://doi.org/10.1016/S0196-8904(01)00094-2

Gustafsson, J., 2012. Visual Minteq, A Free Equilibrium Speciation Model. KTH, Department of Land and Water Resources Engineering.

Gwenzi, W., Mangori, L., Danha, C., Chaukura, N., Dunjana, N., Sanganyado, E., 2018. Sources, behaviour, and environmental and human health risks of high-technology rare earth elements as emerging contaminants. Sci. Total Environ. 636, 299–313. https://doi.org/10.1016/j.scitotenv.2018.04.235

Haferburg, G., Merten, D., Büchel, G., Kothe, E., 2007. Biosorption of metal and salt tolerant microbial isolates from a former uranium mining area. Their impact on changes in rare earth element patterns in acid mine drainage: Biosorption of metal and salt tolerant microbial isolates. J. Basic Microbiol. 47, 474–484. https://doi.org/10.1002/jobm.200700256

Hanazato, T., 2001. Pesticide e€ ects on freshwater zooplankton: an ecological perspective. Environ. Pollut.

Hao, Z., Li, Y., Li, H., Wei, B., Liao, X., Liang, T., Yu, J., 2015. Levels of rare earth elements, heavy metals and uranium in a population living in Baiyun Obo, Inner Mongolia, China: A pilot study. Chemosphere 128, 161–170. https://doi.org/10.1016/j.chemosphere.2015.01.057

Hasegawa, T., Haraguchi, H., 1992. ICPs in Analytical Atomic Spectrometry, A. Montaser and D.W. Golightly, Eds., 2d ed. VCH, New York

Hayashi, S., Usuda, K., Mitsui, G., Shibutani, T., Dote, E., Adachi, K., Fujihara, M., Shimbo, Y., Sun, W., Kono, R., Tsuji, H., Kono, K., 2006. Urinary Yttrium Excretion and Effects of Yttrium Chloride on Renal Function in Rats. Biol. Trace Elem. Res. 114, 225–236. https://doi.org/10.1385/BTER:114:1:225

He, M.L., Ranz, D., Rambeck, W.A., 2001. Study on the performance enhancing effect of rare earth elements in growing and fattening pigs. J. Anim. Physiol. Anim. Nutr. 85, 263–270. https://doi.org/10.1046/j.1439-0396.2001.00327.x

He, M.L., Wehr, U., Rambeck, W.A., 2010. Effect of low doses of dietary rare earth elements on growth performance of broilers. J. Anim. Physiol. Anim. Nutr. 94, 86–92. https://doi.org/10.1111/j.1439-0396.2008.00884.x

He, X., Zhang, Z., Zhang, H., Zhao, Y., Chai, Z., 2008. Neurotoxicological Evaluation of Long-Term Lanthanum Chloride Exposure in Rats. Toxicol. Sci. 103, 354–361. https://doi.org/10.1093/toxsci/kfn046

He, Z., Li, J., Zhang, H., Ma, M., 2005. Different effects of calcium and lanthanum on the expression of phytochelatin synthase gene and cadmium absorption in Lactuca sativa. Plant Sci. 168, 309–318. https://doi.org/10.1016/j.plantsci.2004.07.001

Heckert, E.G., Seal, S., Self, W.T., 2008. Fenton-Like Reaction Catalyzed by the Rare Earth Inner Transition Metal Cerium. Environ. Sci. Technol. 42, 5014–5019. https://doi.org/10.1021/es8001508

Heller, A., Barkleit, A., Bok, F., Wober, J., 2019. Effect of four lanthanides onto the viability of two mammalian kidney cell lines. Ecotoxicol. Environ. Saf. 173, 469–481. https://doi.org/10.1016/j.ecoenv.2019.02.013

Henríquez-Hernández, L.A., Boada, L.D., Carranza, C., Pérez-Arellano, J.L., González-Antuña, A., Camacho, M., Almeida-González, M., Zumbado, M., Luzardo, O.P., 2017. Blood levels of toxic metals and rare earth elements commonly found in e-waste may exert subtle effects on hemoglobin concentration in sub-Saharan immigrants. Environ. Int. 109, 20–28. https://doi.org/10.1016/j.envint.2017.08.023

Henríquez-Hernández, L.A., González-Antuña, A., Boada, L.D., Carranza, C., Pérez-Arellano, J.L., Almeida-González, M., Camacho, M., Zumbado, M., Fernández-Fuertes, F., Tapia-Martín, M., Luzardo, O.P., 2018. Pattern of blood concentrations of 47 elements in two populations from the same geographical area but with different geological origin and lifestyles: Canary Islands (Spain) vs. Morocco. Sci. Total Environ. 636, 709–716. https://doi.org/10.1016/j.scitotenv.2018.04.311

Herrmann, H., Nolde, J., Berger, S., Heise, S., 2016. Aquatic ecotoxicity of lanthanum – A review and an attempt to derive water and sediment quality criteria. Ecotoxicol. Environ. Saf. 124, 213–238. https://doi.org/10.1016/j.ecoenv.2015.09.033

Hirano, S., Suzuki, K.T., 1996. Exposure, metabolism, and toxicity of rare earths and related compounds. Environ. Health Perspect. 104.

Ho, C.-C., Kang, F., Chang, G.-M., You, S.-J., Wang, Y.-F., 2019. Application of recycled lanthanum-doped TiO2 immobilized on commercial air filter for visible-light photocatalytic degradation of acetone and NO. Appl. Surf. Sci. 465, 31–40. https://doi.org/10.1016/j.apsusc.2018.09.136

Höllriegl, V., González-Estecha, M., Trasobares, E.M., Giussani, A., Oeh, U., Herraiz, M.A., Michalke, B., 2010. Measurement of cerium in human breast milk and blood samples. J. Trace Elem. Med. Biol. 24, 193–199. https://doi.org/10.1016/j.jtemb.2010.03.001

Horvatić, J., Peršić, V., 2007. The Effect of Ni2+, Co2+, Zn2+, Cd2+ and Hg2+ on the Growth Rate of Marine Diatom Phaeodactylum tricornutum Bohlin: Microplate Growth Inhibition Test. Bull. Environ. Contam. Toxicol. 79, 494–498. https://doi.org/10.1007/s00128-007-9291-7

Hose, G.C., Van Den Brink, P.J., 2004. Confirming the Species-Sensitivity Distribution Concept for Endosulfan Using Laboratory, Mesocosm, and Field Data. Arch. Environ. Contam. Toxicol. 47, 511–520. https://doi.org/10.1007/s00244-003-3212-5

Houk, R.S., 1986. Mass spectrometry of inductively coupled plasmas. Anal. Chem. 58 (1), 97A-105A. https://doi.org/10.1021/ac00292a003

Hu, B., Tang, Y., Wang, X., Wu, L., Nong, J., Yang, X., Guo, J., 2021. Cobalt-gadolinium modified biochar as an adsorbent for antibiotics in single and binary systems. Microchem. J. 166, 106235. https://doi.org/10.1016/j.microc.2021.106235

Hu, Q., Zheng, S., Tang, S., Guan, L., 2001. Effects of Sm and Y on growth of Chlorella ellipsoidea. Agro Environ. Prot. (China) 20, 398–404.

Huang, Z., Wu, P., Li, H., Li, W., Zhu, Y., Zhu, N., 2014. Synthesis and catalytic properties of La or Ce doped hydroxy-FeAl intercalated montmorillonite used as heterogeneous photo Fenton catalysts under sunlight irradiation. RSC Adv. 4, 6500. https://doi.org/10.1039/c3ra46729e

Hunter, K., 1994. Ion detection in ICP-mass spectrometry using active film multipliers. Atomic Spectroscopy 15(1), 17–20

Huo, W., Zhu, Y., Li, Zhenjiang, Pang, Y., Wang, B., Li, Zhiwen, 2017. A pilot study on the association between rare earth elements in maternal hair and the risk of neural tube defects in north China. Environ. Pollut. 226, 89–93. https://doi.org/10.1016/j.envpol.2017.03.046

Hurst, C.A., 2010. China's ace in the hole rare earth elements. Leavenworth: FOREIGN MILITARY STUDIES OFFICE (ARMY) FORT LEAVENWORTH KS

Hussain, S., Al-Nsour, F., Rice, A.B., Marshburn, J., Yingling, B., Ji, Z., Zink, J.I., Walker, N.J., Garantziotis, S., 2012. Cerium Dioxide Nanoparticles Induce Apoptosis and Autophagy in Human Peripheral Blood Monocytes. ACS Nano 6, 5820–5829. https://doi.org/10.1021/nn302235u

Hutton, R.C., Eaton, A.N., Gosland, R.M., 1990. Application of a Dual-Mode Detection System for ICP-MS. Part I: Determination of Majors, Minors, and Traces in Geostandards. Applied Spectroscopy 44(2), 238–242. https://doi.org/10.1366/0003702904085697

Inaba, T., Kobayashi, E., Suwazono, Y., Uetani, M., Oishi, M., Nakagawa, H., Nogawa, K., 2005. Estimation of cumulative cadmium intake causing Itai–itai disease. Toxicol. Lett. 159, 192–201. https://doi.org/10.1016/j.toxlet.2005.05.011

Ismail, M., Akhtar, K., Khan, M.I., Kamal, T., Khan, M.A., M. Asiri, A., Seo, J., Khan, S.B., 2019. Pollution, Toxicity and Carcinogenicity of Organic Dyes and their Catalytic Bio-Remediation. Curr. Pharm. Des. 25, 3645–3663. https://doi.org/10.2174/1381612825666191021142026

ISO 8692:2012 water quality - fresh water algal growth inhibition test with unicellular green algae. 2012a

ISO 10253:2016 water quality – marine Al gal growth inhibition test with Skeletonema sp. and Phaeodactylum tricornutum. 2016

ISO 11269-1:2012 soil quality - determination of the effects of pollutants on soil flora - part 1: method for the measurement of inhibition of root growth. 2012b

ISO 29200 soil quality—assessment of genotoxic effects on higher plants—Vicia faba micronucleus test, 2013

Jalal, A., Oliveira Junior, J.C.D., Ribeiro, J.S., Fernandes, G.C., Mariano, G.G., Trindade, V.D.R., Reis, A.R.D., 2021. Hormesis in plants: Physiological and biochemical responses. Ecotoxicol. Environ. Saf. 207, 111225. https://doi.org/10.1016/j.ecoenv.2020.111225

Jenkins, W., Perone, P., Walker, K., Bhagavathula, N., Aslam, M.N., DaSilva, M., Dame, M.K., Varani, J., 2011. Fibroblast Response to Lanthanoid Metal Ion Stimulation: Potential Contribution to Fibrotic Tissue Injury. Biol. Trace Elem. Res. 144, 621–635. https://doi.org/10.1007/s12011-011-9041-x

Jha, A.M., Singh, A.C., 1994. Clastogenicity of lanthanides — induction of micronuclei in root tips of Vicia faba. Mutat. Res. Toxicol. 322, 169–172. https://doi.org/10.1016/0165-1218(94)90003-5

Jiang, D.G., n.d. A Survey of 16 Rare Earth Elements in the Major Foods in China. Biomed Env. Sci.

Jin, X., Chu, Z., Yan, F., Zeng, Q., 2009. Effects of lanthanum(III) and EDTA on the growth and competition of Microcystis aeruginosa and Scenedesmus quadricauda. Limnologica 39, 86–93. https://doi.org/10.1016/j.limno.2008.03.002

Johannesson, K.H., Stetzenbach, K.J., Hodge, V.F., Berry Lyons, W., 1996. Rare earth element complexation behavior in circumneutral pH groundwaters: Assessing the role of carbonate and phosphate ions. Earth Planet. Sci. Lett. 139, 305–319. https://doi.org/10.1016/0012-821X(96)00016-7

Jongeneelen, F.J., Anzion, R.B.M., Henderson, P.Th., 1987. Determination of hydroxylated metabolites of polycyclic aromatic hydrocarbons in urine. J. Chromatogr. B. Biomed. Sci. App. 413, 227–232. https://doi.org/10.1016/0378-4347(87)80230-X

Joonas, E., Aruoja, V., Olli, K., Syvertsen-Wiig, G., Vija, H., Kahru, A., 2017. Potency of (doped) rare earth oxide particles and their constituent metals to inhibit algal growth and induce direct toxic effects. Sci. Total Environ. 593–594, 478–486. https://doi.org/10.1016/j.scitotenv.2017.03.184

Ju, L., Chen, Z., Fang, L., Dong, W., Zheng, F., Shen, M., 2011. Sol-Gel Synthesis and Photo-Fenton-Like Catalytic Activity of EuFeO 3 Nanoparticles: Sol-Gel Synthesis and Photo-Fenton-Like Catalytic Activity. J. Am. Ceram. Soc. 94, 3418–3424. https://doi.org/10.1111/j.1551-2916.2011.04522.x

Kajjumba, G.W., Attene-Ramos, M., Marti, E.J., 2021. Toxicity of lanthanide coagulants assessed using four in vitro bioassays. Sci. Total Environ. 800, 149556. https://doi.org/10.1016/j.scitotenv.2021.149556

Kajjumba, G.W., Marti, E.J., 2022. A review of the application of cerium and lanthanum in phosphorus removal during wastewater treatment: Characteristics, mechanism, and recovery. Chemosphere 309, 136462. https://doi.org/10.1016/j.chemosphere.2022.136462

Kamal, A., Rashid, A., 2014. Benzene exposure among auto-repair workers from workplace ambience: A pioneer study from Pakistan. Int. J. Occup. Med. Environ. Health 27, 830–839. https://doi.org/10.2478/s13382-014-0295-3

Kang, L., Shen, Z., Jin, C., 2000. Neodymium cations Nd 3+ were transported to the interior of Euglena gracilis 277. Chin. Sci. Bull. 45, 585–592. https://doi.org/10.1007/BF02886032

Karadaş, C., Kara, D., Fisher, A., 2011. Determination of rare earth elements in seawater by inductively coupled plasma mass spectrometry with off-line column preconcentration using 2,6-diacetylpyridine functionalized Amberlite XAD-4. Anal. Chim. Acta 689, 184–189. https://doi.org/10.1016/j.aca.2011.01.049

Karri, R.R., Ravindran, G., Dehghani, M.H., 2021. Wastewater—Sources, toxicity, and their consequences to human health. In Soft Computing Techniques in Solid Waste and Wastewater Management. Elsevier: Amsterdam, The Netherlands, 3–33

Karunakaran, C., Gomathisankar, P., Manikandan, G., 2010. Preparation and characterization of antimicrobial Ce-doped ZnO nanoparticles for photocatalytic detoxification of cyanide. Mater. Chem. Phys. 123, 585–594. https://doi.org/10.1016/j.matchemphys.2010.05.019

Kastury, F., Ritch, S., Rasmussen, P.E., Juhasz, A.L., 2020. Influence of household smoking habits on inhalation bioaccessibility of trace elements and light rare earth elements in Canadian house dust. Environ. Pollut. 262, 114132. https://doi.org/10.1016/j.envpol.2020.114132

Katsnelson, B.A., Panov, V.G., Minigalieva, I.A., Bushueva, T.V., Gurvich, V.B., Privalova, L.I., Klinova, S.V., Sutunkova, M.P., 2021. On an extended understanding of the term "hormesis" for denoting alternating directions of the organism's response to increasing adverse exposures. Toxicology 447, 152629. https://doi.org/10.1016/j.tox.2020.152629

Keerthana, S.P., Yuvakkumar, R., Kumar, P.S., Ravi, G., Velauthapillai, D., 2021. Rare earth metal (Sm) doped zinc ferrite (ZnFe2O4) for improved photocatalytic elimination of toxic dye from aquatic system. Environ. Res. 197, 111047. https://doi.org/10.1016/j.envres.2021.111047

Khan, S.B., Faisal, M., Rahman, M.M., Jamal, A., 2011. Exploration of CeO2 nanoparticles as a chemi-sensor and photo-catalyst for environmental applications. Sci. Total Environ. 409, 2987–2992. https://doi.org/10.1016/j.scitotenv.2011.04.019

Kim, B.-M., Rhee, J.-S., Jeong, C.-B., Seo, J.S., Park, G.S., Lee, Y.-M., Lee, J.-S., 2014. Heavy metals induce oxidative stress and trigger oxidative stress-mediated heat shock protein (hsp) modulation in the intertidal copepod Tigriopus japonicus. Comp. Biochem. Physiol. Part C Toxicol. Pharmacol. 166, 65–74. https://doi.org/10.1016/j.cbpc.2014.07.005

Kim, E.B., Seo, J.M., Kim, G.W., Lee, S.Y., Park, T.J., 2016. In vivo synthesis of europium selenide nanoparticles and related cytotoxicity evaluation of human cells. Enzyme Microb. Technol. 95, 201–208. https://doi.org/10.1016/j.enzmictec.2016.08.012

Kim, Y.-S., Lim, C.-H., Shin, S.-H., Kim, J.-C., 2017. Twenty-Eight-Day Repeated Inhalation Toxicity Study of Nano-Sized Neodymium Oxide in Male Sprague-Dawley Rats. Toxicol. Res. 33, 239–253. https://doi.org/10.5487/TR.2017.33.3.239

Kooijman, S.A.L.M., 1987. A safety factor for LC50 values allowing for differences in sensitivity among species. Water Res. 21, 269–276. https://doi.org/10.1016/0043-1354(87)90205-3

Kraus, J.M., Pomeranz, J.P., 2020. Cross-ecosystem linkages and trace metals at the landwater interface. Contaminants and Ecological Subsidies. 91–109. https://doi.org/10.1007/978-3-030-49480-3_5

Kuang, J.C., 2014. Characteristics of Electron Structure and 4f Orbital of Rare Earths and Their Reinforcement of Wastewater Degradation. Adv. Mater. Res. 1022, 72–75. https://doi.org/10.4028/www.scientific.net/AMR.1022.72

Kuchma, M.H., Komanski, C.B., Colon, J., Teblum, A., Masunov, A.E., Alvarado, B., Babu, S., Seal, S., Summy, J., Baker, C.H., 2010. Phosphate ester hydrolysis of biologically relevant molecules by cerium oxide nanoparticles. Nanomedicine Nanotechnol. Biol. Med. 6, 738–744. https://doi.org/10.1016/j.nano.2010.05.004

Kulaksız, S., Bau, M., 2013. Anthropogenic dissolved and colloid/nanoparticle-bound samarium, lanthanum and gadolinium in the Rhine River and the impending destruction of the natural rare earth element distribution in rivers. Earth Planet. Sci. Lett. 362, 43–50. https://doi.org/10.1016/j.epsl.2012.11.033

Kulaksız, S., Bau, M., 2007. Contrasting behaviour of anthropogenic gadolinium and natural rare earth elements in estuaries and the gadolinium input into the North Sea. Earth Planet. Sci. Lett. 260, 361–371. https://doi.org/10.1016/j.epsl.2007.06.016

Kumar, V., Shah, M.P., 2021. Advanced oxidation processes for complex wastewater treatment. In Advanced Oxidation Processes for Effluent Treatment Plants. Elsevier: Amsterdam, The Netherlands, 1–31

Kutty, V.R., Abraham, S., Kartha, C.C., 1996. Geographical Distribution of Endomyocardial Fibrosis in South Kerala. Int. J. Epidemiol. 25, 1202–1207. https://doi.org/10.1093/ije/25.6.1202

Lam J.W., McLaren, J.W., 1990. Use of aerosol processing and nitrogen-argon plasmas for reduction of oxide interference in inductively coupled plasma mass spectrometry. J. Anal. Atom. Spectom. 5, 419–424. https://doi.org/10.1039/JA9900500419

Lattanzio, S.M., Imbesi, F., 2020. Fibromyalgia associated with repeated gadolinium contrast-enhanced MRI examinations. Radiol. Case Rep. 15, 534–541. https://doi.org/10.1016/j.radcr.2020.02.002

Laveuf, C., Cornu, S., 2009. A review on the potentiality of Rare Earth Elements to trace pedogenetic processes. Geoderma 154, 1–12. https://doi.org/10.1016/j.geoderma.2009.10.002

Lawrence, M.G., Ort, C., Keller, J., 2009. Detection of anthropogenic gadolinium in treated wastewater in South East Queensland, Australia. Water Res. 43, 3534–3540. https://doi.org/10.1016/j.watres.2009.04.033

Lee, Y.-M., Lee, D.-H., 2019. Mitochondrial Toxins and Healthy Lifestyle Meet at the Crossroad of Hormesis. Diabetes Metab. J. 43, 568. https://doi.org/10.4093/dmj.2019.0143

Lefticariu, L., Klitzing, K.L., Kolker, A., 2020. Rare Earth Elements and Yttrium (REY) in coal mine drainage from the Illinois Basin, USA. Int. J. Coal Geol. 217, 103327. https://doi.org/10.1016/j.coal.2019.103327

León-Mejía, G., Luna-Rodríguez, I., Trindade, C., Oliveros-Ortíz, L., Anaya-Romero, M., Luna-Carrascal, J., Navarro-Ojeda, N., Ruiz-Benitez, M., Franco-Valencia, K., Da Silva, J., Henriques, J.A.P., Muñoz-Acevedo, A., Quintana-Sosa, M., 2019. Cytotoxic and genotoxic effects in mechanics occupationally exposed to diesel engine exhaust. Ecotoxicol. Environ. Saf. 171, 264–273. https://doi.org/10.1016/j.ecoenv.2018.12.067

Li, H., Li, W., Wang, F., Liu, X., Ren, C., 2017. Fabrication of two lanthanides co-doped Bi2MoO6 photocatalyst: Selection, design and mechanism of Ln1/Ln2 redox couple for enhancing photocatalytic activity. Appl. Catal. B Environ. 217, 378–387. https://doi.org/10.1016/j.apcatb.2017.06.015

Li, H., Li, W., Wang, F., Liu, X., Ren, C., Miao, X., 2018. Fabrication of Pt nanoparticles decorated Gd-doped Bi2MoO6 nanosheets: Design, radicals regulating and mechanism of Gd/Pt-Bi2MoO6 photocatalyst. Appl. Surf. Sci. 427, 1046–1053. https://doi.org/10.1016/j.apsusc.2017.09.106

Li, H.-R., Xiang, H.-M., Zhong, J.-W., Ren, X.-Q., Wei, H., Zhang, J.-E., Xu, Q.-Y., Zhao, B.-L., 2020. Acid Rain Increases Impact of Rice Blast on Crop Health via Inhibition of Resistance Enzymes. Plants 9, 881. https://doi.org/10.3390/plants9070881

Li, J., Hong, M., Yin, X., Liu, J., 2010. Effects of the accumulation of the rare earth elements on soil macrofauna community. J. Rare Earths 28, 957–964. https://doi.org/10.1016/S1002-0721(09)60233-7

Li, M., Zhuang, L., Zhang, G., Lan, C., Yan, L., Liang, R., Hao, C., Li, Z., Zhang, J., Lu, Q., Wang, B., 2021. Association between exposure of light rare earth elements and outcomes of in vitro fertilization-embryo transfer in North China. Sci. Total Environ. 762, 143106. https://doi.org/10.1016/j.scitotenv.2020.143106

Li, X., Chen, Zhi-biao, Chen, Zhi-qiang, 2014. Distribution and fractionation of rare earth elements in soil–water system and human blood and hair from a mining area in southwest Fujian Province, China. Environ. Earth Sci. 72, 3599–3608. https://doi.org/10.1007/s12665-014-3271-0

Li, X., Chen, Zhibiao, Chen, Zhiqiang, Zhang, Y., 2013. A human health risk assessment of rare earth elements in soil and vegetables from a mining area in Fujian Province, Southeast China. Chemosphere 93, 1240–1246. https://doi.org/10.1016/j.chemosphere.2013.06.085

Li, X., Li, W., Liu, X., Geng, L., Fan, H., Khan, A., Ma, X., Dong, M., Qiu, H., 2022. The construction of Yb/Er/Pr triple-doped Bi2WO6 superior photocatalyst and the regulation of superoxide and hydroxyl radicals. Appl. Surf. Sci. 592, 153311. https://doi.org/10.1016/j.apsusc.2022.153311

Li, X., Wu, P., 2017. Geochemical characteristics of dissolved rare earth elements in acid mine drainage from abandoned high-As coal mining area, southwestern China. Environ. Sci. Pollut. Res. 24, 20540–20555. https://doi.org/10.1007/s11356-017-9670-5

Li, Y., Yu, H., Li, P., Bian, Y., 2017. Assessment the Exposure Level of Rare Earth Elements in Workers Producing Cerium, Lanthanum Oxide Ultrafine and Nanoparticles. Biol. Trace Elem. Res. 175, 298–305. https://doi.org/10.1007/s12011-016-0795-z

Li, Y., Yu, H., Zheng, S., Miao, Y., Yin, S., Li, P., Bian, Y., 2016. Direct Quantification of Rare Earth Elements Concentrations in Urine of Workers Manufacturing Cerium, Lanthanum Oxide Ultrafine and Nanoparticles by a Developed and Validated ICP-MS. Int. J. Environ. Res. Public. Health 13, 350. https://doi.org/10.3390/ijerph13030350

Lian, H., Qin, C., Zhang, L., Zhang, C., Li, H., Zhang, S., 2019. Lanthanum nitrate improves phosphorus-use efficiency and tolerance to phosphorus-deficiency stress in Vigna angularis seedlings. Protoplasma 256, 383–392. https://doi.org/10.1007/s00709-018-1304-3

Liang, C., Wang, W., 2013. Antioxidant response of soybean seedlings to joint stress of lanthanum and acid rain. Environ. Sci. Pollut. Res. 20, 8182–8191. https://doi.org/10.1007/s11356-013-1776-9

Liang, C.-H., Hou, M.-F., Zhou, S.-G., Li, F.-B., Liu, C.-S., Liu, T.-X., Gao, Y.-X., Wang, X.-G., Lü, J.-L., 2006. The effect of erbium on the adsorption and photodegradation of orange I in aqueous Er3+-TiO2 suspension. J. Hazard. Mater. 138, 471–478. https://doi.org/10.1016/j.jhazmat.2006.05.066

Liang, Q., Yin, H., Li, J., Zhang, L., Hou, R., Wang, S., 2018. Investigation of rare earth elements in urine and drinking water of children in mining area. Medicine (Baltimore) 97, e12717. https://doi.org/10.1097/MD.0000000000012717

Liang, T., Li, K., Wang, L., 2014. State of rare earth elements in different environmental components in mining areas of China. Environ. Monit. Assess. 186, 1499–1513. https://doi.org/10.1007/s10661-013-3469-8

Libralato, G., Costa Devoti, A., Zanella, M., Sabbioni, E., Mičetić, I., Manodori, L., Pigozzo, A., Manenti, S., Groppi, F., Volpi Ghirardini, A., 2016a. Phytotoxicity of ionic, micro- and nano-sized iron in three plant species. Ecotoxicol. Environ. Saf. 123, 81–88. https://doi.org/10.1016/j.ecoenv.2015.07.024

Libralato, G., Gentile, E., Volpi Ghirardini, A., 2016b. Wastewater effects on Phaeodactylum tricornutum (Bohlin): Setting up a classification system. Ecol. Indic. 60, 31–37. https://doi.org/10.1016/j.ecolind.2015.06.014

Lin, W., Huang, Y., Zhou, X.-D., Ma, Y., 2006. Toxicity of Cerium Oxide Nanoparticles in Human Lung Cancer Cells. Int. J. Toxicol. 25, 451–457. https://doi.org/10.1080/10915810600959543

Liu, H., Wang, J., Yang, Z., Wang, K., 2015. Serum Proteomic Analysis Based on iTRAQ in Miners Exposed to Soil Containing Rare Earth Elements. Biol. Trace Elem. Res. 167, 200–208. https://doi.org/10.1007/s12011-015-0312-9

Liu, H., Liu, Haiyan, Yang, Z., Wang, K., 2021. Bone Mineral Density in Population Long-Term Exposed to Rare Earth Elements from a Mining Area of China. Biol. Trace Elem. Res. 199, 453–464. https://doi.org/10.1007/s12011-020-02165-0

Liu, L., Wang, L., Ni, W., Pan, Y., Chen, Y., Xie, Q., Liu, Y., Ren, A., 2021. Rare earth elements in umbilical cord and risk for orofacial clefts. Ecotoxicol. Environ. Saf. 207, 111284. https://doi.org/10.1016/j.ecoenv.2020.111284

Liu, S., 1978. Electronic structure of rare earth metals. Handb. Phys. Chem. Rare Earths 1, 233–335

Liu, W.-S., Guo, M.-N., Liu, C., Yuan, M., Chen, X.-T., Huot, H., Zhao, C.-M., Tang, Y.-T., Morel, J.L., Qiu, R.-L., 2019. Water, sediment and agricultural soil contamination from an ion-adsorption rare earth mining area. Chemosphere 216, 75–83. https://doi.org/10.1016/j.chemosphere.2018.10.109

Liu, Y., Wu, M., Zhang, L., Bi, J., Song, L., Wang, L., Liu, B., Zhou, A., Cao, Z., Xiong, C., Yang, S., Xu, S., Xia, W., Li, Y., Wang, Y., 2019. Prenatal exposure of rare earth elements cerium and ytterbium and neonatal thyroid stimulating hormone levels: Findings from a birth cohort study. Environ. Int. 133, 105222. https://doi.org/10.1016/j.envint.2019.105222

Loell, M., Albrecht, C., Felix-Henningsen, P., 2011. Rare earth elements and relation between their potential bioavailability and soil properties, Nidda catchment (Central Germany). Plant Soil 349, 303–317. https://doi.org/10.1007/s11104-011-0875-y

Lofrano, G., Libralato, G., Carotenuto, M., Guida, M., Inglese, M., Siciliano, A., Meriç, S., 2016. Emerging Concern from Short-Term Textile Leaching: A Preliminary Ecotoxicological Survey. Bull. Environ. Contam. Toxicol. 97, 646–652. https://doi.org/10.1007/s00128-016-1937-x

Lofrano, G., Libralato, G., Casaburi, A., Siciliano, A., Iannece, P., Guida, M., Pucci, L., Dentice, E.F., Carotenuto, M., 2018. Municipal wastewater spiramycin removal by conventional treatments and heterogeneous photocatalysis. Sci. Total Environ. 624, 461–469. https://doi.org/10.1016/j.scitotenv.2017.12.145

Lofrano, G., Rizzo, L., Grassi, M., Belgiorno, V., 2009. Advanced oxidation of catechol: A comparison among photocatalysis, Fenton and photo-Fenton processes. Desalination 249, 878–883. https://doi.org/10.1016/j.desal.2009.02.068

Long, K. R. (2011). The future of rare earth elements—will these high-tech industry elements continue in short supply? Reston, VA: U.S. Geological Survey. Open-File Report 2011–1189. http://pubs.usgs.gov/of/2011/1189/

Longbottom, J.E., Martin, T.D., Edgell, K.W., Long, S.E., Plantz, M.R., Warden, B.E., 1994. Determination of trace elements in water by inductively coupled plasma-mass spectrometry: collaborative study. J. AOAC Internat. 77:1104

Lopes, I., Gonçalves, F., Soares, A.M.V.M., Ribeiro, R., 1999. Discriminating the Ecotoxicity due to Metals and to Low pH in Acid Mine Drainage. Ecotoxicol. Environ. Saf. 44, 207–214. https://doi.org/10.1006/eesa.1999.1825

Loveridge, A., Smith, D.S., McGeer, J.C., 2021. Dissolved Organic Matter Mitigates the Acute Toxicity of Thulium to Hyalella azteca but Ca, Mg and Na Do Not. Arch. Environ. Contam. Toxicol. 81, 637–647. https://doi.org/10.1007/s00244-021-00898-0

Lu, V.M., Crawshay-Williams, F., White, B., Elliot, A., Hill, M.A., Townley, H.E., 2019. Cytotoxicity, dose-enhancement and radiosensitization of glioblastoma cells with rare earth nanoparticles. Artif. Cells Nanomedicine Biotechnol. 47, 132–143. https://doi.org/10.1080/21691401.2018.1544564

Luan, J., Liu, W., Yao, Y., Ma, B., Niu, B., Yang, G., Wei, Z., 2022. Synthesis and Property Examination of Er2FeSbO7/BiTiSbO6 Heterojunction Composite Catalyst and Light-Catalyzed Retrogradation of Enrofloxacin in Pharmaceutical Waste Water under Visible Light Irradiation. Materials 15, 5906. https://doi.org/10.3390/ma15175906

Lürling, M., Tolman, Y., 2010. Effects of lanthanum and lanthanum-modified clay on growth, survival and reproduction of Daphnia magna. Water Res. 44, 309–319. https://doi.org/10.1016/j.watres.2009.09.034

Lürling, M., Van Oosterhout, F., 2013. Case study on the efficacy of a lanthanum-enriched clay (Phoslock®) in controlling eutrophication in Lake Het Groene Eiland (The Netherlands). Hydrobiologia 710, 253–263. https://doi.org/10.1007/s10750-012-1141-x

Ma, J.Y., Mercer, R.R., Barger, M., Schwegler-Berry, D., Scabilloni, J., Ma, J.K., Castranova, V., 2012. Induction of pulmonary fibrosis by cerium oxide nanoparticles. Toxicol. Appl. Pharmacol. 262, 255–264. https://doi.org/10.1016/j.taap.2012.05.005

Ma, J.Y.C., Young, S.-H., Mercer, R.R., Barger, M., Schwegler-Berry, D., Ma, J.K., Castranova, V., 2014. Interactive effects of cerium oxide and diesel exhaust nanoparticles on inducing pulmonary fibrosis. Toxicol. Appl. Pharmacol. 278, 135–147. https://doi.org/10.1016/j.taap.2014.04.019

Ma, Y., Wang, J., Peng, C., Ding, Y., He, X., Zhang, P., Li, N., Lan, T., Wang, D., Zhang, Zhaohui, Sun, F., Liao, H., Zhang, Zhiyong, 2016. Toxicity of cerium and thorium on Daphnia magna. Ecotoxicol. Environ. Saf. 134, 226–232. https://doi.org/10.1016/j.ecoenv.2016.09.006

MacMillan, G.A., Clayden, M.G., Chételat, J., Richardson, M.C., Ponton, D.E., Perron, T., Amyot, M., 2019. Environmental Drivers of Rare Earth Element Bioaccumulation in Freshwater Zooplankton. Environ. Sci. Technol. 53, 1650–1660. https://doi.org/10.1021/acs.est.8b05547

Macnair, M.R., 1993. The genetics of metal tolerance in vascular plants. New Phytol. 124, 541–559. https://doi.org/10.1111/j.1469-8137.1993.tb03846.x

Magnusson, B., and Ornemark, U., 2014. Eurachem Guide: The Fitness for Purpose of Analytical Methods - a laboratory guide to method validation and related topics. 2nd edition. Available at: https://www.eurachem.org/images/stories/Guides/pdf/MV_guide_2nd_ed_EN.pdf

Maier, T.J., Ricciotti, E., Rook, G.A.W., Editors, C.A.L., 2022. Evolution, Biodiversity and a Reassessment of the Hygiene Hypothesis.

Malhotra, N., Hsu, H.-S., Liang, S.-T., Roldan, M.J.M., Lee, J.-S., Ger, T.-R., Hsiao, C.-D., 2020. An Updated Review of Toxicity Effect of the Rare Earth Elements (REEs) on Aquatic Organisms. Animals 10, 1663. https://doi.org/10.3390/ani10091663

Manier, N., Bado-Nilles, A., Delalain, P., Aguerre-Chariol, O., Pandard, P., 2013. Ecotoxicity of non-aged and aged CeO2 nanomaterials towards freshwater microalgae. Environ. Pollut. 180, 63–70. https://doi.org/10.1016/j.envpol.2013.04.040

Manusadžianas, L., Vitkus, R., Gylytė, B., Cimmperman, R., Džiugelis, M., Karitonas, R., Sadauskas, K., 2020. Ecotoxicity Responses of the Macrophyte Algae Nitellopsis obtusa and Freshwater Crustacean Thamnocephalus platyurus to 12 Rare Earth Elements. Sustainability 12, 7130. https://doi.org/10.3390/su12177130

Martino, C., Bonaventura, R., Byrne, M., Roccheri, M., Matranga, V., 2017. Effects of exposure to gadolinium on the development of geographically and phylogenetically distant sea urchins species. Mar. Environ. Res. 128, 98–106. https://doi.org/10.1016/j.marenvres.2016.06.001

Marubashi, K., Hirano, S., Suzuki, K.T., 1998. Effects of intratracheal pretreatment with yttrium chloride (YCl3) on inflammatory responses of the rat lung following intratracheal instillation of YCl3. Toxicol. Lett. 99, 43–51. https://doi.org/10.1016/S0378-4274(98)00137-4

Marwani, H.M., Ahmad, S., Rahman, M.M., 2022. Catalytic Reduction of Environmental Pollutants with Biopolymer Hydrogel Cross-Linked Gelatin Conjugated Tin-Doped Gadolinium Oxide Nanocomposites. Gels 8, 86. https://doi.org/10.3390/gels8020086

Marzec-Wróblewska, U., Kamiński, P., Łakota, P., Ludwikowski, G., Szymański, M., Wasilow, K., Stuczyński, T., Buciński, A., Jerzak, L., 2015. Determination of Rare Earth Elements in Human Sperm and Association with Semen Quality. Arch. Environ. Contam. Toxicol. 69, 191–201. https://doi.org/10.1007/s00244-015-0143-x

Matos, A.R.D., Faria, M.C.S., Freire, B.M., Pereira, R.M., Batista, B.L., Rodrigues, J.L., 2022. Determination of 14 trace elements in blood, serum and urine after environmental disaster in the Doce River basin: Relationship between mining waste and metal concentration in the population. J. Trace Elem. Med. Biol. 70, 126920. https://doi.org/10.1016/j.jtemb.2021.126920

Medas, D., Cidu, R., De Giudici, G., Podda, F., 2013. Geochemistry of rare earth elements in water and solid materials at abandoned mines in SW Sardinia (Italy). J. Geochem. Explor. 133, 149–159. https://doi.org/10.1016/j.gexplo.2013.05.005

Medina-Estévez, F., Zumbado, M., Luzardo, O.P., Rodríguez-Hernández, Á., Boada, L.D., Fernández-Fuertes, F., Santandreu-Jimenez, M.E., Henríquez-Hernández, L.A., 2020. Association between Heavy Metals and Rare Earth Elements with Acute Ischemic Stroke: A Case-Control Study Conducted in the Canary Islands (Spain). Toxics 8, 66. https://doi.org/10.3390/toxics8030066

Meryem, B., Ji, H., Gao, Y., Ding, H., Li, C., 2016. Distribution of rare earth elements in agricultural soil and human body (scalp hair and urine) near smelting and mining areas of Hezhang, China. J. Rare Earths 34, 1156–1167. https://doi.org/10.1016/S1002-0721(16)60148-5

Miazek, K., Iwanek, W., Remacle, C., Richel, A., Goffin, D., 2015. Effect of Metals, Metalloids and Metallic Nanoparticles on Microalgae Growth and Industrial Product Biosynthesis: A Review. Int. J. Mol. Sci. 16, 23929–23969. https://doi.org/10.3390/ijms161023929

Migaszewski, Z.M., Gałuszka, A., 2015. The Characteristics, Occurrence, and Geochemical Behavior of Rare Earth Elements in the Environment: A Review. Crit. Rev. Environ. Sci. Technol. 45, 429–471. https://doi.org/10.1080/10643389.2013.866622

Minganti, V., Drava, G., 2018. Tree bark as a bioindicator of the presence of scandium, yttrium and lanthanum in urban environments. Chemosphere 193, 847–851. https://doi.org/10.1016/j.chemosphere.2017.11.074

Minqin, R., Xiao, C., Yi, Z., Hao, S., Qingguang, R., Yong, L., Frank, W., 2013. Sub-100-nm STIM imaging and PIXE quantification of rare earth elements in algae cells: Sub-100-nm STIM imaging and PIXE quantification of rare earth elements. X-Ray Spectrom. 42, 237–241. https://doi.org/10.1002/xrs.2480

Mittal, S., Pandey, A.K., 2014. Cerium Oxide Nanoparticles Induced Toxicity in Human Lung Cells: Role of ROS Mediated DNA Damage and Apoptosis. BioMed Res. Int. 2014, 1–14. https://doi.org/10.1155/2014/891934

Mongelli, G., Boni, M., Buccione, R., Sinisi, R., 2014. Geochemistry of the Apulian karst bauxites (southern Italy): Chemical fractionation and parental affinities. Ore Geol. Rev. 63, 9–21. https://doi.org/10.1016/j.oregeorev.2014.04.012

Mongelli, G., Boni, M., Oggiano, G., Mameli, P., Sinisi, R., Buccione, R., Mondillo, N., 2017. Critical metals distribution in Tethyan karst bauxite: The cretaceous Italian ores. Ore Geol. Rev. 86, 526–536. https://doi.org/10.1016/j.oregeorev.2017.03.017

Mongelli, G., Buccione, R., Sinisi, R., 2015. Genesis of autochthonous and allochthonous Apulian karst bauxites (Southern Italy): Climate constraints. Sediment. Geol. 325, 168–176. https://doi.org/10.1016/j.sedgeo.2015.06.005

Montasser, A., 1998. Inductively Coupled Plasma Mass Spectrometry. ed. Wiley-VCH, Berlin

Montaser, A., Golightly, D.W., 1992. Inductively coupled plasmas in analytical atomic spectrometry. 2nd ed. VCH Publlishers, Inc, New York, N.Y.

Moreira, A., Henriques, B., Leite, C., Libralato, G., Pereira, E., Freitas, R., 2020. Potential impacts of lanthanum and yttrium through embryotoxicity assays with Crassostrea gigas. Ecol. Indic. 108, 105687. https://doi.org/10.1016/j.ecolind.2019.105687

Na, J., Chen, H., An, H., Li, N., Yan, L., Ye, R., Li, Z., 2022. Association of Rare Earth Elements with Passive Smoking among Housewives in Shanxi Province, China. Int. J. Environ. Res. Public. Health 19, 559. https://doi.org/10.3390/ijerph19010559

Naccarato, A., Tassone, A., Cavaliere, F., Elliani, R., Pirrone, N., Sprovieri, F., Tagarelli, A., Giglio, A., 2020. Agrochemical treatments as a source of heavy metals and rare earth elements in agricultural

soils and bioaccumulation in ground beetles. Sci. Total Environ. 749, 141438. https://doi.org/10.1016/j.scitotenv.2020.141438

Nalabotu, S.K., Kolli, M.B., Triest, W.E., Ma, J.Y., Manne, N.D., Katta, A., Addagarla, H.S., Rice, K.M., Blough, E.R., 2011. Intratracheal instillation of cerium oxide nanoparticles induces hepatic toxicity in male Sprague-Dawley rats. Int. J. Nanomedicine 6, 2327–2335. https://doi.org/10.2147/IJN.S25119

Nelms, S., 2005. Inductively coupled plasma mass spectrometry Handbook. Blackwell Science, Cambridge, Mass

Nemmar, A., Al-Salam, S., Beegam, S., Yuvaraju, P., Ali, B.H., 2017. The acute pulmonary and thrombotic effects of cerium oxide nanoparticles after intratracheal instillation in mice. Int. J. Nanomedicine 12, 2913–2922. https://doi.org/10.2147/IJN.S127180

Newman, M.C., Ownby, D.R., Mézin, L.C.A., Powell, D.C., Christensen, T.R.L., Lerberg, S.B., Anderson, B.A., 2000. Applying species-sensitivity distributions in ecological risk assessment: Assumptions of distribution type and sufficient numbers of species. Environ. Toxicol. Chem. 19, 508–515. https://doi.org/10.1002/etc.5620190233

Nie, Y., Zhang, L., Li, Y.-Y., Hu, C., 2015. Enhanced Fenton-like degradation of refractory organic compounds by surface complex formation of LaFeO3 and H2O2. J. Hazard. Mater. 294, 195–200. https://doi.org/10.1016/j.jhazmat.2015.03.065

Nitti, M., Marengo, B., Furfaro, A.L., Pronzato, M.A., Marinari, U.M., Domenicotti, C., Traverso, N., 2022. Hormesis and Oxidative Distress: Pathophysiology of Reactive Oxygen Species and the Open Question of Antioxidant Modulation and Supplementation. Antioxidants 11, 1613. https://doi.org/10.3390/antiox11081613

Nkrumah, P.N., Erskine, P.D., Erskine, J.D., Van Der Ent, A., 2021. Rare earth elements (REE) in soils and plants of a uranium-REE mine site and exploration target in Central Queensland, Australia. Plant Soil 464, 375–389. https://doi.org/10.1007/s11104-021-04956-3

Nothdurft, L.D., Webb, G.E., Kamber, B.S., 2004. Rare earth element geochemistry of Late Devonian reefal carbonates, Canning Basin, Western Australia: confirmation of a seawater REE proxy in ancient limestones. Geochim. Cosmochim. Acta 68, 263–283. https://doi.org/10.1016/S0016-7037(03)00422-8

Olías, M., Cánovas, C.R., Basallote, M.D., Lozano, A., 2018. Geochemical behaviour of rare earth elements (REE) along a river reach receiving inputs of acid mine drainage. Chem. Geol. 493, 468–477. https://doi.org/10.1016/j.chemgeo.2018.06.029

Olivares, J.A., Houk, R.S., 1986. Suppression of Analyte Signal by Various Concomitant Salts in Inductively Coupled Plasma Mass Spectrometry. Anal. Chem. 58, 20-25

Oliverio, M., Nardi, M., Costanzo, P., Di Gioia, M., Procopio, A., 2018. Erbium Salts as Non-Toxic Catalysts Compatible with Alternative Reaction Media. Sustainability 10, 721. https://doi.org/10.3390/su10030721

Onozuka, K., Kawakami, Y., Imai, H., Yokoi, T., Tatsumi, T., Kondo, J.N., 2012. Perovskite-type La2Ti2O7 mesoporous photocatalyst. J. Solid State Chem. 192, 87–92. https://doi.org/10.1016/j.jssc.2012.03.055

Oral, R., Bustamante, P., Warnau, M., D'Ambra, A., Guida, M., Pagano, G., 2010. Cytogenetic and developmental toxicity of cerium and lanthanum to sea urchin embryos. Chemosphere 81, 194–198. https://doi.org/10.1016/j.chemosphere.2010.06.057

Oral, R., Pagano, G., Siciliano, A., Gravina, M., Palumbo, A., Castellano, I., Migliaccio, O., Thomas, P.J., Guida, M., Tommasi, F., Trifuoggi, M., 2017. Heavy rare earth elements affect early life stages in Paracentrotus lividus and Arbacia lixula sea urchins. Environ. Res. 154, 240–246. https://doi.org/10.1016/j.envres.2017.01.011

Orge, C.A., Órfão, J.J.M., Pereira, M.F.R., Duarte De Farias, A.M., Fraga, M.A., 2012. Ceria and cerium-based mixed oxides as ozonation catalysts. Chem. Eng. J. 200–202, 499–505. https://doi.org/10.1016/j.cej.2012.06.088

Oturan, M.A., Aaron, J.-J., 2014. Advanced Oxidation Processes in Water/Wastewater Treatment: Principles and Applications. A Review. Crit. Rev. Environ. Sci. Technol. 44, 2577–2641. https://doi.org/10.1080/10643389.2013.829765

Ouyang, W., Zhou, Y., Fei, X., Bai, Y., Wang, H., Wu, Z., 2022. Simultaneous removal of NO and dichloromethane (CH2Cl2) over Nb-loaded cerium nanotubes catalyst. J. Environ. Sci. 111, 175–184. https://doi.org/10.1016/j.jes.2021.03.022

Pagano, G., 2017. Rare earth elements in human and environmental health: At the crossroads between toxicity and safety. New York, NY: CRC Press.

Pagano, G., Aliberti, F., Guida, M., Oral, R., Siciliano, A., Trifuoggi, M., Tommasi, F., 2015a. Rare earth elements in human and animal health: State of art and research priorities. Environ. Res. 142, 215–220. https://doi.org/10.1016/j.envres.2015.06.039

Pagano, G., Brouziotis, A.A., Lyons, D., Čarapar, I., Oral, R., Tez, S., Thomas, P.J., Tommasi, F., Libralato, G., Guida, M., Trifuoggi, M., 2023. Hormetic Effects of Cerium, Lanthanum and Their Combination at Sub-micromolar Concentrations in Sea Urchin Sperm. Bull. Environ. Contam. Toxicol. 110, 65. https://doi.org/10.1007/s00128-023-03701-z

Pagano, G., Esposito, A., Giordano, G.G., 1982. Fertilization and larval development in sea urchins following exposure of gametes and embryos to cadmium. Arch. Environ. Contam. Toxicol. 11, 47–55. https://doi.org/10.1007/BF01055185

Pagano, G., Guida, M., Siciliano, A., Oral, R., Koçbaş, F., Palumbo, A., Castellano, I., Migliaccio, O., Thomas, P.J., Trifuoggi, M., 2016. Comparative toxicities of selected rare earth elements: Sea urchin embryogenesis and fertilization damage with redox and cytogenetic effects. Environ. Res. 147, 453–460. https://doi.org/10.1016/j.envres.2016.02.031

Pagano, G., Guida, M., Tommasi, F., Oral, R., 2015b. Health effects and toxicity mechanisms of rare earth elements—Knowledge gaps and research prospects. Ecotoxicol. Environ. Saf. 115, 40–48. https://doi.org/10.1016/j.ecoenv.2015.01.030

Pagano, G., Guida, M., Trifuoggi, M., Thomas, P., Palumbo, A., Romano, G., Oral, R., 2017. Sea Urchin Bioassays in Toxicity Testing: I. Inorganics, Organics, Complex Mixtures and Natural Products. Expert Opin. Environ. Biol. 06. https://doi.org/10.4172/2325-9655.1000142

Pagano, G., Thomas, P.J., Di Nunzio, A., Trifuoggi, M., 2019. Human exposures to rare earth elements: Present knowledge and research prospects. Environ. Res. 171, 493–500. https://doi.org/10.1016/j.envres.2019.02.004

Pairon, J.C., Roos, F., Iwatsubo, Y., Janson, X., Billon-Galland, M.A., Bignon, J., Brochard, P., 1994. Lung retention of cerium in humans. Occup. Environ. Med. 51, 195–199. https://doi.org/10.1136/oem.51.3.195

Pairon, J.-C., Roos, F., Sébastien, P., Chamak, B., Abd-Alsamad, I., Bernaudin, J.-F., Bignon, J., Brochard, P., 1995. Biopersistence of cerium in the human respiratory tract and ultrastructural findings. Am. J. Ind. Med. 27, 349–358. https://doi.org/10.1002/ajim.4700270304

Paiva, A.V., De Oliveira, M.S., Yunes, S.N., De Oliveira, L.G., Cabral-Neto, J.B., De Almeida, C.E.B., 2009. Effects of Lanthanum on Human Lymphocytes Viability and DNA Strand Break. Bull. Environ. Contam. Toxicol. 82, 423–427. https://doi.org/10.1007/s00128-008-9596-1

Pang, X., Peng, A., 2002. Application of rare-earth elements in the agriculture of China and its environmental behavior in soil. Env. Sci.

Pang, Y., Jiang, J., Li, K., Yan, L., Feng, Y., Wang, J., Cao, X., Li, Z., Wang, B., 2021. Effects of Rare Earth Elements on Blood Pressure and Their Exposure Biomarkers: Evidence from Animal Experiments. Int. J. Environ. Res. Public. Health 18, 9836. https://doi.org/10.3390/ijerph18189836

Park, E.-J., Choi, J., Park, Y.-K., Park, K., 2008. Oxidative stress induced by cerium oxide nanoparticles in cultured BEAS-2B cells. Toxicology 245, 90–100. https://doi.org/10.1016/j.tox.2007.12.022

Pedrazzani, R., Bertanza, G., Brnardić, I., Cetecioglu, Z., Dries, J., Dvarionienė, J., García-Fernández, A.J., Langenhoff, A., Libralato, G., Lofrano, G., Škrbić, B., Martínez-López, E., Meriç, S., Pavlović, D.M., Papa, M., Schröder, P., Tsagarakis, K.P., Vogelsang, C., 2019. Opinion paper about organic trace pollutants in wastewater: Toxicity assessment in a European perspective. Sci. Total Environ. 651, 3202–3221. https://doi.org/10.1016/j.scitotenv.2018.10.027

Peng, R., Pan, X., Xie, Q., 2003. [Relationship of the hair content of rare earth elements in young children aged 0 to 3 years to that in their mothers living in a rare earth mining area of Jiangxi]. Zhonghua Yu Fang Yi Xue Za Zhi 37, 20–22.

Perone, P.A., Weber, S.L., DaSilva, M., Paruchuri, T., Bhagavathula, N., Aslam, M.N., Dame, M.K., Johnson, K.J., Swartz, R.D., Varani, J., 2010. Collagenolytic Activity Is Suppressed in Organ-Cultured Human Skin Exposed to a Gadolinium-Based MRI Contrast Agent: Invest. Radiol. 45, 42–48. https://doi.org/10.1097/RLI.0b013e3181bf95eb

Perry, J., Minaei, E., Engels, E., Ashford, B.G., McAlary, L., Clark, J.R., Gupta, R., Tehei, M., Corde, S., Carolan, M., Ranson, M., 2020. Thulium oxide nanoparticles as radioenhancers for the treatment of metastatic cutaneous squamous cell carcinoma. Phys. Med. Biol. 65, 215018. https://doi.org/10.1088/1361-6560/abaa5d

Pešić, M., Podolski-Renić, A., Stojković, S., Matović, B., Zmejkoski, D., Kojić, V., Bogdanović, G., Pavićević, A., Mojović, M., Savić, A., Milenković, I., Kalauzi, A., Radotić, K., 2015. Anti-cancer effects of cerium oxide nanoparticles and its intracellular redox activity. Chem. Biol. Interact. 232, 85–93. https://doi.org/10.1016/j.cbi.2015.03.013

Pham, L.H., Nguyen, H.T., Van Tran, C., Nguyen, H.M., Nguyen, T.H., Tu, M.B., 2017. Arsenic and other trace elements in groundwater and human urine in Ha Nam province, the Northern Vietnam: contamination characteristics and risk assessment. Environ. Geochem. Health 39, 517–529. https://doi.org/10.1007/s10653-016-9831-3

Pichini, S., Pacifici, R., 2013a. Linne guida per la determinazione delle sostanze d'abuso nella matrice pilifera. Istituto Superiore di Sanità.

Pichini, S., Pacifici, R., 2013b. Linne guida per la determinazione delle sostanze d'abuso nelle urine. Istituto Superiore di Sanità.

Pierscionek, B.K., Li, Y., Yasseen, A.A., Colhoun, L.M., Schachar, R.A., Chen, W., 2010. Nanoceria have no genotoxic effect on human lens epithelial cells. Nanotechnology 21, 035102. https://doi.org/10.1088/0957-4484/21/3/035102

Pinto, J., Costa, M., Leite, C., Borges, C., Coppola, F., Henriques, B., Monteiro, R., Russo, T., Di Cosmo, A., Soares, A.M.V.M., Polese, G., Pereira, E., Freitas, R., 2019. Ecotoxicological effects of lanthanum in Mytilus galloprovincialis: Biochemical and histopathological impacts. Aquat. Toxicol. 211, 181–192. https://doi.org/10.1016/j.aquatox.2019.03.017

Piovár, J., Stavrou, E., Kaduková, J., Kimáková, T., Bačkor, M., 2011. Influence of long-term exposure to copper on the lichen photobiont Trebouxia erici and the free-living algae Scenedesmus quadricauda. Plant Growth Regul. 63, 81–88. https://doi.org/10.1007/s10725-010-9515-4

Poniedziałek, B., Rzymski, Paweł, Pięt, M., Niedzielski, P., Mleczek, M., Wilczak, M., Rzymski, Piotr, 2017. Rare-earth elements in human colostrum milk. Environ. Sci. Pollut. Res. 24, 26148–26154. https://doi.org/10.1007/s11356-017-0359-6

Ponnurangam, A., Bau, M., Brenner, M., Koschinsky, A., 2016. Mussel shells of <i>Mytilus edulis</i> as bioarchives of the distribution of rare earth elements and yttrium in seawater and the potential impact of pH and temperature on their partitioning behavior. Biogeosciences 13, 751–760. https://doi.org/10.5194/bg-13-751-2016

Porru, S., Placidi, D., Quarta, C., Sabbioni, E., Pietra, R., Fortaner, S., 2001. The potencial role of rare earths in the pathogenesis of interstitial lung disease: a case report of movie projectionist as investigated by neutron activation analysis. J. Trace Elem. Med. Biol. 14, 232–236. https://doi.org/10.1016/S0946-672X(01)80008-0

Posthuma, Leo, Glenn W. Suter II, and Traas, T.P., 2002. Species Sensitivity Distributions in Ecotoxicology. Lewis, Boca Raton.

Prati, M.V., Costagliola, M.A., Zuccheroso, A., Napolitano, P., 2019. Assessment of Euro 5 diesel vehicle NOx emissions by laboratory and track testing. Environ. Sci. Pollut. Res. 26, 10576–10586. https://doi.org/10.1007/s11356-019-04486-7

Priya, A.K., Gnanasekaran, L., Rajendran, S., Qin, J., Vasseghian, Y., 2022. Occurrences and removal of pharmaceutical and personal care products from aquatic systems using advanced treatment- A review. Environ. Res. 204, 112298. https://doi.org/10.1016/j.envres.2021.112298

Protano, G., Riccobono, F., 2002. High contents of rare earth elements (REEs) in stream waters of a Cu–Pb–Zn mining area. Environ. Pollut. 117, 499–514. https://doi.org/10.1016/S0269-7491(01)00173-7

Purwadi, I., Van Der Werff, H., Lievens, C., 2019. Reflectance spectroscopy and geochemical analysis of rare earth element-bearing tailings: A case study of two abandoned tin mine sites in Bangka Island, Indonesia. Int. J. Appl. Earth Obs. Geoinformation 74, 239–247. https://doi.org/10.1016/j.jag.2018.09.006

Qiang, T., Xiao-rong, W., Li-qing, T., Le-mei, D., 1994. Bioaccumulation of the rare earth elements lanthanum, gadolinium and yttrium in carp (Cyprinus carpio). Environ. Pollut. 85, 345–350. https://doi.org/10.1016/0269-7491(94)90057-4

Ramos, S.J., Dinali, G.S., Oliveira, C., Martins, G.C., Moreira, C.G., Siqueira, J.O., Guilherme, L.R.G., 2016. Rare Earth Elements in the Soil Environment. Curr. Pollut. Rep. 2, 28–50. https://doi.org/10.1007/s40726-016-0026-4

Ren, Q.G., Hua, Y., Shen, H., Zhong, L., Jin, C.Z., Mi, Y., Yao, H.Y., Xie, Y.N., Wei, S.Q., Zhou, L.W., 2007. Cytochemical behavior of rare earth ions in Euglena gracilis studied by XAFS. J. Radioanal. Nucl. Chem. 272, 359–362. https://doi.org/10.1007/s10967-007-0529-y

Riaño, S., Regadío, M., Binnemans, K., Vander Hoogerstraete, T., 2016. Practical guidelines for best practice on Total Reflection X-ray Fluorescence spectroscopy: Analysis of aqueous solutions. Spectrochim. Acta Part B At. Spectrosc. 124, 109–115. https://doi.org/10.1016/j.sab.2016.09.001

Rim, K.-T., 2016. Effects of rare earth elements on the environment and human health: A literature review. Toxicol. Environ. Health Sci. 8, 189–200. https://doi.org/10.1007/s13530-016-0276-y

Rim, K.T., Koo, K.H., Park, J.S., 2013. Toxicological Evaluations of Rare Earths and Their Health Impacts to Workers: A Literature Review. Saf. Health Work 4, 12–26. https://doi.org/10.5491/SHAW.2013.4.1.12

Rodea-Palomares, I., Gonzalo, S., Santiago-Morales, J., Leganés, F., García-Calvo, E., Rosal, R., Fernández-Piñas, F., 2012. An insight into the mechanisms of nanoceria toxicity in aquatic photosynthetic organisms. Aquat. Toxicol. 122–123, 133–143. https://doi.org/10.1016/j.aquatox.2012.06.005

Rodushkin, I., Axelsson, M.D., 2000. Application of double focusing sector field ICP-MS for multielemental characterization of human hair and nails. Part II. A study of the inhabitants of northern Sweden꞉.

Romero, F.M., Prol-Ledesma, R.M., Canet, C., Alvares, L.N., Pérez-Vázquez, R., 2010rim. Acid drainage at the inactive Santa Lucia mine, western Cuba: Natural attenuation of arsenic, barium and lead, and geochemical behavior of rare earth elements. Appl. Geochem. 25, 716–727. https://doi.org/10.1016/j.apgeochem.2010.02.004

Romero-Freire, A., Joonas, E., Muna, M., Cossu-Leguille, C., Vignati, D.A.L., Giamberini, L., 2019. Assessment of the toxic effects of mixtures of three lanthanides (Ce, Gd, Lu) to aquatic biota. Sci. Total Environ. 661, 276–284. https://doi.org/10.1016/j.scitotenv.2019.01.155

Romero-Freire, A., Minguez, L., Pelletier, M., Cayer, A., Caillet, C., Devin, S., Gross, E.M., Guérold, F., Pain-Devin, S., Vignati, D.A.L., Giamberini, L., 2018. Assessment of baseline ecotoxicity of sediments from a prospective mining area enriched in light rare earth elements. Sci. Total Environ. 612, 831–839. https://doi.org/10.1016/j.scitotenv.2017.08.128

Roncati, L., Gatti, A.M., Barbolini, G., Piscioli, F., Pusiol, T., Maiorana, A., 2018. In Vivo Uptake of Rare Earth Metals by Triple-Negative Breast Cancer Cells. Pathol. Oncol. Res. 24, 161–165. https://doi.org/10.1007/s12253-017-0209-3

Rout, P.R., Zhang, T.C., Bhunia, P., Surampalli, R.Y., 2021. Treatment technologies for emerging contaminants in wastewater treatment plants: A review. Sci. Total Environ. 753, 141990. https://doi.org/10.1016/j.scitotenv.2020.141990

Rowell, J.A., Fillion, M.A., Smith, S., Wilkinson, K.J., 2018. Determination of the speciation and bioavailability of samarium to Chlamydomonas reinhardtii in the presence of natural organic matter. Environ. Toxicol. Chem. 37, 1623–1631. https://doi.org/10.1002/etc.4106

Rubio, L., Annangi, B., Vila, L., Hernández, A., Marcos, R., 2016. Antioxidant and anti-genotoxic properties of cerium oxide nanoparticles in a pulmonary-like cell system. Arch. Toxicol. 90, 269–278. https://doi.org/10.1007/s00204-015-1468-y

Rucki, M., Kejlova, K., Vlkova, A., Jirova, D., Dvorakova, M., Svobodova, L., Kandarova, H., Letasiova, S., Kolarova, H., Mannerstrom, M., Heinonen, T., 2021. Evaluation of toxicity profiles of rare earth elements salts (lanthanides). J. Rare Earths 39, 225–232. https://doi.org/10.1016/j.jre.2020.02.011

Rumbo, C., Espina, C.C., Popov, V.V., Skokov, K., Tamayo-Ramos, J.A., 2021. Toxicological evaluation of MnAl based permanent magnets using different in vitro models. Chemosphere 263, 128343. https://doi.org/10.1016/j.chemosphere.2020.128343

Rustad, J.R., 2012. Peak Nothing: Recent Trends in Mineral Resource Production. Environ. Sci. Technol. 46, 1903–1906. https://doi.org/10.1021/es203065g

Rydahl, C., Thomsen, H.S., Marckmann, P., 2008. High Prevalence of Nephrogenic Systemic Fibrosis in Chronic Renal Failure Patients Exposed to Gadodiamide, a Gadolinium-Containing Magnetic Resonance Contrast Agent: Invest. Radiol. 43, 141–144. https://doi.org/10.1097/RLI.0b013e31815a3407

Sabbioni, E., Pietra, R., Gaglione, P., Vocaturo, G., Colombo, F., Zanoni, M., Rodi, F., 1982. Long-term occupational risk of rare-earth pneumoconiosis A case report as investigated by neutron activation analysis. Sci. Total Environ. 26, 19–32. https://doi.org/10.1016/0048-9697(82)90093-6

Sack, M., Alili, L., Karaman, E., Das, S., Gupta, A., Seal, S., Brenneisen, P., 2014. Combination of Conventional Chemotherapeutics with Redox-Active Cerium Oxide Nanoparticles—A Novel Aspect in Cancer Therapy. Mol. Cancer Ther. 13, 1740–1749. https://doi.org/10.1158/1535-7163.MCT-13-0950

Sajeevan, A.C., Sajith, V., 2013. Diesel Engine Emission Reduction Using Catalytic Nanoparticles: An Experimental Investigation. J. Eng. 2013, e589382. https://doi.org/10.1155/2013/589382

Sakata K., Kawabata, K., 1994. Reduction of fundamental polyatomic ions in inductively coupled plasma mass spectrometry. Spectrochimica Acta 49B(10), 1027-1038. https://doi.org/10.1016/0584-8547(94)80088-X

Salminen, R., 2005. Foregs Geochemical Atlas of Europe, Part 1-Background Information, Methodology, and Maps. Electric Publication URL address. http://gtk/publ/foregsatlas

Sam, A.D., Morasch, M.D., Collins, J., Song, G., Chen, R., Pereles, F.S., 2003. Safety of gadolinium contrast angiography in patients with chronic renal insufficiency. J. Vasc. Surg. 38, 313–318. https://doi.org/10.1016/S0741-5214(03)00315-X

Santos, A.S.E., Martins, A.A.F., Simões Gonçalves, E., Meyer, A., 2020. Mortality from Selected Cancers among Brazilian Mechanics. Asian Pac. J. Cancer Prev. 21, 1779–1786. https://doi.org/10.31557/APJCP.2020.21.6.1779

Schettino, A., Turco, E., 2011. Tectonic history of the western Tethys since the Late Triassic. Geol. Soc. Am. Bull. 123, 89–105. https://doi.org/10.1130/B30064.1

Schindelin, J., Rueden, C.T., Hiner, M.C., Eliceiri, K.W., 2015. The ImageJ ecosystem: An open platform for biomedical image analysis: T HE I MAGEJ E COSYSTEM. Mol. Reprod. Dev. 82, 518–529. https://doi.org/10.1002/mrd.22489

Schirrmacher, V., 2021. Less Can Be More: The Hormesis Theory of Stress Adaptation in the Global Biosphere and Its Implications. Biomedicines 9, 293. https://doi.org/10.3390/biomedicines9030293

Schlüter, M., Steuber, T., Parente, M., 2008. Chronostratigraphy of Campanian–Maastrichtian platform carbonates and rudist associations of Salento (Apulia, Italy). Cretac. Res. 29, 100–114. https://doi.org/10.1016/j.cretres.2007.04.005

Schmied, A., Murawski, A., Kolossa-Gehring, M., Kujath, P., 2021. Determination of trace elements in urine by inductively coupled plasma-tandem mass spectrometry – Biomonitoring of adults in the German capital region. Chemosphere 285, 131425. https://doi.org/10.1016/j.chemosphere.2021.131425

Selvaraj, V., Bodapati, S., Murray, E., Blough, E., Winston, N., Rice, K., Shokufar, T., Zhao, Y., 2014. Cytotoxicity and genotoxicity caused by yttrium oxide nanoparticles in HEK293 cells. Int. J. Nanomedicine 1379. https://doi.org/10.2147/IJN.S52625

Semelka, R.C., Commander, C.W., Jay, M., Burke, L.M.B., Ramalho, M., 2016. Presumed Gadolinium Toxicity in Subjects With Normal Renal Function: A Report of 4 Cases. Invest. Radiol. 51, 661–665. https://doi.org/10.1097/RLI.0000000000000318

Seroglazova, A.S., Chebanenko, M.I., Nevedomskyi, V.N., Popkov, V.I., 2023. Solution combustion synthesis of novel PrFeO3/CeO2 nanocomposite with enhanced photo-Fenton activity under visible light. Ceram. Int. 49, 15468–15479. https://doi.org/10.1016/j.ceramint.2023.01.132

Seroglazova, A.S., Popkov, V.I., 2022. Synthesis of highly active and visible-light-driven PrFeO3 photocatalyst using solution combustion approach and succinic acid as fuel. Nanosyst. Phys. Chem. Math. 13, 649–654. https://doi.org/10.17586/2220-8054-2022-13-6-649-654

Shahnaz, T., Vishnu Priyan, V., Jayakumar, A., Narayanasamy, S., 2022. Magnetic nanocellulose from Cyperus rotundas grass in the absorptive removal of rare earth element cerium (III): Toxicity studies and interpretation. Chemosphere 287, 131912. https://doi.org/10.1016/j.chemosphere.2021.131912

Sharma, R., Bansal, S., Singhal, S., 2016. Augmenting the catalytic activity of $CoFe_2O_4$ by substituting rare earth cations into the spinel structure. RSC Adv. 6, 71676–71691. https://doi.org/10.1039/C6RA14325C

Sharmin, F., Basith, M.A., 2022. Highly efficient photocatalytic degradation of hazardous industrial and pharmaceutical pollutants using gadolinium doped BiFeO3 nanoparticles. J. Alloys Compd. 901, 163604. https://doi.org/10.1016/j.jallcom.2021.163604

Sharp, B.L., 1980. Analytical Atomic Spectrometry 3, 613

Shen, H., Ren, Q.G., Mi, Y., Shi, X.F., Yao, H.Y., Jin, C.Z., Huang, Y.Y., He, W., Zhang, J., Liu, B., 2002. Investigation of metal ion accumulation in Euglena gracilis by fluorescence methods. Nucl. Instrum. Methods Phys. Res. Sect. B Beam Interact. Mater. At. 189, 506–510. https://doi.org/10.1016/S0168-583X(01)01132-6

Shen, L., Lan, Z., Sun, X., Shi, L., Liu, Q., Ni, J., 2010. Proteomic analysis of lanthanum citrate-induced apoptosis in human cervical carcinoma SiHa cells. BioMetals 23, 1179–1189. https://doi.org/10.1007/s10534-010-9368-3

Shi, X., Cui, C., Zhang, L., Zhang, J., Liu, G., 2019. FeOCl/Ln (Ln = La or Y): efficient photo-Fenton catalysts for ibuprofen degradation. New J. Chem. 43, 16273–16280. https://doi.org/10.1039/C9NJ03746B

Shi, Z., Yong, L., Liu, Z., Wang, Y., Sui, H., Mao, W., Zhang, L., Li, Y., Liu, J., Wei, S., Song, Y., 2022. Risk assessment of rare earth elements in fruits and vegetables from mining areas in China. Environ. Sci. Pollut. Res. 29, 48694–48703. https://doi.org/10.1007/s11356-022-19080-7

Shibamoto, Y., Nakamura, H., 2018. Overview of Biological, Epidemiological, and Clinical Evidence of Radiation Hormesis. Int. J. Mol. Sci. 19, 2387. https://doi.org/10.3390/ijms19082387

Shin, S.-H., Kim, H.-O., Rim, K.-T., 2019. Worker Safety in the Rare Earth Elements Recycling Process From the Review of Toxicity and Issues. Saf. Health Work 10, 409–419. https://doi.org/10.1016/j.shaw.2019.08.005

Siciliano, A., Guida, M., Pagano, G., Trifuoggi, M., Tommasi, F., Lofrano, G., Padilla Suarez, E.G., Gjata, I., Brouziotis, A.A., Liguori, R., Libralato, G., 2021a. Cerium, gadolinium, lanthanum, and neodymium effects in simplified acid mine discharges to Raphidocelis subcapitata, Lepidium sativum, and Vicia faba. Sci. Total Environ. 787, 147527. https://doi.org/10.1016/j.scitotenv.2021.147527

Siciliano, A., Guida, M., Serafini, S., Micillo, M., Galdiero, E., Carfagna, S., Salbitani, G., Tommasi, F., Lofrano, G., Padilla Suarez, E.G., Gjata, I., Brouziotis, A.A., Trifuoggi, M., Liguori, R., Race, M., Fabbricino, M., Libralato, G., 2021b. Long-term multi-endpoint exposure of the microalga Raphidocelis subcapitata to lanthanum and cerium. Sci. Total Environ. 790, 148229. https://doi.org/10.1016/j.scitotenv.2021.148229

Siciliano, A., Sabatino, M., Paone, A., Padilla Suarez, E.G., Toscanesi, M., Brouziotis, A.A., Gambino, E., Saviano, L., Trifuoggi, M., Guida, M., Libralato, G., 2022. A first attempt to evaluate the toxicity to Phaeodactylum tricornutum Bohlin exposed to rare earth elements. Front. Environ. Sci. 10, 957943. https://doi.org/10.3389/fenvs.2022.957943

Silva, L.F.O., Crissien, T.J., Tutikian, B.F., Sampaio, C.H., 2020. Rare Earth Elements and carbon nanotubes in coal mine around spontaneous combustions. J. Clean. Prod. 253, 120068. https://doi.org/10.1016/j.jclepro.2020.120068

Sin, J.-C., Lam, S.-M., Lee, K.-T., Mohamed, A.R., 2013. Preparation and photocatalytic properties of visible light-driven samarium-doped ZnO nanorods. Ceram. Int. 39, 5833–5843. https://doi.org/10.1016/j.ceramint.2013.01.004

Singh, L., Rekha, P., Chand, S., 2016. Cu-impregnated zeolite Y as highly active and stable heterogeneous Fenton-like catalyst for degradation of Congo red dye. Sep. Purif. Technol. 170, 321–336. https://doi.org/10.1016/j.seppur.2016.06.059

Singh, S., Kumar, A., Karakoti, A., Seal, S., Self, W.T., 2010. Unveiling the mechanism of uptake and sub-cellular distribution of cerium oxide nanoparticles. Mol. Biosyst. 6, 1813. https://doi.org/10.1039/c0mb00014k

Slezakova, K., Pereira, M.C., Alvim-Ferraz, M.C., 2009. Influence of tobacco smoke on the elemental composition of indoor particles of different sizes. Atmos. Environ. 43, 486–493. https://doi.org/10.1016/j.atmosenv.2008.10.017

Snow, S.J., McGee, J., Miller, D.B., Bass, V., Schladweiler, M.C., Thomas, R.F., Krantz, T., King, C., Ledbetter, A.D., Richards, J., Weinstein, J.P., Conner, T., Willis, R., Linak, W.P., Nash, D., Wood, C.E., Elmore, S.A., Morrison, J.P., Johnson, C.L., Gilmour, M.I., Kodavanti, U.P., 2014. Inhaled Diesel Emissions Generated with Cerium Oxide Nanoparticle Fuel Additive Induce Adverse Pulmonary and Systemic Effects. Toxicol. Sci. 142, 403–417. https://doi.org/10.1093/toxsci/kfu187

Song, J., Ma, N., Chen, W., Chen, J., Dai, Q., 2022. Insights into mechanism of catalytic ozonation of cinnamyl alcohol over core–shell Fe3O4@SiO2@La2O3 catalyst. Sep. Purif. Technol. 282, 119969. https://doi.org/10.1016/j.seppur.2021.119969

Soyol-Erdene, T.O., Valente, T., Grande, J.A., De La Torre, M.L., 2018. Mineralogical controls on mobility of rare earth elements in acid mine drainage environments. Chemosphere 205, 317–327. https://doi.org/10.1016/j.chemosphere.2018.04.095

Spasiano, D., Siciliano, A., Race, M., Marotta, R., Guida, M., Andreozzi, R., Pirozzi, F., 2016. Biodegradation, ecotoxicity and UV254/H2O2 treatment of imidazole, 1-methyl-imidazole and N,N'-alkyl-imidazolium chlorides in water. Water Res. 106, 450–460. https://doi.org/10.1016/j.watres.2016.10.026

Squadrone, S., Brizio, P., Stella, C., Mantia, M., Battuello, M., Nurra, N., Sartor, R.M., Orusa, R., Robetto, S., Brusa, F., Mogliotti, P., Garrone, A., Abete, M.C., 2019. Rare earth elements in marine and terrestrial matrices of Northwestern Italy: Implications for food safety and human health. Sci. Total Environ. 660, 1383–1391. https://doi.org/10.1016/j.scitotenv.2019.01.112

Stauber, J., Binet, M., 2000. Canning River Phoslock Field Trials–Ecotoxicity Testing Final Report. CSIRO & the WA Waters and Rivers Commission Report No: ET 317R.

Stebbing, A.R., 1982, Hormesis - the stimulation of growth by low levels of inhibitors. Sci. Total Environ. 22, 213–234. https://doi.org/10.1016/0048-9697(82)90066-3

Steiner, S., Mueller, L., Popovicheva, O.B., Raemy, D.O., Czerwinski, J., Comte, P., Mayer, A., Gehr, P., Rothen-Rutishauser, B., Clift, M.J.D., 2012. Cerium dioxide nanoparticles can interfere with the associated cellular mechanistic response to diesel exhaust exposure. Toxicol. Lett. 214, 218–225. https://doi.org/10.1016/j.toxlet.2012.08.026

Stewart, B.W., Capo, R.C., Hedin, B.C., Hedin, R.S., 2017. Rare earth element resources in coal mine drainage and treatment precipitates in the Appalachian Basin, USA. Int. J. Coal Geol. 169, 28–39. https://doi.org/10.1016/j.coal.2016.11.002

Su, X., Zheng, X., Ni, J., 2009. Lanthanum citrate induces anoikis of Hela cells. Cancer Lett. 285, 200–209. https://doi.org/10.1016/j.canlet.2009.05.018

Sun, D., He, N., Chen, Q., Duan, S., 2019. Effects of Lanthanum on the Photosystem II Energy Fluxes and Antioxidant System of Chlorella Vulgaris and Phaeodactylum Tricornutum. Int. J. Environ. Res. Public. Health 16, 2242. https://doi.org/10.3390/ijerph16122242

Sun, G., Li, Z., Liu, T., Chen, J., Wu, T., Feng, X., 2017. Rare earth elements in street dust and associated health risk in a municipal industrial base of central China. Environ. Geochem. Health 39, 1469–1486. https://doi.org/10.1007/s10653-017-9982-x

Sverjensky, D. A., 1984. Europium redox equilibria in aqueous solution. Earth Planet. Sci. Lett. 67, 70–78. https://doi.org/10.1016/0012-821X(84)90039-6

Szabadvary, F., 1988. Chapter 73 The history of the discovery and separation of the rare earths. Handb. Phys. Chem. Rare Earths 11, 33–80. https://doi.org/10.1016/S0168-1273(88)11005-2

Tai, P., Zhao, Q., Su, D., Li, P., Stagnitti, F., 2010. Biological toxicity of lanthanide elements on algae. Chemosphere 80, 1031–1035. https://doi.org/10.1016/j.chemosphere.2010.05.030

Takaya, Y., Yasukawa, K., Kawasaki, T., Fujinaga, K., Ohta, J., Usui, Y., Nakamura, K., Kimura, J.-I., Chang, Q., Hamada, M., Dodbiba, G., Nozaki, T., Iijima, K., Morisawa, T., Kuwahara, T., Ishida, Y., Ichimura, T., Kitazume, M., Fujita, T., Kato, Y., 2018. The tremendous potential of deep-sea mud as a source of rare-earth elements. Sci. Rep. 8, 5763. https://doi.org/10.1038/s41598-018-23948-5

Takyi, S.A., Basu, N., Arko-Mensah, J., Dwomoh, D., Houessionon, K.G., Fobil, J.N., 2021. Biomonitoring of metals in blood and urine of electronic waste (E-waste) recyclers at Agbogbloshie, Ghana. Chemosphere 280, 130677. https://doi.org/10.1016/j.chemosphere.2021.130677

Tamás, M., Sharma, S., Ibstedt, S., Jacobson, T., Christen, P., 2014. Heavy Metals and Metalloids As a Cause for Protein Misfolding and Aggregation. Biomolecules 4, 252–267. https://doi.org/10.3390/biom4010252

Tanner, S.D., Douglas, D.J., French, J.B., 1994. Gas and Ion Dynamics of a Three-Aperture Vacuum Interface for Inductively Coupled Plasma-Mass Spectrometry. Appl. Spectrosc. 48(11), 1373-1378. https://doi.org/10.1366/0003702944028137

Tarnuzzer, R.W., Colon, J., Patil, S., Seal, S., 2005. Vacancy Engineered Ceria Nanostructures for Protection from Radiation-Induced Cellular Damage. Nano Lett. 5, 2573–2577. https://doi.org/10.1021/nl052024f

Taylor, N.S., Merrifield, R., Williams, T.D., Chipman, J.K., Lead, J.R., Viant, M.R., 2016. Molecular toxicity of cerium oxide nanoparticles to the freshwater alga Chlamydomonas reinhardtii is associated with supra-environmental exposure concentrations. Nanotoxicology 10, 32–41. https://doi.org/10.3109/17435390.2014.1002868

Técher, D., Grosjean, N., Sohm, B., Blaudez, D., Le Jean, M., 2020. Not merely noxious? Time-dependent hormesis and differential toxic effects systematically induced by rare earth elements in Escherichia coli. Environ. Sci. Pollut. Res. 27, 5640–5649. https://doi.org/10.1007/s11356-019-07002-z

Thomas, P.J., Carpenter, D., Boutin, C., Allison, J.E., 2014. Rare earth elements (REEs): Effects on germination and growth of selected crop and native plant species. Chemosphere 96, 57–66. https://doi.org/10.1016/j.chemosphere.2013.07.020

Thomas, R., 2001. Spectroscopy Tutorial: A Beginner's Guide to ICP-MS, Part IV: The Interface Region. Spectroscopy 16(7), 26–34

Thomsen, HenrikS., 2004. Gadolinium-based contrast media may be nephrotoxic even at approved doses. Eur. Radiol. 14. https://doi.org/10.1007/s00330-004-2379-0

Thomson, B.A., Douglas, D.J., Corr, J.J., Hager, J.W., Joliffe, C.A., 1995. Improved Collisionally Activated Dissociation Efficiency and Mass Resolution on a Triple Quadrupole Mass Spectrometer SystemAnal. Chem. 67, 1696–1704. https://doi.org/10.1021/ac00106a008

Tian, S., Li, K., Møller, P., Ying, S.C., Wang, L., Li, Z., Roursgaard, M., Liang, T., 2020. Assessment of reactive oxygen species production and genotoxicity of rare earth mining dust: Implications for public health and mining management. Sci. Total Environ. 740, 139759. https://doi.org/10.1016/j.scitotenv.2020.139759

Tian, S., Liang, T., Li, K., 2019. Fine road dust contamination in a mining area presents a likely air pollution hotspot and threat to human health. Environ. Int. 128, 201–209. https://doi.org/10.1016/j.envint.2019.04.050

Tikhanova, S.M., Lebedev, L.A., Martinson, K.D., Chebanenko, M.I., Buryanenko, I.V., Semenov, V.G., Nevedomskiy, V.N., Popkov, V.I., 2021. The synthesis of novel heterojunction h-$YbFeO_3$/o-$YbFeO_3$ photocatalyst with enhanced Fenton-like activity under visible-light. New J. Chem. 45, 1541–1550. https://doi.org/10.1039/D0NJ04895J

Tokunaga, S., Haron, M.J., Wasay, S.A., Wong, K.F., Laosangthum, K., Uchiumi, A., 1995. Removal of fluoride ions from aqueous solutions by multivalent metal compounds. Int. J. Environ. Stud. 48, 17–28. https://doi.org/10.1080/00207239508710973

Tommasi, F., Thomas, P.J., Pagano, G., Perono, G.A., Oral, R., Lyons, D.M., Toscanesi, M., Trifuoggi, M., 2021. Review of Rare Earth Elements as Fertilizers and Feed Additives: A Knowledge Gap Analysis. Arch. Environ. Contam. Toxicol. 81, 531–540. https://doi.org/10.1007/s00244-020-00773-4

Tong, S., Yang, L., Gong, H., Wang, L., Li, H., Yu, J., Li, Y., Deji, Y., Nima, C., Zhao, S., Gesang, Z., Kong, C., Wang, X., Men, Z., 2022. Association of selenium, arsenic, and other trace elements in drinking water and urine in residents of the plateau region in China. Environ. Sci. Pollut. Res. 29, 26498–26512. https://doi.org/10.1007/s11356-021-17418-1

Tong, S.-L., Zhu, W.-Z., Gao, Z.-H., Meng, Y.-X., Peng, R.-L., Lu, G.-C., 2004. Distribution Characteristics of Rare Earth Elements in Children's Scalp Hair from a Rare Earths Mining Area in Southern China. J. Environ. Sci. Health Part A 39, 2517–2532. https://doi.org/10.1081/ESE-200026332

Towett, E.K., Shepherd, K.D., Cadisch, G., 2013. Quantification of total element concentrations in soils using total X-ray fluorescence spectroscopy (TXRF). Sci. Total Environ. 463–464, 374–388. https://doi.org/10.1016/j.scitotenv.2013.05.068

Trapasso, G., Chiesa, S., Freitas, R., Pereira, E., 2021a. What do we know about the ecotoxicological implications of the rare earth element gadolinium in aquatic ecosystems? Sci. Total Environ. 781, 146273. https://doi.org/10.1016/j.scitotenv.2021.146273

Trapasso, G., Coppola, F., Queirós, V., Henriques, B., Soares, A.M.V.M., Pereira, E., Chiesa, S., Freitas, R., 2021b. How Ulva lactuca can influence the impacts induced by the rare earth element Gadolinium in Mytilus galloprovincialis? The role of macroalgae in water safety towards marine wildlife. Ecotoxicol. Environ. Saf. 215, 112101. https://doi.org/10.1016/j.ecoenv.2021.112101

Trifuoggi, M., Pagano, G., Guida, M., Palumbo, A., Siciliano, A., Gravina, M., Lyons, D.M., Burić, P., Levak, M., Thomas, P.J., Giarra, A., Oral, R., 2017. Comparative toxicity of seven rare earth

elements in sea urchin early life stages. Environ. Sci. Pollut. Res. 24, 20803–20810. https://doi.org/10.1007/s11356-017-9658-1

Tseng, M.T., Lu, X., Duan, X., Hardas, S.S., Sultana, R., Wu, P., Unrine, J.M., Graham, U., Butterfield, D.A., Grulke, E.A., Yokel, R.A., 2012. Alteration of hepatic structure and oxidative stress induced by intravenous nanoceria. Toxicol. Appl. Pharmacol. 260, 173–182. https://doi.org/10.1016/j.taap.2012.02.008

Turra, C., Fernandes, E.A.N., Bacchi, M.A., n.d. Evaluation on rare earth elements of Brazilian agricultural supplies.

Uchida, S., Tagami, K., Tabei, K., Hirai, I., 2006. Concentrations of REEs, Th and U in river waters collected in Japan. J. Alloys Compd. 408–412, 525–528. https://doi.org/10.1016/j.jallcom.2004.12.104

Ugwu, E.I., Karri, R.R., Nnaji, C.C., John, J., Padmanaban, V., Othmani, A., Ikechukwu, E.L., Helal, W.M., 2022. Application of green nanocomposites in removal of toxic chemicals, heavy metals, radioactive materials, and pesticides from aquatic water bodies. In Sustainable Nanotechnology for Environmental Remediation. Elsevier: Amsterdam, The Netherlands, 321–346

UNI CEI EN ISO/IEC 17025:2018. General requirements for the competence of testing and calibration laboratories. Available at: http://store.uni.com/catalogo/unicei-en-iso-iec-17025-2018

US DOE UDoE, 2012. Critical materials strategy. 196.

US Environmental Protection Agency, 1994. Determination of trace elements in waters and wastes by inductively coupled plasma-mass spectrometry; Method 200.8. Environmental Monitoring Systems Laboratory, Cincinati, Ohio

US Environmental Protection Agency, 2012. Rare earth elements: A review of production, processing, recycling, and associated environmental issues. Washington, DC: U.S. Environmental Protection Agency. EPA 600/R-12/572 www.epa.gov/ord

USGS (2022). "Rare earths," in U.S. Mineral commodity summaries 2022 (Reston, VA: U.S. Geological Survey), 134–135

Valcheva-Traykova, M., Saso, L., Kostova, I., 2014. Involvement of Lanthanides in the Free Radicals Homeostasis. Curr. Top. Med. Chem. 14, 2508–2519. https://doi.org/10.2174/1568026614666141203123620

Valiathan, M.S., Kartha, C.C., Panday, V.K., Gang, H.S., Sunta, C.M., 1986. A geochemical basis for endomyocardial fibrosis. Cardiovasc. Res. 20, 679–682. doi:10.1093/cvr/20.9.679

Van Gosen, B. S., Verplanck, P. L., Seal, R. R., Long, K. R., and Gambogi, J., 2017. "Rare-Earth elements," in Chapter O" in Critical mineral resources of the United States—economic and environmental geology and prospects for future supply. Editors K. J. Schulz, J. H. DeYoungJr., and R. R. Seal (Bradley, D.C.: U.S. Geological Survey), O1–O31. Professional Paper 1802

Van Oosterhout, F., Goitom, E., Roessink, I., Lürling, M., 2014. Lanthanum from a modified clay used in eutrophication control is bioavailable to the marbled crayfish (Procambarus fallax f. virginalis). PLoS ONE 9. https://doi.org/10.1371/journal.pone.0102410

Varani, J., DaSilva, M., Warner, R.L., Deming, M.O., Barron, A.G., Johnson, K.J., Swartz, R.D., 2009. Effects of Gadolinium-Based Magnetic Resonance Imaging Contrast Agents on Human Skin

in Organ Culture and Human Skin Fibroblasts: Invest. Radiol. 44, 74–81. https://doi.org/10.1097/RLI.0b013e31818f76b5

Vargas Hernández, J., Coste, S., García Murillo, A., Carrillo Romo, F., Kassiba, A., 2017. Effects of metal doping (Cu, Ag, Eu) on the electronic and optical behavior of nanostructured TiO2. J. Alloys Compd. 710, 355–363. https://doi.org/10.1016/j.jallcom.2017.03.275

Vass, C.R., Noble, A., Ziemkiewicz, P.F., 2019. The Occurrence and Concentration of Rare Earth Elements in Acid Mine Drainage and Treatment By-products: Part 1—Initial Survey of the Northern Appalachian Coal Basin. Min. Metall. Explor. 36, 903–916. https://doi.org/10.1007/s42461-019-0097-z

Verlicchi, P., Al Aukidy, M., Zambello, E., 2012. Occurrence of pharmaceutical compounds in urban wastewater: Removal, mass load and environmental risk after a secondary treatment—A review. Sci. Total Environ. 429, 123–155. https://doi.org/10.1016/j.scitotenv.2012.04.028

Verplanck, P.L., Nordstrom, D.K., Taylor, H.E., Kimball, B.A., 2004. Rare earth element partitioning between hydrous ferric oxides and acid mine water during iron oxidation. Appl. Geochem. 19, 1339–1354. https://doi.org/10.1016/j.apgeochem.2004.01.016

Verrey, D., Durand, S., Thomas, O., Lelévrier, V., Quénel, P., Le Bot, B., 2019. A new washing procedure for inorganic element analysis of hair. J. Expo. Sci. Environ. Epidemiol. 29, 706–717. https://doi.org/10.1038/s41370-018-0112-3

Vinosha, P.A., Vinsla, J.V.A., Madhavan, J., Devanesan, S., AlSalhi, M.S., Nicoletti, M., Xavier, B., 2022. Impact of dysprosium doped (Dy) zinc ferrite (ZnFe2o4) nanocrystals in photo- fenton exclusion of recalcitrant organic pollutant. Environ. Res. 203, 111913. https://doi.org/10.1016/j.envres.2021.111913

Vocaturo, G., Colombo, F., Zanoni, M., Rodi, F., Sabbioni, E., Pietra, R., 1983. Human Exposure to Heavy Metals. Chest 83, 780–783. https://doi.org/10.1378/chest.83.5.780

Vogler, A., Kunkely, H., 2006. Excited state properties of lanthanide complexes: Beyond ff states. Inorganica Chim. Acta 359, 4130–4138. https://doi.org/10.1016/j.ica.2006.05.025

Volokh, A. A., Gorbunov, A. V., Gundorina, S. F., Revich, B. A., Frontasyeva, M. V., Pal, C. S., 1990. Phosphorus fertilizer production as a source of rare-earth elements pollution of the environment. Sci. Total Environ. 95, 141–148. https://doi.org/10.1016/0048-9697(90)90059-4

Vukov, O., 2015. Developing a Site Specific Understanding of the Toxicity of Rare Earth Elements , Cerium and Dysprosium , To Daphnia Pulex and Hyalella Azteca.

Vukov, O., Smith, D.S., McGeer, J.C., 2016. Acute dysprosium toxicity to Daphnia pulex and Hyalella azteca and development of the biotic ligand approach. Aquat. Toxicol. 170, 142–151. https://doi.org/10.1016/j.aquatox.2015.10.016

Wagner, C., Løkke, H., 1991. Estimation of ecotoxicological protection levels from NOEC toxicity data. Water Res. 25, 1237–1242. https://doi.org/10.1016/0043-1354(91)90062-U

Wall, F., 2013. Rare earth elements, in: Gunn, G. (Ed.), Critical Metals Handbook. John Wiley & Sons, Oxford, pp. 312–339. https://doi.org/10.1002/9781118755341.ch13

Wang, B., Yan, L., Huo, W., Lu, Q., Cheng, Z., Zhang, J., Li, Z., 2017. Rare earth elements and hypertension risk among housewives: A pilot study in Shanxi Province, China. Environ. Pollut. 220, 837–842. https://doi.org/10.1016/j.envpol.2016.10.066

Wang, B., Zhu, Y., Pang, Y., Xie, J., Hao, Y., Yan, H., Li, Z., Ye, R., 2018. Indoor air pollution affects hypertension risk in rural women in Northern China by interfering with the uptake of metal elements: A preliminary cross-sectional study. Environ. Pollut. 240, 267–272. https://doi.org/10.1016/j.envpol.2018.04.097

Wang, C., He, M., Chen, B., Hu, B., 2020. Study on cytotoxicity, cellular uptake and elimination of rare-earth-doped upconversion nanoparticles in human hepatocellular carcinoma cells. Ecotoxicol. Environ. Saf. 203, 110951. https://doi.org/10.1016/j.ecoenv.2020.110951

Wang, C., He, M., Shi, W., Wong, J., Cheng, T., Wang, X., Hu, L., Chen, F., 2011. Toxicological effects involved in risk assessment of rare earth lanthanum on roots of Vicia faba L. seedlings. J. Environ. Sci. 23, 1721–1728. https://doi.org/10.1016/S1001-0742(10)60598-0

Wang, L., He, J., Xia, A., Cheng, M., Yang, Q., Du, C., Wei, H., Huang, X., Zhou, Q., 2017. Toxic effects of environmental rare earth elements on delayed outward potassium channels and their mechanisms from a microscopic perspective. Chemosphere 181, 690–698. https://doi.org/10.1016/j.chemosphere.2017.04.141

Wang, L., Huang, X., Zhou, Q., 2009. Protective Effect of Rare Earth Against Oxidative Stress Under Ultraviolet-B Radiation. Biol. Trace Elem. Res. 128, 82–93. https://doi.org/10.1007/s12011-008-8250-4

Wang, L., Li, J., Zhou, Q., Yang, G., Ding, X.L., Li, X., Cai, C.X., Zhang, Z., Wei, H.Y., Lu, T.H., Deng, X.W., Huang, X.H., 2014a. Rare earth elements activate endocytosis in plant cells. Proc. Natl. Acad. Sci. 111, 12936–12941. https://doi.org/10.1073/pnas.1413376111

Wang, L., Liang, T., 2014. Accumulation and fractionation of rare earth elements in atmospheric particulates around a mine tailing in Baotou, China. Atmos. Environ. 88, 23–29. https://doi.org/10.1016/j.atmosenv.2014.01.068

Wang, L., Wang, P., Chen, W.-Q., Wang, Q.-Q., Lu, H.-S., 2020. Environmental impacts of scandium oxide production from rare earths tailings of Bayan Obo Mine. J. Clean. Prod. 270, 122464. https://doi.org/10.1016/j.jclepro.2020.122464

Wang, L., Wang, W., Zhou, Q., Huang, X., 2014b. Combined effects of lanthanum (III) chloride and acid rain on photosynthetic parameters in rice. Chemosphere 112, 355–361. https://doi.org/10.1016/j.chemosphere.2014.04.069

Wang, M., You, M., Guo, P., Tang, H., Lv, C., Zhang, Y., Zhu, T., Han, J., 2017. Hydrothermal synthesis of Sm-doped Bi2MoO6 and its high photocatalytic performance for the degradation of Rhodamine B. J. Alloys Compd. 728, 739–746. https://doi.org/10.1016/j.jallcom.2017.09.066

Wang, N., Zheng, T., Zhang, G., Wang, P., 2016. A review on Fenton-like processes for organic wastewater treatment. J. Environ. Chem. Eng. 4, 762–787. https://doi.org/10.1016/j.jece.2015.12.016

Wang, S., 2008. A Comparative study of Fenton and Fenton-like reaction kinetics in decolourisation of wastewater. Dyes Pigments 76, 714–720. https://doi.org/10.1016/j.dyepig.2007.01.012

Wang, W., Zhu, Q., Qin, F., Dai, Q., Wang, X., 2018. Fe doped CeO2 nanosheets as Fenton-like heterogeneous catalysts for degradation of salicylic acid. Chem. Eng. J. 333, 226–239. https://doi.org/10.1016/j.cej.2017.08.065

Wang, X., Jin, Y., Chen, W., Zou, R., Xie, J., Tang, Y., Li, X., Li, L., 2021. Electro-catalytic activity of CeOx modified graphite felt for carbamazepine degradation via E-peroxone process. Front. Environ. Sci. Eng. 15, 122. https://doi.org/10.1007/s11783-021-1410-x

Wang, Y., Li, J., Lü, Y., Jin, H., Deng, S., Zeng, Y., 2012. Effects of cerium on growth and physiological characteristics of Anabaena flosaquae. J. Rare Earths 30, 1287–1292. https://doi.org/10.1016/S1002-0721(12)60222-1

Wang, Y.-L., Wang, X.-D., Zhao, B., Wang, Y.-C., 2007. Reduction of hyperhydricity in the culture of Lepidium meyenii shoots by the addition of rare earth elements. Plant Growth Regul. 52, 151–159. https://doi.org/10.1007/s10725-007-9185-z

Wang, Zaosheng, Shu, J., Wang, Zhaoru, Qin, X., Wang, S., 2022. Geochemical behavior and fractionation characteristics of rare earth elements (REEs) in riverine water profiles and sentinel Clam (Corbicula fluminea) across watershed scales: Insights for REEs monitoring. Sci. Total Environ. 803, 150090. https://doi.org/10.1016/j.scitotenv.2021.150090

Waring, P.M., Watling, R.J., 1990. Rare earth deposits in a deceased movie projectionist: A new case of rare earth pneumoconiosis? Med. J. Aust. 153, 726–730. https://doi.org/10.5694/j.1326-5377.1990.tb126334.x

Wei, B., Li, Y., Li, H., Yu, J., Ye, B., Liang, T., 2013. Rare earth elements in human hair from a mining area of China. Ecotoxicol. Environ. Saf. 96, 118–123. https://doi.org/10.1016/j.ecoenv.2013.05.031

Wei, J., Wang, C., Yin, S., Pi, X., Jin, L., Li, Z., Liu, J., Wang, L., Yin, C., Ren, A., 2020. Concentrations of rare earth elements in maternal serum during pregnancy and risk for fetal neural tube defects. Environ. Int. 137, 105542. https://doi.org/10.1016/j.envint.2020.105542

Wennmalm, Å., Gunnarsson, B., 2009. Pharmaceutical management through environmental product labeling in Sweden. Environ. Int. 35, 775–777. https://doi.org/10.1016/j.envint.2008.12.008

Werkneh, A.A., Rene, E.R., 2019. Applications of nanotechnology and biotechnology for sustainable water and wastewater treatment. In Water and Wastewater Treatment Technologies. Springer: Berlin/Heidelberg, Germany, 405–430

White, G.W., Gibby, W.A., Tweedle, M.F., 2006. Comparison of Gd(DTPA-BMA) (Omniscan) Versus Gd(HP-DO3A) (ProHance) Relative to Gadolinium Retention in Human Bone Tissue by Inductively Coupled Plasma Mass Spectroscopy: Invest. Radiol. 41, 272–278. https://doi.org/10.1097/01.rli.0000186569.32408.95

Wiesinger, B., Kehlbach, R., Bebin, J., Hemsen, J., Bantleon, R., Schmehl, J., Dietz, K., Claussen, C.D., Wiskirchen, J., 2010. Effects of MRI Contrast Agents on Human Embryonic Lung Fibroblasts: Invest. Radiol. 45, 513–519. https://doi.org/10.1097/RLI.0b013e3181eb2fe7

World Medical Association, 2013. Declaration of Helsinki – ethical principles for medical research involving human subjects. Available at: https://www.wma.net/policies-post/wmadeclaration-of-helsinki-ethical-principles-for-medical-research-involving-human-subjects/

Wu, D., Li, C., Zhang, D., Wang, L., Zhang, X., Shi, Z., Lin, Q., 2019. Enhanced photocatalytic activity of Gd3+ doped TiO2 and Gd2O3 modified TiO2 prepared via ball milling method. J. Rare Earths 37, 845–852. https://doi.org/10.1016/j.jre.2018.10.011

Wu, J., Yang, J., Liu, Q., Wu, S., Ma, H., Cai, Y., 2013. Lanthanum Induced Primary Neuronal Apoptosis Through Mitochondrial Dysfunction Modulated by Ca2+ and Bcl-2 Family. Biol. Trace Elem. Res. 152, 125–134. https://doi.org/10.1007/s12011-013-9601-3

Wysocka, I., Vassileva, E., 2017. Method validation for high resolution sector field inductively coupled plasma mass spectrometry determination of the emerging contaminants in the open ocean: Rare earth elements as a case study. Spectrochim. Acta Part B At. Spectrosc. 128, 1–10. https://doi.org/10.1016/j.sab.2016.12.004

Wyttenbach, A., Furrer, V., Schleppi, P., Tobler, L., n.d. Rare earth elements in soil and in soil-grown plants.

Xia, B., Sun, Z., Wang, L., Zhou, Q., Huang, X., 2017. Analysis of the combined effects of lanthanum and acid rain, and their mechanisms, on nitrate reductase transcription in plants. Ecotoxicol. Environ. Saf. 138, 170–178. https://doi.org/10.1016/j.ecoenv.2016.12.034

Xia, T., Kovochich, M., Liong, M., Mädler, L., Gilbert, B., Shi, H., Yeh, J.I., Zink, J.I., Nel, A.E., 2008. Comparison of the Mechanism of Toxicity of Zinc Oxide and Cerium Oxide Nanoparticles Based on Dissolution and Oxidative Stress Properties. ACS Nano 2, 2121–2134. https://doi.org/10.1021/nn800511k

Xie, Y., Yuan, C., 2003. Visible-light responsive cerium ion modified titania sol and nanocrystallites for X-3B dye photodegradation. Appl. Catal. B Environ. 46, 251–259. https://doi.org/10.1016/S0926-3373(03)00211-X

Xin, Z., Wenchao, Z., Zhenguang, Y., Yiguo, H., Zhengtao, L., Xianliang, Y., Xiaonan, W., Tingting, L., Liming, Z., 2015. Species sensitivity analysis of heavy metals to freshwater organisms. Ecotoxicology 24, 1621–1631. https://doi.org/10.1007/s10646-015-1500-2

Xu, D., Shen, Z., Dou, C., Dou, Z., Li, Y., Gao, Y., Sun, Q., 2022. Effects of soil properties on heavy metal bioavailability and accumulation in crop grains under different farmland use patterns. Sci. Rep. 12, 9211. https://doi.org/10.1038/s41598-022-13140-1

Xu, L., Wang, J., 2012. Magnetic Nanoscaled Fe_3O_4/CeO_2 Composite as an Efficient Fenton-Like Heterogeneous Catalyst for Degradation of 4-Chlorophenol. Environ. Sci. Technol. 46, 10145–10153. https://doi.org/10.1021/es300303f

Xu, L., Xue, Y., Xia, J., Qu, X., Lei, B., Yang, T., Zhang, X., Li, N., Zhao, H., Wang, M., Luo, M., Zhang, C., Du, Y., Yan, C., 2020. Construction of high quality ultrathin lanthanide oxyiodide nanosheets for enhanced CT imaging and anticancer drug delivery to efficient cancer theranostics. Biomaterials 230, 119670. https://doi.org/10.1016/j.biomaterials.2019.119670

Xu, Q., Fu, Y., Min, H., Cai, S., Sha, S., Cheng, G., 2012. Laboratory assessment of uptake and toxicity of lanthanum (La) in the leaves of Hydrocharis dubia (Bl.) Backer. Environ. Sci. Pollut. Res. 19, 3950–3958. https://doi.org/10.1007/s11356-012-0982-1

Xu, T., Zhang, M., Hu, J., Li, Z., Wu, T., Bao, J., Wu, S., Lei, L., He, D., 2017. Behavioral deficits and neural damage of Caenorhabditis elegans induced by three rare earth elements. Chemosphere 181, 55–62. https://doi.org/10.1016/j.chemosphere.2017.04.068

Xu, X., Ge, Y., Li, B., Fan, F., Wang, F., 2014. Shape evolution of Eu-doped Bi 2 WO 6 and their photocatalytic properties. Mater. Res. Bull. 59, 329–336. https://doi.org/10.1016/j.materresbull.2014.07.050

Xu, X., Zhu, W., Wang, Z., Witkamp, G.-J., 2002. Distributions of rare earths and heavy metals in field-grown maize after application of rare earth-containing fertilizer. Sci. Total Environ. 293, 97–105. https://doi.org/10.1016/S0048-9697(01)01150-0

Yang, L., Wang, X., Nie, H., Shao, L., Wang, G., Liu, Y., 2016. Residual levels of rare earth elements in freshwater and marine fish and their health risk assessment from Shandong, China. Mar. Pollut. Bull. 107, 393–397. https://doi.org/10.1016/j.marpolbul.2016.03.034

Yang, Y., Zhou, Z., Wei, Z.-Z., Qin, Q.-P., Yang, L., Liang, H., 2021. High anticancer activity and apoptosis- and autophagy-inducing properties of novel lanthanide(III) complexes bearing 8-hydroxyquinoline- *N* -oxide and 1,10-phenanthroline. Dalton Trans. 50, 5828–5834. https://doi.org/10.1039/D1DT00450F

Yayapao, O., Thongtem, T., Phuruangrat, A., Thongtem, S., 2013. Ultrasonic-assisted synthesis of Nd-doped ZnO for photocatalysis. Mater. Lett. 90, 83–86. https://doi.org/10.1016/j.matlet.2012.09.027

Yin, H., Wang, J., Zeng, Y., Shen, X., He, Y., Ling, L., Cao, L., Fu, X., Peng, L., Chun, C., 2021. Effect of the Rare Earth Element Lanthanum (La) on the Growth and Development of Citrus Rootstock Seedlings. Plants 10, 1388. https://doi.org/10.3390/plants10071388

Yongxing, W., Xiaorong, W., Zichun, H., 2000. Genotoxicity of Lanthanum (III) and Gadolinium (III) in Human Peripheral Blood Lymphocytes. Bull. Environ. Contam. Toxicol. 64, 611–616. https://doi.org/10.1007/s001280000047

Yoon, H.K., 2005. Dendriform pulmonary ossification in patient with rare earth pneumoconiosis. Thorax 60, 701–703. https://doi.org/10.1136/thx.2003.006270

Younes, H.A., Taha, M., Khaled, R., Mahmoud, H.M., Abdelhameed, R.M., 2023. Perovskite/metal-organic framework photocatalyst: A novel nominee for eco-friendly uptake of pharmaceuticals from wastewater. J. Alloys Compd. 930, 167322. https://doi.org/10.1016/j.jallcom.2022.167322

Yu, C., Wu, Z., Liu, R., He, H., Fan, W., Xue, S., 2016. The effects of Gd 3+ doping on the physical structure and photocatalytic performance of Bi 2 MoO 6 nanoplate crystals. J. Phys. Chem. Solids 93, 7–13. https://doi.org/10.1016/j.jpcs.2016.02.008

Yu, L., Dai, Y., Yuan, Z., Li, J., 2007. Effects of rare earth elements on telomerase activity and apoptosis of human peripheral blood mononuclear cells. Biol. Trace Elem. Res. 116.

Yuan, X.-Z., Pan, G., Chen, H., Tian, B.-H., 2009. Phosphorus fixation in lake sediments using LaCl3-modified clays. Ecol. Eng. 35, 1599–1602. https://doi.org/10.1016/j.ecoleng.2008.08.002

Zaichick, S., Zaichick, V., Karandashev, V., Nosenko, S., 2011. Accumulation of rare earth elements in human bone within the lifespan. Metallomics 3, 186–194. https://doi.org/10.1039/C0MT00069H

Zhang, A., Zhang, J., 2010. Effects of europium doping on the photocatalytic behavior of BiVO4. J. Hazard. Mater. 173, 265–272. https://doi.org/10.1016/j.jhazmat.2009.08.079

Zhang, H., Feng, J., Zhu, W., Liu, C., Xu, S., Shao, P., Wu, D., Yang, W., Gu, J., 2000. Chronic Toxicity of Rare-Earth Elements on Human Beings : Implications of Blood Biochemical Indices in

REE-high Regions, South Jiangxi. Biol. Trace Elem. Res. 73, 1–18. https://doi.org/10.1385/BTER:73:1:1

Zhang, H., He, X., Bai, W., Guo, X., Zhang, Z., Chai, Z., Zhao, Y., 2010. Ecotoxicological assessment of lanthanum with Caenorhabditis elegans in liquid medium. Metallomics 2, 806. https://doi.org/10.1039/c0mt00059k

Zhang, L., Chen, B., He, M., Hu, B., 2013. Polymer monolithic capillary microextraction combined on-line with inductively coupled plasma MS for the determination of trace rare earth elements in biological samples: Sample Preparation. J. Sep. Sci. 36, 2158–2167. https://doi.org/10.1002/jssc.201300100

Zhang, N., Chen, J., Fang, Z., Tsang, E.P., 2019. Ceria accelerated nanoscale zerovalent iron assisted heterogenous Fenton oxidation of tetracycline. Chem. Eng. J. 369, 588–599. https://doi.org/10.1016/j.cej.2019.03.112

Zhang, R., Wang, L., Li, Y., Li, H., Xu, Y., 2020. Distribution Characteristics of Rare Earth Elements and Selenium in Hair of Centenarians Living in China Longevity Region. Biol. Trace Elem. Res. 197, 15–24. https://doi.org/10.1007/s12011-019-01970-6

Zhang, Y., Fu, L.-J., Li, J.-X., Yang, X.-G., Yang, X.-D., Wang, K., 2009. Gadolinium promoted proliferation and enhanced survival in human cervical carcinoma cells. BioMetals 22, 511–519. https://doi.org/10.1007/s10534-009-9208-5

Zhang, Y., Zhang, H., Xu, Y., Wang, Y., 2003. Europium doped nanocrystalline titanium dioxide: preparation, phase transformation and photocatalytic properties. J. Mater. Chem. 13, 2261. https://doi.org/10.1039/b305538h

Zhang, Z.-H., Balasubramanian, R., 2017. Effects of Cerium Oxide and Ferrocene Nanoparticles Addition As Fuel-Borne Catalysts on Diesel Engine Particulate Emissions: Environmental and Health Implications. Environ. Sci. Technol. 51, 4248–4258. https://doi.org/10.1021/acs.est.7b00920

Zhao, C.-M., Shi, X., Xie, S.-Q., Liu, W.-S., He, E.-K., Tang, Y.-T., Qiu, R.-L., 2019. Ecological Risk Assessment of Neodymium and Yttrium on Rare Earth Element Mine Sites in Ganzhou, China. Bull. Environ. Contam. Toxicol. 103, 565–570. https://doi.org/10.1007/s00128-019-02690-2

Zhao, F., Cong, Z., Sun, H., Ren, D., 2007. The geochemistry of rare earth elements (REE) in acid mine drainage from the Sitai coal mine, Shanxi Province, North China. Int. J. Coal Geol. 70, 184–192. https://doi.org/10.1016/j.coal.2006.01.009

Zhao, H., Cheng, Z., Hu, R., Chen, J., Hong, M., Zhou, M., Gong, X., Wang, L., Hong, F., 2011. Oxidative Injury in the Brain of mice Caused by Lanthanid. Biol. Trace Elem. Res. 142, 174–189. https://doi.org/10.1007/s12011-010-8759-1

Zhao, L., Liu, L., 2018. Assessing the impact of lanthanum on the bivalve Corbicula fluminea in the Rhine River. Sci. Total Environ. 640–641, 830–839. https://doi.org/10.1016/j.scitotenv.2018.05.351

Zhong, Z.W., Na, S.N., Quan, M.S., Chao, Z.Z., Yu, C., Chao, Z., n.d. Hormetic Effects of Yttrium on Male Sprague-Dawley Rats. Biomed Env. Sci.

Zhou, F., Wang, H., Zhou, S., Liu, Y., Yan, C., 2020. Fabrication of europium-nitrogen co-doped TiO2/Sepiolite nanocomposites and its improved photocatalytic activity in real wastewater treatment. Appl. Clay Sci. 197, 105791. https://doi.org/10.1016/j.clay.2020.105791

Zhu, W., Xu, S., Shao, P., Zhang, H., Wu, D., Yang, W., Feng, J., 1997. Bioelectrical activity of the central nervous system among populations in a rare earth element area. Biol. Trace Elem. Res. 57, 71–77. https://doi.org/10.1007/BF02803871

Zhu, W., Xu, S., Shao, P., Zhang, H., Wu, D., Yang, W., Feng, J., Feng, L., 2005. Investigation on Liver Function Among Population in High Background of Rare Earth Area in South China. Biol. Trace Elem. Res. 104, 001–008. https://doi.org/10.1385/BTER:104:1:001

Zhu, Y., 2020. Determination of rare earth elements in seawater samples by inductively coupled plasma tandem quadrupole mass spectrometry after coprecipitation with magnesium hydroxide. Talanta 209, 120536. https://doi.org/10.1016/j.talanta.2019.120536

Zhuang, G., Zhou, Y., Lu, H., Lu, W., Zhou, M., Wang, Y., Tan, M., 1996. Concentration of rare earth elements, As, and Th in human brain and brain tumors, determined by neutron activation analysis. Biol. Trace Elem. Res. 53, 45–49. https://doi.org/10.1007/BF02784543

Zhuang, M., Wang, L., Wu, G., Wang, K., Jiang, X., Liu, T., Xiao, P., Yu, L., Jiang, Y., Song, J., Zhang, J., Zhou, J., Zhao, J., Chu, Z., 2017a. Health risk assessment of rare earth elements in cereals from mining area in Shandong, China. Sci. Rep. 7, 9772. https://doi.org/10.1038/s41598-017-10256-7

Zhuang, M., Zhao, J., Li, S., Liu, D., Wang, K., Xiao, P., Yu, L., Jiang, Y., Song, J., Zhou, J., Wang, L., Chu, Z., 2017b. Concentrations and health risk assessment of rare earth elements in vegetables from mining area in Shandong, China. Chemosphere 168, 578–582. https://doi.org/10.1016/j.chemosphere.2016.11.023

Zinatloo-Ajabshir, S., Emsaki, M., Hosseinzadeh, G., 2022. Innovative construction of a novel lanthanide cerate nanostructured photocatalyst for efficient treatment of contaminated water under sunlight. J. Colloid Interface Sci. 619, 1–13. https://doi.org/10.1016/j.jcis.2022.03.112

Zumbado, M., Luzardo, O.P., Rodríguez-Hernández, Á., Boada, L.D., Henríquez-Hernández, L.A., 2019. Differential exposure to 33 toxic elements through cigarette smoking, based on the type of tobacco and rolling paper used. Environ. Res. 169, 368–376. https://doi.org/10.1016/j.envres.2018.11.021

Appendix: Other contributions

Summer schools

1. 1st PANORAMA summer school. Lisbon, Portugal. 23-27/05/2022
2. 2nd Panorama summer school. Hamburg, Germany. 31/10/2022 – 04/11/2022
3. 3rd PANORAMA summer school. Antwerp, Belgium. 22-26/05/2023

Workshops

1. 1st PANORAMA workshop. Bremen, Germany. 21-23/04/2021
2. 2nd PANORAMA workshop. Paris, France. 13-15/12/2021

Courses UNINA

1. Cell biology and physiology
2. Biodiversity at sea
3. Marine biotechnology
4. Genome editing
5. Bioplastics
6. Gene expression in model systems
7. Italian language level B1
8. Italian language level B2
9. Mass spectrometry

Courses Accelopment

1. Data management
2. Gender in research
3. Research project management
4. Scientific communication
5. Funding opportunities
6. Transferable skills

This research has received funding from European Union’s Horizon 2020 research and innovation program under the Marie Sklodowska-Curie Grant Agreement N°857989